

Characterization of the PLP- dependent decarboxylases GADL1 and CSAD

Elaheh Mahootchi

Thesis for the degree of Philosophiae Doctor (PhD)
University of Bergen, Norway
2022

UNIVERSITY OF BERGEN



Characterization of the PLP-dependent decarboxylases GADL1 and CSAD

Elaheh Mahootchi



Thesis for the degree of Philosophiae Doctor (PhD)
at the University of Bergen

Date of defense: 31.03.2022

© Copyright Elaheh Mahootchi

The material in this publication is covered by the provisions of the Copyright Act.

Year: 2022

Title: Characterization of the PLP-dependent decarboxylases GADL1 and CSAD

Name: Elaheh Mahootchi

Print: Skipnes Kommunikasjon / University of Bergen

Scientific environment

The presented work has been carried out at the Department of Biomedicine, University of Bergen, during 2015-2021. It was supervised by Professor Jan Haavik and co-supervised by Professor Petri Kursula. Funding was provided by the University of Bergen and K.G. Jebsen Centre for Research on Neuropsychiatric disorders. The Norwegian Neuroscience School (NRSN), Digital Life of Norway (DLN), and Norwegian Biochemistry Society (NBS) supported courses and conference participation. In addition, the synchrotron-radiation facilities and the outstanding beamline support at EMBL/DESY, SOLEIL, and ESRF are gratefully acknowledged at this work.

Acknowledgments

First and foremost, I would like to express my sincere appreciation to my main supervisor Professor Jan Haavik for his tremendous support and excellent supervision. Thank you for devoting your time generously to the progress of this project. I am so grateful for having this great opportunity to learn lab techniques, earn experiences and complete my PhD in your group. Your continuous support and incredible expertise helped me a lot during this journey. Also, I have deep gratitude to my co-supervisor, Professor Petri Kursula for his inspiring guidance and amazing ideas. From both of you, I received insightful feedback and suggestions that have been vital to the progress of this work. Thank you for all your supports and your patience during scientific and technical challenges.

All my co-authors are acknowledged for their invaluable contributions. Thank you for the great collaborations and scientific inspiration. This goal was not achievable without your inputs and help.

I am so blessed to have wonderful colleagues and co-workers who created an inspiring, fabulous working atmosphere at the Neurotargeting group at BBB. Working with you was a great pleasure for me and from each one of you, I learned a life lesson. Thank you to all the nice people in Lab A since I started: Sidsel Riise, Ingeborg Winge, Rune Kleppe, Sadaf Ghorbani, Hanne Hollås, Ann Kari Grindheim, Anni Vedeler, Erik Hallin, Nibal Betari, Lisa Vårdal, Tor-Arne Hegvik, Peter Daniel Szigetvari, Anne Bauman, Arne Raasakka, Gyrid Nygård, Lucia Wagner, Selina Cannon Homaei, Oda Krokengen, Berit Skretting Solberg, Tore Ivar Malmei Aarsland, Johanne Instanes, Tatyana Zayats, Sudarshan Patil, Kazi Asraful Alam, Sunil Pandey, Kai Waløen and Ju Xu. Special thanks to Marte Innselset Flydal from Lab E.

Completing a PhD is a long journey, full of happy and sad moments. There are many days of success and satisfaction in achieving the goals and of course, days of frustrations and long, unsuccessful hours of work. For me, going through this journey would not be

possible without the unconditional love of my amazing family who supported me in every possible way that one can be supported. My dear father, Shahram, who raised me with big dreams and the courage to follow them. My beautiful mum, Ashraf, for her kind words and motivations along the way. From both of you, I always received warm, positive vibes from miles away. My lovely sisters, Elham and Azadeh, for being sources of motivation and hope. Thank you for sending me love and support from the other side of the ocean. My dearest friend, a true friend forever, Zahra Aghabozorg, who shared my laughs and tears for the last 25 years. Yes, such a long, wonderful friendship is one of the best gifts in my life. Also, many thanks to my friend Roald Wie.

And finally, to my amazing husband, Dr. Jalal Safari, for all his supports and help through this journey and for being a great inspiration of hard work, persistence, and kindness. And to my little Sofia, who patiently bears with me all the long working hours in the evenings and weekends.

Elaheh Mahootchi

Bergen, December 2021

To my amazing parents

Shahram Mahootchi and Ashraf Akrami

Contents

Scientific environment	3
Acknowledgments.....	5
Abstract	11
List of publications	13
Paper I.....	13
Paper II	13
Paper III	13
Paper IV	13
Abbreviations	14
1. Introduction.....	16
1.1. Brain-related disorders, a global concern	16
1.2. Pyridoxal 5'-phosphate-dependent enzymes	17
1.2.1. PLP-dependent enzyme classification	18
1.2.3. PLP-dependent enzymes, related diseases, and therapeutic potential	22
1.2.4. CSAD	23
1.2.5. GADL1	24
1.3. Histidine-containing dipeptides.....	27
1.3.1. Carnosine	27
1.3.1.4. The role of carnosine in muscle contraction	31
1.3.1.5. Therapeutic potential of carnosine	32
1.4. β -Alanine	34
1.5. Antioxidant effects of β -alanine and carnosine	35
2. Aims.....	38

2.1. Specific aims.....	38
3. Overview of the results	39
3.1. Paper I.....	39
3.2. Paper II	40
3.3. Paper III.....	41
3.4. Paper IV.....	42
4. Discussion.....	44
4.1. Methodological considerations.....	44
4.1.1. Generating the knock-out (KO) mouse model.....	44
4.1.1.3. Confirming gene knock-out	47
4.1.2. HPLC.....	47
4.1.3. Protein expression and purification.....	48
4.2. GADL1, the discovery of a “novel” enzyme	48
4.3. Multiple substrates, multiple functions	49
4.4. GADL1 and CSAD structures and biochemical features.....	50
4.4.1. PLP-dependent enzymatic mechanism	50
4.4.2. Substrate specificity of CSAD and GADL1	51
4.4.3. On the k_{cat} value of CSAD and GADL1	52
4.4.4. GADL1 and CSAD, similarities and differences.....	53
4.4.5. Current advances on protein structure studies.....	54
4.4.6. Inhibitors for PLP-DCs.....	54
4.5. GADL1 and CSAD tissue distribution and expression.....	56
4.6. Changes observed in the <i>Gad11</i> ^{-/-} mice	58
4.6.1. β -Alanine biosynthesis and changes in the <i>Gad11</i> ^{-/-} mice	58
4.6.2. Oxidative stress in <i>Gad11</i> ^{-/-} mice.....	59

4.6.3. <i>Gad11</i> ^{-/-} mice behaviour	60
4.7. Discovery of “new” functions for old enzymes	61
4.8. Medical implications	62
4.8.1. Potential biomarkers for brain-related disorders.....	62
5. Concluding remarks	64
6. Future perspectives	65
7. References.....	68

Abstract

Pyridoxal 5'-phosphate (PLP) -dependent enzymes constitute an essential superfamily of enzymes for all living organisms. Due to the chemistry of their cofactor, PLP, these enzymes catalyze a wide variety of reactions. PLP-dependent decarboxylases (PLP-DCs) play key roles in amino acid metabolism and are considered important biocatalysts for the pharmaceutical and chemical industries. In this project, we focused on the recently discovered enzyme glutamate decarboxylase-like 1 (GADL1) and its homolog, cysteine sulfinic acid (CSA) decarboxylase (CSAD). We investigated the expression pattern as well as the structural and biochemical features of both GADL1 and CSAD. Furthermore, we studied the physiological role of GADL1 by developing the first knockout mouse model for this enzyme. In addition, we reported crystal structures of mouse GADL1 (*MmGADL1*) and CSAD (*MmCSAD*).

We found that GADL1 decarboxylates aspartate (Asp) to β -alanine, and consequently, it plays a role in the production of carnosine. Both carnosine and β -alanine are pH buffers, metal chelators, and have antioxidants effects. In addition to β -alanine, we observed that GADL1 decarboxylates CSA to hypotaurine, which leads to the production of taurine, one of the most abundant free amino acids in mammals. Taurine also functions as an antioxidant, membrane stabilizer, and neurotransmitter in the central nervous system (CNS). Similarly, CSAD decarboxylates CSA to hypotaurine and has a higher affinity to CSA than GADL1. The tissue distribution of the two enzymes was investigated, and it was found that in humans, both GADL1 and CSAD are expressed in the brain, whereas only CSAD is found in the liver. In mice, both enzymes are expressed in the brain, olfactory bulb (OB), and skeletal muscle (SKM). In the kidney, GADL1 has lower expression than CSAD and in the liver only the expression of CSAD was found.

To find the physiological role of GADL1 we generated *Gadl1*^{-/-} mice. These mice were deficient in β -alanine, carnosine, and anserine, particularly in the OB, brain, and SKM, indicating a role for GADL1 in carnosine dipeptide production. Furthermore, *Gadl1*^{-/-} mice had increased levels of oxidative stress markers, indicating the

importance of carnosine as a cellular antioxidant. In addition, in different behavioural examinations, *Gad11*^{-/-} mice showed a slightly decreased level of anxiety. Human genetic studies show a strong association of the *GADL1* locus with plasma levels of carnosine, subjective well-being, kidney function, and muscle strength. In addition, investigating the GADL1 active site indicates that the enzyme may have multiple physiological substrates *in vivo*, including Asp and CSA.

Structural studies on *MmGADL1* and *MmCSAD* in this project showed that the overall fold and the conformation of the bound PLP are similar to other PLP-DCs. Both GADL1 and CSAD showed a more loose conformation in solution than in the crystal state, with open/close motions. In addition, in the *MmCSAD* structure, phenylalanine⁹⁴ plays a critical role in substrate binding, and its mutation to serine changed *MmCSAD* affinity towards both CSA and Asp and also affected enzyme stability. The structural studies of *MmGADL1* and *MmCSAD* provided details on substrate recognition in the PLP-DC family. These results are useful for future studies in structure-based inhibitor design and drug discovery.

In conclusion, in this project, the biochemical and physiological roles of CSAD and a novel PLP-DC, GADL1, were investigated. This study also introduces *Gad11* knockout mice as a multi-aspect model to investigate carnosine biology. Using a structural approach, new information was revealed about the structure and features of both *MmGADL1* and *MmCSAD*.

List of publications

Paper I

Winge I, Teigen K, Fossbakk A, Mahootchi E, Kleppe R, Sköldberg F, Kämpe O, Haavik J, 2015. **Mammalian CSAD and GADL1 have distinct biochemical properties and patterns of brain expression.** Neurochem. Int. 90:173-84.

Paper II

Mahootchi E, Homaei SC, Kleppe R, Winge I, Hegvik TA, Megias-Perez R, Totland, C, Mogavero F, Baumann A, Glennon JC, Miletic H, Kursula P, Haavik J, 2020. **GADL1 is a multifunctional decarboxylase with tissue-specific roles in β -alanine and carnosine production.** Sci. Adv. 6:eabb3713.

Paper III

Raasakka A*, Mahootchi E*, Winge I, Luan W, Kursula P, Haavik J, 2018. **Structure of the mouse acidic amino acid decarboxylase GADL1.** Acta Crystallogr. F Struct. Biol. Commun. 74:65-73.

*equal contribution

Paper IV

Mahootchi E*, Raasakka A*, Luan W, Muruganandam G, Loris R, Haavik J, Kursula P, 2020. **Substrate specificity determinants in the taurine biosynthetic enzyme cysteine sulphinic acid decarboxylase (CSAD).** J. Struct. Biol. 213:107674.

*equal contribution

Abbreviations

ADHD	Attention deficit hyperactivity disorder
AMD	Age-related macular degeneration
APS1	Autoimmune polyendocrine syndrome type 1
Asp	Aspartate
CA	Cysteic acid
CARNS1	Carnosine synthase 1
CDO	Cysteine dioxygenase
CN1/2	Carnosinase
CNDP1/2	Carnosinase coding gene
CNS	Central nervous system
CSA	Cysteine sulfinic acid
CSAD	CSA decarboxylase
ECT	Electroconvulsive therapy
GAD	Glutamate decarboxylase
GADL1	Glutamate decarboxylase like 1
GABA	γ -aminobutyric acid
GABA-T	GABA aminotransferase
Glu	Glutamate
GPX	Glutathione peroxidase
GSH	Glutathione
GSR	Glutathione reductase
GSSG	Glutathione disulfide
HCD	Histidine-containing dipeptide
His	Histidine
HPLC	High-performance liquid chromatography
HsCSAD	Human CSAD
KO	Knockout
LC-MS	Liquid chromatography-mass spectrometry

Lys	Lysine
MmGADL1	Mouse GADL1
MnSOD	Manganese superoxide dismutase
MS	Mass spectrometry
OPA	<i>o</i> -phtaldialdehyde
PDB	Protein Data Bank
Phe	Phenylalanine
PLP	Pyridoxal 5'-phosphate
PLP-DCs	PLP-dependent decarboxylases
qRT-PCR	Quantitative real-time polymerase chain reaction
ROS	Reactive oxygen species
RP-HPLC	Reverse-phase HPLC
SAXS	Small-angle X-ray scattering
Ser	Serine
SKM	Skeletal muscle
SOD	Superoxide dismutase
TAT	Tyrosine aminotransferase
WW	Wet weight
WT	Wild type

1. Introduction

1.1. Brain-related disorders, a global concern

Brain-related disorders, including neuropsychiatric and neurodegenerative disorders, are a huge medical and economical problem worldwide. Based on WHO statistics, 10-20% of children and adolescents in the world suffer from mental or behavioural disorders, such as major depressive disorder, bipolar disorder, attention deficit hyperactivity disorder (ADHD), or schizophrenia. Every year, approximately 1 million people commit suicide, and suicide is the second-leading cause of death among 15-29-year-olds. Four of the six leading causes of years lived with disability are due to neuropsychiatric disorders. Globally, more than 264 million people suffer from depression (1). Furthermore, as populations are growing and aging, the prevalence of neurodegenerative disorders, such as Alzheimer's disease and Parkinson's disease, is increasing dramatically (2, 3). Hence, there is an immediate need for intense studies investigating the biology of brain-related disorders, which might pave the way for new therapeutic approaches and novel treatment methods.

One of the most effective pharmacological agents used in psychiatry is lithium salts. The use of lithium in psychiatry goes back to the mid-19th century. However, early works were soon forgotten and in 1949, the effects of lithium as a mood-stabilizer for bipolar patients were rediscovered, and since then it has been a drug of choice for this condition (4, 5). In a paper published in 2014 by Chen *et al.*, a strong genetic association between variants in the human glutamate (Glu) decarboxylase-like 1 (*GADL1*) gene and the response to lithium therapy in bipolar patients was reported (6). Although these findings could not be replicated in other clinical studies (7), the results were intriguing and triggered further research on this novel pyridoxal 5'-phosphate (PLP)-dependent enzyme, *GADL1*, which will be described in detail in the next chapters.

1.2. Pyridoxal 5'-phosphate-dependent enzymes

PLP (Fig.1A), the active form of vitamin B6 (Fig.1B), is an essential coenzyme in a variety of enzymatic reactions. Hence, PLP has an important role in the human body. For example, inadequate levels of PLP in the brain can cause neurological dysfunction and lead to neurological diseases, such as epilepsy (8).

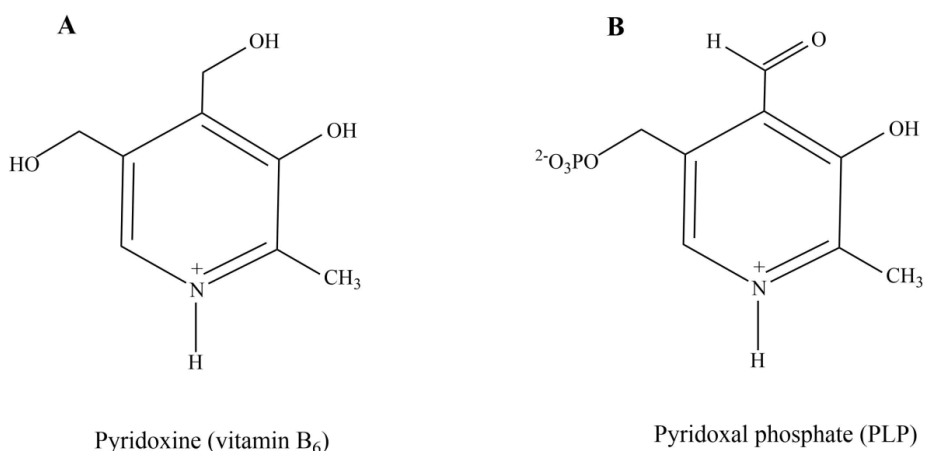


Fig. 1. Comparing the structure of vitamin B₆ (A) to pyridoxal 5'-phosphate (PLP) (B). PLP is the metabolically active form of vitamin B6 which serves as a coenzyme in many enzymatic reactions

On the other hand, it has been shown that abnormal metabolism (9) and accumulation of PLP, may result in hypophosphatasia (HPP) (10). HPP is a rare disease caused by a loss of function mutation (11) and is involved in defects in bone and tooth mineralization (12). Increased level of PLP is used as a biomarker with the highest diagnostic sensitivity in children and adults affected by HPP (13, 14).

As a cofactor, PLP has unique chemical properties. The stabilization of the C_α-anion is facilitated by the delocalization of the negative charge through the π system of the cofactor. For this reason, PLP is often described as an electron sink. This feature allows PLP to catalyze many reactions slowly even in the absence of an enzyme (15). The

formation of an external aldimine intermediate with the substrate is a common step in the PLP-dependent reactions (16). This is described in more detail in chapter 4.4.1.

A total of 145 different enzyme activities, which is around 4% of all known enzyme catalytic activities, are classified as PLP-dependent by the Enzyme Commission (EC) (17, 18). Almost 1.5% of all genes in most prokaryotic genomes encode PLP-dependent enzymes, showing their importance in basic biochemical pathways (18). PLP-dependent enzymes play key roles in amino acid metabolism (19), and they are considered important biocatalysts for the pharmaceutical, chemical, and food industries (20). They have recently drawn extra attention as powerful tools in biotechnology, for the *green chemistry* production of a whole range of specific amino acids and their derivatives (21). Furthermore, genetic engineering of metabolic pathways catalyzed by PLP-dependent enzymes is considered a promising strategy to provide cells with unnatural amino acids that are produced inside the cells from simple carbon sources or precursors (22).

1.2.1. PLP-dependent enzyme classification

PLP-dependent enzymes are of multiple evolutionary origins. Therefore, the common mechanistic features of these enzymes are not only historical traits passed on from one common ancestor, but also reflect evolutionary or chemical necessities (23). This feature makes their classification challenging. The B6 database (<http://bioinformatics.unipr.it/cgi-bin/bioinformatics/B6db/home.pl>) is a curated repository of biochemical and molecular information about PLP-dependent enzymes, providing a resource for the identification, classification, and comparative studies on these enzymes (24).

PLP-dependent enzymes were first classified into five different fold types. Fold types I to V were suggested by Grishin *et al.* (25). Then, two additional fold types VI and VII were added to the list by Percudani *et al.* in 2009 (24). Currently, the PLP-dependent enzymes are classified into seven different fold types based on their structure (20, 25), which most likely corresponds to seven independent evolutionary lineages (23, 26). Liang *et al.* published an update on the diversity of PLP-dependent enzyme fold types.

The following brief overview of PLP-dependent enzyme structures is in accordance with the terminology used by Liang *et al.* (27).

Fold I, the α -family, also known as the aminotransferase superfamily, is the largest family. This group includes aminotransferases, such as tyrosine aminotransferase (TAT) and γ -aminobutyric acid aminotransferase (GABA-T), and decarboxylases, such as Glu decarboxylase (GAD), GADL1, and cysteine sulfinic acid decarboxylase (CSAD) which are further described in this thesis. Fold II, also known as the β -family, catalyzes reactions at the β -carbon. Some examples of this group are serine (Ser) racemase and cystathionine β -synthase. Fold III, the alanine racemase family, primarily contains racemases and some decarboxylases. Eukaryotic ornithine decarboxylase (ODC) belongs to this group (25). Fold IV contains only D-amino acid and branched-chain amino acid aminotransferases, and Fold V only contains glycogen phosphorylase (18, 28). Fold VI and fold VII includes D-lysine-5,6-aminomutase and lysine 2,3-aminomutase respectively. Fig. 2 shows a summary of the PLP-dependent enzyme classification.

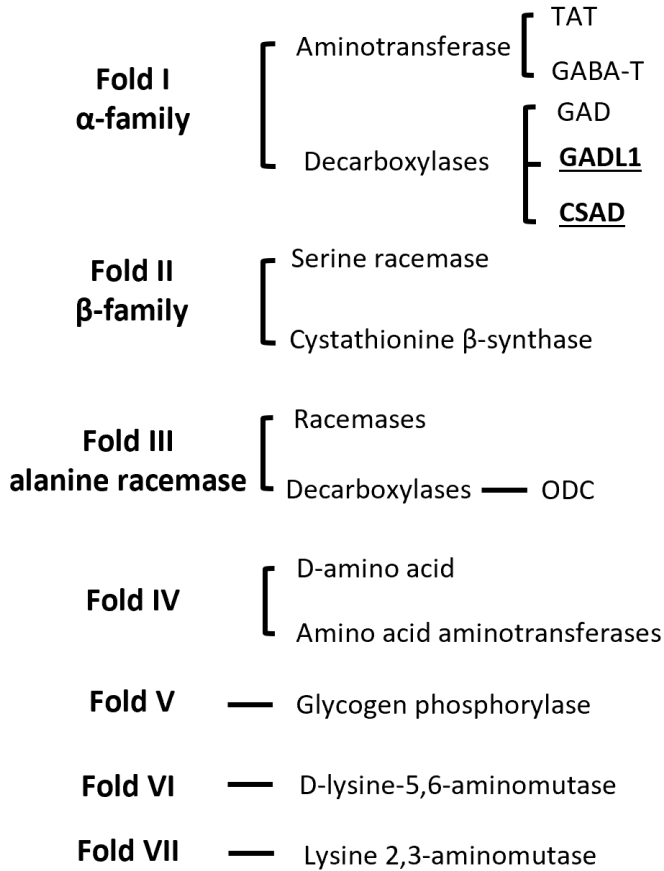
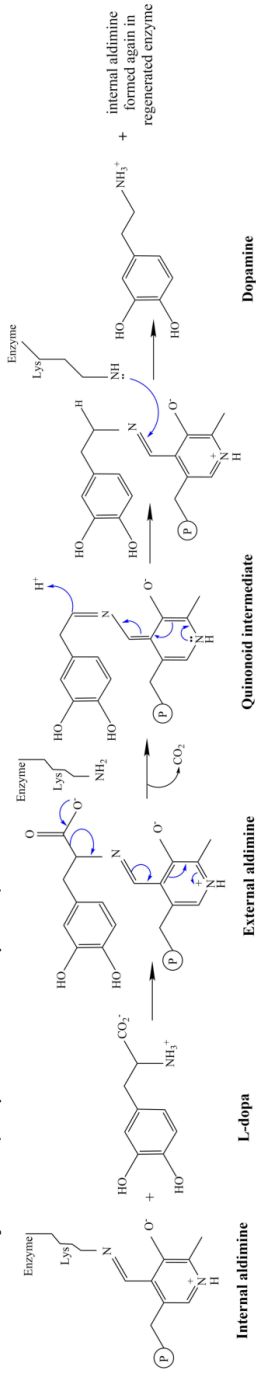


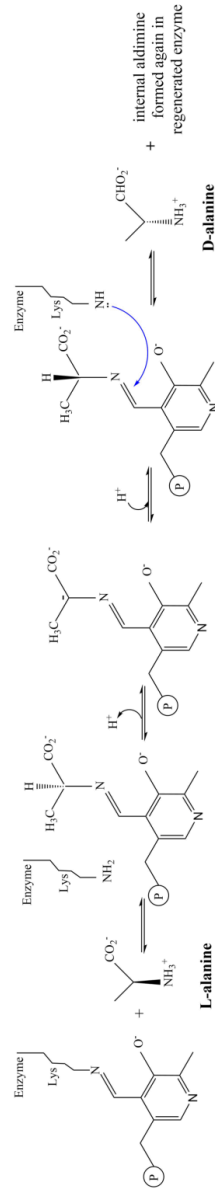
Fig. 2. Structure-based classification of PLP-dependent enzymes. The enzymes which are the subjects of this study are in boldface and underlined.

New biosynthetic pathways recently described in fungi (29), provide evidence of the high catalytic activity and versatility of PLP-dependent enzymes in nature. Particularly, the oxygen reactivity of PLP-dependent enzymes could be of great physiological interest because of the roles of PLP-dependent enzymes in the production of important neurotransmitters and neuromodulators (30), whose effects could be greatly affected by redox conditions (31). Fig. 3. shows some examples of the reactions performed by PLP-dependent enzymes.

Decarboxylation (dopa decarboxylase)



Racemization (Alanine racemase)



Transamination (aspartate aminotransferase first half-reaction)

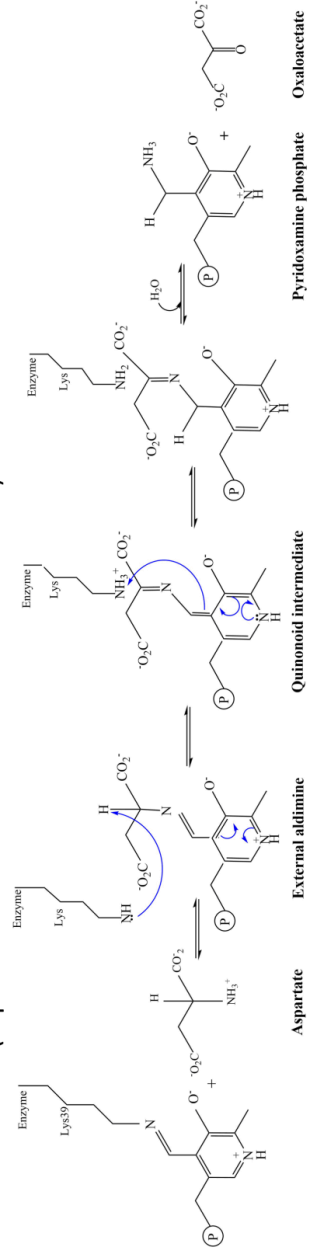


Fig. 3. Some of the reactions' mechanism catalysed by PLP-dependent enzymes. Reaction mechanism of decarboxylation, racemization and transamination is shown.

1.2.2. PLP-dependent enzyme structures

Most of the PLP-dependent enzymes have a conserved lysine (Lys) residue in the active site for the PLP binding. The ϵ -amino group of the Lys residue forms a Schiff-base structure with the aldehyde group of PLP which is referred as internal aldimine (27). This is explained in detail in chapter 4.4.1.

Among the PLP-dependent enzymes, PLP-DCs have high catalytic and structural similarities. Many of them have multiple substrates (15, 27, 32, 33) which may have metabolic advantages. In the PLP-DCs, the Schiff-base Lys residue is near C-terminus forming a Gly-rich group that is involved in the binding of the PLP phosphate group (25, 27). Most of the PLP-DCs are homodimers or homotetramers. Each subunit has a PLP molecule bonded and the active site is in the interface of subunits, composed of residues from both subunits (34-36).

1.2.3. PLP-dependent enzymes, related diseases, and therapeutic potential

Genetic deficiencies affecting PLP-dependent enzymes have been associated with many diseases, such as primary hyperoxaluria type 1, which is caused by mutations in alanine-glyoxylate aminotransferase (37, 38). Furthermore, some PLP-dependent enzymes are autoantigens in autoimmune disease, for example, aromatic L-amino-acid decarboxylase (DOPA decarboxylase) in autoimmune polyendocrine syndrome type 1 (APS1) (39), soluble liver antigen/liver-pancreas (SLA/LP) in autoimmune hepatitis (40, 41) and, GAD in type I diabetes (42).

GAD is one of the most studied PLP-DCs that decarboxylate Glu to the brain inhibitory neurotransmitter, GABA (43-45). GAD has two isoforms, GAD65 and GAD67 (46-49). The role of GAD in the mechanism of seizures in the epilepsy has been studied for a long time (50). Clinical studies shows that reduction in the GAD activity is associated with several forms of epilepsy (51-53).

Many PLP-dependent enzymes have been studied as targets for therapeutic agents. A few are known targets of approved drugs, and about twenty are recognized as potential

drug targets (17). Some of the PLP-dependent enzymes that have already commercially available drugs are GABA aminotransferase (epilepsy), DOPA decarboxylase, serine hydroxymethyltransferase (tumors and malaria), ornithine decarboxylase (tumors), alanine racemase (antibacterial agents), and cytosolic branched-chain aminotransferase (pathological states associated to the GABA/Glu equilibrium concentrations) (17).

1.2.4. CSAD

CSAD is a PLP-DC and plays an important role in the production of taurine from cysteine sulfinic acid (CSA) (54). Taurine, which is the most common free amino acid in the body, is found at high concentrations in the heart, kidney, liver, muscle, and brain. Taurine is involved in many physiological functions, such as antioxidation, membrane stabilization, and modulation of calcium signaling. Taurine has attracted increasing attention as a biomarker for many diseases (55-57). In the olfactory bulb (OB), taurine has been shown to activate stem cells and neural precursors to differentiate into neurons rather than astrocytes (58). Taurine deficiency can lead to a delay in cell differentiation and migration in the cerebellum, pyramidal cells, and visual cortex in cats (59) and monkeys (60, 61). In the CSAD knock-out (KO) mice (*Csad*^{-/-}), the plasma level of taurine was reduced by 83%, and most offspring in the second generation died shortly after birth (62). This illustrates the vital importance of taurine in higher organisms.

The crystal structure of human CSAD (*HsCSAD*) was deposited in the Protein Data Bank (PDB) by Collins *et al* (PDB ID: 2JIS). However, no further analysis or comparison with other enzymes in the PLP-DC family was reported.

In mammalian tissues, taurine is mainly synthesized in three steps: oxidation of cysteine by Cysteine dioxygenase (CDO), decarboxylation of CSA by CSAD, and finally oxidation of hypotaurine to taurine (63) (Fig.2). Another enzyme that can decarboxylate CSA is GADL1.

1.2.5. GADL1

Although PLP-DCs have been studied for many years, GADL1 is a recently identified enzyme. Liu *et al.* first described the tissue distribution, substrates, and possible role of GADL1 in taurine biosynthesis *in vitro* in 2012 (63). Apparently, there have been no other reports about GADL1 until 2014 when an article about the association between *GADL1* variants and response to lithium therapy in bipolar patients was published (mentioned in chapter 1.1) (6). There haven't been articles showing that these findings were replicated in other clinical studies (7, 64). Still, these findings motivated more research on GADL1.

Studies on GADL1 substrate specificity have shown that GADL1 is using CSA as the substrate to produce hypotaurine in a similar process as CSAD. GADL1 decarboxylates Asp to β -alanine as well. However, CSAD has higher affinity towards CSA than GADL1 and GADL1 has higher affinity towards Asp than CSAD (63, 65) (Fig. 4).

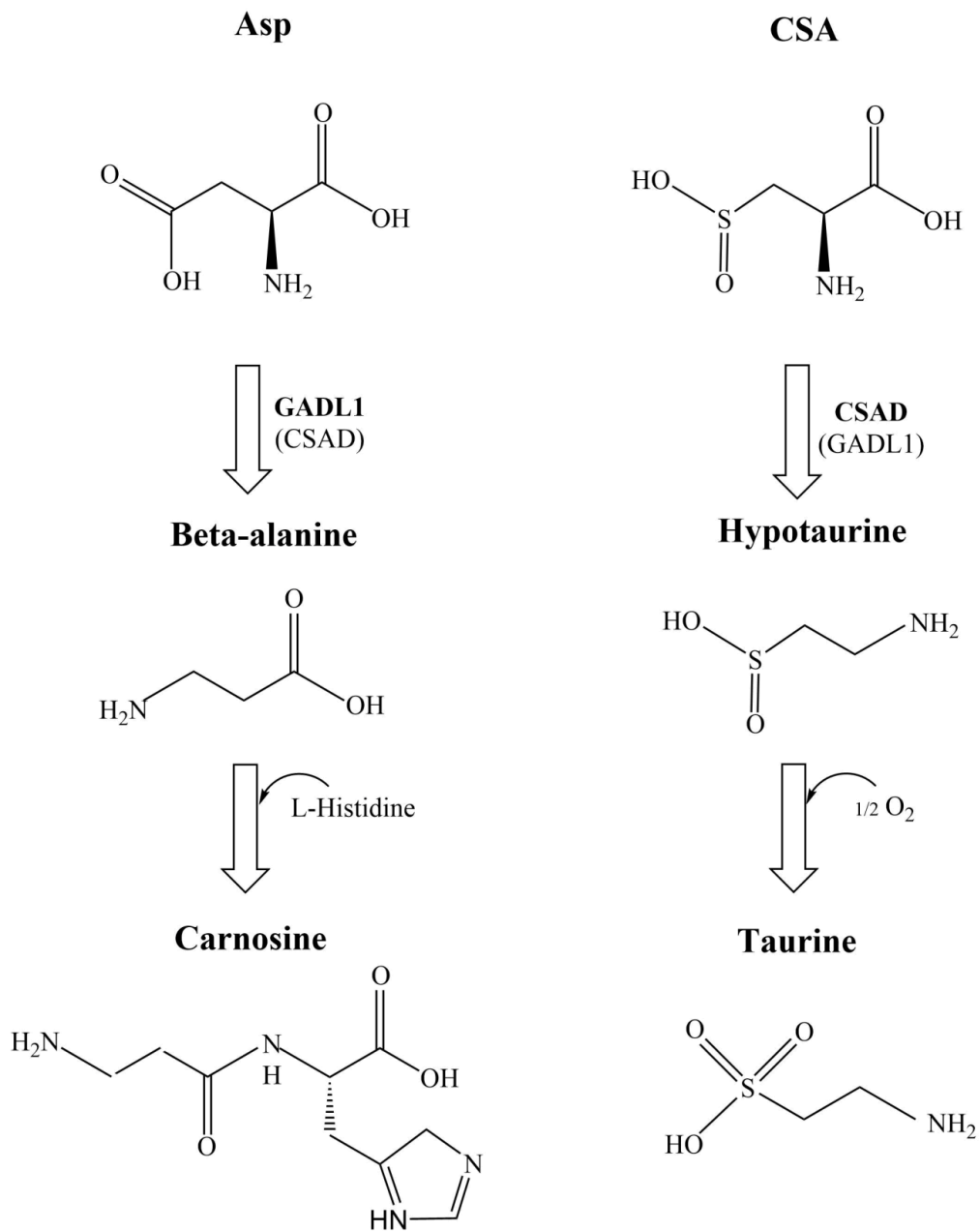


Fig. 4. CSAD and GADL1 pathway.

Although both GADL1 and CSAD are cytoplasmic enzymes, they have a distinct pattern of tissue distribution (Fig. 5). GADL1 is generally expressed at low levels, but the relatively highest abundance is observed in skeletal muscle (SKM) (63, 65), OB (65), and kidneys (63). CSAD has been isolated from the liver, kidney, and brain (66-68).

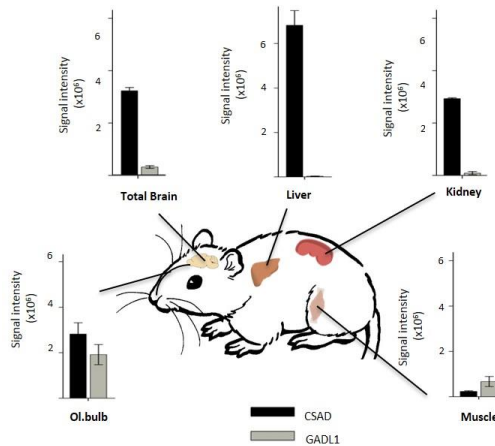


Fig. 5. Tissue distribution of CSAD and GADL1 in mice. CSAD is highly expressed in the brain, liver, kidney, and olfactory bulb, while GADL1 is most abundant in the olfactory bulb and, skeletal muscle. Adapted from (65).

Based on RNA transcript and protein analyses of mice, rats, and humans, both GADL1 and CSAD are cytosolic proteins expressed in neurons. In the CNS, GADL1 appears to be expressed in oligodendrocytes whereas CSAD is expressed in astrocytes. GADL1 has been found in the OB, whereas CSAD was detected in the cerebellum and hippocampus (63, 65, 69, 70). The expression level of these proteins has been reported in several databases including the human protein atlas protein database (<https://www.proteinatlas.org/>). However, these data are not completely consistent and may be dependent on experimental conditions. For instance, according to the protein atlas, RNA expression of GADL1 was found in fibroblasts but apparently, there is no

other literature reporting these findings. Thus, some of the data on the databases should be considered preliminary.

1.3. Histidine-containing dipeptides

Histidine (Fig. 7A) is an essential amino acid in humans. Due to its side chain imidazole ring properties, histidine is an important component of proteins and participates in a variety of enzymatic functions (78). Many of the proteins and dipeptides having histidine as a component, function as scavengers of free radicals, chelate metal ions, and act as proton buffers at physiological pH, because of the basicity of the imidazole ring (63, 71, 72).

The physiological presence of some of the HCDs, specifically carnosine (Fig.7B), in the brain and their ability to cross the blood-brain barrier (73), as well as evidence from *in vitro*, animal, and human studies, may indicate that these compounds may be promising biomarkers and therapeutic agents in brain disorders (74, 75). Carnosine and anserine have been proposed as biomarkers of habitual meat consumption in plasma (76). However, more studies need to be done before proposing them as biomarkers.

1.3.1. Carnosine

Carnosine (β -alanyl-L-histidine) (Fig. 6 B), belongs to a group of related β -alanine and HCDs (77, 78). It was first isolated from minced meat by Dr. Vladimir Gulevic at the University of Moscow in 1900, and it is named after the Latin term *caro or carnis* (meat) (79). In 1906, Krimberg classified it as a histidine-containing dipeptide that is synthesized from the amino acids β -alanine and L-histidine (80). Carnosine is found in high concentrations in the SKM and cardiac muscle of both vertebrates and non-vertebrates, as well as in the CNS, spinal cord, and some specific brain regions, such as OB, that have a high content of carnosine (81, 82). Some studies show that in the vertebrate nervous system, carnosine peptides are typically expressed in sensory organs (77, 83, 84). In mammals, carnosine has also been found in many other organs, including the spleen and kidneys (77). In humans, biological fluids, such as plasma, the

concentration of carnosine is regulated by carnosine synthase 1 (CARNS1) (73, 85, 86) and carnosinase (CN1) (87), both considered metalloprotease enzymes (88) which are discussed more in chapter 1.3.1.2.

Although carnosine has been studied for a long time, it has been only in recent years that it has gained more attention in the fields of nutrition, food science, neuroscience, biochemistry, and molecular biology (89-92). Many lines of evidence suggest multiple roles for carnosine, such as antioxidant, anti-age, anti-fatigue, neuroprotective, calcium regulator in the cells, and proton buffer (93). However, its exact mechanism of action and physiological importance are still being debated.

1.3.1.1. Carnosine distribution in different species

The concentration of carnosine in SKM is higher in males compared to females in both rodents and humans (94, 95). Among different species, the abundance of carnosine is strikingly different (77). Among mammals, mice appear to have the lowest level of carnosine, only 1-3 mmol/kg wet weight (WW), i.e., approximately 1-3 mM or ~ 0.04% of the muscle WW. In humans, the concentration of carnosine in SKM can be up to 20mM. In the vertebrate brain, carnosine can be found at 0.7-2 mM concentration (77, 96, 97).

Physiological investigation of different species shows that organisms with a high demand of non-oxidative forms of energy production, and which experience regular challenges to acid-base homeostasis, have a higher abundance of HCDs (98). For example, the wallaby and blue whale have the highest HCD concentrations, around 50 – 60 mmol/kg, corresponding to > 1% of the muscle WW. In addition, many fish species have a high abundance of HCDs (77). This shows that acid-base regulation may be an important feature of the HCDs, which makes them suitable physiological buffers in these animals.

1.3.1.2. Enzymes involved in carnosine metabolism

The following key enzymes are known to be involved in the synthesis and degradation of carnosine:

- **Carnosine synthesis 1 (CARNS1):** The key enzyme for synthesizing carnosine from β -alanine and L-histidine.
- **Carnosinase (CN):** Degrades carnosine and exists as two isoforms, CN1 and CN2.
- **Carnosine N-methyltransferase (CARNMT1):** Methylates carnosine

Both CN1 and CN2 are members of the M20 family of metalloproteases (88) and show 53% sequence identity in humans (99). CN1 specifically degrades both carnosine and homocarnosine (another HCD) (100), while CN2 is a cytosolic non-specific dipeptidase able to degrade carnosine and other dipeptides, but not homocarnosine (88). Fig. 6 is a schematic picture illustrating the enzymes involved in Asp, carnosine, and β -alanine metabolism in different tissues.

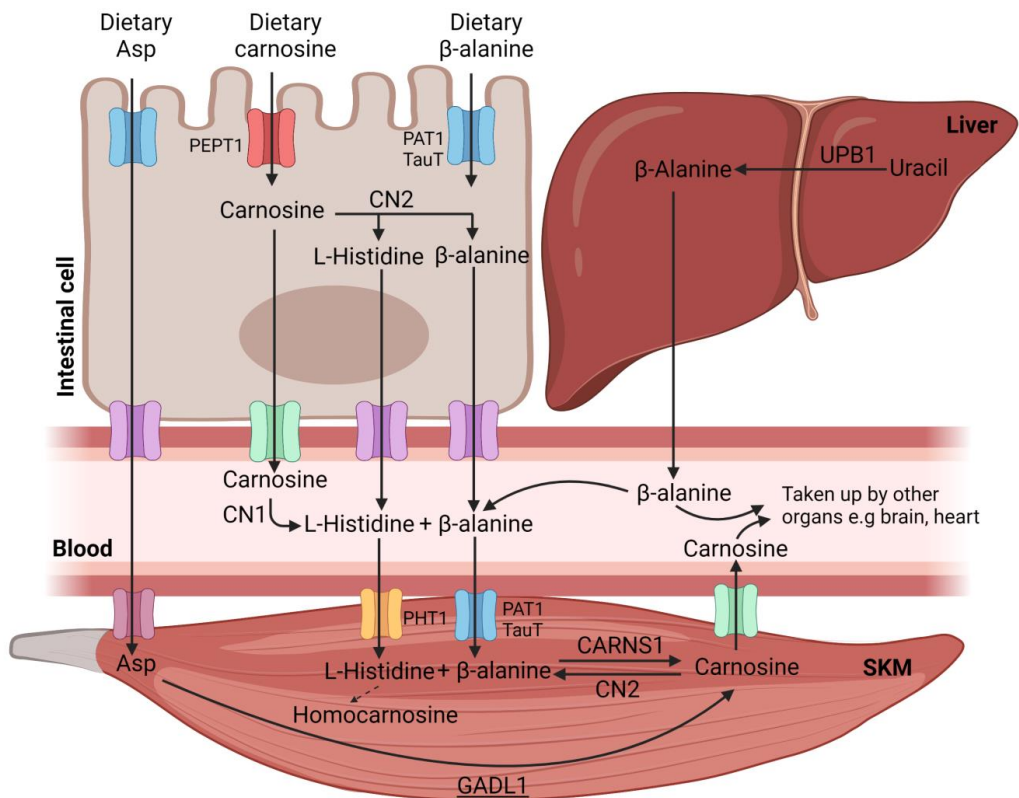


Fig. 6. A schematic picture of Asp, carnosine and β -alanine absorption, metabolism and the involved enzymes. The carnosine level in the blood depends on CN1 activity. The pathway shown for β -alanine in the liver represents pathways in rodents and humans. For clarity, the transporters on the cell membranes have not been named. Illustration created with BioRender (BioRender.com).

The expression and activity of CN1 are increased in patients with diabetic nephropathy. Thus, it has been proposed that the level of CN1 in serum is involved in the development of diabetic nephropathy and has a promising therapeutic potential for the treatment of diabetic nephropathy (101).

The decarboxylation activity of GADL1 toward Asp and its possible role in the production of carnosine has been suggested (63, 65). Furthermore, a genetic study showed that single-nucleotide polymorphisms in the *GADL1* intron are strongly

associated with the levels of acetylcarnosine in human blood (102); acetylcarnosine is also strongly correlated with carnosine levels (78).

1.3.1.3. Carnosine in the brain

In vitro and immunostaining studies showed that glial cells, including oligodendrocytes, possess carnosine synthase activity (103-105). In humans, oligodendrocytes appear to be the only brain cells that express CARNS1, whereas in mice it is only expressed in newly formed and myelinating oligodendrocytes (106). Taken together, carnosine metabolism in the brain appears to be mostly concentrated in four cell classes: oligodendrocytes, astrocytes, microglia, and macrophages.

1.3.1.4. The role of carnosine in muscle contraction

It has been reported that muscle carnosine content is ergogenic (i.e. increasing physical performance) during anaerobic exercise (107, 108). Carnosine plays an important role as an anti-fatigue agent in SKM (109-112) and has a higher effect in high-intensity interval exercise, rather than short-term training (107) and endurance exercise (108). However, the ergogenic role of carnosine peptides in humans is still being debated. The effect of carnosine supplements is discussed further in chapter 1.3.1.5.

On the other hand, a study on the role of carnosine in both SKM and cardiac muscle using the *Carns1*^{-/-} rat model showed no effect on exercise capacity or SKM force production. However, there was significant impairment of contractile function in the cardiac muscle of these rats which was confirmed both *in vivo* and *ex vivo*. Impaired systolic and diastolic dysfunction were accompanied by reduced intracellular Ca²⁺ peaks and slowed Ca²⁺ removal, which shows that carnosine in cardiac muscle is involved in the regulation of Ca²⁺ and excitation-contraction coupling (113).

1.3.1.5. Therapeutic potential of carnosine

One of the first studies on the therapeutic potential of carnosine showed that adding carnosine to rat diet may prevent the synthesis and negative effects of β -amyloid peptides. These peptides form plaques in Alzheimer's patient brains (96). Furthermore, a study on the transgenic mouse model of Alzheimer's disease proved that a treatment with carnosine (5 mg/day) for 6 weeks improved cognitive deficits and reverted oxidative stress and microglial activation in the hippocampus (114). Moreover, it was shown that carnosine may pass the blood-brain barrier, reach the brain and activate glial cells, which promotes the repair of damaged neurons in neurodegenerative diseases, such as Alzheimer's disease (73) and multiple sclerosis. In a study on the plasma metabolomic changes in age-related macular degeneration (AMD) patients, it was found that carnosine was 50% decreased in these patients, revealing possible carnosine deficiency. Thus, it was suggested that the relative deficiency in carnosine could contribute to AMD pathogenesis (115).

Concerning the effect of carnosine supplements on elderly people, it was reported that dietary supplementation of carnosine (250–350 mg/day) and anserine (650–750 mg/daily) for 13 weeks can improve cognitive function (116, 117) and physical activity (117), preserve verbal episodic memory and brain perfusion (116, 118), and modulate network connectivity changes associated with cognitive function (116). In a review by Caruso *et al.* on four double-blind, randomized, placebo-controlled trials on the effects of carnosine against cognitive decline, it was shown that supplementation with 500 mg carnosine per day for 12 weeks improved global cognitive function and verbal memory in elderly subjects and mild cognitive impairment patients, whereas no effects were detected on depressive symptoms (119). Also, consumption of carnosine may prevent chronic diseases, such as diabetes, atherosclerosis, and cognitive impairment (120, 121).

In the field of neuropsychiatry, there have been many studies on the health benefits of carnosine showing that carnosine supplementations may improve core and secondary symptoms of some neuropsychiatric diseases, such as schizophrenia, ADHD, major depressive disorder, and obsessive-compulsive disorder (OCD) (75, 122-125). Some

studies are reporting the short-term positive effects of carnosine treatment on both attention and hyperactivity in ADHD and autism patients which could be explained by the carnosine role in the regulation of N-methyl-D-aspartate (NMDA) receptors and GABA levels (126, 127). On the other hand, some studies showed no effect on autism severity and only decreased sleep deprivation (128). For possible carnosine supplementation side effects, there has been a study reporting the effects of carnosine on schizophrenia patients. In this study, 75 adults patients were randomly assigned to 2 g of carnosine a day as an adjunctive treatment. The group that received carnosine displayed significantly improved strategic efficiency and made fewer perseverative errors compared with placebo. However, in this study, the treated patients also showed some side effects such as dry mouth, weight change, and itchiness (129). Therefore, the role of carnosine as adjunctive treatment to improve dysfunction in schizophrenia patients might have to be reconsidered. Nevertheless, the majority of studies show that oral carnosine supplement is considered safe if it is used appropriately (130).

1.3.1.6. Carnosinemia

As mentioned in chapter 1.3.1.2, carnosinase (CN1) is an enzyme degrading carnosine. CN1 is coded by the *CNDPI* gene (99). Carnosinase deficiency may lead to the accumulation of carnosine in the blood. This condition is called carnosinemia, a rare inherited (131) metabolic disorder (132) that may be the result of a mutation in the *CNDPI* gene (131). Carnosinemia is associated with severe neurological symptoms in humans. It was first discovered in 1968 by Perry and colleagues, who showed that patients with carnosinemia have an excess of carnosine in the urine, little or no serum carnosinase activity, and develop progressive neurologic symptoms characterized by mental defects and intellectual disability (132-134). Carnosinemia affects males and females equally. Until today, 30 cases of carnosinemia have been reported in the medical literature registered by National Organization for Rare Disorders (NORD) (<https://rarediseases.org/rare-diseases/carnosinemia/>).

According to www.clinicaltrials.gov (a service of the U.S. National Institutes of Health, which shares information on current clinical trials), there are currently 24 studies using carnosine or zinc L-carnosine as a treatment for various diseases, such as bipolar disorder, schizophrenia, and Alzheimer's disease, but none of them targets carnosinemia or homocarnosinemia (133-135).

1.4. β -Alanine

It is generally believed that β -alanine (Fig. 7C) is supplied by the diet or synthesized in the liver, through uracil and thymine degradation (136). Many studies have shown that the consumption of β -alanine supplements may increase carnosine concentration in human muscles, which leads to increased well-being and improves athletic performance (137, 138). For instance, a study by Furst *et al.* on 12 human subjects between the ages of 60 and 70 showed that β -alanine supplementation (2.4 g/day) for 28 days increased physical performance and improved executive function following endurance exercise (139).

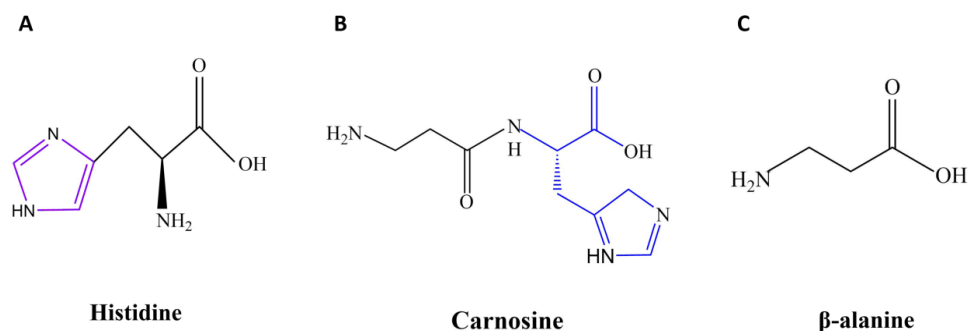


Fig. 7. The chemical structure of histidine (A), carnosine (B), and β -alanine (C). (A) The imidazole ring in histidine structure is shown in magenta. (B) In the carnosine structure, histidine is shown in blue, and β -alanine is shown in black. (C) β -alanine chemical structure.

β -Alanine, as well as its dipeptide derivatives, may also act as neurotransmitters or neuromodulators in the CNS, especially in the OB (77). Furthermore, β -alanine can increase brain-derived growth factor (BDNF) levels in the hippocampus and has anxiolytic effects (140). In a study on the link between vitamin B6 deficiency and cardiac function, β -alanine was proposed as a potential circulating biomarker to identify the onset of cardiac dysfunction (141).

1.5. Antioxidant effects of β -alanine and carnosine

β -Alanine, carnosine, and their metabolic derivatives have neuromodulator and antioxidant properties both *in vitro* and *in vivo* (77, 142). Reactive oxygen species (ROS) damage has been reported in many diseases, such as cancer, and carnosine is involved in the inhibition of cancer cell proliferation using its antioxidant effect (143). Carnosine can perform antioxidant activity directly and indirectly. First, it can directly decrease the intracellular level of ROS, such as superoxide anions and hydroxyl radicals (144, 145), NO (146), cytotoxic carbonyl species (147), and aldehydes (148). Carnosine can also indirectly promote the endogenous system of antioxidant protection (149, 150).

Several studies on oxidative stress have used the levels and the activity of superoxide dismutase (SOD), glutathione reductase (GSR), or glutathione peroxidase (GPX) as markers for oxidative stress (151). SOD, possibly the most powerful antioxidant in the cell (79), belongs to a large group of metalloenzymes. SOD enzymes are divided into four groups: copper-zinc SOD (CuZnSOD), manganese SOD (MnSOD/SOD2), iron SOD (FeSOD) and nickel SOD (NiSOD) (152). CuZnSOD is a cytosolic enzyme expressed in the mitochondrial matrix. In the brain, CuZnSOD is considered an important endogenous antioxidant. Another SOD enzyme, MnSOD, is mainly expressed in mitochondria (152, 153). Both are considered important antioxidant enzymes. SODs catalyze the dismutation of the superoxide radicals (O_2^-) to molecular oxygen (O_2) and hydrogen peroxide (H_2O_2) (152). With aging, the natural amount of these enzymes decreases, which leads to a higher risk of oxidative stress-related diseases, such as cancer, diabetes, and Alzheimer's disease (153). Any alternations in the activity of SOD

can affect the ROS homeostasis changes and result in the activation of particular redox-sensitive pathways involving nonreceptor protein tyrosine kinases (PTKs), protein kinase C (PKC), and protein phosphatases (PTPs) (152, 154).

Glutathione, probably the most important antioxidant in the body, is synthesized from cysteine, glycine, and Glu. Glutathione peroxidase (GPX) oxidizes glutathione to glutathione disulfide (GSSG), and glutathione reductase (GSR) reduces it to reduced glutathione (GSH). A ratio of GSH to GSSG can be used to determine the level of oxidative stress that has occurred in cells. In mitochondria, GSR reduces GSSG to GSH using electrons (e^-) from dihydro nicotinamide adenine dinucleotide phosphate (NADPH). Then, by using its thiol group, GSH neutralizes molecules such as ROS. Hence, GSR, a flavin adenine dinucleotide (FAD)-dependent enzyme, plays an indirect, but critical role in controlling cellular ROS (152, 155, 156).

The link between carnosine levels and these antioxidant enzymes is very intriguing. Some studies showed that carnosine supplementation increased the activity and expression of GSH and SODs (157). It has been shown that using carnosine as a pre-treatment for the oxidative stress-induced rat models may result in a 25% increase in the activity of CuZnSOD (158). In addition, Aydin *et al.* have shown that in the aged male rat liver, daily doses of carnosine (250 mg/kg) during one month caused a significant reduction in the activity of GSH and SOD (157). Furthermore, another study showed that 100 mg/kg of carnosine supplements per day may lead to a higher activity of GPX and SOD in the plasma, liver, and muscle of pigs. Also, in this study, the expression levels of GPX and SOD genes were increased in the muscle tissue (159).

Another antioxidant enzyme, MnSOD, has limited effects on the growth of cancer cells. A significant decrease in cellular ROS levels and increase in MnSOD expression have been reported when carnosine is used as an inhibitor for the proliferation of cancer cells *in vitro* (143). However, most of the studies focused on exogenous carnosine, and there are not so many studies on the effect of endogenous carnosine on antioxidant enzymes. Therefore, more research on the biology of β -alanine and carnosine is needed to answer many open question about them, and to validate the available findings.

2. Aims

The main aim of this study was to characterize the novel PLP-DC, GADL1, both *in vivo* and *in vitro*. Furthermore, we wanted to compare the structure, biochemical properties, and expression pattern of GADL1 with the closely homologous enzyme, CSAD.

A long-term goal is to provide knowledge that may lead to the identification of new metabolomic pathways and signalling molecules and enable the development of novel biomarkers and target therapies for different diseases, in particular brain disorders.

2.1. Specific aims

1. Identify the natural substrates, tissue distribution, and inhibitors of GADL1 and CSAD. **Paper I**
2. Explore the physiology of GADL1 using a constitutive knockout mouse model and human genetic data. **Paper II**
3. Solve the crystal structure of mouse GADL1 with bound substrates. **Paper III**
4. Solve the crystal structure of mouse CSAD and compare it with other PLP-DCs to identify determinants of substrate specificity and catalytic activity. **Paper IV**

3. Overview of the results

3.1. Paper I

Title: Mammalian CSAD and GADL1 have distinct biochemical properties and patterns of brain expression.

In this article, we explored the biochemical features and brain expression patterns of GADL1 and compared it to CSAD. We investigated the role of both GADL1 and CSAD in taurine biosynthesis and other possible pathways, in which the two enzymes could be involved.

Using quantitative reverse transcription-polymerase chain reaction (qRT-PCR) and western blotting analysis, we showed that GADL1 is expressed in the OB during early brain development in mice and humans. The mRNA of GADL1 was found only in neurons, whereas its homolog, CSAD, was found in both neurons and astrocytes. Moreover, we found that the relative expression level of GADL1 mRNA was significantly lower than CSAD in the adult brain. However, in contrast to CSAD, the mRNA of GADL1 was also detected in SKM.

We found that both GADL1 and CSAD can decarboxylate CSA, cysteic acid (CA), homocysteic acid, and Asp, but the most favored substrate for both enzymes appeared to be CSA. By measuring enzyme activity with HPLC, we determined the K_m , k_{cat} , and V_{max} of GADL1 and CSAD using CSA and Asp as substrates. This showed that the k_{cat} value of GADL1 is approximately, 10-fold higher than CSAD using Asp as substrate. On the other hand, k_{cat} value of CSAD is approximately, 2-fold higher than GADL1 using CSA as substrate. Furthermore, upon using *in silico* screening and molecular docking with the homology model of GADL1, combined with *in vitro* assays, we discovered several substrate analogs that were weak inhibitors for both GADL1 and CSAD, such as bis-(carboxymethyl)-trithiocarbonate and ethylxanthogenacetic acid. Different concentrations of the inhibitors were tested and some inhibitor specificity for each enzyme was reported. Lithium had minimal effect on the enzyme activities of CSAD or GADL1.

Based on these findings, we concluded that the biosynthesis of taurine in mammals involves two structurally related PLP-DCs, GADL1, and CSAD. These two homologous enzymes have partially overlapped catalytic properties but different tissue distribution, suggesting that the enzymes may have different physiological roles *in vivo*. In addition, further studies on selective inhibitors targeting these enzymes may lead to a better understanding of their structures to help the development of compounds that could potentially be used as therapeutic agents.

3.2. Paper II

Title: GADL1 is a multifunctional decarboxylase with tissue-specific roles in β -alanine and carnosine production

In this study, we investigated the metabolic role of GADL1 by using a novel mouse model lacking the *Gad1l* gene. First, we collected tissues of *Gad1l*^{-/-}, *Gad1l*^{-/+} and *Gad1l*^{+/+} mice and performed an untargeted metabolomic analysis using liquid chromatography mass-spectrometry (LC-MS). We found that carnosine peptides were the most affected metabolites in *Gad1l*^{-/-} compared to *Gad1l*^{-/+} and *Gad1l*^{+/+}. The most affected tissue is the brain, in particular OB. β -Alanine was also significantly reduced in the OB, but this reduction was nonsignificant in other regions of the brain and SKM, and it was unaltered in the liver of *Gad1l*^{-/-} mice. On the other hand, acetylcarnosine and anserine were significantly decreased in the brain and SKM.

Furthermore, we observed increased levels of oxidative stress markers in the SKM, brain and specifically in the OB. This increase is in line with elevated glutathione synthesis and could be an indication of increased oxidative stress. Several disorders, including neurodegenerative diseases and cancers, are believed to be caused by oxidative stress damage. Since β -alanine and carnosine supplementation has been used in protection against oxidative stress (77), we suggested that the *Gad1l*^{-/-} mouse model can be used as a new tool for further research in the field of oxidative stress-related diseases and the effects of carnosine dipeptides on these diseases. Moreover, we observed some phenotypical and behavioural changes in the *Gad1l*^{-/-} mice. The *Gad1l*^{-/-} mice had

significantly lower weight compared to *Gadli*^{+/+} after 30 weeks of age. Also, lower anxiety was observed in the 22-week-old male mice. In addition, previously reported human data showed that common variants in the human *GADLI* locus were associated with plasma levels of acetylcarnosine, muscle strength, kidney function, and subjective well-being (102, 160-162). The low score of subjective well-being has been genetically related to low energy, anxiety, and depression, which can all be related to brain and muscle levels of carnosine peptides (163). Combining this with our behavioural analysis data of *Gadli*^{-/-} mice, we conclude that the link between the *GADLI* gene and anxiety is particularly interesting and needs further investigation.

These results showed that the GADL1 enzyme plays an important role in the synthesis of β -alanine and carnosine peptides in the brain, SKM and OB. In the future, studying the relation between the GADL1 enzyme and the level of oxidative stress and the connection between *GADLI* gene expression and anxiety using the *Gadli*^{-/-} mouse model might reveal more information about this enzyme and its therapeutic potential.

3.3. Paper III

Title: Structure of the mouse acidic amino acid decarboxylase GADL1

Here, the structure of *MmGADL1* and a solution model based on small-angle X-ray scattering (SAXS) data are described. Histidine-tagged *MmGADL1* was expressed in *Escherichia coli*, purified, and crystallized using sitting-drop vapor diffusion. The crystals were subjected to X-ray diffraction analysis. We also used SAXS to validate the crystal structure and to determine the conformation of *MmGADL1* in solution.

The *MmGADL1* crystal structure showed a single *MmGADL1* homodimer in the asymmetric unit. This was expected based on other PLP-DCs structures. However, it is important to note that although *MmGADL1* overall folding and the bound PLP conformation are similar to other PLP-DCs, GADL1 adopts a looser conformation in solution. This feature might have functional relevance in substrate binding and catalysis

and will be investigated more in the future for a better understanding of PLP-DC enzyme family structures and their physiological roles.

3.4. Paper IV

Title: Structure and substrate specificity determinants of the taurine biosynthetic enzyme cysteine sulphinic acid decarboxylase (CSAD)

In this paper, we studied the crystal structure of *MmCSAD*, an enzyme that plays a critical role in the taurine synthesis and compared it with the structure of other enzymes in the PLP-DC family. SAXS data on *MmCSAD* structure demonstrated that *MmCSAD* shows open/close motions in solution. Investigating the apo-CSAD structure revealed that the active site of the enzyme gets more ordered by the binding of PLP and internal aldimine formation.

By comparing the active sites of CSAD and GAD, we observed that phenylalanine (Phe)94 plays a critical role in the binding of substrate. Phe94 makes the CSAD active site so tight that Glu cannot productively bind. The same residue in GAD is a Ser instead of Phe. Thus, we hypothesized that by mutating Phe94 to Ser in the active site of *MmCSAD*, Glu may productively bind to the active site, and the activity of CSAD could change. This mutation indeed changed the stability and the activity of the enzyme, but Glu still could not productively bind to the active site. Testing other substrates, CSA and Asp, showed that the mutation affects the K_m and k_{cat} of the enzyme in the way that the mutated enzyme has a turnover number 5-10 times lower than the wild-type (WT) CSAD, which indicates an overall effect of the mutation on catalysis.

Hence, we concluded that Phe94 plays an important role in the substrate binding of *MmCSAD*, but changing the structure of the active site so that Glu can productively bind needs further studies. This study revealed new information about *MmCSAD* structure and highlighted the molecular mechanism of taurine synthesis and the enzymes involved.

4. Discussion

In this project, the biochemical properties, physiological function, and crystal structure of CSAD and the novel PLP-dependent enzyme, GADL1 were studied. The role of GADL1 in β -alanine and carnosine peptide production and its role in the oxidative stress process was investigated by using the *Gad11*^{-/-} mouse. In addition, the *Gad11*^{-/-} mouse was introduced as a new animal model to study β -alanine and carnosine biosynthetic pathways.

4.1. Methodological considerations

4.1.1. Generating the knock-out (KO) mouse model

In order to choose the best strategy for knocking out the *Gad11* gene, there were several considerations. In this chapter, the possible strategies for knocking out the *Gad11* gene and the logic behind the chosen method are briefly explained.

4.1.1.1. Structure of *Gad11* gene

Bioinformatic analysis showed that the *Gad11* gene is located on chromosome 27 and is composed of 20 exons. ATG initiation codons are located in exons 3 and 5, while the stop codons are located in exons 19 and 20. The length of the mouse *Gad11* gene is 183.6 kilobases (kb).

The *Gad11* gene has two isoforms:

- *Gad11* isoform 1 that encodes for 550 amino acids, an experimentally validated protein.
- *Gad11* isoform 2 that corresponds to the alternative use of exon 19 leading to a premature stop codon and would encode for 526 amino acids, a predicted protein.

There are 5 overlapping putative genes (*LOC102633399*, *LOC102633324*, *LOC102633106*, *CB272377*, *AK015508*) near *Gad1l* gene. These putative genes all encode non-coding RNAs (Fig. 8).

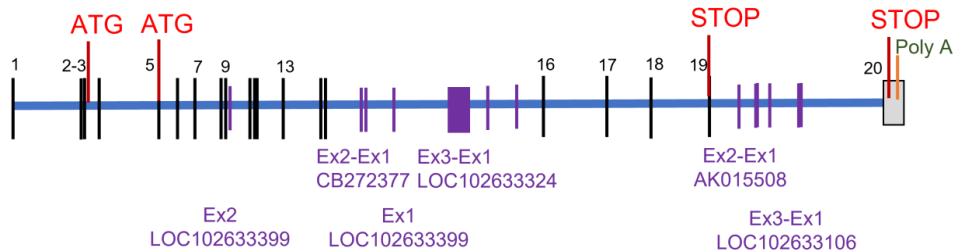


Fig. 8. The structure of *Gad1l* gene. The ATG start codon and stop codon are shown in red. The overlapping putative genes are shown in magenta.

The neighboring gene of *Gad1l* is the *Tgfb2* gene, encoding an important receptor with a role in growth and survival (shown in Fig. 9). The distance between *Gad1l* and *Tgfb2* is approximately 8 kb. Therefore, we had to apply a safe, conservative knocking-out strategy, to minimize the risk of disrupting the *Tgfb2* gene function. In addition, the presence of 5 overlapping genes was considered in choosing the knocking-out strategy.

4.1.1.2. Knocking out *Gad1l*

We aimed to eliminate *Gad1l* gene expression in specific tissues using conditional KO mice. In this project, these mice were also used to generate a constitutive KO mouse model. Possible approaches for generating a KO mouse model and avoiding the risk of expression of truncated proteins containing a functional domain were:

- Deletion of the ATG start codon to disrupt *Gad1l* translation
- Deletion of the part of the gene that codes for the PLP binding site to eliminate the protein activity

- Deletion of the stop codons to generate an unstable *Gad11* mRNA

To avoid disrupting any gene expression regulatory element, we decided to only delete part of the gene that codes for the PLP binding site, exon 7, to eliminate enzymatic activity. To achieve this aim, we used the *Cre/loxP* method. The *loxP* sites were inserted into intron 6 and intron 7, together with the neomycin (neo)–positive selection cassette in intron 6 (Fig.9).

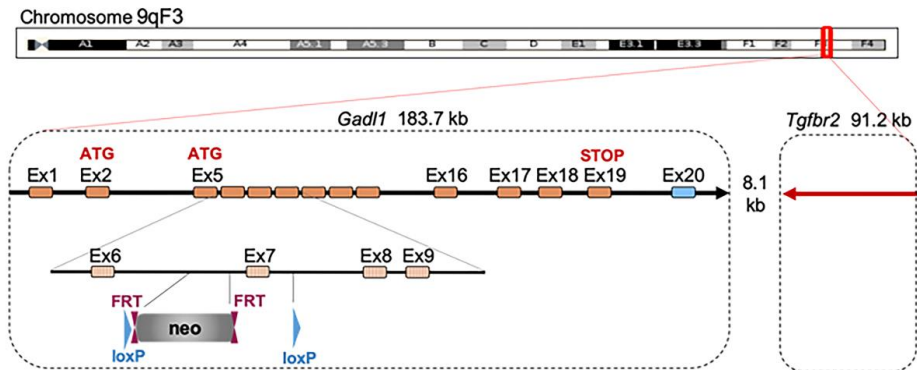


Fig. 9. Targeting strategy for knocking out the *Gad11* gene in the mice. *Gad11* coding sequences (hatched rectangles) were targeted for knocking out the *Gad11* gene expression. Noncoding exon portions are shown as blue rectangles, and chromosome sequences are shown as orange rectangles. The neomycin (neo)–positive selection cassette is shown between *loxP* sites (shown as blue triangles), and Flippase recognition target (FRT) sites (shown as magenta triangles). Figure adapted from (164).

This approach results in out-of-frame splicing and leads to a premature stop codon in exon 8 of both the 550- and 526-amino acid GADL1 isoforms. The mRNA would be non-functional, unstable, and rapidly degraded by nonsense-mediated decay. This insertion stops the transcription of *Gad11*, and in the unlikely event of an mRNA being produced, it would encode for a 152-residue polypeptide devoid of any functional domain.

For generating conditional KO mice, it is possible to combine the *Cre-loxP* method with clustered regularly interspaced short palindromic repeats (CRISPR) associated protein 9 (Cas9) technology (165). This combination has been also tested in cells (166) and is a novel method for gene editing with low off-target effects. We are considering using this combination for generating a conditional *Gad11* KO mouse model in the future.

4.1.1.3. Confirming gene knock-out

DNA sequencing and Southern blotting showed that exon 7 was eliminated from the *Gad11* gene in the mouse genome. However, we observed that in the OB and SKM of *Gad11*^{-/-} mice, some *Gad11* mRNA species were detectable, although subsequent RNA sequencing and qRT-PCR of individual exons showed that *Gad11*^{-/-} mice lacked exon 7 on the *Gad11* gene. Bioinformatic analyses showed that the deletion of exon 7 led to the generation of a new RNA splicing site in *Gad11*^{-/-} mice. We confirmed the knocking out of the gene by Western blotting, which revealed that the KO mice do not express GADL1 protein. We did an additional KO verification by expressing the KO protein (protein lacking segments coded by exons 7) recombinantly in *Escherichia coli*. Compared to the full-length protein, the KO protein yield was very low, and it was enzymatically inactive, confirming that the gene elimination was successful and *Gad11*^{-/-} mice probably do not have any residual GADL1 enzyme activity.

4.1.2. HPLC

During method development for this study, different mobile phases and columns were tested for the high-performance liquid chromatography (HPLC) based methods. The instability of *o*-phthalaldehyde (OPA) derivatization caused some problems for reproducibility, both between individual replicates and runs. To minimize this problem, internal standards were injected between the samples, and the peak areas of the standards were used for the normalization of all the sample peak areas. In addition, by experience, we learned that pre-incubation of OPA with β -mercaptoethanol for 30 minutes significantly increased the stability of the analysis.

Another method for measuring enzyme activity is using circular dichroism spectroscopy (CD). Tramonti *et al.* recently reported that it is possible to measure CSAD enzyme activity using CD, as the substrate and product of the reaction have different optical properties (167). CD is a common method to investigate protein structure and has been used in biochemistry to obtain a quantitative assessment of the secondary structure content of biomolecules (168). However, most studies in the field of enzymology have used HPLC to measure enzyme activities. Reported HPLC assays for measuring taurine (169, 170) or carnosine (171) production have used ion-exchange or reversed-phase separation, which provide the possibility of separation and measurement of complex samples. One of the most important features of using HPLC for measuring enzyme activity is that the change in both substrate and product concentration can be measured simultaneously. Therefore, HPLC has a high potential for enzyme activity assays and has been employed in many studies on enzyme activities (172-174).

4.1.3. Protein expression and purification

Part of this study includes the characterization and crystallization of GADL1 and CSAD. For this aim, biophysical techniques were used, and controlled conditions were employed during and between all the experiments, including expression and purification processes. Having proteins with a high degree of purity and stability was vital for the experiments. Hence, the possible effects of aggregation and degradation were avoided. The quality of the purified proteins was checked by sodium dodecyl sulfate-polyacrylamide gel electrophoresis (SDS-PAGE) and size-exclusion chromatography with multiple angle laser light scattering (SEC-MALS) before and after the experiments.

4.2. GADL1, the discovery of a “novel” enzyme

The initiation of our studies on GADL1 was in 1998, when in a collaborative study between the University of Bergen and Uppsala University, it was found that some patients with APS1 have antibodies against tryptophan hydroxylase, tyrosine hydroxylase, and the PLP-dependent enzyme aromatic amino acid decarboxylase

(DOPA decarboxylase) that are involved in the production of serotonin and dopamine (175-180). In the course of these investigations, it was also found that a subgroup of patients produced antibodies against a novel antigen that was later identified as GADL1 in Paper I. During the assembly of mouse genome databases, this gene had originally received the name “GAD-like 1” because of the high sequence similarity to GAD (45–47% amino acid identity). Based on this similarity, GADL1 was assigned a possible role in GABA synthesis. However, later we and others (63) found that GADL1 does not have biologically significant GAD activity, and sequence comparison shows that it is more similar to CSAD (61% amino acid identity) (65).

4.3. Multiple substrates, multiple functions

Many PLP-dependent enzymes have multiple substrates (18). It is assumed that in the earliest phase of metabolism, enzymes were acting more generally and each enzyme had several substrates (181). Then, during evolution, most of the enzymes became more and more active, selective, and specific towards a single substrate (182-184). However, for some enzymes, having multiple physiological substrates is an advantage for fitness. Hence, for these enzymes, this feature has been selected or retained during evolution (181). One example of a PLP-dependent enzyme with multiple substrates is omega (ω)-transaminase, which is active on two types of substrates, hydrophobic amines and amino acids (27). Some other PLP-dependent enzymes also have several substrates (185).

Having multiple substrates does not mean that the enzyme must have the same affinity towards both substrates and act with the same efficiency on them. Sometimes the cell needs the product at a very low level, so even a slow reaction would be beneficial for the cell (181). For example, it has been shown that Ser racemase, which belongs to Fold II type of PLP-dependent enzymes, is involved in D-aspartate biosynthesis (186), and phylogenetic analysis indicated that animal Ser racemase and Asp racemase are not separated by their particular racemase function and form a Ser/Asp racemase family cluster (187). Nevertheless, Ser racemase catalytic efficiency for Asp racemization is 550-fold lower than that of Ser racemization (186).

Both GADL1 and CSAD are examples of PLP-DCs with multiple substrates. Each of them has a different affinity towards each substrate. CSA is the preferred substrate for both CSAD and GADL1. Nonetheless, apparently, CSAD has a higher affinity towards CSA than GADL1. Both enzymes decarboxylate Asp, but the mouse GADL1 decarboxylates Asp approximately 10 times faster (higher V_{\max}) than CSAD (Paper I). This may also have roots in structural differences in the active sites of CSAD and GADL1 that will be further discussed in chapter 4.4.2 on substrate specificity.

4.4. GADL1 and CSAD structures and biochemical features

Part of this project was studying the structure of CSAD and GADL1. We solved the crystal structure of GADL1 and CSAD in paper III and paper IV, respectively. In addition, in paper I, we have characterized these two enzymes from a biochemical point of view and suggested some new inhibitors for both of them. In this chapter, GADL1 and CSAD structure, substrate preferences, and catalytic activities are discussed.

4.4.1. PLP-dependent enzymatic mechanism

In the reactions performed by the PLP-dependent enzyme family, the formation of an external aldimine intermediate with the substrate is a common step (16). In this enzyme family, PLP is covalently bound to the active site of the enzyme, forming an internal aldimine (Fig. 10A). The covalent bond is formed between an aldehyde group of PLP and the ϵ -amino group of a Lys residue in the enzyme active site (Schiff-base linkage) (188, 189). When the substrate binds, the Lys ϵ -amino group is displaced by an amino group from the substrate, which leads to the formation of a substrate-PLP adduct, referred to as an external aldimine (Fig. 10B) (190).

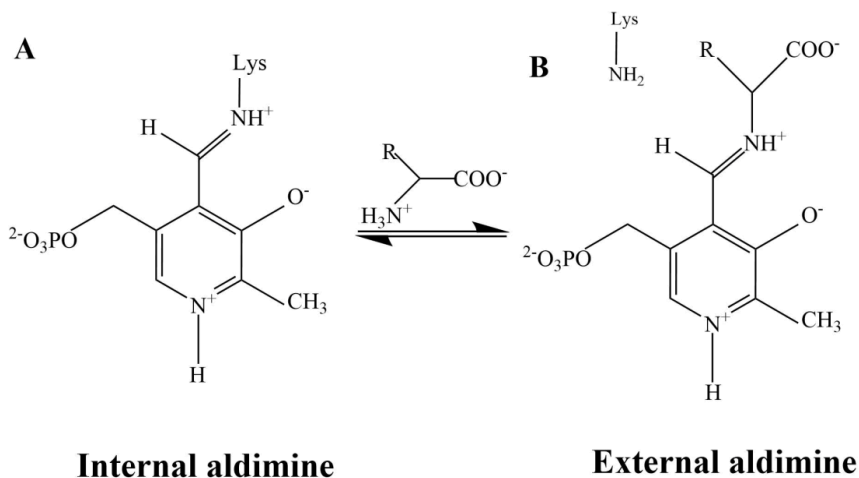


Fig.10. The common initial step in PLP-dependent enzymes reactions. The formation of an internal aldimine (A) and then an external aldimine (B) is the first step in all the PLP-dependent enzyme reactions, including those catalyzed by GADL1 and CSAD.

4.4.2. Substrate specificity of CSAD and GADL1

In paper I, we showed that both GADL1 and CSAD can decarboxylate CSA, CA, and Asp but both of them preferred CSA as substrate. These findings are in line with previous studies (63). On the other hand, it was found that cysteine may inactivate the CSA and Asp decarboxylase activity of GADL1 and CSAD in a concentration-dependent manner. Thus, in the presence of cysteine, β -alanine production from Asp by GADL1 is diminished. The inactivation was shown to be due to the interaction between cysteine and bound PLP in the enzyme structure, and it depends on the relative position of cysteine and the PLP bound to the active site (191).

The substrate specificity of GADL1 (63, 65) and CSAD (68, 167) towards Glu has been debated. In paper I, we reported that neither GADL1 nor CSAD decarboxylates Glu. Tappaz *et al.* also reported that CSAD is unable to decarboxylate Glu (192). However, using a more sensitive detection system, in paper IV, we observed a trace level of activity for CSAD with Glu as substrate. Moreover, Tramonti and colleagues found

some activity of CSAD with Glu, although with very low k_{cat} and V_{max} , possibly low efficiency (167). From one point of view, since CSAD has high sequence similarity with the GAD enzymes, it is expected to observe an activity between CSAD and Glu (192). This applies to GADL1 as well. On the other hand, investigating the structures of CSAD and GADL1 active sites shows that both enzymes have some differences compared to GAD. In a closer look, Phe94 in the CSAD active site, and Tyr in the same position in the GADL1 active site, should prevent Glu from binding. GAD has a serine in the corresponding residue position (described in detail in paper IV). Furthermore, CSA, Asp, and Glu, the substrates of CSAD, GADL1, and GAD, are different in size and shape (illustrated in paper II, Fig. 3h). Therefore, it was predicted that CSAD and GADL1 have a very low activity towards Glu, since Glu cannot productively bind to the CSAD and GADL1 active sites.

4.4.3. On the k_{cat} value of CSAD and GADL1

The k_{cat} value, the maximal turnover rate of an enzyme, is one of the fundamental properties of an enzyme, and it is important for the study of metabolic systems that the enzyme is involved in. Many models of cellular metabolism include k_{cat} values as key inputs to predict the behaviour of metabolic pathways and networks (193, 194). Reaching highly efficient enzymes is a great challenge in enzyme engineering (195).

In paper I, we reported the K_{m} and k_{cat} of CSAD and GADL1. In addition, in paper IV, we measured the activity of CSAD expressed and purified using another vector that contained a His-tag. Based on these values, CSAD has a low k_{cat} value towards its substrates. The same is true for the GADL1 k_{cat} value. But does this mean that GADL1 and CSAD are “not very active enzymes”? Perhaps not. Although k_{cat} is supposed to be a constant value and is part of the enzyme identity, many factors can affect the k_{cat} value. One possibility could be that the enzyme was not correctly folded during expression and purification. Thus, optimization of purification conditions may improve enzyme activity. Furthermore, it has been reported that when tagged enzymes are used for

measuring kinetics, it may have resulted in enzyme instability or interference with catalysis (196). We can see this difference in k_{cat} values between cleaved and non-cleaved enzymes in paper I (numbers are shown in Table 1 of paper I). In addition, there is an ongoing debate on comparing the enzyme assay conditions *in vivo* and *in vitro*. There is always a question of how similar the *in vitro* enzyme assay condition is to the *in vivo*, and if enzymes have different catalytic properties *in vivo* (197). Davidi and colleagues proposed a proteomics method for measuring the catalytic activity of enzymes *in vivo* (198, 199). Using such methods in future studies for estimating the maximal catalytic rates of GADL1 and CSAD *in vivo* may help in promoting our understanding of PLP-DCs substrate affinity, activity, and roles in metabolism.

4.4.4. GADL1 and CSAD, similarities and differences

In papers III and IV, we reported the crystal structure of *Mm*GADL1 and *Mm*CSAD, respectively. The structure of both enzymes reveals a homodimer that adopts an open conformation for the cofactor and substrate binding. The active sites are fully occupied with PLP, except the CSAD apo structure. Both enzymes adopt a loose conformation in solution, possibly explaining the affinities of CSAD and GADL1 toward multiple substrates. In the active site of CSAD, there is Phe94 that is important for substrate binding. GADL1 has a Tyr in the corresponding site. This minor difference may explain why GADL1 is more active than CSAD using Asp as substrate. Fig. 11 shows the structures of *Mm*GADL1 (A) and *Mm*CSAD (B) using the PDB entries 6ENZ and 6ZEK, respectively.

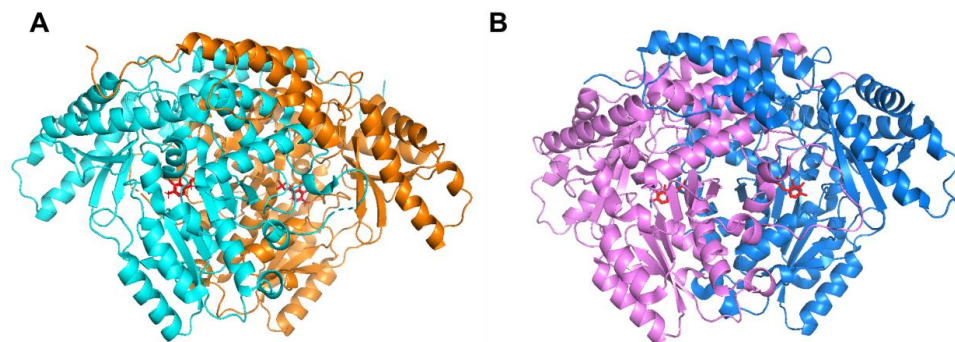


Figure 11. *MmGADL1* (A) and *MmCSAD* (B) crystal structures. PLP is shown in red. Different colors were chosen based on the chains for clarification. The figure was created in PyMol (2.4.1).

4.4.5. Current advances on protein structure studies

Studying the structure of a protein helps in better understanding its biochemical features, interaction with other proteins, biological functions, and predicting its therapeutic potential. There have been many studies on predicting protein structures based on their amino acid sequence or based on homologous proteins in the same family (200-202). Recently, there has been a breakthrough in protein structure prediction by artificial intelligence. AlphaFold2 is one example of software that is using a novel approach for predicting protein structures and potentially changing the future of protein structure science (203). Similarly, the RoseTTAFold protein modelling software is another very recent tool for protein structure prediction (204). However, experimental techniques are still needed to validate predicted structures.

4.4.6. Inhibitors for PLP-DCs

Considering the wide variety of their action mechanism and their versatility, PLP-dependent enzymes are attractive targets for designing specific inhibitors. Among the PLP-DCs, DOPA decarboxylase (DDC) and its inhibitor, carbidopa, have been studied

more than other PLP-DCs and their inhibitors, because of their role in the treatment of Parkinson's disease (205-207).

Parkinson's disease is characterized by losing neurons involved in the production of one of the most important neurotransmitters in the brain, dopamine (208). DDC, also known as aromatic L-amino acid decarboxylase, decarboxylates L-DOPA to dopamine. DDC is expressed by neurons in the CNS, liver, kidney, pancreas, and T lymphocytes (209). L-DOPA (levodopa) (Fig. 12A) is the most common drug for the treatment of Parkinson's disease (210). Intake of levodopa results in the systemic production of dopamine, which has side effects and may limit the production of dopamine in the CNS. Activation of peripheral dopamine receptors results in nausea and vomiting. Another drug that is commonly used by Parkinson's patients to control the effects of L-DOPA is carbidopa (Fig. 12B).

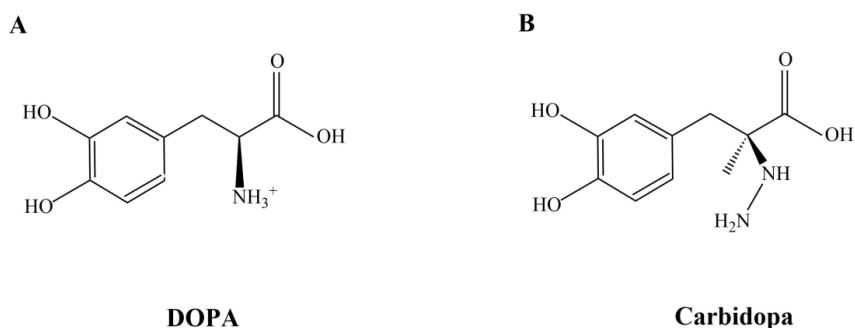


Fig.12. Chemical structure of DOPA and carbidopa.

Carbidopa is an inhibitor of DDC (211) and does not cross the blood-brain barrier, thus inhibiting the conversion of levodopa to dopamine outside of the brain, in the peripheral tissues (212), increasing the L-DOPA half-life and decreasing the unwanted side effects of dopamine on organs located outside of CNS (213-218). However, it has been shown that carbidopa inhibits T cell activation *in vitro* and *in vivo* (213). Carbidopa is an analogue of L-DOPA and inhibits DDC by forming a covalent bond to PLP and blocking the active site (206, 212). The crystal structure of the DDC and carbidopa complex is

available at the PDB (number 1JS3) (206) and may be used for designing inhibitors for other PLP-DCs with a similar mechanism of action.

Another example of an inhibitor of PLP-dependent enzymes is cycloserine, which has irreversible inhibition effects on GABA transaminases (219-221). Cycloserine is a cyclic analogue of alanine or serine and is approved for clinical use (222-224). Similarly to carbidopa, the cycloserine mechanism of inhibition is by making a covalent bond with PLP, therefore inhibiting the enzyme reaction (219, 222, 223).

In paper I, we introduced the “first generation” of inhibitors against GADL1 and CSAD that were designed based on *in silico* binding predictions and the substrate structures. Another approach for designing mechanism-based inhibitors could be to directly target the formation of the external aldimine during the catalytic cycle. Since this method targets a common step of all PLP-dependent enzyme reactions, it may lead to identifying inhibitors with less specificity but possibly higher affinity. Thus, it might be more efficient to use analogues of different stages of the enzyme reaction instead of using substrate analogues as inhibitors that may have a low affinity towards the enzyme.

4.5. GADL1 and CSAD tissue distribution and expression

In paper I, we showed that GADL1 is expressed in the SKM, brain, and particularly in the OB. Our data in paper II confirmed this by showing that OB is the most affected tissue in the *Gadl1*^{-/-} mice. A recent paper by Wang-Eckhardt and colleagues on the KO mouse model of CARNS1 also shows-depletion of HCDs in the OB. (225). It has been proposed that carnosine is present in OB and nasal olfactory epithelium (82) and possibly plays a role in the smelling sense.

In addition to the OB, other regions of the brain are also affected in the *Gadl1*^{-/-} mice. It has been proposed that in the brain, carnosine would act as a neurotransmitter (226) and the level of carnosine was reduced in the brain of *Gadl1*^{-/-} mice. However, the morphology of the brain in *Gadl1*^{-/-} mice did not change compared to *Gadl1*^{+/+} mice (Fig. 3D-F in paper II and supplementary Fig. 5A in paper II). Moreover, we observed

no major abnormalities in the behaviour and activities of *Gad11*^{-/-} mice, except for a small decrease in anxiety, and there was no significant difference in the phenotypes across the genotypes. However, the level of homocarnosine was upregulated, which might be a compensatory mechanism for the reduction against carnosine.

GADL1 is also expressed in SKM. Miyamoto-Mikami *et al.* reported that the expression levels of *CARNS1* and *GADL1* in SKM are significantly increased by high-intensity interval training, indicating the roles of these enzymes in SKM performance and carnosine importance in muscle function (227). However, it was recently reported that in *Carns1*^{-/-} mice, the pH buffering capacity and SKM contraction were unaltered, although a lack of *CARNS1* caused depletion of HCDs in the SKM (225). One possibility could be that in *Carns1*^{-/-} mice, the lack of carnosine is compensated by up-regulation of other physiological buffers, so the muscle contraction was not affected. This would be in line with our findings in Paper II, that mice lacking carnosine had increased levels of homocarnosine.

In *Csad*^{-/-} mice, the expression of GADL1 was relatively upregulated in the brain and SKM, which partially compensates for the lack of taurine, indicating an important role for GADL1 in maintaining the taurine level in some tissues (228). On the other hand, Liu *et al.* (63) found a high expression of GADL1 in the kidney. However, this high level of expression was not reproduced by us (65) or other groups (228). Since CSAD is highly expressed in the kidney, it is possible that the antibody used in the study (63) was nonspecific and bound to CSAD instead of GADL1 in the kidney.

Our experiments showed that GADL1 is not expressed at high levels in any of the tissues examined. However, its expression may be upregulated in response to environmental or physiological challenges, such as oxidative stress. For example, it has been shown that in the mouse model of amyotrophic lateral sclerosis (ALS), the expression of GADL1 was increased 1.52-fold in response to damage occurring during the course of disease in oligodendrocytes (229). Considering the antioxidant feature of carnosine, there is a possibility that GADL1 expression is also regulated based on the level of oxidative stress

markers and oxygen in the cell. This could be tested by inducing oxidative stress in animals (230) or cell culture and checking for changes in GADL1 expression.

There are several examples of enzymes that are upregulated because of oxidative stress (231-233) such as SOD enzymes described in chapter 1.5 (234). Another example of an enzyme that is expressed in specific tissue at a certain time window is plasmin, one of the most reactive serine proteases, involved in cancer progression. The proteolytic activity of plasmin is tightly regulated through activation of its precursor, plasminogen, but only at specific times and in defined locations (235).

4.6. Changes observed in the *Gad11*^{-/-} mice

Using LC-MS, we performed a metabolic analysis of different tissues taken from *Gad11*^{-/-} and *Gad11*^{+/+} mice. Between 541-720 metabolites were identified in the OB, SKM, brain, heart, serum, and kidney. In this chapter, some of the most significant and crucial changes observed in the *Gad11*^{-/-} mouse are discussed.

4.6.1. β -Alanine biosynthesis and changes in the *Gad11*^{-/-} mice

In paper II, we have shown that the β -alanine level was significantly decreased in the *Gad11*^{-/-} mouse OB. The most obvious reduction of β -alanine levels was observed in OB, and this is expected since GADL1 is mostly expressed in OB. However, it is possible that in other tissues with a high demand for β -alanine, such as SKM and brain, upregulation of alternative enzymes involved in β -alanine synthesis maintain β -alanine cellular levels. For example, β -ureidopropionase 1 produces β -alanine from uracil (136, 236-238). Possibly, upregulation of β -ureidopropionase was one of the ways for the mice's body to compensate for the reduced production of β -alanine in the absence of GADL1.

Dietary β -alanine, anserine, and taurine have been shown to reduce muscle fatigue, play roles as antioxidants and improve metabolic profiles in animals and humans (239-243). Nevertheless, some negative effects have also been reported (244). One of the most

widely known side effects of β -alanine supplements is paraesthesia (tingling), reported in individuals using more than 800 mg of β -alanine in non-sustained release form (245, 246). Moreover, there have been studies on the toxicity of taurine and ethanol in combination, which increases concerns for young people mixing taurine-containing energy drinks with alcohol (247). However, a review published in 2008 found no documented negative or positive health effects of taurine energy drinks, and it was concluded that the amount of taurine in energy drinks is too low to have any therapeutic benefits or negative effects (248). Evidently, more research is needed to determine the positive or negative effects of taurine and β -alanine supplementation.

On the other hand, β -alanine supplementation leads to a reduction in the abundance of taurine in the mouse SKM (249, 250). This is because one way of transporting β -alanine into the cells is *via* a transporter called taurine transporter-SLC6A6 (TauT), which is a Na^+ and Cl^- -dependent transmembrane transporter managed by transmembrane Na^+ flux (251, 252). This β -amino acid transporter transports both β -alanine and taurine (253, 254). Sharing the same transporter leads to a lower taurine uptake in the cell. Reduction of taurine caused elevated oxidative stress (250) and changes in energy metabolism (255).

4.6.2. Oxidative stress in *Gad11*^{-/-} mice

Oxidative stress is believed to contribute to many diseases, such as cancer, diabetes, and neurological disorders, including Alzheimer's disease (256, 257). There are many factors involved in this process. One of the main causes could be changes in the cell chemical profile and expression levels of the enzymes involved in the production of essential chemical substances. Carnosine (77, 142), β -alanine (258, 259), and taurine (239, 240) may protect against oxidative stress.

The therapeutic potential of carnosine against oxidative stress (260) and its role in suppressing Alzheimer's disease has been extensively studied (258, 259). The antioxidative stress effect of carnosine could be explained by its function as a ROS quencher (77, 142). ROS may cause a reduction in the levels of antioxidant enzymes,

such as SOD and GPX. Carnosine supplementation may increase the levels of these enzymes (77).

In our study, we found that in *Gad11*^{-/-} animals, the levels of oxidative stress markers were increased. This is consistent with the antioxidative stress effect of carnosine in the SKM. On the other hand, in the *Carns1*^{-/-} rat model, although the level of carnosine was very low, the levels of antioxidant markers in cardiac muscle were unaltered, indicating that in cardiac tissues, the absence of carnosine does not result in increased oxidative stress, and antioxidant defense is not a primary physiological role of carnosine in the cardiac muscle (113).

4.6.3. *Gad11*^{-/-} mice behaviour

The expression of high levels of GADL1 in the OB is intriguing and might provide additional information about the physiological role(s) of this enzyme. The sense of smell is essential for a wide range of mouse behaviour including navigation, ability to find food, bond formation, mate selection, and sexual and parental behaviour (261-264). Many behavioural tests designed for mice are based on the function of OB, including social behaviour tests, such as the resident intruder paradigm and three-chamber social interaction test that were employed on *Gad11*^{-/-} mice in paper II, and some learning and memory tests. Our results showed that in the resident intruder paradigm, both genotypes attack faster on the second day of the test. In the three-chamber social interaction test, the time spent at each cylinder for both genotypes was similar, and the differences were not significant. Both genotypes preferred the social cylinder. However, neither of these tests is specifically designed for examining OB function. More specific tests for the OB could be a buried food test or the olfactory habituation/dishabituation test. The buried food test, which relies on the animal's natural ability to use smelling senses for finding food, is used to confirm the ability to smell different odors. What is measured in this test is the time it takes for the mouse to find a piece of food buried under a layer of cage bedding. In addition, the olfactory habituation/dishabituation test, relies on the animal's ability to investigate new smells, is used to check if the animal can detect and differentiate different odors (265). It has been shown in the *Carns1*^{-/-} mice that lacking

carosine causes defects in the olfactory system in old age (225). In addition, a neuroprotective role for carosine in the olfactory system of mice after vanadium inhalation was suggested (266). Thus, accurate assessment of OB function is critical for proper interpretation of the *Gad11^{-/-}* mice behaviour, determination of the physiological role of GADL1, and investigating the particular role of carosine in the OB.

4.7. Discovery of “new” functions for old enzymes

The first paper describing GADL1 was published in 2012. In this report, the possible role of GADL1 in the synthesis of taurine or β -alanine and consequently in the production of carosine was discussed (63). However, in this paper, the role of GADL1 in taurine biosynthesis was more emphasized than its possible role in carosine production, as also reflected in the title of their study: “Role of glutamate decarboxylase-like protein 1 (GADL1) in taurine biosynthesis.” In contrast, in paper II, we clearly demonstrated the role of GADL1 in carosine production using a *Gad11^{-/-}* mouse model. The discovery of new and sometimes unexpected roles of previously characterized genes and proteins is quite common. One example of an old enzyme with a new function is the neutral endopeptidase (NEP) enzyme. NEP, also known as neprilysin, is considered to be one of the key enzymes in the metabolism of many active peptide hormones. At first, NEP was known to be the key enzyme in terminating the action of neuroendocrine mediators (267) and has a role in neurodegeneration and neuroprotection (268). Later, it was shown that NEP also plays role in fat accumulation and obesity by using a NEP-deficient mouse model. In the same study, the inhibition of NEP in mice with an enzyme inhibitor led to delayed rapid body mass. Therefore, a lack of NEP activity, genetically or pharmacologically, would result in gaining fat (269) and NEP serves as a good example of finding new role(s) of an old enzyme.

4.8. Medical implications

4.8.1. Potential biomarkers for brain-related disorders

The signs and symptoms of brain-related disorders, including neuropsychiatric and neurological disorders, can be unspecific and diverse, which makes diagnosis challenging. Detection of specific biomarkers to understand disease pathogenesis, improve diagnosis and provide treatment options is therefore essential. For brain-related disorders, early diagnosis has great importance, since early treatment can significantly slow down the progress of the disease. Therefore, finding biomarkers for neurological disorders is vital for early diagnosis.

Some biomarkers have been introduced for a few neuropsychiatric disorders, such as fragile X syndrome, Huntington's disease, and Rett syndrome (270). However, there are no reliable biomarkers for schizophrenia, ADHD, bipolar disorder, and major depressive disorders.

Recently, promising studies have been published on blood metabolic markers for many neuropsychiatric disorders (271). Since neuropsychiatric symptoms are often linked to metabolic disturbances, many studies have been done on metabolic biomarkers for neuropsychiatric disorders (272). These studies have shown that metabolomics-based technologies have the potential to identify biochemical changes happening in diseases and, thus, provide an opportunity to develop diagnostic tools that can be used as indicators of pathological abnormalities even before the emergence of clinical symptoms of neuropsychiatric disorders. Such studies have proposed multiple signaling molecules and pathways that are important in health and disease. In particular, amino acids, peptides, and amino acid derivatives, such as taurine, carnosine, β -alanine, and anserine, have recently received increasing attention as biomarkers in plasma and cerebrospinal fluid samples from neuropsychiatric patients (56, 57, 75). Therefore, studying taurine, carnosine, β -alanine and the enzymes involved in their synthesis may possibly lead to identifying novel biomarkers.

5. Concluding remarks

Using a wide range of methods, including LC-MS, HPLC, screening of putative substrates, enzyme kinetics, and western blotting, we explored the physiological roles and tissue distribution of GADL1 and CSAD. Furthermore, we discovered the first generation of partially selective inhibitors and solved the crystal structures of both enzymes. This has highlighted important details on the molecular mechanisms of the biosynthesis of taurine, carnosine, and β -alanine that could be used to develop new and more potent inhibitors aiming to affect the pathways where these metabolites are involved. Using gene elimination with the generation of a novel mouse model, we demonstrated that GADL1 plays an essential role in the production of β -alanine and its derivatives, such as carnosine peptides, particularly in the brain, OB, and SKM. Mice lacking GADL1 had multiple metabolomic alterations, including altered oxidative stress markers, and several age-related changes, underscoring the biological importance of GADL1. However, overall, the mice appeared normal and had only minor behavioural changes. By bringing together data from many large genetic studies, we showed that common variants in the human *GADL1* locus are associated with plasma levels of acetylcarnosine, muscle strength, kidney function, and subjective well-being.

To summarize, this study has provided new information about GADL1 and CSAD structures and biochemical features. In addition, the possible physiological role of GADL1 in mice is reported. These data can be used for studying other PLP-DCs. Furthermore, the therapeutic potential of GADL1 and CSAD direct and indirect products, β -alanine, carnosine, and taurine is the subject for further studies.

6. Future perspectives

PLP-dependent enzymes are involved in a variety of physiological reactions and metabolic pathways. Recently, their therapeutic potential in different fields, including enzyme inhibition and dietary supplementation therapy, has gained much attention (273). However, the diversity and structural complexity of these enzymes make it challenging to study this family. In this project, we explored the structures and physiological roles of two PLP-DCs, GADL1 and CSAD. Although the results have provided us with a better understanding of the biochemical features of this enzyme family, both *in vivo* and *in vitro*, there are still many open questions that remain unanswered. Therefore, many topics would be interesting for further investigation, some of which are highlighted below.

By screening multiple naturally occurring putative substrates, we demonstrated that both CSAD and GADL1 have a broad substrate specificity. However, it is possible that these enzymes may still use additional substrates and be involved in additional physiological functions. Further investigation on metabolomic changes in model organisms, such as the *Gad1^{-/-}* mouse, may lead to discovering other metabolic pathways affected by GADL1. As metabolomic studies showed that *Gad1^{-/-}* mice had multiple metabolic alterations and delayed growth, GADL1 could be involved in overall energy metabolism. By using tools to monitor mouse metabolism, for example, metabolic cages, to determine the rate of carbon dioxide production (V_{CO_2}) to the oxygen consumption (VO_2) of individual animals that were used in other studies (274, 275), one can estimate energy levels and possible metabolic alterations in the mice. One can also measure the food intake of individual mice and test different diets, such as a high or low-fat diet with or without taurine, β -alanine, or carnosine supplements.

Another method for studying the metabolic changes at the cellular level could be to isolate mitochondria from mouse tissues, for example from the OB of *Gad1^{-/-}* mice, measuring mitochondrial metabolic rates in a closed chamber system (276, 277). The

changes in the oxygen level can be recorded by a sensor in the chamber, and from the rate of oxygen reduction, the respiratory rate of the mitochondria can be measured.

Moreover, it would be interesting to generate a tissue-specific conditional *Gad11*^{-/-} mouse model and investigate the enzyme functions in specific cell types, such as oligodendrocytes. Such models could also improve our understanding of how the absence of GADL1 affects downstream signalling molecules, and which signalling and metabolic pathways are affected in each cell type or tissue. Since GADL1 and CSAD have overlapping substrate specificities, the generation of a double KO *Gad11*^{-/-} and *Csad*^{-/-} mouse model would help us towards a better understanding of the synergy between these enzymes.

One of the important aspects of studying GADL1 and CSAD is to explore how GADL1 and CSAD activities are regulated, and how this regulation affects their physiological roles. Interestingly, our preliminary studies revealed several phosphorylation sites in purified GADL1 and CSAD. Further biochemical and structural studies are needed to determine how phosphorylation may regulate these enzymes and the possible physiological consequences. This would improve our knowledge about protein functional modifications for further protein-protein interactions in this enzyme family.

From the structural point of view, important future work could be concentrated on high-resolution structural details of the substrate and inhibitor binding of GADL1, and on comparing these data with CSAD, GAD, and other PLP-DCs. Important questions to address would be the details of substrate specificity and the relevance of the conformational changes in substrate binding to the catalytic cycle of PLP-DCs. Such studies would be instrumental in structure-based drug design.

Finally, the potential of taurine, carnosine, and β -alanine as biomarkers for neurological disorders should be investigated. For instance, it has been shown that the levels of taurine in plasma samples of patients with major depressive disorder are increased after ECT (56, 57). In addition, carnosine has been proposed as a biomarker of habitational meat consumption (76) and food intake (278), and it has the potential as a biomarker for different diseases. For instance, analysis of serum samples from different patient groups

could help clarify whether carnosine or other HCDs should be studied further as candidate biomarkers for disease.

7. References

1. Disease GBD, Injury I, Prevalence C. Global, regional, and national incidence, prevalence, and years lived with disability for 354 diseases and injuries for 195 countries and territories, 1990-2017: a systematic analysis for the Global Burden of Disease Study 2017. *Lancet*. 2018;392(10159):1789-858.
2. Xia X, Jiang Q, McDermott J, Han JJ. Aging and Alzheimer's disease: Comparison and associations from molecular to system level. *Aging Cell*. 2018;17(5):e12802.
3. Reeve A, Simcox E, Turnbull D. Ageing and Parkinson's disease: why is advancing age the biggest risk factor? *Ageing Res Rev*. 2014;14:19-30.
4. Rybakowski JK. Lithium - past, present, future. *Int J Psychiatry Clin Pract*. 2020;24(4):330-40.
5. Shorter E. The history of lithium therapy. *Bipolar Disord*. 2009;11 Suppl 2:4-9.
6. Chen CH, Lee CS, Lee MT, Ouyang WC, Chen CC, Chong MY, et al. Variant GADL1 and response to lithium therapy in bipolar I disorder. *N Engl J Med*. 2014;370(2):119-28.
7. Cruceanu C, Alda M, Dion PA, Turecki G, Rouleau GA. No evidence for GADL1 variation as a bipolar disorder susceptibility factor in a Caucasian lithium-responsive cohort. *Am J Psychiatry*. 2015;172(1):94-5.
8. Clayton PT. B6-responsive disorders: a model of vitamin dependency. *J Inherit Metab Dis*. 2006;29(2-3):317-26.
9. Bianchi ML. Hypophosphatasia: an overview of the disease and its treatment. *Osteoporos Int*. 2015;26(12):2743-57.
10. Martos-Moreno GA, Calzada J, Couce ML, Argente J. [Hypophosphatasia: Clinical manifestations, diagnostic recommendations and therapeutic options]. *An Pediatr (Engl Ed)*. 2018;88(6):356 e1- e11.
11. Mornet E. Hypophosphatasia. *Orphanet J Rare Dis*. 2007;2:40.
12. Linglart A, Bioso-Duplan M. Hypophosphatasia. *Curr Osteoporos Rep*. 2016;14(3):95-105.
13. Whyte MP. Hypophosphatasia - aetiology, nosology, pathogenesis, diagnosis and treatment. *Nat Rev Endocrinol*. 2016;12(4):233-46.
14. Villa-Suarez JM, Garcia-Fontana C, Andujar-Vera F, Gonzalez-Salvatierra S, de Haro-Munoz T, Contreras-Bolivar V, et al. Hypophosphatasia: A Unique Disorder of Bone Mineralization. *Int J Mol Sci*. 2021;22(9).
15. Eliot AC, Kirsch JF. Pyridoxal phosphate enzymes: mechanistic, structural, and evolutionary considerations. *Annu Rev Biochem*. 2004;73:383-415.
16. Gayathri SC, Manoj N. Crystallographic Snapshots of the Dunathan and Quinonoid Intermediates provide Insights into the Reaction Mechanism of Group II Decarboxylases. *J Mol Biol*. 2020;432(24):166692.
17. Amadasi A, Bertoldi M, Contestabile R, Bettati S, Cellini B, di Salvo ML, et al. Pyridoxal 5'-phosphate enzymes as targets for therapeutic agents. *Curr Med Chem*. 2007;14(12):1291-324.
18. Percudani R, Peracchi A. A genomic overview of pyridoxal-phosphate-dependent enzymes. *EMBO Rep*. 2003;4(9):850-4.
19. Singh R, Spyraakis F, Cozzini P, Paiardini A, Pascarella S, Mozzarelli A. Chemogenomics of pyridoxal 5'-phosphate dependent enzymes. *J Enzyme Inhib Med Chem*. 2013;28(1):183-94.
20. Rocha JF, Pina AF, Sousa SF, Cerqueira NMFSA. PLP-dependent enzymes as important biocatalysts for the pharmaceutical, chemical and food industries: a structural and mechanistic perspective. *Catalysis Science & Technology*. 2019;9(18):4864-76.
21. Di Salvo ML, Fesko K, Phillips RS, Contestabile R. Editorial: PLP-Dependent Enzymes: Extraordinary Versatile Catalysts and Ideal Biotechnological Tools for the Production of Unnatural Amino Acids and Related Compounds. *Front Bioeng Biotechnol*. 2020;8:52.
22. Ma Y, Biava H, Contestabile R, Budisa N, di Salvo ML. Coupling bioorthogonal chemistries with artificial metabolism: intracellular biosynthesis of azidohomoalanine and its incorporation into recombinant proteins. *Molecules*. 2014;19(1):1004-22.
23. Mehta PK, Christen P. The molecular evolution of pyridoxal-5'-phosphate-dependent enzymes. *Adv Enzymol Relat Areas Mol Biol*. 2000;74:129-84.
24. Percudani R, Peracchi A. The B6 database: a tool for the description and classification of vitamin B6-dependent enzymatic activities and of the corresponding protein families. *BMC Bioinformatics*. 2009;10:273.
25. Grishin NV, Phillips MA, Goldsmith EJ. Modeling of the spatial structure of eukaryotic ornithine decarboxylases. *Protein Sci*. 1995;4(7):1291-304.
26. Christen P, Mehta PK. From cofactor to enzymes. The molecular evolution of pyridoxal-5'-phosphate-dependent enzymes. *Chem Rec*. 2001;1(6):436-47.
27. Liang J, Han Q, Tan Y, Ding H, Li J. Current Advances on Structure-Function Relationships of Pyridoxal 5'-Phosphate-Dependent Enzymes. *Front Mol Biosci*. 2019;6:4.
28. Rossignoli G, Phillips RS, Astegno A, Menegazzi M, Voltattorni CB, Bertoldi M. Phosphorylation of pyridoxal 5'-phosphate enzymes: an intriguing and neglected topic. *Amino Acids*. 2018;50(2):205-15.
29. Dai GZ, Han WB, Mei YN, Xu K, Jiao RH, Ge HM, et al. Pyridoxal-5'-phosphate-dependent bifunctional enzyme catalyzed biosynthesis of indolizidine alkaloids in fungi. *Proc Natl Acad Sci U S A*. 2020;117(2):1174-80.

30. Paiardini A, Giardina G, Rossignoli G, Voltattorni CB, Bertoldi M. New Insights Emerging from Recent Investigations on Human Group II Pyridoxal 5'-Phosphate Decarboxylases. *Curr Med Chem.* 2017;24(3):226-44.
31. Bisello G, Longo C, Rossignoli G, Phillips RS, Bertoldi M. Oxygen reactivity with pyridoxal 5'-phosphate enzymes: biochemical implications and functional relevance. *Amino Acids.* 2020;52(8):1089-105.
32. Toney MD. Reaction specificity in pyridoxal phosphate enzymes. *Arch Biochem Biophys.* 2005;433(1):279-87.
33. Hayashi H. Pyridoxal enzymes: mechanistic diversity and uniformity. *J Biochem.* 1995;118(3):463-73.
34. Schneider G, Kack H, Lindqvist Y. The manifold of vitamin B6 dependent enzymes. *Structure.* 2000;8(1):R1-6.
35. Han Q, Cai T, Tagle DA, Robinson H, Li J. Substrate specificity and structure of human amino adipate aminotransferase/kynurenine aminotransferase II. *Biosci Rep.* 2008;28(4):205-15.
36. Milano T, Paiardini A, Grgurina I, Pascarella S. Type I pyridoxal 5'-phosphate dependent enzymatic domains embedded within multimodular nonribosomal peptide synthetase and polyketide synthase assembly lines. *BMC Struct Biol.* 2013;13:26.
37. Oppici E, Fodor K, Paiardini A, Williams C, Voltattorni CB, Wilmanns M, et al. Crystal structure of the S187F variant of human liver alanine: glyoxylate [corrected] aminotransferase associated with primary hyperoxaluria type I and its functional implications. *Proteins.* 2013;81(8):1457-65.
38. Oppici E, Roncador A, Montioli R, Bianconi S, Cellini B. Gly161 mutations associated with Primary Hyperoxaluria Type I induce the cytosolic aggregation and the intracellular degradation of the apo-form of alanine:glyoxylate aminotransferase. *Biochim Biophys Acta.* 2013;1832(12):2277-88.
39. Hegvik TA, Husebye ES, Haavik J. Autoantibodies targeting neurotransmitter biosynthetic enzymes in attention-deficit/hyperactivity disorder (ADHD). *Eur Child Adolesc Psychiatry.* 2014;23(2):115-7.
40. Paiardini A, Contestabile R, Buckle AM, Cellini B. PLP-dependent enzymes. *Biomed Res Int.* 2014;2014:856076.
41. Paiardini A, Pascarella S. Structural mimicry between SLA/LP and Rickettsia surface antigens as a driver of autoimmune hepatitis: insights from an in silico study. *Theor Biol Med Model.* 2013;10:25.
42. Fenalti G, Buckle AM. Structural biology of the GAD autoantigen. *Autoimmun Rev.* 2010;9(3):148-52.
43. Yogeswara IBA, Maneerat S, Haltrich D. Glutamate Decarboxylase from Lactic Acid Bacteria-A Key Enzyme in GABA Synthesis. *Microorganisms.* 2020;8(12).
44. Ghit A, Assal D, Al-Shami AS, Hussein DEE. GABAA receptors: structure, function, pharmacology, and related disorders. *J Genet Eng Biotechnol.* 2021;19(1):123.
45. Bown AW, Shelp BJ. The Metabolism and Functions of [gamma]-Aminobutyric Acid. *Plant Physiol.* 1997;115(1):1-5.
46. Erlander MG, Tillakaratne NJ, Feldblum S, Patel N, Tobin AJ. Two genes encode distinct glutamate decarboxylases. *Neuron.* 1991;7(1):91-100.
47. Kim J, Richter W, Aanstoot HJ, Shi Y, Fu Q, Rajotte R, et al. Differential expression of GAD65 and GAD67 in human, rat, and mouse pancreatic islets. *Diabetes.* 1993;42(12):1799-808.
48. Soghomonian JJ, Martin DL. Two isoforms of glutamate decarboxylase: why? *Trends Pharmacol Sci.* 1998;19(12):500-5.
49. Tavazzani E, Tritto S, Spaiardi P, Botta L, Manca M, Prigioni I, et al. Glutamic acid decarboxylase 67 expression by a distinct population of mouse vestibular supporting cells. *Front Cell Neurosci.* 2014;8:428.
50. Wood JD. The role of gamma-aminobutyric acid in the mechanism of seizures. *Prog Neurobiol.* 1975;5(1):77-95.
51. Zhang Y, Vanmeert M, Siekierska A, Ny A, John J, Callewaert G, et al. Inhibition of glutamate decarboxylase (GAD) by ethyl ketopentenoate (EKP) induces treatment-resistant epileptic seizures in zebrafish. *Sci Rep.* 2017;7(1):7195.
52. Lloyd KG, Bossi L, Morselli PL, Munari C, Rougier M, Loiseau H. Alterations of GABA-mediated synaptic transmission in human epilepsy. *Adv Neurol.* 1986;44:1033-44.
53. Giometto B, Nicolao P, Macucci M, Tavalato B, Foxon R, Bottazzo GF. Temporal-lobe epilepsy associated with glutamic-acid-decarboxylase autoantibodies. *Lancet.* 1998;352(9126):457.
54. de la Rosa J, Stipanuk MH. Evidence for a rate-limiting role of cysteinesulfinate decarboxylase activity in taurine biosynthesis in vivo. *Comp Biochem Physiol B.* 1985;81(3):565-71.
55. Lourenco R, Camilo ME. Taurine: a conditionally essential amino acid in humans? An overview in health and disease. *Nutr Hosp.* 2002;17(6):262-70.
56. Samuelsson M, Gerdin G, Ollinger K, Vrethem M. Taurine and glutathione levels in plasma before and after ECT treatment. *Psychiatry Res.* 2012;198(1):53-7.
57. Samuelsson M, Skogh E, Lundberg K, Vrethem M, Ollinger K. Taurine and glutathione in plasma and cerebrospinal fluid in olanzapine treated patients with schizophrenia. *Psychiatry Res.* 2013;210(3):819-24.
58. Hernandez-Benitez R, Ramos-Mandujano G, Pasantes-Morales H. Taurine stimulates proliferation and promotes neurogenesis of mouse adult cultured neural stem/progenitor cells. *Stem Cell Res.* 2012;9(1):24-34.
59. Hayes KC, Trautwein EA. Taurine deficiency syndrome in cats. *Vet Clin North Am Small Anim Pract.* 1989;19(3):403-13.
60. Neuringer M, Sturman J. Visual acuity loss in rhesus monkey infants fed a taurine-free human infant formula. *J Neurosci Res.* 1987;18(4):597-601.
61. Sturman JA. Taurine in development. *J Nutr.* 1988;118(10):1169-76.
62. Park E, Park SY, Dobkin C, Schuller-Levis G. Development of a novel cysteine sulfinic Acid decarboxylase knockout mouse: dietary taurine reduces neonatal mortality. *J Amino Acids.* 2014;2014:346809.

63. Liu P, Ge X, Ding H, Jiang H, Christensen BM, Li J. Role of glutamate decarboxylase-like protein 1 (GADL1) in taurine biosynthesis. *J Biol Chem.* 2012;287(49):40898-906.
64. Wu TN, Chen CK, Liu IC, Wu LS, Cheng AT. Effects of GADL1 overexpression on cell migration and the associated morphological changes. *Sci Rep.* 2019;9(1):5298.
65. Winge I, Teigen K, Fossbakk A, Mahootchi E, Kleppe R, Skoldberg F, et al. Mammalian CSAD and GADL1 have distinct biochemical properties and patterns of brain expression. *Neurochem Int.* 2015.
66. Heinamaki AA, Peramaa AK, Piha RS. Characterization of cerebral cysteine sulfinic acid decarboxylase. Molecular parameters and inhibition studies. *Acta Chem Scand B.* 1982;36(5):287-90.
67. Tang XW, Hsu CC, Sun Y, Wu E, Yang CY, Wu JY. Multiplicity of Brain Cysteine Sulfinic Acid Decarboxylase - Purification, Characterization and Subunit Structure. *J Biomed Sci.* 1996;3(6):442-53.
68. Tappaz M, Reymond I, Bitoun M, Sergeant A. Cysteine sulfinate decarboxylase (CSD): molecular cloning, sequence and genomic expression in brain. *Adv Exp Med Biol.* 1998;442:25-32.
69. Chan-Palay V, Palay SL, Wu JY. Sagittal cerebellar microbands of taurine neurons: immunocytochemical demonstration by using antibodies against the taurine-synthesizing enzyme cysteine sulfinic acid decarboxylase. *Proc Natl Acad Sci U S A.* 1982;79(13):4221-5.
70. Reymond I, Almarghini K, Tappaz M. Immunocytochemical localization of cysteine sulfinate decarboxylase in astrocytes in the cerebellum and hippocampus: a quantitative double immunofluorescence study with glial fibrillary acidic protein and S-100 protein. *Neuroscience.* 1996;75(2):619-33.
71. Hartman PE, Hartman Z, Ault KT. Scavenging of singlet molecular oxygen by imidazole compounds: high and sustained activities of carboxy terminal histidine dipeptides and exceptional activity of imidazole-4-acetic acid. *Photochem Photobiol.* 1990;51(1):59-66.
72. Li S, Hong M. Protonation, tautomerization, and rotameric structure of histidine: a comprehensive study by magic-angle-spinning solid-state NMR. *J Am Chem Soc.* 2011;133(5):1534-44.
73. Yamashita S, Sato M, Matsumoto T, Kadooka K, Hasegawa T, Fujimura T, et al. Mechanisms of carnosine-induced activation of neuronal cells. *Biosci Biotechnol Biochem.* 2018;82(4):683-8.
74. Perrin RJ, Craig-Schapiro R, Malone JP, Shah AR, Gilmore P, Davis AE, et al. Identification and validation of novel cerebrospinal fluid biomarkers for staging early Alzheimer's disease. *PLoS One.* 2011;6(1):e16032.
75. Schon M, Mousa A, Berk M, Chia WL, Ukropec J, Majid A, et al. The Potential of Carnosine in Brain-Related Disorders: A Comprehensive Review of Current Evidence. *Nutrients.* 2019;11(6).
76. Mitry P, Wawro N, Rohrmann S, Giesbertz P, Daniel H, Linseisen J. Plasma concentrations of anserine, carnosine and pi-methylhistidine as biomarkers of habitual meat consumption. *Eur J Clin Nutr.* 2019;73(5):692-702.
77. Boldyrev AA, Aldini G, Derave W. Physiology and pathophysiology of carnosine. *Physiol Rev.* 2013;93(4):1803-45.
78. Chaleckis R, Murakami I, Takada J, Kondoh H, Yanagida M. Individual variability in human blood metabolites identifies age-related differences. *Proc Natl Acad Sci U S A.* 2016;113(16):4252-9.
79. Ighodaro OM, Akinloye OA. First line defence antioxidants-superoxide dismutase (SOD), catalase (CAT) and glutathione peroxidase (GPX): Their fundamental role in the entire antioxidant defence grid. *Alexandria Journal of Medicine.* 2018;54(4):287-93.
80. Krimberg R. Zur Kenntnis der Extraktivstoffe der Muskeln. IV. Mitteilung. Über das Vorkommen des Carnosins, Carnitins und Methylguanidins im Fleisch. 1906;48.
81. Tallon MJ, Harris RC, Maffulli N, Tarnopolsky MA. Carnosine, taurine and enzyme activities of human skeletal muscle fibres from elderly subjects with osteoarthritis and young moderately active subjects. *Bogerontology.* 2007;8(2):129-37.
82. Margolis FL. Carnosine in the primary olfactory pathway. *Science.* 1974;184(4139):909-11.
83. Bonfanti L, Peretto P, De Marchis S, Fasolo A. Carnosine-related dipeptides in the mammalian brain. *Prog Neurobiol.* 1999;59(4):333-53.
84. De Marchis S, Modena C, Peretto P, Migheli A, Margolis FL, Fasolo A. Carnosine-related dipeptides in neurons and glia. *Biochemistry (Mosc).* 2000;65(7):824-33.
85. Lenney JF, George RP, Weiss AM, Kucera CM, Chan PW, Rinzler GS. Human serum carnosinase: characterization, distinction from cellular carnosinase, and activation by cadmium. *Clin Chim Acta.* 1982;123(3):221-31.
86. Chmielewska K, Dzierzbicka K, Inkielewicz-Stepniak I, Przybylowska M. Therapeutic Potential of Carnosine and Its Derivatives in the Treatment of Human Diseases. *Chem Res Toxicol.* 2020;33(7):1561-78.
87. Lenney JF, Peppers SC, Kucera-Orallo CM, George RP. Characterization of human tissue carnosinase. *Biochem J.* 1985;228(3):653-60.
88. Teufel M, Saudek V, Ledig JP, Bernhardt A, Boularand S, Carreau A, et al. Sequence identification and characterization of human carnosinase and a closely related non-specific dipeptidase. *J Biol Chem.* 2003;278(8):6521-31.
89. Derave W, De Courten B, Baba SP. An update on carnosine and anserine research. *Amino Acids.* 2019;51(1):1-4.
90. Kim EH, Kim ES, Shin D, Kim D, Choi S, Shin YJ, et al. Carnosine Protects against Cerebral Ischemic Injury by Inhibiting Matrix-Metalloproteinases. *Int J Mol Sci.* 2021;22(14).
91. Prakash MD, Fraser S, Boer JC, Plebanski M, de Courten B, Apostolopoulos V. Anti-Cancer Effects of Carnosine-A Dipeptide Molecule. *Molecules.* 2021;26(6).
92. Turner MD, Sale C, Garner AC, Hipkiss AR. Anti-cancer actions of carnosine and the restoration of normal cellular homeostasis. *Biochim Biophys Acta Mol Cell Res.* 2021;1868(11):119117.

93. Jukic I, Kolobaric N, Stupin A, Matic A, Kozina N, Mihaljevic Z, et al. Carnosine, Small but Mighty-Prospect of Use as Functional Ingredient for Functional Food Formulation. *Antioxidants* (Basel). 2021;10(7).
94. Everaert I, Mooyaart A, Baguet A, Zutinic A, Baelde H, Achten E, et al. Vegetarianism, female gender and increasing age, but not CNDP1 genotype, are associated with reduced muscle carnosine levels in humans. *Amino Acids*. 2011;40(4):1221-9.
95. Penafiel R, Ruzafa C, Monserrat F, Cremades A. Gender-related differences in carnosine, anserine and lysine content of murine skeletal muscle. *Amino Acids*. 2004;26(1):53-8.
96. Preston JE, Hipkiss AR, Himsworth DT, Romero IA, Abbott JN. Toxic effects of beta-amyloid(25-35) on immortalised rat brain endothelial cell: protection by carnosine, homocarnosine and beta-alanine. *Neurosci Lett*. 1998;242(2):105-8.
97. Mannion AF, Jakeman PM, Dunnett M, Harris RC, Willan PL. Carnosine and anserine concentrations in the quadriceps femoris muscle of healthy humans. *Eur J Appl Physiol Occup Physiol*. 1992;64(1):47-50.
98. Dolan E, Saunders B, Harris RC, Bicudo J, Bishop DJ, Sale C, et al. Comparative physiology investigations support a role for histidine-containing dipeptides in intracellular acid-base regulation of skeletal muscle. *Comp Biochem Physiol A Mol Integr Physiol*. 2019;234:77-86.
99. Peters V, Zschocke J, Schmitt CP. Carnosinase, diabetes mellitus and the potential relevance of carnosinase deficiency. *J Inherit Metab Dis*. 2018;41(1):39-47.
100. Miyaji T, Sato M, Maemura H, Takahata Y, Morimatsu F. Expression profiles of carnosine synthesis-related genes in mice after ingestion of carnosine or ss-alanine. *J Int Soc Sports Nutr*. 2012;9(1):15.
101. Zhou Z, Liu XQ, Zhang SQ, Qi XM, Zhang Q, Yard B, et al. Correlation between serum carnosinase concentration and renal damage in diabetic nephropathy patients. *Amino Acids*. 2021;53(5):687-700.
102. Shin SY, Fauman EB, Petersen AK, Krumsiek J, Santos R, Huang J, et al. An atlas of genetic influences on human blood metabolites. *Nat Genet*. 2014;46(6):543-50.
103. Bauer K. Carnosine and homocarnosine, the forgotten, enigmatic peptides of the brain. *Neurochem Res*. 2005;30(10):1339-45.
104. De Marchis S, Melcangi RC, Modena C, Cavaretta I, Peretto P, Agresti C, et al. Identification of the glial cell types containing carnosine-related peptides in the rat brain. *Neurosci Lett*. 1997;237(1):37-40.
105. Bakardjiev A. Biosynthesis of carnosine in primary cultures of rat olfactory bulb. *Neurosci Lett*. 1997;227(2):115-8.
106. Zhang Y, Sloan SA, Clarke LE, Caneda C, Plaza CA, Blumenthal PD, et al. Purification and Characterization of Progenitor and Mature Human Astrocytes Reveals Transcriptional and Functional Differences with Mouse. *Neuron*. 2016;89(1):37-53.
107. Derave W, Everaert I, Beeckman S, Baguet A. Muscle carnosine metabolism and beta-alanine supplementation in relation to exercise and training. *Sports Med*. 2010;40(3):247-63.
108. Parkhouse WS, McKenzie DC. Possible contribution of skeletal muscle buffers to enhanced anaerobic performance: a brief review. *Med Sci Sports Exerc*. 1984;16(4):328-38.
109. Boldyrev AA, Severin SE. The histidine-containing dipeptides, carnosine and anserine: distribution, properties and biological significance. *Adv Enzyme Regul*. 1990;30:175-94.
110. Boldyrev AA. [Biological role of histidine-containing dipeptides]. *Biokhimiia*. 1986;51(12):1930-43.
111. Culbertson JY, Kreider RB, Greenwood M, Cooke M. Effects of beta-alanine on muscle carnosine and exercise performance: a review of the current literature. *Nutrients*. 2010;2(1):75-98.
112. Abe H. Role of histidine-related compounds as intracellular proton buffering constituents in vertebrate muscle. *Biochemistry (Mosc)*. 2000;65(7):757-65.
113. Goncalves LS, Sales LP, Saito TR, Campos JC, Fernandes AL, Natali J, et al. Histidine dipeptides are key regulators of excitation-contraction coupling in cardiac muscle: Evidence from a novel CARN1 knockout rat model. *Redox Biol*. 2021;44:102016.
114. Herculano B, Tamara M, Ohba A, Shimatani M, Kutsuna N, Hisatsune T. beta-alanyl-L-histidine rescues cognitive deficits caused by feeding a high fat diet in a transgenic mouse model of Alzheimer's disease. *J Alzheimers Dis*. 2013;33(4):983-97.
115. Chao de la Barca JM, Rondet-Courbis B, Ferre M, Muller J, Buisset A, Leruez S, et al. A Plasma Metabolomic Profiling of Exudative Age-Related Macular Degeneration Showing Carnosine and Mitochondrial Deficiencies. *J Clin Med*. 2020;9(3).
116. Rokicki J, Li L, Imabayashi E, Kaneko J, Hisatsune T, Matsuda H. Daily Carnosine and Anserine Supplementation Alters Verbal Episodic Memory and Resting State Network Connectivity in Healthy Elderly Adults. *Front Aging Neurosci*. 2015;7:219.
117. Szczesniak D, Budzen S, Kopec W, Rymaszewska J. Anserine and carnosine supplementation in the elderly: Effects on cognitive functioning and physical capacity. *Arch Gerontol Geriatr*. 2014;59(2):485-90.
118. Hisatsune T, Kaneko J, Kurashige H, Cao Y, Satsu H, Totsuka M, et al. Effect of Anserine/Carnosine Supplementation on Verbal Episodic Memory in Elderly People. *J Alzheimers Dis*. 2016;50(1):149-59.
119. Caruso G, Godos J, Castellano S, Micek A, Murabito P, Galvano F, et al. The Therapeutic Potential of Carnosine/Anserine Supplementation against Cognitive Decline: A Systematic Review with Meta-Analysis. *Biomedicines*. 2021;9(3).
120. Brown BE, Kim CH, Torpy FR, Bursill CA, McRobb LS, Heather AK, et al. Supplementation with carnosine decreases plasma triglycerides and modulates atherosclerotic plaque composition in diabetic apo E(-/-) mice. *Atherosclerosis*. 2014;232(2):403-9.

121. Coyle JT, Puttfarcken P. Oxidative stress, glutamate, and neurodegenerative disorders. *Science*. 1993;262(5134):689-95.
122. Menon K, Cameron JD, de Courten M, de Courten B. Use of carnosine in the prevention of cardiometabolic risk factors in overweight and obese individuals: study protocol for a randomised, double-blind placebo-controlled trial. *BMJ Open*. 2021;11(5):e043680.
123. Hipkiss AR. Possible Benefit of Dietary Carnosine towards Depressive Disorders. *Aging Dis*. 2015;6(5):300-3.
124. Shen Y, Hu WW, Chen Z. [Carnosine and diseases of central nervous system]. *Zhejiang Da Xue Xue Bao Yi Xue Ban*. 2007;36(2):199-203.
125. Berezhnoy DS, Stvolinsky SL, Lopachev AV, Devyatov AA, Lopacheva OM, Kulikova OI, et al. Carnosine as an effective neuroprotector in brain pathology and potential neuromodulator in normal conditions. *Amino Acids*. 2019;51(1):139-50.
126. Ghajar A, Aghajan-Nashtaei F, Afarideh M, Mohammadi MR, Akhondzadeh S. L-Carnosine as Adjunctive Therapy in Children and Adolescents with Attention-Deficit/Hyperactivity Disorder: A Randomized, Double-Blind, Placebo-Controlled Clinical Trial. *J Child Adolesc Psychopharmacol*. 2018;28(5):331-8.
127. Hajizadeh-Zaker R, Ghajar A, Mesgarpour B, Afarideh M, Mohammadi MR, Akhondzadeh S. L-Carnosine As an Adjunctive Therapy to Risperidone in Children with Autistic Disorder: A Randomized, Double-Blind, Placebo-Controlled Trial. *J Child Adolesc Psychopharmacol*. 2018;28(1):74-81.
128. Mehrazad-Saber Z, Kheirouri S, Noorazar SG. Effects of L-Carnosine Supplementation on Sleep Disorders and Disease Severity in Autistic Children: A Randomized, Controlled Clinical Trial. *Basic Clin Pharmacol Toxicol*. 2018;123(1):72-7.
129. Chengappa KN, Turkin SR, DeSanti S, Bowie CR, Brar JS, Schlicht PJ, et al. A preliminary, randomized, double-blind, placebo-controlled trial of L-carnosine to improve cognition in schizophrenia. *Schizophr Res*. 2012;142(1-3):145-52.
130. Sato M, Karasawa N, Shimizu M, Morimatsu F, Yamada R. Safety evaluation of chicken breast extract containing carnosine and anserine. *Food Chem Toxicol*. 2008;46(2):480-9.
131. Willi SM, Zhang Y, Hill JB, Phelan MC, Michaelis RC, Holden KR. A deletion in the long arm of chromosome 18 in a child with serum carnosinase deficiency. *Pediatr Res*. 1997;41(2):210-3.
132. Perry TL, Hansen S, Tischler B, Bunting R, Berry K. Carnosinemia. A new metabolic disorder associated with neurologic disease and mental defect. *N Engl J Med*. 1967;277(23):1219-27.
133. Bessman SP, Baldwin R. Imidazole aminoaciduria in cerebromacular degeneration. *Science*. 1962;135(3506):789-91.
134. Levenson J, Lindahl-Kiessling K, Rayner S. Carnosine Excretion in Juvenile Amaurotic Idiocy. *Lancet*. 1964;2(7362):756-7.
135. Caruso G, Caraci F, Jolivet RB. Pivotal role of carnosine in the modulation of brain cells activity: Multimodal mechanism of action and therapeutic potential in neurodegenerative disorders. *Prog Neurobiol*. 2019;175:35-53.
136. Matthews MM, Traut TW. Regulation of N-carbamoyl-beta-alanine amidohydrolase, the terminal enzyme in pyrimidine catabolism, by ligand-induced change in polymerization. *J Biol Chem*. 1987;262(15):7232-7.
137. del Favero S, Roschel H, Solis MY, Hayashi AP, Artioli GG, Otaduy MC, et al. Beta-alanine (Carnosyn) supplementation in elderly subjects (60-80 years): effects on muscle carnosine content and physical capacity. *Amino Acids*. 2012;43(1):49-56.
138. Varanoske AN, Hoffman JR, Church DD, Coker NA, Baker KM, Dodd SJ, et al. beta-Alanine supplementation elevates intramuscular carnosine content and attenuates fatigue in men and women similarly but does not change muscle l-histidine content. *Nutr Res*. 2017;48:16-25.
139. Furst T, Massaro A, Miller C, Williams BT, LaMacchia ZM, Horvath PJ. beta-Alanine supplementation increased physical performance and improved executive function following endurance exercise in middle aged individuals. *J Int Soc Sports Nutr*. 2018;15(1):32.
140. Murakami T, Furuse M. The impact of taurine- and beta-alanine-supplemented diets on behavioral and neurochemical parameters in mice: antidepressant versus anxiolytic-like effects. *Amino Acids*. 2010;39(2):427-34.
141. Kumrungsee T, Nirmagustina DE, Arima T, Onishi K, Sato K, Kato N, et al. Novel metabolic disturbances in marginal vitamin B6-deficient rat heart. *J Nutr Biochem*. 2019;65:26-34.
142. Boldyrev AA. Carnosine: new concept for the function of an old molecule. *Biochemistry (Mosc)*. 2012;77(4):313-26.
143. Rybakova YS, Kalen AL, Eckers JC, Fedorova TN, Goswami PC, Sarsour EH. [Increased manganese superoxide dismutase and cyclin B1 expression in carnosine-induced inhibition of glioblastoma cell proliferation]. *Biomed Khim*. 2015;61(4):510-8.
144. Gorbunov NV, Erin AN. [Mechanism of antioxidant action of carnosine]. *Biull Eksp Biol Med*. 1991;111(5):477-8.
145. Caruso G, Fresta CG, Siegel JM, Wijesinghe MB, Lunte SM. Microchip electrophoresis with laser-induced fluorescence detection for the determination of the ratio of nitric oxide to superoxide production in macrophages during inflammation. *Anal Bioanal Chem*. 2017;409(19):4529-38.
146. Caruso G, Distefano DA, Parlascino P, Fresta CG, Lazzarino G, Lunte SM, et al. Receptor-mediated toxicity of human amylin fragment aggregated by short- and long-term incubations with copper ions. *Mol Cell Biochem*. 2017;425(1-2):85-93.
147. Aldini G, Facino RM, Beretta G, Carini M. Carnosine and related dipeptides as quenchers of reactive carbonyl species: from structural studies to therapeutic perspectives. *Biofactors*. 2005;24(1-4):77-87.
148. Hipkiss AR, Preston JE, Himsforth DT, Worthington VC, Keown M, Michaelis J, et al. Pluripotent protective effects of carnosine, a naturally occurring dipeptide. *Ann N Y Acad Sci*. 1998;854:37-53.

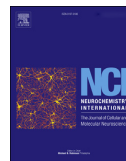
149. Ukeda H, Hasegawa Y, Harada Y, Sawamura M. Effect of carnosine and related compounds on the inactivation of human Cu,Zn-superoxide dismutase by modification of fructose and glycolaldehyde. *Biosci Biotechnol Biochem*. 2002;66(1):36-43.
150. Choi SY, Kwon HY, Kwon OB, Kang JH. Hydrogen peroxide-mediated Cu,Zn-superoxide dismutase fragmentation: protection by carnosine, homocarnosine and anserine. *Biochim Biophys Acta*. 1999;1472(3):651-7.
151. Mao C, Yuan JQ, Lv YB, Gao X, Yin ZX, Kraus VB, et al. Associations between superoxide dismutase, malondialdehyde and all-cause mortality in older adults: a community-based cohort study. *BMC Geriatr*. 2019;19(1):104.
152. Wang Y, Branicky R, Noe A, Hekimi S. Superoxide dismutases: Dual roles in controlling ROS damage and regulating ROS signaling. *J Cell Biol*. 2018;217(6):1915-28.
153. Carillon J, Rouanet JM, Cristol JP, Brion R. Superoxide dismutase administration, a potential therapy against oxidative stress related diseases: several routes of supplementation and proposal of an original mechanism of action. *Pharm Res*. 2013;30(11):2718-28.
154. Lin MT, Beal MF. Mitochondrial dysfunction and oxidative stress in neurodegenerative diseases. *Nature*. 2006;443(7113):787-95.
155. Lu SC. Regulation of glutathione synthesis. *Mol Aspects Med*. 2009;30(1-2):42-59.
156. Wu G, Fang YZ, Yang S, Lupton JR, Turner ND. Glutathione metabolism and its implications for health. *J Nutr*. 2004;134(3):489-92.
157. Aydin AF, Kucukgergin C, Ozdemirler-Erata G, Kocak-Toker N, Uysal M. The effect of carnosine treatment on prooxidant-antioxidant balance in liver, heart and brain tissues of male aged rats. *Biogerontology*. 2010;11(1):103-9.
158. Stvolinskii SL, Fedorova TN, Yuneva MO, Boldyrev AA. Protective effect of carnosine on Cu,Zn-superoxide dismutase during impaired oxidative metabolism in the brain in vivo. *Bull Exp Biol Med*. 2003;135(2):130-2.
159. Ma XY, Jiang ZY, Lin YC, Zheng CT, Zhou GL. Dietary supplementation with carnosine improves antioxidant capacity and meat quality of finishing pigs. *J Anim Physiol Anim Nutr (Berl)*. 2010;94(6):e286-95.
160. Sekula P, Goek ON, Quaye L, Barrios C, Levey AS, Romisch-Margl W, et al. A Metabolome-Wide Association Study of Kidney Function and Disease in the General Population. *J Am Soc Nephrol*. 2016;27(4):1175-88.
161. Wade TD, Gordon S, Medland S, Bulik CM, Heath AC, Montgomery GW, et al. Genetic variants associated with disordered eating. *Int J Eat Disord*. 2013;46(6):594-608.
162. Wuttke M, Li Y, Li M, Sieber KB, Feitosa MF, Gorski M, et al. A catalog of genetic loci associated with kidney function from analyses of a million individuals. *Nat Genet*. 2019;51(6):957-72.
163. Babzhayev MA. Biochemical, Biomedical and Metabolic Aspects of Imidazole-Containing Dipeptides with the Inherent Complexity to Neurodegenerative Diseases and Various States of Mental Well-Being: A Challenging Correction and Neurotherapeutic Pharmaceutical Biotechnology for Treating Cognitive Deficits, Depression and Intellectual Disabilities. *Curr Pharm Biotechnol*. 2014;15(8):738-78.
164. Mahootchi E, Cannon Homaei S, Kleppe R, Winge I, Hegvik TA, Megias-Perez R, et al. GADL1 is a multifunctional decarboxylase with tissue-specific roles in beta-alanine and carnosine production. *Sci Adv*. 2020;6(29):eabb3713.
165. Noiman T, Kahana C. A Simple Combined Use of CRISPR-Cas9 and Cre-LoxP Technologies for Generating Conditional Gene Knockouts in Mammalian Cells. *CRISPR J*. 2018;1:278-85.
166. Li Y, Zhang W, Zhao J, Li S, Shan L, Zhu J, et al. Establishing a dual knock-out cell line by lentivirus based combined CRISPR/Cas9 and Loxp/Cre system. *Cytotechnology*. 2018;70(6):1595-605.
167. Tramonti A, Contestabile R, Florio R, Nardella C, Barile A, Di Salvo ML. A Novel, Easy Assay Method for Human Cysteine Sulfinic Acid Decarboxylase. *Life (Basel)*. 2021;11(5).
168. Kelly SM, Price NC. The application of circular dichroism to studies of protein folding and unfolding. *Biochim Biophys Acta*. 1997;1338(2):161-85.
169. Hopkins PC, Kay IS, Davies WE. A rapid method for the determination of taurine in biological tissue. *Neurochem Int*. 1989;15(4):429-32.
170. Zheng G, Lin S. [Determination of taurine in foods by high performance liquid chromatography]. *Wei Sheng Yan Jiu*. 1998;27(4):266-8.
171. Kumagai M, Kato S, Arakawa N, Otsuka M, Hamano T, Kashiwagi N, et al. Quantification of Histidine-Containing Dipeptides in Dolphin Serum Using a Reversed-Phase Ion-Pair High-Performance Liquid Chromatography Method. *Separations*. 2021;8(8).
172. Welling GW, Scheffer AJ, Welling-Wester S. Determination of enzyme activity by high-performance liquid chromatography. *J Chromatogr B Biomed Appl*. 1994;659(1-2):209-25.
173. Rossomando EF. High-performance liquid chromatography in enzymatic analysis. Opening lecture. *J Chromatogr*. 1991;566(2):275-86.
174. Lambeth DO, Muhonen WW. High-performance liquid chromatography-based assays of enzyme activities. *J Chromatogr B Biomed Appl*. 1994;656(1):143-57.
175. Ekwall O, Hedstrand H, Grimelius L, Haavik J, Perheentupa J, Gustafsson J, et al. Identification of tryptophan hydroxylase as an intestinal autoantigen. *Lancet*. 1998;352(9124):279-83.
176. Hedstrand H, Ekwall O, Haavik J, Landgren E, Betterle C, Perheentupa J, et al. Identification of tyrosine hydroxylase as an autoantigen in autoimmune polyendocrine syndrome type I. *Biochem Biophys Res Commun*. 2000;267(1):456-61.
177. Husebye ES, Boe AS, Rorsman F, Kampe O, Aakvaag A, Rygh T, et al. Inhibition of aromatic L-amino acid decarboxylase activity by human autoantibodies. *Clin Exp Immunol*. 2000;120(3):420-3.

178. Ekwall O, Hedstrand H, Haavik J, Perheentupa J, Betterle C, Gustafsson J, et al. Pteridin-dependent hydroxylases as autoantigens in autoimmune polyendocrine syndrome type I. *J Clin Endocrinol Metab.* 2000;85(8):2944-50.
179. Bratland E, Wolff AS, Haavik J, Kampe O, Skoldberg F, Perheentupa J, et al. Epitope mapping of human aromatic L-amino acid decarboxylase. *Biochem Biophys Res Commun.* 2007;353(3):692-8.
180. Bratland E, Magitta NF, Boe Wolff AS, Ekern T, Knappskog PM, Kampe O, et al. Autoantibodies against aromatic amino acid hydroxylases in patients with autoimmune polyendocrine syndrome type 1 target multiple antigenic determinants and reveal regulatory regions crucial for enzymatic activity. *Immunobiology.* 2013;218(6):899-909.
181. Peracchi A. The Limits of Enzyme Specificity and the Evolution of Metabolism. *Trends Biochem Sci.* 2018;43(12):984-96.
182. Nam H, Lewis NE, Lerman JA, Lee DH, Chang RL, Kim D, et al. Network context and selection in the evolution to enzyme specificity. *Science.* 2012;337(6098):1101-4.
183. Mannervik B, Runarsson A. The quest for molecular quasi-species in ligand-activity space and its application to directed enzyme evolution. *FEBS Lett.* 2010;584(12):2565-71.
184. Khersonsky O, Tawfik DS. Enzyme promiscuity: a mechanistic and evolutionary perspective. *Annu Rev Biochem.* 2010;79:471-505.
185. Martino L, di Salvo NB, and, Contestabile R. <plp-dependent_enzymes_a_powerful_tool_for_metabolic_synthesis_of_non-canonical_amino_acids_.pdf>. Beilstein Bozen Symposium on Molecular Engineering and Control. 2012.
186. Ito T, Hayashida M, Kobayashi S, Muto N, Hayashi A, Yoshimura T, et al. Serine racemase is involved in d-aspartate biosynthesis. *J Biochem.* 2016;160(6):345-53.
187. Uda K, Abe K, Dehara Y, Mizobata K, Sogawa N, Akagi Y, et al. Distribution and evolution of the serine/aspartate racemase family in invertebrates. *Amino Acids.* 2016;48(2):387-402.
188. Carmen López SDR, Josep López-Santín, Gloria Caminal, Gregorio Álvaro. Immobilization of PLP-dependent enzymes with cofactor retention and enhanced stability. *Biochemical Engineering Journal.* 2010;49(3):414-21.
189. Schirch D, Delle Fratte S, Iurescia S, Angelaccio S, Contestabile R, Bossa F, et al. Function of the active-site lysine in *Escherichia coli* serine hydroxymethyltransferase. *J Biol Chem.* 1993;268(31):23132-8.
190. Du YL, Ryan KS. Pyridoxal phosphate-dependent reactions in the biosynthesis of natural products. *Nat Prod Rep.* 2019;36(3):430-57.
191. Liu P, Torrens-Spence MP, Ding H, Christensen BM, Li J. Mechanism of cysteine-dependent inactivation of aspartate/glutamate/cysteine sulfinic acid alpha-decarboxylases. *Amino Acids.* 2013;44(2):391-404.
192. Tappaz M, Bitoun M, Reymond I, Sergeant A. Characterization of the cDNA coding for rat brain cysteine sulfinate decarboxylase: brain and liver enzymes are identical proteins encoded by two distinct mRNAs. *J Neurochem.* 1999;73(3):903-12.
193. Labhsetwar P, Cole JA, Roberts E, Price ND, Luthey-Schulten ZA. Heterogeneity in protein expression induces metabolic variability in a modeled *Escherichia coli* population. *Proc Natl Acad Sci U S A.* 2013;110(34):14006-11.
194. Karr JR, Sanghvi JC, Macklin DN, Gutschow MV, Jacobs JM, Bolival B, Jr., et al. A whole-cell computational model predicts phenotype from genotype. *Cell.* 2012;150(2):389-401.
195. Goldsmith M, Tawfik DS. Enzyme engineering: reaching the maximal catalytic efficiency peak. *Curr Opin Struct Biol.* 2017;47:140-50.
196. Waugh DS. An overview of enzymatic reagents for the removal of affinity tags. *Protein Expr Purif.* 2011;80(2):283-93.
197. Garcia-Contreras R, Vos P, Westerhoff HV, Booger FC. Why in vivo may not equal in vitro - new effectors revealed by measurement of enzymatic activities under the same in vivo-like assay conditions. *FEBS J.* 2012;279(22):4145-59.
198. Davidi D, Noor E, Liebermeister W, Bar-Even A, Flamholz A, Tummler K, et al. Global characterization of in vivo enzyme catalytic rates and their correspondence to in vitro kcat measurements. *Proc Natl Acad Sci U S A.* 2016;113(12):3401-6.
199. Davidi D, Milo R. Lessons on enzyme kinetics from quantitative proteomics. *Curr Opin Biotechnol.* 2017;46:81-9.
200. Fetrow JS, Skolnick J. Method for prediction of protein function from sequence using the sequence-to-structure-to-function paradigm with application to glutaredoxins/thioredoxins and T1 ribonucleases. *J Mol Biol.* 1998;281(5):949-68.
201. Dunbrack RL, Jr. Sequence comparison and protein structure prediction. *Curr Opin Struct Biol.* 2006;16(3):374-84.
202. Deng H, Jia Y, Zhang Y. Protein structure prediction. *Int J Mod Phys B.* 2018;32(18).
203. Service RF. 'The game has changed.' AI triumphs at protein folding. *Science.* 2020;370(6521):1144-5.
204. Georgoulia PS, Bjelic S. Prediction of Protein-Protein Binding Interactions in Dimeric Coiled Coils by Information Contained in Folding Energy Landscapes. *Int J Mol Sci.* 2021;22(3).
205. Daidone F, Montiolari R, Paiardini A, Cellini B, Macchiarulo A, Giardina G, et al. Identification by virtual screening and in vitro testing of human DOPA decarboxylase inhibitors. *PLoS One.* 2012;7(2):e31610.
206. Burkhard P, Dominici P, Borri-Voltattorni C, Jansonius JN, Malashkevich VN. Structural insight into Parkinson's disease treatment from drug-inhibited DOPA decarboxylase. *Nat Struct Biol.* 2001;8(11):963-7.
207. Montiolari R, Voltattorni CB, Bertoldi M. Parkinson's Disease: Recent Updates in the Identification of Human Dopa Decarboxylase Inhibitors. *Curr Drug Metab.* 2016;17(5):513-8.
208. Brichta L, Greengard P, Flajolet M. Advances in the pharmacological treatment of Parkinson's disease: targeting neurotransmitter systems. *Trends Neurosci.* 2013;36(9):543-54.

209. Zhu MY, Juorio AV. Aromatic L-amino acid decarboxylase: biological characterization and functional role. *Gen Pharmacol.* 1995;26(4):681-96.
210. Fahn S. The history of dopamine and levodopa in the treatment of Parkinson's disease. *Mov Disord.* 2008;23 Suppl 3:S497-508.
211. Sletzing M, Chmerda JM, Bollinger FW. Potent Decarboxylase Inhibitors. Analogs of Methylodopa. *J Med Chem.* 1963;6:101-3.
212. Bartholini G, Pletscher A. Decarboxylase inhibitors. *Pharmacol Ther B.* 1975;1(3):407-21.
213. Zhu H, Lemos H, Bhatt B, Islam BN, Singh A, Gurav A, et al. Carbidopa, a drug in use for management of Parkinson disease inhibits T cell activation and autoimmunity. *PLoS One.* 2017;12(9):e0183484.
214. Corvol JC, Mariani LL. [Therapeutic and pharmacologic perspectives in Parkinson's disease]. *Rev Prat.* 2018;68(5):515-9.
215. Ebada MA, Alkanj S, Ebada M, Abdelkarim AH, Diab A, Aziz MAE, et al. Safety and Efficacy of Levetiracetam for the Management of Levodopa- Induced Dyskinesia in Patients with Parkinson's Disease: A Systematic Review. *CNS Neurol Disord Drug Targets.* 2019;18(4):317-25.
216. Romagnolo A, Merola A, Artusi CA, Rizzone MG, Zibetti M, Lopiano L. Levodopa-Induced Neuropathy: A Systematic Review. *Mov Disord Clin Pract.* 2019;6(2):96-103.
217. Ogungbenro K, Pertinez H, Aarons L. Empirical and semi-mechanistic modelling of double-peaked pharmacokinetic profile phenomenon due to gastric emptying. *AAPS J.* 2015;17(1):227-36.
218. Gandhi KR, Saadabadi A. Levodopa (L-Dopa). *StatPearls.* Treasure Island (FL)2021.
219. Dindo M, Grottelli S, Annunziato G, Giardina G, Pieroni M, Pampalone G, et al. Cycloserine enantiomers are reversible inhibitors of human alanine:glyoxylate aminotransferase: implications for Primary Hyperoxaluria type 1. *Biochem J.* 2019;476(24):3751-68.
220. Soper TS, Manning JM. Different modes of action of inhibitors of bacterial D-amino acid transaminase. A target enzyme for the design of new antibacterial agents. *J Biol Chem.* 1981;256(9):4263-8.
221. Polc P, Pieri L, Bonetti EP, Scherschlicht R, Moehler H, Kettler R, et al. L-cycloserine: behavioural and biochemical effects after single and repeated administration to mice, rats and cats. *Neuropharmacology.* 1986;25(4):411-8.
222. Amorim Franco TM, Favrot L, Vergnolle O, Blanchard JS. Mechanism-Based Inhibition of the Mycobacterium tuberculosis Branched-Chain Aminotransferase by d- and l-Cycloserine. *ACS Chem Biol.* 2017;12(5):1235-44.
223. Lowther J, Yard BA, Johnson KA, Carter LG, Bhat VT, Raman MC, et al. Inhibition of the PLP-dependent enzyme serine palmitoyltransferase by cycloserine: evidence for a novel decarboxylative mechanism of inactivation. *Mol Biosyst.* 2010;6(9):1682-93.
224. Prosser GA, de Carvalho LP. Reinterpreting the mechanism of inhibition of Mycobacterium tuberculosis D-alanine:D-alanine ligase by D-cycloserine. *Biochemistry.* 2013;52(40):7145-9.
225. Wang-Eckhardt L, Bastian A, Bruegmann T, Sasse P, Eckhardt M. Carnosine synthase deficiency is compatible with normal skeletal muscle and olfactory function but causes reduced olfactory sensitivity in aging mice. *J Biol Chem.* 2020;295(50):17100-13.
226. Horning MS, Blakemore LJ, Trombley PQ. Endogenous mechanisms of neuroprotection: role of zinc, copper, and carnosine. *Brain Res.* 2000;852(1):56-61.
227. Miyamoto-Mikami E, Tsuji K, Horii N, Hasegawa N, Fujie S, Homma T, et al. Gene expression profile of muscle adaptation to high-intensity intermittent exercise training in young men. *Sci Rep.* 2018;8(1):16811.
228. Park E, Park SY, Cho IS, Kim BS, Schuller-Levis G. A Novel Cysteine Sulfinic Acid Decarboxylase Knock-Out Mouse: Taurine Distribution in Various Tissues With and Without Taurine Supplementation. *Adv Exp Med Biol.* 2017;975 Pt 1:461-74.
229. Sun S, Sun Y, Ling SC, Ferraiuolo L, McAlonis-Downes M, Zou Y, et al. Translational profiling identifies a cascade of damage initiated in motor neurons and spreading to glia in mutant SOD1-mediated ALS. *Proc Natl Acad Sci U S A.* 2015;112(50):E6993-7002.
230. Koch RE, Hill GE, Costantini D. An assessment of techniques to manipulate oxidative stress in animals. *Functional Ecology.* 2016;31(1):9-21.
231. Limaye PV, Raghuram N, Sivakami S. Oxidative stress and gene expression of antioxidant enzymes in the renal cortex of streptozotocin-induced diabetic rats. *Mol Cell Biochem.* 2003;243(1-2):147-52.
232. Franco AA, Odum RS, Rando TA. Regulation of antioxidant enzyme gene expression in response to oxidative stress and during differentiation of mouse skeletal muscle. *Free Radic Biol Med.* 1999;27(9-10):1122-32.
233. Dunning S, Ur Rehman A, Tiebosch MH, Hannivoort RA, Hajjer FW, Woudenberg J, et al. Glutathione and antioxidant enzymes serve complementary roles in protecting activated hepatic stellate cells against hydrogen peroxide-induced cell death. *Biochim Biophys Acta.* 2013;1832(12):2027-34.
234. Hayyan M, Hashim MA, AlNashef IM. Superoxide Ion: Generation and Chemical Implications. *Chem Rev.* 2016;116(5):3029-85.
235. Deryugina EI, Quigley JP. Cell surface remodeling by plasmin: a new function for an old enzyme. *J Biomed Biotechnol.* 2012;2012:564259.
236. Traut TW, Loechel S. Pyrimidine catabolism: individual characterization of the three sequential enzymes with a new assay. *Biochemistry.* 2002;23(11):2533-9.
237. Caravaca J, Grisolia S. Enzymatic decarbamylation of carbamyl beta-alanine and carbamyl beta-aminoisobutyric acid. *J Biol Chem.* 1958;231(1):357-65.

238. Campbell LL. Reductive degradation of pyrimidines. 5. Enzymatic conversion of N-carbamyl-beta-alanine to beta-alanine, carbon dioxide, and ammonia. *J Biol Chem.* 1960;235:2375-8.
239. Schaffer SW, Azuma J, Mozaffari M. Role of antioxidant activity of taurine in diabetes. *Can J Physiol Pharmacol.* 2009;87(2):91-9.
240. Huxtable RJ. Physiological actions of taurine. *Physiol Rev.* 1992;72(1):101-63.
241. Bloedon TK, Braithwaite RE, Carson IA, Klimis-Zacas D, Lehnhard RA. Impact of anthocyanin-rich whole fruit consumption on exercise-induced oxidative stress and inflammation: a systematic review and meta-analysis. *Nutr Rev.* 2019.
242. Hobson RM, Saunders B, Ball G, Harris RC, Sale C. Effects of beta-alanine supplementation on exercise performance: a meta-analysis. *Amino Acids.* 2012;43(1):25-37.
243. Wu G. Important roles of dietary taurine, creatine, carnosine, anserine and 4-hydroxyproline in human nutrition and health. *Amino Acids.* 2020;52(3):329-60.
244. Artioli GG, Gualano B, Smith A, Stout J, Lancha AH, Jr. Role of beta-alanine supplementation on muscle carnosine and exercise performance. *Med Sci Sports Exerc.* 2010;42(6):1162-73.
245. Trexler ET, Smith-Ryan AE, Stout JR, Hoffman JR, Wilborn CD, Sale C, et al. International society of sports nutrition position stand: Beta-Alanine. *J Int Soc Sports Nutr.* 2015;12:30.
246. Harris RC, Tallon MJ, Dunnett M, Boobis L, Coakley J, Kim HJ, et al. The absorption of orally supplied beta-alanine and its effect on muscle carnosine synthesis in human vastus lateralis. *Amino Acids.* 2006;30(3):279-89.
247. Andrey Taranukhin PSSO. <Janus-faced taurine, protection or toxicity.pdf>. SpringerPlus. 2015.
248. Clauson KA, Shields KM, McQueen CE, Persad N. Safety issues associated with commercially available energy drinks. *J Am Pharm Assoc (2003).* 2008;48(3):e55-63; quiz e4-7.
249. Horvath DM, Murphy RM, Mollica JP, Hayes A, Goodman CA. The effect of taurine and beta-alanine supplementation on taurine transporter protein and fatigue resistance in skeletal muscle from mdx mice. *Amino Acids.* 2016;48(11):2635-45.
250. Shetewy A, Shimada-Takaura K, Warner D, Jong CJ, Mehdi AB, Alexeyev M, et al. Mitochondrial defects associated with beta-alanine toxicity: relevance to hyper-beta-alaninemia. *Mol Cell Biochem.* 2016;416(1-2):11-22.
251. Jessen H. Taurine and beta-alanine transport in an established human kidney cell line derived from the proximal tubule. *Biochim Biophys Acta.* 1994;1194(1):44-52.
252. Goncalves LS, Kratz C, Santos L, Carvalho VH, Sales LP, Nemezio K, et al. Insulin does not stimulate beta-alanine transport into human skeletal muscle. *Am J Physiol Cell Physiol.* 2020;318(4):C777-C86.
253. Caruso J, Charles J, Unruh K, Giebel R, Learmonth L, Potter W. Ergogenic effects of beta-alanine and carnosine: proposed future research to quantify their efficacy. *Nutrients.* 2012;4(7):585-601.
254. Vadgama JV, Chang K, Kopple JD, Idriss JM, Jonas AJ. Characteristics of taurine transport in rat liver lysosomes. *J Cell Physiol.* 1991;147(3):447-54.
255. Gemelli T, de Andrade RB, Rojas DB, Bonorino NF, Mazzola PN, Tortorelli LS, et al. Effects of beta-alanine administration on selected parameters of oxidative stress and phosphoryltransfer network in cerebral cortex and cerebellum of rats. *Mol Cell Biochem.* 2013;380(1-2):161-70.
256. Forman HJ, Zhang H. Targeting oxidative stress in disease: promise and limitations of antioxidant therapy. *Nat Rev Drug Discov.* 2021;20(9):689-709.
257. Valko M, Leibfritz D, Moncol J, Cronin MT, Mazur M, Telser J. Free radicals and antioxidants in normal physiological functions and human disease. *Int J Biochem Cell Biol.* 2007;39(1):44-84.
258. Hipkiss AR. Could carnosine or related structures suppress Alzheimer's disease? *J Alzheimers Dis.* 2007;11(2):229-40.
259. Hipkiss AR. Would carnosine or a carnivorous diet help suppress aging and associated pathologies? *Ann N Y Acad Sci.* 2006;1067:369-74.
260. Hipkiss AR. Is carnosine a naturally occurring suppressor of oxidative damage in olfactory neurones? *Rejuvenation Res.* 2004;7(4):253-5.
261. Doty RL. Odor-guided behavior in mammals. *Experientia.* 1986;42(3):257-71.
262. Brennan PA, Keverne EB. Something in the air? New insights into mammalian pheromones. *Curr Biol.* 2004;14(2):R81-9.
263. Keverne EB. Importance of olfactory and vomeronasal systems for male sexual function. *Physiol Behav.* 2004;83(2):177-87.
264. Restrepo D, Arellano J, Oliva AM, Schaefer ML, Lin W. Emerging views on the distinct but related roles of the main and accessory olfactory systems in responsiveness to chemosensory signals in mice. *Horm Behav.* 2004;46(3):247-56.
265. Yang M, Crawley JN. Simple behavioral assessment of mouse olfaction. *Curr Protoc Neurosci.* 2009;Chapter 8:Unit 8 24.
266. Colin-Barenque L, Bizarro-Neves P, Gonzalez Villalva A, Pedraza-Chaverri J, Medina-Campos ON, Jimenez-Martinez R, et al. Neuroprotective effect of carnosine in the olfactory bulb after vanadium inhalation in a mouse model. *Int J Exp Pathol.* 2018;99(4):180-8.
267. Scholzen TE, Luger TA. Neutral endopeptidase and angiotensin-converting enzyme -- key enzymes terminating the action of neuroendocrine mediators. *Exp Dermatol.* 2004;13 Suppl 4:22-6.
268. Turner AJ, Nalivaeva NN. New insights into the roles of metalloproteinases in neurodegeneration and neuroprotection. *Int Rev Neurobiol.* 2007;82:113-35.

269. Becker M, Siems WE, Kluge R, Gembardt F, Schultheiss HP, Schirner M, et al. New function for an old enzyme: NEP deficient mice develop late-onset obesity. *PLoS One*. 2010;5(9).
270. Z WA, McClure EA, Gray KM, Danielson CK, Treiber FA, Ruggiero KJ. Mobile devices for the remote acquisition of physiological and behavioral biomarkers in psychiatric clinical research. *J Psychiatr Res*. 2017;85:1-14.
271. Suman Patel1 aAR. Patent on Biomarkers in Medical Research: A Focus on Neuropsychiatric Disorders. 2013;24(7):715-22.
272. Suman Patel AR. Patent on Biomarkers in Medical Research: A Focus on Neuropsychiatric Disorders. 2013.
273. El-Sayed AS. Microbial L-methioninase: production, molecular characterization, and therapeutic applications. *Appl Microbiol Biotechnol*. 2010;86(2):445-67.
274. Aubi O, Prestegard KS, Jung-Kc K, Shi TS, Ying M, Grindheim AK, et al. The Pah-R261Q mouse reveals oxidative stress associated with amyloid-like hepatic aggregation of mutant phenylalanine hydroxylase. *Nat Commun*. 2021;12(1):2073.
275. Kaiyala KJ, Wisse BE, Lighton JRB. Validation of an equation for energy expenditure that does not require the respiratory quotient. *PLoS One*. 2019;14(2):e0211585.
276. Sperling JA, Sakamuri S, Albuck AL, Sure VN, Evans WR, Peterson NR, et al. Measuring Respiration in Isolated Murine Brain Mitochondria: Implications for Mechanistic Stroke Studies. *Neuromolecular Med*. 2019;21(4):493-504.
277. Andersen JV, Jakobsen E, Waagepetersen HS, Aldana BI. Distinct differences in rates of oxygen consumption and ATP synthesis of regionally isolated non-synaptic mouse brain mitochondria. *J Neurosci Res*. 2019;97(8):961-74.
278. Cuparencu C, Pratico G, Hemeryck LY, Sri Harsha PSC, Noerman S, Rombouts C, et al. Biomarkers of meat and seafood intake: an extensive literature review. *Genes Nutr*. 2019;14:35.



Mammalian CSAD and GADL1 have distinct biochemical properties and patterns of brain expression



Ingeborg Winge^a, Knut Teigen^a, Agnete Fossbakk^a, Elaheh Mahootchi^a, Rune Kleppe^a, Filip Sköldbberg^b, Olle Kämpe^{b,d}, Jan Haavik^{a,c,*}

^a K.G. Jebsen Centre for Research on Neuropsychiatric Disorders, Department of Biomedicine, University of Bergen, Norway

^b Department of Medical Sciences, University Hospital, Uppsala University, Uppsala, Sweden

^c Division of Psychiatry, Haukeland University Hospital, Bergen, Norway

^d Centre of Molecular Medicine (CMM L8:01), Dept. of Medicine (Solna), Karolinska Institutet, Stockholm, Sweden

ARTICLE INFO

Article history:

Received 17 April 2015

Received in revised form

30 July 2015

Accepted 22 August 2015

Available online 1 September 2015

Keywords:

Taurine

Cysteine sulfinic acid decarboxylase

Aspartate

Brain

Pyridoxal-phosphate

Lithium

ABSTRACT

Variants in the gene encoding the enzyme glutamic acid decarboxylase like 1 (GADL1) have been associated with response to lithium therapy. Both GADL1 and the related enzyme cysteine sulfinic acid decarboxylase (CSAD) have been proposed to be involved in the pyridoxal-5'-phosphate (PLP)-dependent biosynthesis of taurine. In the present study, we compared the catalytic properties, inhibitor sensitivity and expression profiles of GADL1 and CSAD in brain tissue. In mouse and human brain we observed distinct patterns of expression of the PLP-dependent decarboxylases CSAD, GADL1 and glutamic acid decarboxylase 67 (GAD67). CSAD levels were highest during prenatal and early postnatal development; GADL1 peaked early in prenatal development, while GAD67 increased rapidly after birth. Both CSAD and GADL1 are being expressed in neurons, whereas only CSAD mRNA was detected in astrocytes. Cysteine sulfinic acid was the preferred substrate for both mouse CSAD and GADL1, although both enzymes also decarboxylated cysteic acid and aspartate. *In silico* screening and molecular docking using the crystal structure of CSAD and *in vitro* assays led to the discovery of eight new enzyme inhibitors with partial selectivity for either CSAD or GADL1. Lithium had minimal effect on their enzyme activities. In conclusion, taurine biosynthesis in vertebrates involves two structurally related PLP-dependent decarboxylases (CSAD and GADL1) that have partially overlapping catalytic properties but different tissue distribution, indicating divergent physiological roles. Development of selective enzyme inhibitors targeting these enzymes is important to further dissect their (patho)physiological roles.

© 2015 The Authors. Published by Elsevier Ltd. This is an open access article under the CC BY license (<http://creativecommons.org/licenses/by/4.0/>).

1. Introduction

Lithium salts are among the most effective pharmacological agents used in psychiatry. Although several molecular targets have been identified, including protein kinases and enzymes involved in phosphoinositide metabolism, lithium's mode of action at the

cellular and molecular level is still being debated (Malhi et al., 2013). A strong genetic association between variants in the human glutamic acid decarboxylase like 1 (GADL1) gene and the response to lithium therapy in bipolar patients was recently reported (Chen et al., 2014). Although these findings were not replicated in other clinical samples (Cristiana et al., 2015), these results are intriguing and warrants a biochemical investigation on GADL1 and the effects of lithium on this enzyme.

Human GADL1 was recently found to function as a cysteine sulfinic acid decarboxylase and postulated to be involved in taurine and possibly also β -alanine and carnosine production *in vivo* (Liu et al., 2012). The sulfur amino acid taurine (2-amino-ethane-sulfonic acid) is abundant in mammalian tissues and has been implicated in many physiological functions. Taurine has a regulatory role in maintenance of osmotic pressure and preservation of structural integrity of biological membranes (Hoffmann and

Abbreviations: AADC, Aromatic amino acid decarboxylase; ADC, Aspartate decarboxylase; APS-1, Autoimmune polyendocrine syndrome type 1; BSA, Bovine serum albumin; CA, Cysteic acid; CDO, Cysteine oxidase; CSA, Cysteine sulfinic acid; CSAD, CSA decarboxylase; GABA, Gamma-amino-butyric acid; GAD, Glutamate decarboxylase; GADL1, Glutamate decarboxylase like 1; HDC, Histidine decarboxylase; ITT, *in vitro* transcription/translation system; OPA, *o*-phthalaldehyde; MBP, Maltose-binding protein; PCW, Post conception week; PLP, Pyridoxal-5'-phosphate; TEV, Tobacco Etch Virus protease.

* Corresponding author. Dept. of Biomedicine, University of Bergen, Jonas Lies vei 91, 5009, Bergen, Norway.

E-mail address: jan.haavik@biomed.uib.no (J. Haavik).

<http://dx.doi.org/10.1016/j.neuint.2015.08.013>

0197-0186/© 2015 The Authors. Published by Elsevier Ltd. This is an open access article under the CC BY license (<http://creativecommons.org/licenses/by/4.0/>).

Pedersen, 2006; Schaffer et al., 2010). In the nervous system, taurine may modulate protein phosphorylation (Lombardini, 1994), serve as a trophic factor (Hernandez-Benitez et al., 2010; Pasantes-Morales and Hernandez-Benitez, 2010), or act as a neurotransmitter/neuromodulator (Jia et al., 2008). In several species, taurine deficiency has been linked to specific disease states (Schaffer et al., 2010) and also in humans dietary intake of taurine in the form of energy drinks or vitamin supplements is widespread, although with unclear health implications (Bigard, 2010).

In mammalian tissues taurine is mainly synthesized from cysteine in a three step sequential pathway, involving oxidation by cysteine dioxygenase (CDO, E.C. 1.13.11.20), decarboxylation by cysteine sulfenic acid decarboxylase (CSAD, E.C. 4.1.1.29) and finally oxidation of hypotaurine to taurine. Alternatively, taurine may be formed from cysteamine by cysteamine dioxygenase (E.C. 1.13.11.19). The tissue distribution of the various enzymes involved in cysteine metabolism seems to reflect different metabolic demands of these tissues (Stipanuk et al., 2006). Thus, the protein levels of liver CDO, which is rate limiting in the degradation of the potentially toxic amino acid cysteine are tightly regulated in response to cysteine load (Stipanuk et al., 2009).

In comparison, the physiological role and regulation of CSAD and GADL1 are less understood. Mammalian CSAD has been isolated from liver, kidney and brain where it exists as a dimer with a reported subunit molecular mass of approx. 43–55 kDa (Heinamaki et al., 1982; Tang et al., 1996; Tappaz et al., 1998). GADL1 is expressed in muscle and kidney tissue (Liu et al., 2012). However, its pattern of expression in other tissues, including brain is not known. CSAD and GADL1 belong to a large family of pyridoxal-5'-phosphate (PLP)-dependent enzymes that catalyze a range of different reactions, such as decarboxylation, transamination, racemization or eliminations using amino acids or related substrates (Toney, 2011). Crystal structures of many PLP-dependent enzymes, including CSAD, have been published (<http://www.rcsb.org/pdb/explore/explore.do?structureid=2JIS>).

In the brain, CSAD has mainly been detected in astrocytes in cerebellum and hippocampus (Reymond et al., 1996a), although there are also reports of CSAD being found in neurons (Chan-Palay et al., 1982). Based on the different tissue distribution of CDO and CSAD, it was proposed that the taurine synthesis pathway is initiated in neurons and completed in astrocytes (Dominy et al., 2004). More recently, taurine biosynthesis from cysteine in murine neurons and astrocytes was reported, indicating that the complete enzymatic machinery for taurine synthesis is present in both cell types (Vitvitsky et al., 2011). However, the identity of the enzymes involved in the synthesis in the two cells types is not known.

A CSAD knockout mouse was recently described (Park et al., 2014). The plasma levels of taurine were reduced by 83% in CSAD^{-/-} mice and most offspring from 2nd generation CSAD^{-/-} mice died shortly after birth, indicating an important physiological role of CSAD.

The aims of our study were (i) to determine the effects of lithium on GADL1 and CSAD, (ii) to compare the substrate specificities of these enzymes, to use this knowledge to find inhibitors of the enzymes and (iii) to study their cellular, regional and temporal patterns of expression in the mammalian brain.

2. Experimental procedure

2.1. Source of materials

Chromatography materials for enzyme purification were purchased from GE Healthcare Life Sciences (Uppsala, Sweden), unless otherwise indicated, and all other reagents were from Sigma (St Louis, MO, USA).

2.2. Molecular modeling/docking of substrates in GADL1 and CSAD

To determine the structural relationships of GADL1, CSAD, and other decarboxylases, we created a homology model of GADL1. The sequence of GADL1 was aligned with that of CSAD in DeepView (Guex and Peitsch, 1997) and submitted to the Swiss-Model server (Schwede et al., 2003) to prepare a homology model of GADL1 (see Fig. 2). A virtual library of 8 million commercially available compounds was obtained from the ZINC database (Irwin et al., 2012) and docked into the active site of CSAD with the Glide software (Friesner et al., 2004) from Schrodinger®. A grid centered on the PLP cofactor in the CSAD binding site was defined with dimensions 17 Å in all three dimensions. The compounds were initially docked following the high throughput virtual screening protocol. The top 100,000 compounds were redocked following the standard precision protocol. Finally, the 10,000 top scoring compounds from this procedure were docked into the active site with the extra precision (Friesner et al., 2006) protocol.

2.3. Expression vectors

Multiple mRNA transcripts of CSAD and GADL1 have been described, probably due to alternative initiation codons and splicing events (Tappaz et al., 1999). The UniProt database (<http://www.uniprot.org/uniprot/>) lists three human CSAD sequences with 346–520 amino acids, two human GADL1 isoforms with 418–521 amino acids and two mouse GADL1 isoforms with 526–550 amino acids. We obtained cDNA clones corresponding to the 550 amino acids (62 kDa; Q80WP8-2) isoform of mouse GADL1

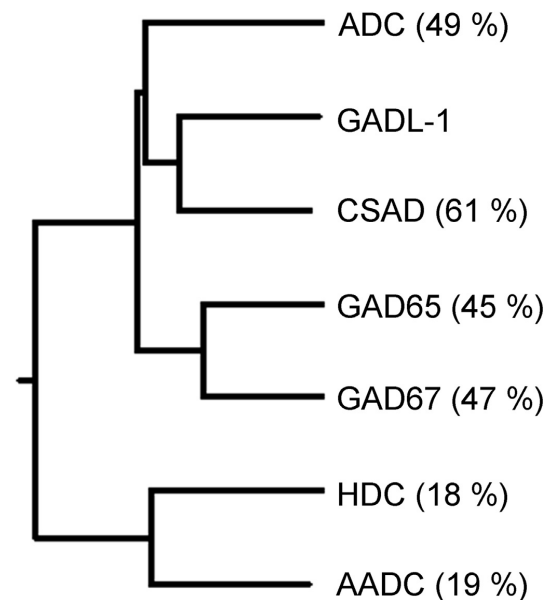


Fig. 1. Phylogenetic tree of PLP-dependent decarboxylases. Amino acid sequences of PLP-dependent decarboxylases were aligned using ClustalW version 2 software (2007) (Larkin et al., 2007). The phylogenetic tree was constructed by the neighbor-joining method based on alignment using the data base accession numbers: Q80WP8 (GADL1), Q9DBE0 (CSAD), P48318 (GAD1), P48320 (GAD2), O88533 (AADC), P23738 (HDC), A7U8C7 (ADC). The percentages of the amino acid sequence similarity to GADL1 are given in parenthesis. All the sequences are from *Mus musculus*, except for ADC, which is from *Tribolium castaneum*.

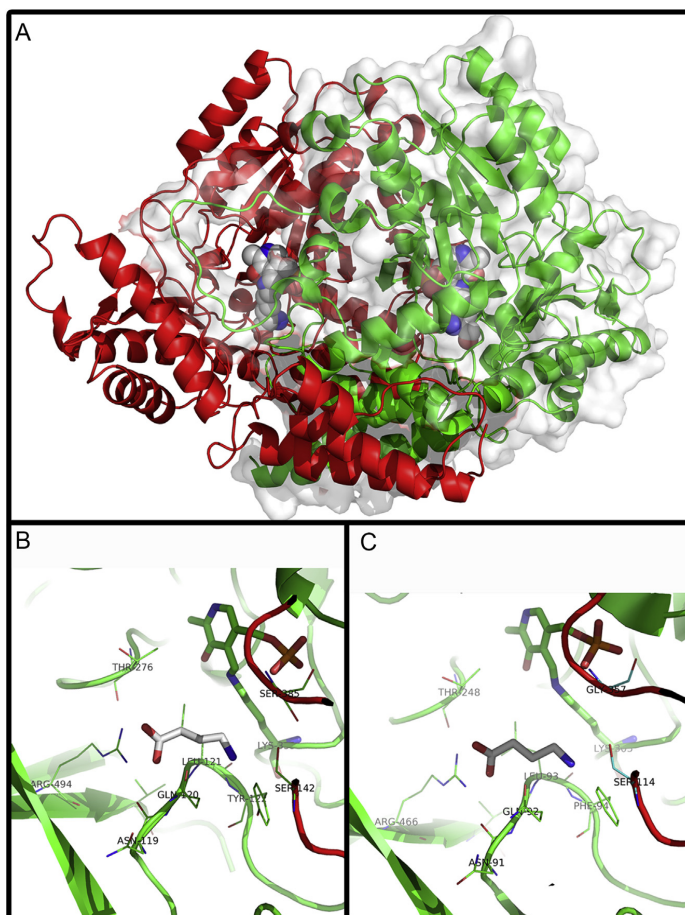


Fig. 2. **A** Homology model of dimeric GADL1 based on CSAD (pdb code 2JJS). One of the subunits (colored green) is represented with transparent surface to get an impression of the overall structure. The PLP cofactor is represented by spheres with size corresponding to the Van der Waal radius, colored by atom type and covalently linked to Lys333 (not shown) in the active site. **B** Representation of the putative substrate binding site in GADL1 with highlighted amino acids in close proximity to the substrate. PLP is shown with a covalent bond to Lys333. The model of GADL1 with GABA in the putative substrate binding site was prepared by aligning the GADL1 homology model with the coordinates of GAD67 in complex with GABA (pdb code 2OKJ). **C** Representation of the substrate binding site in CSAD with highlighted amino acids in close proximity to the substrate; Arg466, Gln92 and Leu93. PLP is shown with a covalent bond to Lys305. The model of CSAD with GABA in the putative substrate binding site was prepared by aligning the CSAD coordinate file (2JJS) with the coordinates of GAD67 in complex with GABA (pdb code 2OKJ).

and the 493 amino acids (55 kDa; Q9DBE0) isoform of mouse CSAD. Three different expression vectors were used using maltose-binding protein (MBP) as a fusion partner; pETM41: for 6×His-MBP-CSAD and 6×His-MBP-GADL1 expression in *Escherichia coli* and pCMV-SPORT 6: for expression of native CSAD and pCRII-Topo for native GADL1 in an *in vitro* transcription/translation system (ITT), essentially as described previously (McKinney et al., 2005). The sequences of all CSAD and GADL1 expression clones were verified by DNA sequencing.

2.4. Cell free transcription and translation of CSAD and GADL1

A rabbit reticulocyte lysate (Promega, Madison, WI) was used to express CSAD and GADL1 where 1 µg of plasmid DNA per reaction (50 µL) and 1 h incubation (30 °C) was used. Enzyme activity was

assayed immediately following removal of unincorporated amino acids by gel filtration using 0.5 mL pre-packed Zeba™ spin columns (Pierce, Rockford, IL, USA), which were prerinsed with buffer: 20 mM NaHepes 200 mM NaCl and 10% glycerol. Specific expression levels were determined after gel filtration and separation on 12% SDS-PAGE by integration of [³⁵S] methionine labeled CSAD and GADL1 band intensities using the Personal Molecular Imager™ System and Quantity One Software v. 4.5.2 (Bio-Rad, Hercules, CA, USA).

2.5. Analysis of CSAD and GADL1 expressed in *E. coli*

Heterologous expression of CSAD and GADL1 fusion proteins in *E. coli* was essentially performed as described (Winge et al., 2007) except for the following changes: BL21-CodonPlus (DE3)-RIPL

(Stratagene, La Jolla, CA) was used as expression host and the induction temperature was reduced to 20 °C. Cell pellets were lysed by sonication in 20 mM Hepes pH 7.4, 200 mM NaCl, 10% glycerol, 10 mM benzimidazole, 1 mg/mL lysozyme, 1 µg/mL pepstatin A, 4.6 µg/mL leupeptin. PMSF was added immediately following sonication to a concentration of 1 mM. The cell lysate was fractionated into soluble and insoluble parts by centrifugation at 10,000 × g for 30 min. An equal volume of lysate buffer was added to the pelleted fraction and homogenized. Specific expression levels of fusion proteins were determined by analyzing equal amounts (30 µg) of the soluble fractions by separation on 12% SDS-PAGE. Coomassie stained 6 × HisMBP-CSAD and GADL1 fusion protein band intensities were integrated using the VersaDoc MP 4000 imaging system and Quantity One Software (Bio-Rad, Hercules, CA, USA).

2.6. Activity assays

Activities of CSAD, GADL1 and GAD65 were measured using both ITT-expressed protein and *E. coli* expressed protein. A reaction mixture of 100 µl containing varying amounts of purified recombinant proteins and amino-acids was prepared in 60 mM potassium phosphate (pH 7.4) containing 5 mM DTT, 50 mM sucrose and 0.5 or 100 µM PLP. Adding 1 mM of the amino acid substrate started the reaction. Samples of 30 µl were taken at 15–60 min and the reaction stopped by addition of an equal volume of ice-cold ethanol with 5% acetic acid. The samples were then centrifuged at 15,700 × g for 10 min before the supernatant was being transferred to a microtiter plate and analyzed by HPLC. Samples were diluted to 50% in solvent (24% ethanol in 50 mM Na-phosphate pH 6.0), and 4.2% *o*-phthalaldehyde (OPA)-reagent was added before injection into a Zorbax Eclipse XDB-C18 column. Determination of product in the reaction-mixture was based on fluorescence detection of OPA-bound amino acid at 366/455 nm.

In order to perform inhibition assays on the two enzymes, different concentrations of the inhibitors were tested (0.001–50 mM). The assay was performed as described above at 37 °C for 60 min and stopped by addition of equal volume of ice-cold ethanol with 5% acetic acid.

2.7. Gene expression assays

Total RNA was obtained from Clontech laboratories, Mountain View, California, USA (brain, liver, muscle and kidney) and Sciencell, Carlsbad, USA (neurons and astrocytes). Total cDNA was obtained using High Capacity RNA-to-cDNA kit from Applied Biosystems (Foster city, CA). Gene-specific primers (Suppl. Table 1), TaqMan[®] Minor Groove Binder (MGB) probes and Assay-on-Demand[™] PCR reagents were from Applied Biosystems and were designed to be gene-specific and target all reported splice variants of GADL1 and CSAD (Suppl. Table 2). Each real-time PCR reaction was run in triplicate and contained 1 µl TaqMan[®] primer/probe. Cycling parameters were 95 °C for 10 min, followed by 40 cycles of 95 °C for 15 s and 60 °C for 1 min. Serial diluted standards were used to prepare a standard curve, which was run on the same plate and used to calculate relative gene expression abundance. The results were quantified by the $\Delta\Delta C_t$ method using the housekeeping genes GAPDH and β -actin as endogenous controls to adjust for unequal amounts of RNA and efficiency of cDNA synthesis. None of the samples showed signs of DNA contamination when reverse transcriptase was omitted from the cDNA reaction. The relative gene expression levels are presented as $2^{\Delta\Delta C_t}$ using CSAD as the control.

2.8. Western blot analysis

Frozen mouse tissues (200 µg) were lysed in ice-cold lysis buffer containing protease inhibitors. The lysates were centrifuged at 16,000 × g for 10 min at 4 °C. The supernatants were collected and stored at –80 °C. Protein concentrations were determined and 20 µg of total protein or 10 ng of purified CSAD or GADL1 protein were analyzed on 10% TGX Stain-Free gels (Bio-Rad) for 45 min at 20 mA/gel. The gel was activated and imaged (see “Imaging and data analysis” section below). The activated gel was transferred to an Immun-Blot nitrocellulose membrane (Bio-Rad) in 7 min using the Trans-Blot Turbo Transfer System (Bio-Rad) with Trans-Blot Turbo Midi Transfer Packs. Pre-made western blots of protein samples from mouse brain sampled at 11 different developmental stages (MW-201-D) and adult brain tissues from 14 different species (AW-201) were also obtained from Zyagen Laboratories, San Diego, CA. The membranes were blocked with 5% bovine serum albumin (BSA), 1% glycine and 0.1% Tween-20 in Tris-buffered saline and incubated with custom made affinity purified sheep antibodies generated against purified human CSAD or human GADL1 MBP fusion proteins (James Hastie, University of Dundee). To avoid cross reactivity against these related proteins, the GADL1 antibodies were filtered against purified CSAD and the CSAD antibodies were filtered against purified GADL1. Antigens were detected using horseradish peroxidase-conjugated goat anti-sheep antibody (1:10,000) (Bio-Rad Laboratories, Hercules, CA) as a secondary antibody and enhanced chemiluminescence detection.

We also tested commercial rabbit antibodies against either human CSAD (Sigma–Aldrich HPA039487; 1:2,000, immunogen peptide corresponding to amino acids 52–110 in the CSAD protein sequence), anti-GADL1 (Sigma–Aldrich SAB2103888; 1:1000, immunogen 159–208) or anti-GADL1 (Thermo Scientific, Rockford, IL, PA5-13434; 1:100, immunogen 224–254). The Sigma anti-Glutamic Acid Decarboxylase 65/67 (Anti-GAD65/67) antibody from rabbit (G5163, Immunogen human GAD67 amino acids 579–594) was also used (1:10,000). The commercial CSAD antibodies all reacted against the respective MBP fusion proteins, as well as with the cleaved purified enzymes. Although the antibodies were raised against three different immunogens and marketed to be specific against either of these enzymes, they all showed some cross reactivity with the other enzyme (Suppl. Fig. 1). This lack of specificity is also reflected in the recently published Human protein atlas (<http://www.proteinatlas.org/>), where two commercially available antibodies against each of GADL1 and CSAD show multiple protein bands and little internal consistency.

This is in contrast to our custom made sheep CSAD and GADL1 antibodies that were specific for their respective proteins and were judged to be more reliable in studies of tissues with low levels of expression of these proteins. None of the antibodies showed cross reactivity against hGAD1, whereas the commercial antibody raised against GAD67 showed some cross reactivity against both CSAD and GADL1 (Suppl. Fig. 1).

2.9. Imaging and data analysis

Housekeeping genes as GAPDH are being expressed at different levels in the different tissues (Eaton et al., 2013). It is therefore difficult to find an antibody to use as a loading control when comparing different tissues. Using TGX Stain-Free gels (Bio-Rad) we were able to normalize the western blots with total protein as described in Gurtler et al. (Gurtler et al., 2013). CSAD and GADL1 signals were automatically normalized using ImageLab software with either the intensity values of GAPDH or Stain-Free total lane volumes. The normalized datasets were used for the calculation of CSAD/GADL1 levels. In addition, t-tests (double-sided and paired)

were performed with Microsoft Office Excel for Mac 2011 to evaluate the statistical significance of the calculations.

3. Results

Genome databases contain many sequences within the family of the PLP-dependent enzymes, including GAD65 and GAD67, aromatic amino acid decarboxylase (AADC), histidine decarboxylase (HDC), aspartate decarboxylase (ADC), CSAD and GADL1. Although the terminology “GADL1” probably is based upon its sequence similarity to GAD (45–47% amino acid identity), a sequence comparison shows that it is more similar to ADC (49%) and to CSAD (61%) (Fig. 1). The three-dimensional structure of GADL1 is not known. However, the structures of human CSAD (pdb accession code 2JIS), GAD67 and GAD65 (pdb codes 2OKJ and 2OKK, respectively) are deposited in the protein data bank. This information can be used to model the structure of GADL1.

3.1. Homology modeling

A homology model of GADL1 was prepared with CSAD as template in SwissModel <http://www.rcsb.org/pdb/explore/explore.do?structureId=2JIS> (Fig. 2A). The structure of CSAD was solved in complex with the PLP, without substrate present. However, the structures of GAD67 and GAD65 are of the ternary complexes with both cofactor and product (γ -amino-butyric acid, GABA) present in the proposed substrate-binding site. Superimposition of our GADL1 homology model and CSAD with GAD65 and GAD67 thus provided a structural model of GADL1 and CSAD in ternary complex with cofactor and GABA in the postulated substrate-binding site (Fig. 2B and C).

Inspection of this model revealed some amino acid residues that may be critical for enzyme function. A Schiff base linkage (internal aldimine) between PLP and Lys405 of the active site in GAD65 has been described (Fenalti et al., 2007). In our homology model of GADL1 PLP is covalently attached to Lys333. Furthermore, His219 of GADL1 is involved in base stacking with PLP. This residue corresponds to the conserved base-stacking residue His191 in CSAD and His 291 in GAD67 (Qu et al., 1998). This residue is found in two possible conformations in CSAD and the equivalent His in GAD65/67 is postulated to be involved in regulation of enzymatic activity through interactions with the activation loop.

The activation loop of human GAD65 comprises a stretch of 11 residues from Ala432 to Tyr442 (Ala-Gly-Tyr-Leu-Phe-Gln-Pro-Asp-Lys-Gln-Tyr) with Tyr434 being involved in catalysis. This stretch of amino acids corresponds to 361–371 in GADL1 (Ala-Ser-Tyr-Leu-Phe-Gln-Gln-Asp-Lys-Phe-Tyr) including the conserved catalytic tyrosine residue, Tyr363 in GADL1 (corresponding to Tyr335 in human CSAD and Tyr322 in human AADC).

The carboxyl group of the product (GABA) in GAD67 is found to form a salt bridge with Arg567 and a hydrogen bond with Gln190 (Fenalti et al., 2007). These two residues correspond to Arg494 and Gln120 in our homology model and are thus likely to be involved in interactions with the GADL1 substrate. Furthermore, the structure of GAD from *E. coli* in complex with the substrate analogue glutamate points to Thr62 (corresponding to Gln120 in GADL1) as important for substrate binding.

3.2. GADL1 and CSAD form dimers in solution

Using cDNA of the coding reading frame from mouse, the GADL1 and CSAD sequences were cloned into vectors for both mammalian and bacterial expression. The proteins expressed in bacteria were fused to MBP to increase their solubility and facilitate purification. They were expressed and purified as described in Experimental

Procedures. When purifying the proteins on a gel-filtration column after cleavage with TEV, CSAD and GADL1 had apparent molecular masses of 115 kDa and 137 kDa, respectively, suggesting that they are both present as dimers. Although both proteins have a tendency to aggregate in solution, it appears that GADL1 has the highest solubility (results not shown). When analyzed on SDS-PAGE, CSAD and GADL1 appear at almost the same molecular weight, i.e. as 99 kDa as fusion proteins (MBP-CSAD or MBP-GADL1) or as cleaved proteins at 56 kDa (CSAD) and 59 kDa (GADL1), respectively (MBP has a molecular weight of 45 kDa) (Suppl. Fig. 1).

3.3. GADL1 and CSAD have overlapping substrate specificities

When we performed activity assays with the standard proteogenic amino acids and some abundant occurring dicarboxylic acids as substrates for CSAD, GAD and GADL1, few compounds displayed significant activity with either enzyme (Suppl. Table 3). However, cysteic acid (CA), homocysteic acid, CSA and Asp were decarboxylated by both GADL1 and CSAD at different rates (Fig. 3, Table 1 and data not shown). Notably, no production of GABA from glutamate was observed for either CSAD or GADL1, whereas, as expected, GAD catalyzed this reaction (data not shown). These data suggest that mouse CSAD and GADL1 are more similar to each other than they are to GAD, as the sequence comparison also suggests (Fig. 1).

3.4. Kinetic properties of CSAD and GADL1

Using different concentrations of CSA and Asp, we determined the kinetic properties of CSAD and GADL1 (Table 1). Whether analyzed as fusion proteins with MBP or as pure, cleaved enzymes, the activity towards CSA was higher for CSAD than for GADL1 ($p = 0.0001$), whereas GADL1 had much higher V_{max} values than CSAD for decarboxylation of Asp ($p = 0.003$). For both substrates, the fusion proteins and the purified cleaved enzymes had similar K_m values, but the V_{max} values were highest for the pure decarboxylases. Using CSA as substrate, the specificity constants (K_{cat}/K_m) were much higher for CSAD than for GADL1, whereas the opposite was true using Asp as substrate. The K_m value for decarboxylation of

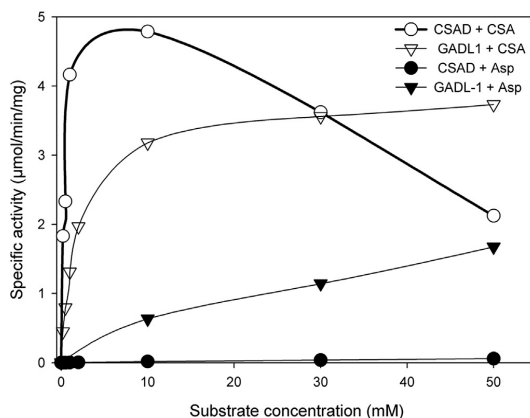


Fig. 3. Substrate dependence and inhibition of CSAD and GADL1. Substrate dependence of purified GADL1 (triangles) and CSAD (circles) using CSA (open symbols) or Asp (filled symbols) as substrates ($n = 10$). The assay was performed as described above at 37 °C for 60 min and stopped by addition of equal volume of ice-cold ethanol with 5% acetic acid.

Table 1
Kinetic parameters of recombinant CSAD and GADL1 using CSA and aspartate as substrates. Activity assays were performed as described in the method-section. The results are presented as means \pm S.E.M. of three separate measurements using different enzyme preparations. The kinetic values were calculated based on predicted subunit masses of 55 kDa (493 aa) for mouse CSAD, 57 kDa (502 aa) for mouse GADL1, 100 kDa for mouse MBP CSAD and 102 kDa for MBP GADL1. Human CSAD has a predicted mass of 55,023 kDa (493 aa) and human GADL1 is predicted to be 59 246 kDa (521 aa). *Substrate inhibition, K_{SI} CSA: 26 \pm 10 mM for cleaved CSAD.

		CSA (0–50 mM)				Aspartate (0–50 mM)			
Enzyme form		V _{max} (μmol/min/mg)	K _m (mM)	k _{cat} (s ⁻¹)	k _{cat} /K _m (mM ⁻¹ s ⁻¹)	V _{max} (μmol/min/mg)	K _m (mM)	k _{cat} (s ⁻¹)	k _{cat} /K _m (mM ⁻¹ s ⁻¹)
Fusion	CSAD	0.33 \pm 0.046*	0.14 \pm 0.11	0.55	3.9	0.025 \pm 0.003	23.0 \pm 6.7	0.04	0.0017
	proteins	GADL1	0.74 \pm 0.055	1.74 \pm 0.56	1.3	0.75	0.66 \pm 0.02	21.3 \pm 1.5	1.2
Cleaved	CSAD	7.22 \pm 1.26*	0.20 \pm 0.06	6.6	33	0.16 \pm 0.027	93 \pm 32	0.14	0.0015
	proteins	GADL1	3.84 \pm 0.034	1.12 \pm 0.06	3.6	0.94	1.41 \pm 0.10	31.7 \pm 4.7	1.3

CSA by recombinant mouse CSAD (0.14–0.20 mM) was similar to that reported for purified rat liver CSAD (0.17 mM) (Guion-Rain and Chatagner, 1972). Although the K_m value for decarboxylation of CSA by mouse GADL1 (1.12–1.74 mM) was similar to recently reported values for human GADL1 (1.14 mM) (Liu et al., 2012), the mouse enzymes had 2–3 fold higher specific activities (Table 1). Interestingly, the K_m values were much higher and the specificity constants for decarboxylation of Asp were much lower for mouse GADL1 and CSAD than reported for the recombinant human GADL1 (Liu et al., 2012). A comparison of these constants revealed that compared to GADL1, CSAD had a 1000-fold higher selectivity towards CSA. A pronounced substrate inhibition by CSA was apparent for CSAD (K_{SI} = 26 \pm 10 mM), but this was not observed for GADL1 in this substrate concentration range (Fig. 3). Both GADL1 and CSAD catalyzed decarboxylation of CA to taurine, at rates of 12–13% of that observed for the conversion of CSA to hypotaurine (data not shown). Using equimolar concentrations of CA and CSA (1 mM), CA decarboxylation by the competing substrate was inhibited by 49–56% for both enzymes, while the CSA decarboxylation was inhibited by only 5–15% for GADL1 and CSAD, respectively; illustrating that CSA is the preferred substrate for both enzymes.

3.5. Effects of metal ions

As reported for pig brain CSAD (Tang et al., 1996), mouse CSAD was activated by addition of manganese ions (52% stimulation in the presence of 0.4 mM MnCl₂, p = 0.003), but this effect was not present for GADL1 using similar assay conditions. The enzyme activities of CSAD and GADL1 were essentially unaffected by Li⁺ using final concentrations of LiCl from 0.05 to 40 mM, however, for GADL1 a weak stimulation was observed in the presence of 0.2–0.4 mM Li⁺ (p = 0.03) (Fig. 4A).

3.6. Inhibitors of CSAD and GADL1

To further characterize the substrate and inhibitor specificities of GADL1 and CSAD, we performed *in silico* docking into the active site of CSAD of a subset of the ZINC database of different compounds [28] and tested the top 20 compounds *in vitro*. As shown in Table 2 and Fig. 4B, bis-carboxymethyl-trithiocarbonate (Compound A) was the compound with highest affinity for both enzymes (K_i \approx 70 and 60 μM for CSAD and GADL1, respectively). Removing the two terminal carboxyl oxygens and substituting the adjacent thioether into an ether increased the selectivity for GADL1 over CSAD (compound B). Removing the central thioketone of Compound A gave rise to Compound C with selectivity for CSAD over GADL1, although at a significantly lower affinity for both. Compound E was the most selective CSAD inhibitor of the compounds tested. Although none of the compounds were potent inhibitors of either enzyme, their relative selectivity might be exploited to produce even more specific compounds.

Glutamate was completely inactive as inhibitor of either CSAD

or GADL1, indicating that none of these enzymes are involved in glutamate metabolism. In contrast to the recently reported insensitivity of CSAD towards inhibition by L-cysteine [40], the latter compound completely inhibited the CSAD activity (>95%) of both

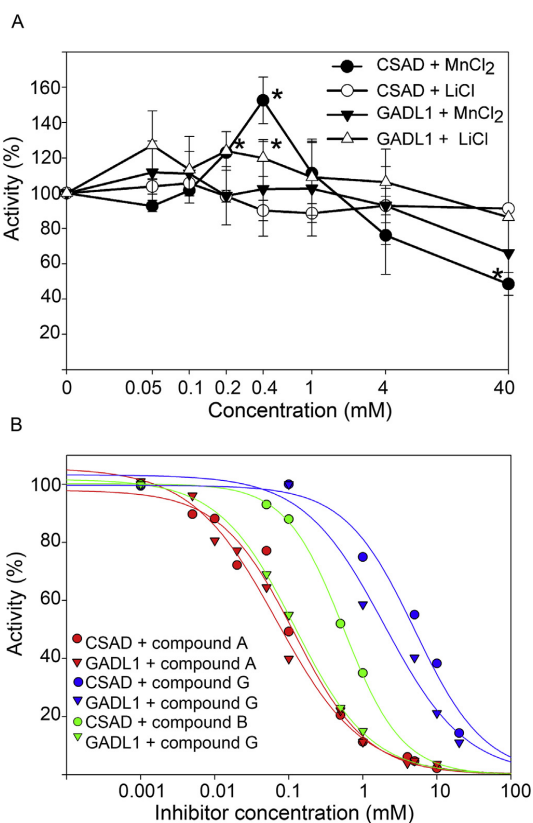
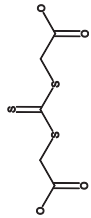
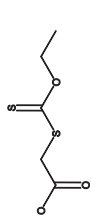

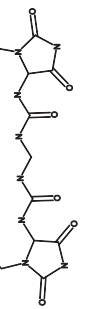
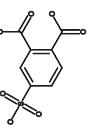
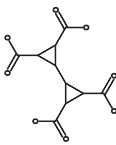
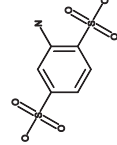
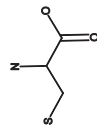


Fig. 4. A. Effect on CSAD (circles) and GADL1 (triangles) by MnCl₂ (closed symbols) and LiCl (open symbols). * Significantly different from control (t-test, p < 0.05). Data are expressed as average \pm STDEV (n = 3) B Inhibition of CSAD (circles) and GADL1 (triangles). The different compounds used are Bis-(carboxymethyl)-trithiocarbonate (Red, compound A), Ethylxanthogenacetic acid (Green, compound B) and 2,5-disulfoaniline (Blue, compound G). Different concentrations of the compounds were tested (0.05–40 mM for the salts and 0.001–50 mM for the inhibitors) using a standard concentration of CSA (100 μM). The assay was performed as described above at 37 °C for 60 min and stopped by addition of equal volume of ice-cold ethanol with 5% acetic acid. Data are expressed as average \pm STDEV (n = 3).

Table 2
 Specificity of CSAD and GADL1 inhibitors. Different concentrations of the inhibitors were tested (0.1–50 mM). The assay was performed as described above at 37 °C for 60 min and stopped by addition of equal volume of ice-cold ethanol with 5% acetic acid.

Compound	Name	Zinc ^a	CSAD IC ₅₀ ± S.E. (mM)	GADL1 IC ₅₀ ± S.E. (mM)	CSAD K _i ± S.E. (mM)	GADL1 K _i ± S.E. (mM)	Selectivity	2D structure
A	Bis-(carboxymethyl)-trithiocarbonate	01661333	0.12 ± 0.029	0.068 ± 0.013	0.07 ± 0.04	0.06 ± 0.03	1.09	
B	Ethykantothenic acid	01760604	0.43 ± 0.23	0.098 ± 0.012	0.25 ± 0.28	0.09 ± 0.02	2.71	
C	Methylenebis thioglycolic acid	01635711	1.6 ± 0.53	2.7 ± 0.21	0.93 ± 0.66	2.55 ± 0.44	0.36	
D	Imidazolidinyl urea	04245708	2.72 ± 0.92	1.30 ± 0.52	1.59 ± 1.14	1.23 ± 1.00	1.29	
E	4 sulfophthalic acid	01693949	0.97 ± 0.3	7.4 ± 0.94	0.57 ± 0.37	7 ± 1.89	0.08	
F	Bi(cyclopropane)-2,2,3,3 tetracarboxylic acid	25722391	7.3 ± 1.3	10.0 ± 0.35	4.26 ± 1.68	9.46 ± 0.81	0.45	
G	2,5-disulfaniline	01687023	5.3 ± 1.0	2.4 ± 0.6	3.09 ± 1.29	2.27 ± 1.17	1.36	
H	L-cysteine	00895042	1.44 ± 0.45	0.92 ± 0.10	0.84 ± 0.56	0.87 ± 0.20	0.97	

^a Accession number in Zinc database (Irwin et al. 2012)

GADL1 and CSAD at concentrations above 10 mM. Kinetic studies showed that the inhibitors were competitive against CSA (data not shown). Furthermore, as the most potent inhibitors were substrate analogs and the inhibition constants were unaffected by 10-fold dilution of target enzyme or the addition of 0.1 mg BSA in the assay, they probably inhibit GADL1 and CSAD by binding to the enzymes' active sites. It is unlikely that the enzyme inhibition is due to the formation of colloidal aggregates by the inhibitors (Feng et al., 2007), or other non-specific effects.

3.7. CSAD and GADL1 expression patterns

The tissue distribution of CSAD has been controversial (Tang et al., 1996; Tappaz et al., 1999; Vitvitsky et al., 2011). Since many studies were done before the discovery of GADL1, it was important to establish whether the reported discrepancies could be due to contamination of CSAD preparations with GADL1. For this purpose, we systematically compared the mRNA and protein levels for CSAD and GADL1 in mouse tissues. The mRNA levels were determined by real-time reverse transcriptase (RT)-PCR quantification using specific DNA probes (Suppl. Table 1). As shown in Fig. 5A, the level of CSAD mRNA was much higher in mouse liver and kidney than in total brain extracts ($4 (p = 1 \times 10^{-6})$ and 7 times ($p = 4 \times 10^{-10}$)

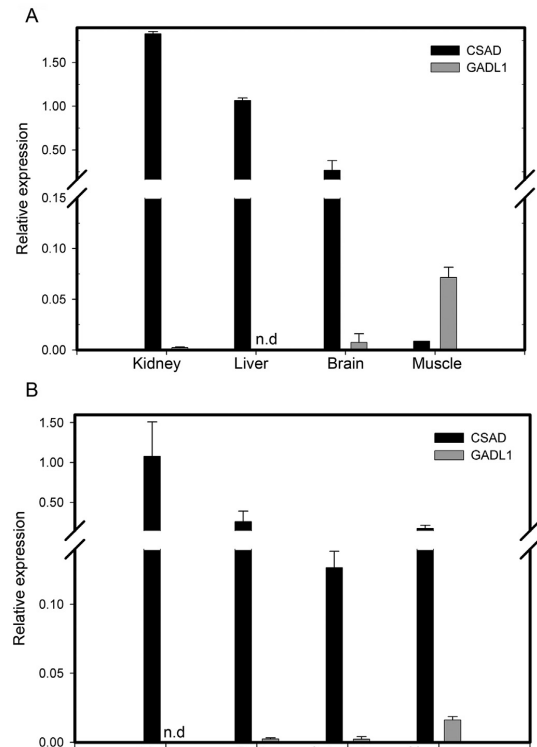


Fig. 5. Gene expression of CSAD and GADL1 in different tissues. **A** Adult mouse tissues. **B** Adult human tissues. Total poly-A + RNA was reverse transcribed and the cDNA amplified by real-time PCR using specific primers for CSAD or GADL1. The PCR products were detected with TaqMan[®] detection assay. PCR values were normalized to those produced with primers for GAPDH and β -actin and presented as average \pm STDEV ($n = 3$). All values were significantly different between tissues and proteins ($p < 0.05$).

higher, respectively), and almost no CSAD mRNA was detected in the muscle, as reported previously (Ide et al., 2002; Park et al., 2002; Raymond et al., 2000). For GADL1 only low levels of mRNA were observed in adult brain compared with CSAD ($p = 0.001$), but was not detected in liver and kidney samples. However, in contrast to CSAD, mRNA of GADL1 was detected in skeletal muscle ($p = 0.005$), as was also reported by Liu et al. (Liu et al., 2012). These results were also confirmed by western blot experiments (Fig. 6), although the amount of CSAD detected in kidney was lower than in brain and liver ($p = 0.01$ and 0.0005).

Although taurine is found in both astrocytes and neurons, CSAD is more abundant in non-neuronal cells (Tappaz et al., 1998). It has been proposed that astrocytes produce taurine via CSAD, while

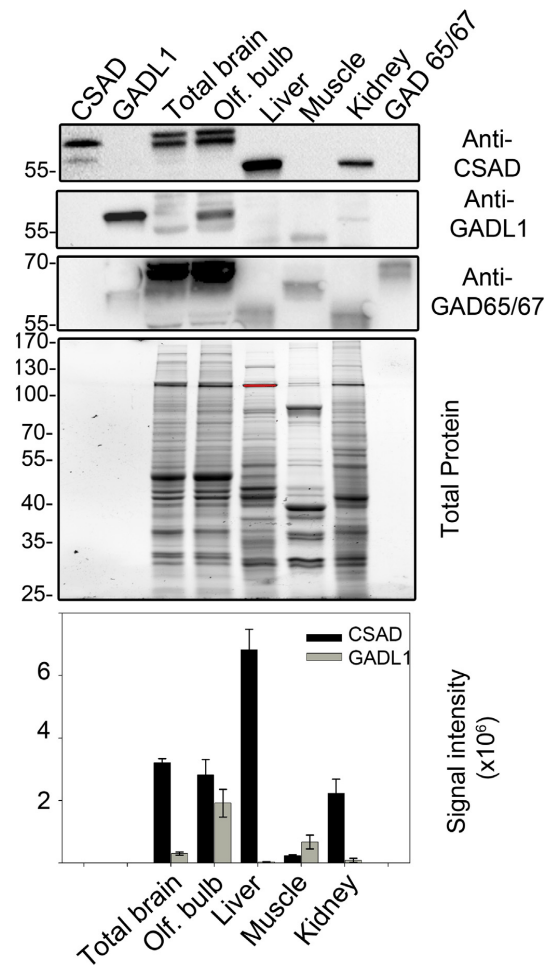


Fig. 6. Protein expression of CSAD and GADL1 in different tissues. Representative western blot image of CSAD, GADL1 and GAPDH in mouse brain, olfactory bulb, liver, muscle and kidney (20 μ g, 3 weeks old, $n = 3$). Recombinant mCSAD, mGADL1 and hGAD1 were used as controls. A representative image of the stain free gel is shown under the immunoblots showing the total protein in the samples. The signals from 3 different samples are expressed as average \pm STDEV in the bar chart. * Significantly different $p < 0.05$. Signals were normalized against both GAPDH and total protein (using stain-free gels from Bio-Rad).

neurons synthesizes taurine via the cysteamine dioxygenase pathway (Vitvitsky et al., 2011). To examine whether CSAD or GADL1 could be involved in taurine biosynthesis in either neurons or astrocytes, CSAD and GADL1 mRNA levels were measured in both cell types. As shown in Fig. 5B, CSAD was expressed at lower levels in human astrocytes than in neuronal cells ($p = 0.0001$), whereas GADL1 was only expressed in neuronal cells. Although the level of GADL1 mRNA was six-fold lower than those of CSAD ($p = 1 \times 10^{-7}$), this enzyme might account for some of the CSAD-activity in neurons (Vitvitsky et al., 2011). The Human Protein Atlas <http://www.proteinatlas.org/> also shows that both proteins are mainly present in neurons. It also indicates the presence of GADL1 in astrocytes in certain tissues such as hippocampus and cerebral cortex. However, these results are uncertain as the antibody used in their study also showed cross reactivity towards CSAD (results not shown).

Publicly available databases, such as the Allen Brain Atlas (<http://www.brain-map.org/>), were also consulted to study the *in situ* RNA hybridization patterns of GAD65/67, CSAD, and GADL1. A comparison of their expression levels showed that although GAD65/67 and CSAD in general are expressed at higher levels than GADL1, certain brain regions, such as the olfactory bulb, have higher levels of GADL1 than CSAD (Suppl. Fig. 2A). At protein levels, GADL1 appeared to be expressed at the same level as CSAD in the olfactory bulb, but at very low levels in total brain lysates ($p = 0.003$) (Fig. 6).

3.8. Developmental pattern of CSAD and GADL1 in mouse brain

In some tissues, CSAD expression has been reported to increase with age (Tappaz et al., 1998), while in zebrafish an important role of CSAD in early embryogenesis was recently reported (Chang et al., 2013). To investigate the pattern of GADL1 and CSAD expression during development and compare it with GAD expression, we immunoblotted total brain extracts from mice at 11 different ages, from embryonic day 17 (E17) to 12 months. As shown in Fig. 7A, striking differences were observed between the staining patterns of the three antibodies. CSAD expression decreased with age, whereas the expression of GAD increased and was strongest in adult brain, consistent with its reported developmental pattern (Kim et al., 2006; Ohkuma et al., 1986). However, when using specific antibodies for GADL1, three weak bands were visible; a high molecular weight species (65 kDa), that had similar developmental pattern as CSAD, and two bands at 58–60 kDa that gradually disappeared after E17. This protein intensity pattern corresponds well with mRNA levels from the Human Brain transcriptome database (<http://hbatlas.org/>), as shown in Suppl. Fig. 2B (Kang et al., 2011). Although the detection of GADL1 in the total brain lysate was weak, we cannot rule out the presence of the protein in specific parts of the brain, such as was seen in the olfactory bulb.

3.9. Cross-species characterization of brain CSAD and GADL1

CSAD purified from many sources and species has been reported with subunit molecular masses of 43, 51, 53, or 55 kDa (Pasantes-Morales et al., 1976; Skoldberg et al., 2004; Tang et al., 1996; Weinstein and Griffith, 1987; Wu, 1982). To examine cross-species reactivity of the CSAD antibodies, and compare their protein levels, total brain homogenates from 14 different species of adult age were analyzed by western blotting (Fig. 7B). Consistent with the strong sequence similarities between mammalian CSAD enzymes, comparable labeling intensity was obtained for most of these species. Only one major CSAD band appeared at around 58 kDa (Fig. 7B). In accordance with the low abundance and mainly embryonic expression pattern of GADL1 expression, much weaker bands appeared when the same samples were analyzed with anti-GADL1 antibodies, making the comparison of this enzyme across

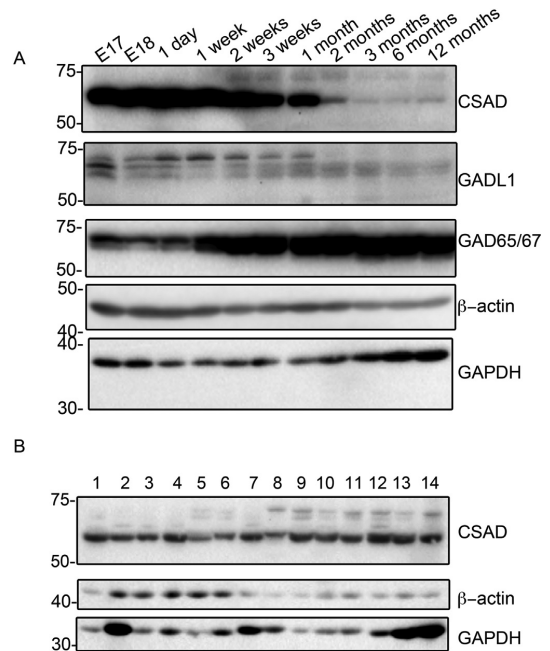


Fig. 7. Protein expression of CSAD and GADL1 in brain. **A** Representative western blot image of CSAD, GADL1, GAD65/67 and Beta-actin/GAPDH in total brain lysates (70 μ g) from mice at different developmental stages and different ages (embryonic day 17 to 12 months old, Zyagen Laboratories). **B** Representative western blot image of CSAD and Beta-actin/GAPDH in total brain lysates (70 μ g) from 14 different species (Zyagen Laboratories) using custom-made CSAD antibody. 1. Human (55 years), 2. Mouse (10 weeks), 3. Rat (10 weeks), 4. Dog (2 years), 5. Rabbit (15 weeks), 6. Guinea Pig (15 weeks), 7. Hamster (10 weeks), 8. Chicken (1 year), 9. Bovine (3 years), 10. Sheep (3.5 years), 11. Porcine (3 years), 12. Equine (5 years), 13. Monkey Cynomolgus (4 years), 14. Mini Pig (2 years).

species more subject to ambiguity (results not shown).

4. Discussion

Here we report a systematic comparison of murine CSAD and GADL1 structures, biochemical properties and tissue expression patterns.

4.1. Biochemical properties of CSAD and GADL1

In order to characterize these two proteins we first developed a new expression and purification protocol. Although both enzymes appeared to have a preference for decarboxylation of CSA, they were also active against other substrates, with different substrate specificities and sensitivity towards inhibitors. Glutamate was completely inactive as substrate or inhibitor of either CSAD or GADL1, indicating that none of these enzymes are involved in glutamate metabolism. Thus, it is also unlikely that the observed strong association between genetic variants GADL1 and response to lithium treatment ($p = 2.52 \times 10^{-37}$) is related to altered production of the inhibitory transmitter γ -aminobutyric acid, as recently suggested (Chen et al., 2014). The effects of metal ions on the enzyme activities were tested using a wide range of concentrations including the therapeutic range of Li^+ used in human pharmacotherapy. The minimal effect of lithium on either CSAD or GADL1

activity further argues against a direct relationship between GADL1 genetic variants and the response to lithium therapy. As lithium is eliminated via kidneys, it has been speculated that the association between GADL1 variants and response to lithium therapy could be mediated by renal GADL1 (Birnbaum et al., 2014). However, as the response to lithium therapy was independent on renal clearance of lithium (Chen et al., 2014) and the kidney levels of GADL1 are very low, we consider this to be unlikely.

Alternative substrates and physiological functions of GADL1 should also be considered. The decarboxylation product of Asp (β -alanine) produced by GADL1 or CSAD (Fig. 3) is a constituent of the dipeptide carnosine. As for taurine, carnosine and its metabolic derivatives may have antioxidant properties and are found in many tissues, including muscle and brain (Boldyrev and Abe, 1999). A role of GADL1 in carnosine production was supported by recent genome wide association studies showing a strong association between human blood levels of N-acetyl carnosine and variants in the GADL1 gene ($p = 3.4 \times 10^{-18}$ for rs7643891) (Shin et al., 2014). Indeed, the tissue distribution of GADL1 seems to be compatible with a physiological role of carnosine in muscle and possibly also brain function. The role of β -alanine in brain function is less clear. However, it is interesting that the plasma levels of this amino acid is altered by selective serotonin reuptake inhibitors, indirectly linking it to brain (dys)function (Woo et al., 2015).

4.2. Expression of CSAD and GADL1

The most striking difference between the enzymes was found in their patterns of tissue expression of both mRNA and protein, where GADL1 was mainly found in muscle and brain, in particularly olfactory bulb, and CSAD was found in liver, kidney and brain tissues, confirming previous reports (Guion-Rain and Chatagner, 1972; Liu et al., 2012; Park et al., 2014, 2002; Reymond et al., 1996a; Reymond et al., 2000; Tang et al., 1996; Tappaz et al., 1994, 1998; Weinstein and Griffith, 1987).

The recent observations that human (Liu et al., 2012) and mouse GADL1 decarboxylate CSA at comparable rates to CSAD (Table 1), raised the possibility that the enzyme "CSADII" described by Tang and coworkers (Tang et al., 1996) is identical to GADL1. This would explain the reported discrepancies between CSAD enzyme activity and mRNA levels in different tissues (Tappaz et al., 1999). However, the low expression levels of GADL1 in adult neurons (Table 3, Fig. 5) indicate that this enzyme probably cannot account for much of the CSAD activity previously reported (Tang et al., 1996; Tappaz et al., 1999). The relative expression levels and catalytic activities of CSAD and GADL1 are in accordance with the recent study of Park et al., who found that CSAD knockout mice had a 83% reduction of plasma taurine levels and a similar reduction in liver and brain taurine levels in offspring of CSAD $-/-$ mice (Park et al., 2014). Based on our estimates of catalytic activity and expression levels, GADL1 probably accounts for a small fraction of the remaining

CSAD activity in CSAD knockout mice, while cysteamine dioxygenase (EC 1.133.11.19) also may contribute to taurine synthesis.

Weinstein and Griffith reported that there was almost no detectable CSAD mRNA in the brain, whereas they could still measure enzyme activity (Weinstein and Griffith, 1987). It was explained by fast turnover of the mRNA, but it could also be due to the existence of several CSAD enzymes with different mRNA sequences (Suppl. Table 2). Western blotting revealed multiple molecular species. This could be due to alternatively spliced variants, as there is evidence for alternative splicing for CSAD and GADL1. The identity and roles of such putative splice variants should be further investigated.

Taurine has mainly been detected in neurons in the cerebellum and hippocampus (Ottersen et al., 1988; Zhang and Ottersen, 1992), and more in fetal tissues than in adults (Terauchi et al., 1998). However, it is unclear whether biosynthesis of taurine occurs exclusively in neurons or glial cells, or both cell types. The use of different antisera may have contributed to the diverging results reported from different research groups. Chan-Palay and coworkers found an exclusive localization of CSAD in rat neurons (Chan-Palay et al., 1982), results that were later confirmed by others (Kuriyama et al., 1985; Magnusson et al., 1988; Ohkuma et al., 1986; Taber et al., 1986; Wu et al., 1987). However, other research groups were not able to detect CSAD in neurons, only in astrocytes (Reymond et al., 1996b; Tappaz et al., 1992). There are several theories for these results. It was recently proposed that taurine is independently produced from cysteine by either astrocytes or neurons (Vitvitsky et al., 2011), while previous reports indicated that taurine is produced by a cooperative exchange of taurine precursors between astrocytes and neurons as each cell type contains incomplete but complementary components of this pathway (Dominy et al., 2004).

As commercially available antibodies against CSAD do not fully discriminate between CSAD and GADL1, the finding of CSAD in both neurons and astrocytes could potentially be due to cross-reactivity. However, the RT-PCR data reported here using gene specific probes establish that CSAD is present in both neurons and astrocytes, consistent with the view that taurine biosynthesis takes place independently in both neurons and astrocytes, and that this activity cannot be attributed to GADL1, as very low levels of GADL1 were detected in neurons, and not in astrocytes (Table 3, Fig. 5B). However, although our data suggest an expression of GADL1 only in the neurons, The Human Protein Atlas suggest protein expression in both neurons and glia cells. Non-specific antibodies, as previously discussed, could explain these discrepancies.

4.3. Developmental patterns

Our mRNA and protein measurements were compared with data deposited in the Allen Brain Atlas (<http://www.brain-map.org/>) and The Human Protein Atlas (<http://www.proteinatlas.org/>). They confirm that the PLP-dependent decarboxylases GADL1, CSAD, GAD65 and GAD67 all have different expression patterns in humans, as well as in mice, which is consistent with distinct physiological roles of these proteins. In particular, CSAD and GADL1 have strikingly different patterns of expression in the human brain, where mRNA levels of GADL1 are lower than CSAD in most brain regions, except olfactory cortex and ventral striatum (Fig. 7A). In the latter region, GADL1 mRNA levels appear to be almost 10 fold higher than for CSAD, indicating a specific physiological role of GADL1 in these structures. Our data also suggest that levels of RNA and protein are lower for GADL1 than for CSAD in most human and mouse tissues (Figs. 5 and 6), except for muscle and olfactory bulb. This is consistent with data in the databases Braineac (www.braineac.org/), Allen Brain Atlas and The Human Protein Atlas.

Table 3

Gene Expression assay with different mouse and human tissues. Total RNA from different tissues was analyzed using RT-PCR and normalized against GAPDH. Results are average \pm stdev for three preparations.

Species	Tissue	CSAD (Δ CtGAPDH)	GADL1 (Δ CtGAPDH)
Human	Brain	-8.07 \pm 0.78	-14.73 \pm 0.47
	Liver	-5.96 \pm 0.61	n.d.
	Astrocytes	-9.02 \pm 0.08	-15.56 \pm 0.36
	Neurons	-8.33 \pm 0.44	-11.9 \pm 0.54
Mouse	Brain	-8.06 \pm 0.62	-13.83 \pm 1.45
	Liver	-6.04 \pm 0.55	n.d.
	Kidney	-5.17 \pm 0.02	-14.86 \pm 0.42
	Muscle	-12.93 \pm 0.24	-9.85 \pm 0.15

The presence of GADL1 in olfactory bulb is particularly interesting as taurine is known to be abundant in this brain structure, exceeding glutamate and GABA in concentration, and has been shown to be important in early stages of olfactory maturation (Steullet et al., 2000).

The highest level of human CSAD mRNA is found during prenatal development, with a maximum around 17 weeks post conception (pcw), although it is also detected in many brain regions in adults (Ohkuma et al., 1986). In contrast, GADL1 appears to be exclusively expressed in brain cortical areas during embryonic development, with highest levels during 12–14 pcw. Except for these weeks, CSAD had a much higher level of expression than GADL1 (Brainspan and Human Brain Atlas). CSAD appears to have the highest level in the intermediate zone, important for neural migration, whereas GADL1 has the highest level in the subplate zone, important in establishing correct wiring and functional maturation of the cerebral cortex. The subplate neurons disappear during postnatal development, and this could explain the low levels of GADL1 in adult brain. When analyzing lysates from total mouse brain, we obtained similar results (Fig. 7A), although three lanes of protein bands were observed. These protein bands could indicate different splice variants. This has not previously been investigated for GADL1, although it has been reported that alternative splicing is frequent during early embryonic development in mice (Revil et al., 2010). Distinct developmental patterns of expression have also been described for other PLP-dependent decarboxylases, such as GAD67 (as shown in Fig. 7A) and AADC (Blechingberg et al., 2010; Liu et al., 2010). Temporal and organ specific splicing events, resulting in many different mRNA and protein species from these genes, indicates a fine tuned physiological regulation of expression, but has also complicated previous studies of these enzymes (Blechingberg et al., 2010; Liu et al., 2010).

4.4. Animal models

The physiological roles of CSAD and particularly GADL1 are not well established. It was recently reported that CSAD is expressed during early embryonic development of the Zebrafish and that knockdown of *Csad* significantly reduced embryonic taurine levels, leading to increased early mortality and cardiac abnormalities (Chang et al., 2013). This is in line with previous studies on taurine transporter (TauT) knockout mice, which showed abnormalities of kidney, liver, brain, retina and olfactory function (Warskulat et al., 2007). In contrast, the CSAD knockout mice had a less severe phenotype (Park et al., 2014).

Unlike CSAD, GADL1 is absent from the Zebrafish genome. Considering the predominantly embryonic pattern of GADL1 expression observed in mice and humans, it is tempting to speculate that GADL1 may have a specific role during embryonic development and that this evolutionary more recent enzyme has replaced some CSAD function in early brain development.

Selective knockdown and knockout studies of GADL1 in combination with CSAD may be needed to resolve the metabolic role of these enzymes. However, since both *CSAD* and *GADL1* appear to be transcribed to multiple tissue-specific transcripts with different in-frame start codons, comprehensive knockdown experiments of these enzymes may be technically challenging (Chang et al., 2013).

4.5. PLP-dependent decarboxylases in human disease

Several PLP-dependent decarboxylases act as autoantigens in different autoimmune disorders, e.g. GAD65 in type 1 diabetes (Baekkeskov et al., 1990), GAD65 and GAD67 in the neurological condition Stiff Person Syndrome (Bjork et al., 1994), and AADC (Rorsman et al., 1995), histidine decarboxylase and CSAD

(Skoldberg et al., 2004) in APS-1. Interestingly, autoantibodies typically recognize evolutionary conserved epitopes on these enzymes and act as strong inhibitors of the enzymatic activity, presumably by binding to epitopes close to the substrate binding or active sites of the enzymes targeted. We have previously observed that serum from a subgroup of APS-1 patients (3 out of 83 individuals) contain antibodies reacting with both CSAD (Skoldberg et al., 2004) and GADL1 protein produced from a mouse cDNA library (data not shown). Although APS-1 patients with these autoantibodies have multiple autoimmune manifestations, it is unclear whether they have any pathogenic significance.

5. Conclusion

Purified murine CSAD and GADL1 both decarboxylate CSA, CA, homocysteic acid and Asp, although with very different affinities. However, we cannot rule out that these enzymes may have still other physiological substrates. The novel enzyme inhibitors identified by *in silico* and *in vitro* screening had relatively low affinities, but could be used as templates to obtain more selective compounds. The two proteins are located in different tissues. The possible role GADL1 in olfactory bulb and embryonic brain development should be investigated further.

Acknowledgments

Sidsel Riise and Guri Matre are thanked for expert technical assistance. Per M. Knappskog is thanked for valuable discussions. This work was supported by the Research Council of Norway, The Swedish Research Council, Western Norway Regional Health Authority (Grant number 911972) and K.G. Jebsen Foundation.

Appendix A. Supplementary data

Supplementary data related to this article can be found at <http://dx.doi.org/10.1016/j.neuint.2015.08.013>.

References

- Baekkeskov, S., Aanstoot, H.J., Christgau, S., Reetz, A., Solimena, M., Cascalho, M., et al., 1990. Identification of the 64K autoantigen in insulin-dependent diabetes as the GABA-synthesizing enzyme glutamic acid decarboxylase. *Nature* 347, 151–156.
- Bigard, A.X., 2010. Risks of energy drinks in youths. *Arch. Pediatr. Organe Off. Soc. française Pédiatr.* 17, 1625–1631.
- Birnbaum, R., Shin, J.H., Weinberger, D., 2014. Variant GADL1 and response to lithium in bipolar I disorder. *N. Engl. J. Med.* 370, 1855–1856.
- Bjork, E., Velloso, L.A., Kampe, O., Karlsson, F.A., 1994. GAD autoantibodies in IDDM, stiff-man syndrome, and autoimmune polyendocrine syndrome type I recognize different epitopes. *Diabetes* 43, 161–165.
- Blechingberg, J., Holm, I.E., Johansen, M.G., Borglum, A.D., Nielsen, A.L., 2010. Aromatic l-amino acid decarboxylase expression profiling and isoform detection in the developing porcine brain. *Brain Res.* 1308, 1–13.
- Boldyrev, A., Abe, H., 1999. Metabolic transformation of neuropeptide carnosine modifies its biological activity. *Cell Mol. Neurobiol.* 19, 163–175.
- Chan-Palay, V., Palay, S.L., Wu, J.Y., 1982. Sagittal cerebellar microbands of taurine neurons: immunocytochemical demonstration by using antibodies against the taurine-synthesizing enzyme cysteine sulfonic acid decarboxylase. *Proc. Natl. Acad. Sci. U. S. A.* 79, 4221–4225.
- Chang, Y.C., Ding, S.T., Lee, Y.H., Wang, Y.C., Huang, M.F., Liu, I.H., 2013. Taurine homeostasis requires de novo synthesis via cysteine sulfonic acid decarboxylase during zebrafish early embryogenesis. *Amino Acids* 44, 615–629.
- Chen, C.H., Lee, C.S., Lee, M.T., Ouyang, W.C., Chen, C.C., Chong, M.Y., et al., 2014. Variant GADL1 and response to lithium therapy in bipolar I disorder. *N. Engl. J. Med.* 370, 119–128.
- Cristiana, C., Martin, A., Patrick, A.D., Gustavo, T., Guy, A.R., 2015. No evidence for GADL1 variation as a bipolar disorder susceptibility factor in a caucasian lithium-responsive cohort. *Am. J. Psychiatry* 172, 94–95.
- Dominy, J., Eller, S., Dawson Jr., R., 2004. Building biosynthetic schools: reviewing compartmentation of CNS taurine synthesis. *Neurochem. Res.* 29, 97–103.
- Eaton, S.L., Roche, S.L., Llaverro Hurtado, M., Oldknow, K.J., Farquharson, C., Gillingwater, T.H., et al., 2013. Total protein analysis as a reliable loading control for quantitative fluorescent Western blotting. *PLoS One* 8, e72457.

- Renalti, G., Law, R.H., Buckle, A.M., Langendorf, C., Tuck, K., Rosado, C.J., et al., 2007. GABA production by glutamic acid decarboxylase is regulated by a dynamic catalytic loop. *Nat. Struct. Mol. Biol.* 14, 280–286.
- Feng, B.Y., Simeonov, A., Jadhav, A., Babaoglu, K., Inglese, J., Shoichet, B.K., et al., 2007. A high-throughput screen for aggregation-based inhibition in a large compound library. *J. Med. Chem.* 50, 2385–2390.
- Friesner, R.A., Banks, J.L., Murphy, R.B., Halgren, T.A., Klicic, J.J., Mainz, D.T., et al., 2004. Glide: a new approach for rapid, accurate docking and scoring. I. Method and assessment of docking accuracy. *J. Med. Chem.* 47, 1739–1749.
- Friesner, R.A., Murphy, R.B., Repasky, M.P., Frye, L.L., Greenwood, J.R., Halgren, T.A., et al., 2006. Extra precision glide: docking and scoring incorporating a model of hydrophobic enclosure for protein-ligand complexes. *J. Med. Chem.* 49, 6177–6196.
- Guex, N., Peitsch, M.C., 1997. SWISS-MODEL and the Swiss-PdbViewer: an environment for comparative protein modeling. *Electrophoresis* 18, 2714–2723.
- Guion-Rain, M.C., Chatagner, F., 1972. Rat liver cysteine sulfinate decarboxylase: some observations about substrate specificity. *Biochim. Biophys. Acta* 276, 272–276.
- Gurtler, A., Kunz, N., Gomolka, M., Hornhardt, S., Friedl, A.A., McDonald, K., et al., 2013. Stain-Free technology as a normalization tool in Western blot analysis. *Anal. Biochem.* 433, 105–111.
- Heinamaki, A.A., Perama, A.K., Pihä, R.S., 1982. Characterization of cerebral cysteine sulfonic acid decarboxylase. Molecular parameters and inhibition studies. *Acta Chem. Scand.* B 36, 287–290.
- Hernandez-Benitez, R., Pasantes-Morales, H., Saldana, I.T., Ramos-Mandujano, G., 2010. Taurine stimulates proliferation of mice embryonic cultured neural progenitor cells. *J. Neurosci. Res.* 88, 1673–1681.
- Hoffmann, E.K., Pedersen, S.F., 2006. Sensors and signal transduction pathways in vertebrate cell volume regulation. *Contrib. Nephrol.* 152, 54–104.
- Ide, T., Kushi, M., Takahashi, Y., Shinohara, K., Cha, S., 2002. mRNA expression of enzymes involved in taurine biosynthesis in rat adipose tissues. *Metabolism* 51, 1191–1197.
- Irwin, J.J., Sterling, T., Mysinger, M.M., Bolstad, E.S., Coleman, R.G., 2012. ZINC: a free tool to discover chemistry for biology. *J. Chem. Inf. Model.* 52 (7), 1757–1768. <http://dx.doi.org/10.1021/ci3001277>.
- Jia, F., Yue, M., Chandra, D., Keramidas, A., Goldstein, P.A., Homanics, G.E., et al., 2008. Taurine is a potent activator of extrasynaptic GABA(A) receptors in the thalamus. *J. Neurosci. Off. J. Soc. Neurosci.* 28, 106–115.
- Kang, H.J., Kawasawa, Y.L., Cheng, F., Zhu, Y., Xu, X., Li, M., et al., 2011. Spatio-temporal transcriptome of the human brain. *Nature* 478, 483–489.
- Kim, H.W., Yoon, S.H., Park, T., Kim, B.K., Park, K.K., Lee, D.H., 2006. Gene expressions of taurine transporter and taurine biosynthetic enzyme during mouse and chicken embryonic development. *Taurine* 6 (583), 69–77.
- Kuriyama, K., Ida, S., Ohkuma, S., Tanaka, Y., 1985. Alteration of cerebral biosynthesis of taurine in spontaneously hypertensive and 3-acetylpyridine intoxicated rats. *Prog. Clin. Biol. Res.* 179, 91–103.
- Larkin, M.A., Blackshields, G., Brown, N.P., Chenna, R., McGettigan, P.A., McWilliam, H., et al., 2007. Clustal W and clustal X version 2.0. *Bioinformatics* 23, 2947–2948.
- Liu, H., Zhang, Y., Li, S., Yan, Y., Li, Y., 2010. Dynamic regulation of glutamate decarboxylase 67 gene expression by alternative promoters and splicing during rat testis maturation. *Mol. Biol. Rep.* 37, 3111–3119.
- Liu, P., Ge, X., Ding, H., Jiang, H., Christensen, B.M., Li, J., 2012. Role of glutamate decarboxylase-like protein 1 (GADL1) in taurine biosynthesis. *J. Biol. Chem.* 287, 40898–40906.
- Lombardini, J.B., 1994. The inhibitory effects of taurine on protein phosphorylation: comparison of various characteristics of the taurine-affected phosphoproteins present in rat retina, brain and heart. *Adv. Exp. Med. Biol.* 359, 9–17.
- Magnusson, K.R., Madl, J.E., Clements, J.R., Wu, J.Y., Larson, A.A., Beitz, A.J., 1988. Colocalization of taurine- and cysteine sulfonic acid decarboxylase-like immunoreactivity in the cerebellum of the rat with monoclonal antibodies against taurine. *J. Neurosci. Off. J. Soc. Neurosci.* 8, 4551–4564.
- Malhi, G.S., Tanius, M., Das, P., Coulston, C.M., Berk, M., 2013. Potential mechanisms of action of lithium in bipolar disorder. *Current understanding. CNS Drugs* 27, 135–153.
- McKinney, J., Knappskog, P.M., Haavik, J., 2005. Different properties of the central and peripheral forms of human tryptophan hydroxylase. *J. Neurochem.* 92, 311–320.
- Ohkuma, S., Tomono, S., Tanaka, Y., Kuriyama, K., Mukainaka, T., 1986. Development of taurine biosynthesizing system in cerebral cortical neurons in primary culture. *Int. J. Dev. Neurosci. Off. J. Int. Soc. Dev. Neurosci.* 4, 383–395.
- Ottersen, O.P., Madsen, S., Storm-Mathisen, J., Somogyi, P., Scopsi, L., Larsson, L.I., 1988. Immunocytochemical evidence suggests that taurine is colocalized with GABA in the Purkinje cell terminals, but that the stellate cell terminals predominantly contain GABA: a light- and electronmicroscopic study of the rat cerebellum. *Exp. Brain Res. Exp. Hirnforsch. Exp. Cereb. Tr.* 72, 407–416.
- Park, E., Park, S.Y., Dobkin, C., Schuller-Levis, G., 2014. Development of a novel cysteine sulfonic acid decarboxylase knockout mouse: dietary taurine reduces neonatal mortality. *J. Amino Acids* 2014, 346809.
- Park, E., Park, S.Y., Wang, C., Xu, J., LaFauci, G., Schuller-Levis, G., 2002. Cloning of murine cysteine sulfonic acid decarboxylase and its mRNA expression in murine tissues. *Biochim. Biophys. Acta* 1574, 403–406.
- Pasantes-Morales, H., Hernandez-Benitez, R., 2010. Taurine and brain development: trophic or cytoprotective actions? *Neurochem. Res.* 35, 1939–1943.
- Pasantes-Morales, H., Mapes, C., Tapia, R., Mandel, P., 1976. Properties of soluble and particulate cysteine sulfinate decarboxylase of the adult and the developing rat brain. *Brain Res.* 107, 575–581.
- Qu, K., Martin, D.L., Lawrence, C.E., 1998. Motifs and structural fold of the cofactor binding site of human glutamate decarboxylase. *Protein Sci. A Publ. Protein Soc.* 7, 1092–1105.
- Revil, T., Gaffney, D., Dias, C., Majewski, J., Jerome-Majewska, L.A., 2010. Alternative splicing is frequent during early embryonic development in mouse. *BMC Genom.* 11, 399.
- Reymond, I., Almaghini, K., Tappaz, M., 1996a. Immunocytochemical localization of cysteine sulfinate decarboxylase in astrocytes in the cerebellum and hippocampus: a quantitative double immunofluorescence study with glial fibrillary acidic protein and S-100 protein. *Neuroscience* 75, 619–633.
- Reymond, I., Bitoun, M., Levillain, O., Tappaz, M., 2000. Regional expression and histological localization of cysteine sulfinate decarboxylase mRNA in the rat kidney. *J. Histochem. Cytochem.* 48, 1461–1468.
- Reymond, I., Sergeant, A., Tappaz, M., 1996b. Molecular cloning and sequence analysis of the cDNA encoding rat liver cysteine sulfinate decarboxylase (CSD). *Biochim. Biophys. Acta* 1307, 152–156.
- Rorsman, F., Husebye, E.S., Winqvist, O., Bjork, E., Karlsson, F.A., Kampe, O., 1995. Aromatic-L-amino-acid decarboxylase, a pyridoxal phosphate-dependent enzyme, is a beta-cell autoantigen. *Proc. Natl. Acad. Sci. U. S. A.* 92, 8626–8629.
- Schaffer, S.W., Jong, C.J., Ramila, K.C., Azuma, J., 2010. Physiological roles of taurine in heart and muscle. *J. Biomed. Sci.* 17 (Suppl. 1), S2.
- Schwede, T., Kopp, J., Guex, N., Peitsch, M.C., 2003. SWISS-MODEL: an automated protein homology-modeling server. *Nucleic Acids Res.* 31, 3381–3385.
- Shin, S.Y., Fauman, E.B., Petersen, A.K., Krumsiek, J., Santos, R., Huang, J., et al., 2014. An atlas of genetic influences on human blood metabolites. *Nat. Genet.* 46, 543–550.
- Skoldberg, F., Rorsman, F., Perheentupa, J., Landin-Olsson, M., Husebye, E.S., Gustafsson, J., et al., 2004. Analysis of antibody reactivity against cysteine sulfonic acid decarboxylase, a pyridoxal phosphate-dependent enzyme, in endocrine autoimmune disease. *J. Clin. Endocrinol. Metab.* 89, 1636–1640.
- Steuillet, P., Cate, H.S., Derby, C.D., 2000. A spatiotemporal wave of turnover and functional maturation of olfactory receptor neurons in the spiny lobster *Panulirus argus*. *J. Neurosci. Off. J. Soc. Neurosci.* 20, 3282–3294.
- Stipanuk, M.H., Dominy Jr., J.E., Lee, J.L., Coloso, R.M., 2006. Mammalian cysteine metabolism: new insights into regulation of cysteine metabolism. *J. Nutr.* 136, 1652S–1659S.
- Stipanuk, M.H., Ueki, I., Dominy Jr., J.E., Simmons, C.R., Hirschberger, L.L., 2009. Cysteine dioxygenase: a robust system for regulation of cellular cysteine levels. *Amino Acids* 37, 55–63.
- Taber, K.H., Lin, C.T., Liu, J.W., Thalmann, R.H., Wu, J.Y., 1986. Taurine in hippocampus: localization and postsynaptic action. *Brain Res.* 386, 113–121.
- Tang, X.W., Hsu, C.C., Sun, Y., Wu, E., Yang, C.Y., Wu, J.Y., 1996. Multiplicity of brain cysteine sulfonic acid decarboxylase – purification, characterization and subunit structure. *J. Biomed. Sci.* 3, 442–453.
- Tappaz, M., Almaghini, K., Do, K., 1994. Cysteine sulfinate decarboxylase in brain: identification, characterization and immunocytochemical location in astrocytes. *Adv. Exp. Med. Biol.* 359, 257–268.
- Tappaz, M., Almaghini, K., Legay, F., Remy, A., 1992. Taurine biosynthesis enzyme cysteine sulfinate decarboxylase (CSD) from brain: the long and tricky trail to identification. *Neurochem. Res.* 17, 849–859.
- Tappaz, M., Bitoun, M., Reymond, I., Sergeant, A., 1999. Characterization of the cDNA coding for rat brain cysteine sulfinate decarboxylase: brain and liver enzymes are identical proteins encoded by two distinct mRNAs. *J. Neurochem.* 73, 903–912.
- Tappaz, M., Reymond, I., Bitoun, M., Sergeant, A., 1998. Cysteine sulfinate decarboxylase (CSD): molecular cloning, sequence and genomic expression in brain. *Adv. Exp. Med. Biol.* 442, 25–32.
- Terauchi, A., Nakazawa, A., Johkura, K., Yan, L., Usuda, N., 1998. Immunohistochemical localization of taurine in various tissues of the mouse. *Amino Acids* 15, 151–160.
- Toney, M.D., 2011. Controlling reaction specificity in pyridoxal phosphate enzymes. *Biochim. Biophys. Acta* 1814, 1407–1418.
- Vitvitsky, V., Garg, S.K., Banerjee, R., 2011. Taurine biosynthesis by neurons and astrocytes. *J. Biol. Chem.* 286, 32002–32010.
- Warskulat, U., Heller-Stilb, B., Oermann, E., Zilles, K., Haas, H., Lang, F., et al., 2007. Phenotype of the taurine transporter knockout mouse. *Methods Enzymol.* 428, 439–458.
- Weinstein, C.L., Griffith, O.W., 1987. Multiple forms of rat liver cysteine sulfinate decarboxylase. *J. Biol. Chem.* 262, 7254–7263.
- Winge, I., McKinney, J.A., Knappskog, P.M., Haavik, J., 2007. Characterization of wild-type and mutant forms of human tryptophan hydroxylase 2. *J. Neurochem.* 100, 1648–1657.
- Woo, H.-I., Chun, M.-R., Yang, J.-S., Lim, S.-W., Kim, M.-J., Kim, S.-W., et al., 2015. Plasma amino acid profiling in major depressive disorder treated with selective serotonin reuptake inhibitors. *CNS Neurosci. Ther.* 21, 417–424.
- Wu, J.Y., 1982. Purification and characterization of cysteine acid and cysteine sulfonic acid decarboxylase and L-glutamate decarboxylase from bovine brain. *Proc. Natl. Acad. Sci. U. S. A.* 79, 4270–4274.
- Wu, J.Y., Johansen, F.F., Lin, C.T., Liu, J.W., 1987. Taurine system in the normal and ischemic rat hippocampus. *Adv. Exp. Med. Biol.* 217, 265–274.
- Zhang, N., Ottersen, O.P., 1992. Differential cellular distribution of two sulphur-containing amino acids in rat cerebellum. An immunocytochemical investigation using antisera to taurine and homocysteine acid. *Exp. Brain Res. Exp. Hirnforsch. Exp. Cereb. J.* 11, 20–20.

Species	cDNA	Accession no	PCR-product (bp)
Human	CSAD	Hs00211126_m1	64
	GADL1	Hs01395974_m1	66
	GAPDH	Hs99999905_m1	122
	β -Actin	Hs99999903_m1	171
Mouse	CSAD	Mm00520087_m1	64
	GADL1	Mm01348767_m1	73
	GAPDH	Mm99999915_g1	107
	β -Actin	Mm00607939_s1	115

Supple. Table 1 Probes used for real-time PCR quantification of GADL1 and CSAD mRNA.

Name	Transcript ID	Length (bp)	Protein ID	Length (aa)	Size (kDa)
CSAD-004	ENST00000267085	2619	ENSP00000267085	520 (1-520)	58
CSAD-003	ENST00000379850	2379	ENSP00000369179	519 (1-519)	57
CSAD-019	ENST00000453446	1774	ENSP00000410648	493 (28-520)	55
CSAD-017	ENST00000444623	2122	ENSP00000415485	493 (28-520)	55
CSAD-201	ENST00000379843	2253	ENSP00000369172	346(1-42 186-493)	38
CSAD-002	ENST00000379846	1962	ENSP00000369175	346(1-42 144-454)	38
CSAD-009	ENST00000437073	581	ENSP00000415314	163 (1-163)	18
CSAD-202	ENST00000542115	1178	ENSP00000439419	152 (1-151)	17
CSAD-005	ENST00000424990	565	ENSP00000401078	146 (1-146)	16
CSAD-020	ENST00000548698	455	ENSP00000449373	135 (1-42 216-309)	15
CSAD-007	ENST00000498635	585	ENSP00000457264	129 (1-129)	14
GADL1-001	ENST00000282538	3759	ENSP00000282538	521 (1-521)	59
GADL1-002	ENST00000454381	4509	ENSP00000427059	418 (1-418)	47

Suppl. Table 2 Splice variants described for human CSAD and GADL1 in Ensemble.

Enzyme	Substrate	Activity	Enzyme	Substrate	Activity
GADL1	CSA	+	CSAD	CSA	+
	L-Cysteic acid	+		Cysteic acid	+
	L-Aspartic acid	+		Aspartic acid	-
	Homocysteine	-		Homocysteine	-
	Histidine	-		Histidine	-
	L-Threonine	-		L-Threonine	-
	Methionine	-		Methionine	-
	DL-Cysteine	-		DL-Cysteine	-
	L-Lysine	-		L-Lysine	-
	L-Tryptophan	-		L-Tryptophan	-
	L-Glutamine	-		L-Glutamine	-
	L-Alanine	-		L-Alanine	-
	L-Glutamic acid	-		L-Glutamic acid	-
	L-Asparagine	-		L-Asparagine	-
	Serine	-		Serine	-
	Tyrosine	-		Tyrosine	-
	Isomaltose	-		Isomaltose	-
	Maltulose	-		Maltulose	-
	Phtalic acid	-		Phtalic acid	-
	Isophtalic acid	-		Isophtalic acid	-
	Trisodium 2 Methylcitrate	-		Trisodium 2 Methylcitrate	-
	Butane carboxylic acid	-		Butane carboxylic acid	-
	Dimethachlor Metabolite	-		Dimethachlor Metabolite	-
	Adenosine 2,3-cyclic Monophosphate	-		Adenosine 2,3-cyclic Monophosphate	-
	Salisyl sulphate disodium salt	-		Salisyl sulphate disodium salt	-
	N-Acetyl-L-Aspartic acid	-		N-Acetyl-L-Aspartic acid	-
	N-Acetyl-L-Carnosine	-		N-Acetyl-L-Carnosine	-
	N-Acetyl-L-aspartic acid-glutamate	-		N-Acetyl-L-aspartic acid- glutamate	-
	Malic acid	-		Malic acid	-
	Cis-oxalic acid	-		Cis-oxalic acid	-
	Isocitric acid Lactone	-		Isocitric acid Lactone	-

Suppl. Table 3 Complete list of compounds tested for activity on CSAD and GADL1.

The assay was performed as described above at 37°C for 60 min and stopped by addition of equal volume of ice-cold ethanol with 5 % acetic acid. The observed effect is denoted with + (positive) or – (negative) activity.

II

BIOCHEMISTRY

GADL1 is a multifunctional decarboxylase with tissue-specific roles in β -alanine and carnosine production

Elaheh Mahootchi¹, Selina Cannon Homaei^{1,2}, Rune Kleppe², Ingeborg Winge¹, Tor-Arne Hegvik¹, Roberto Megias-Perez¹, Christian Totland^{3,4}, Floriana Mogavero⁵, Anne Baumann¹, Jeffrey Colm Glennon^{5,6}, Hrvoje Miletic^{1,7}, Petri Kursula^{1,8}, Jan Haavik^{1,2*}

Copyright © 2020 The Authors, some rights reserved; exclusive licensee American Association for the Advancement of Science. No claim to original U.S. Government Works. Distributed under a Creative Commons Attribution License 4.0 (CC BY).

Carnosine and related β -alanine-containing peptides are believed to be important antioxidants, pH buffers, and neuromodulators. However, their biosynthetic routes and therapeutic potential are still being debated. This study describes the first animal model lacking the enzyme glutamic acid decarboxylase-like 1 (GADL1). We show that *Gadl1*^{-/-} mice are deficient in β -alanine, carnosine, and anserine, particularly in the olfactory bulb, cerebral cortex, and skeletal muscle. *Gadl1*^{-/-} mice also exhibited decreased anxiety, increased levels of oxidative stress markers, alterations in energy and lipid metabolism, and age-related changes. Examination of the GADL1 active site indicated that the enzyme may have multiple physiological substrates, including aspartate and cysteine sulfinic acid. Human genetic studies show strong associations of the *GADL1* locus with plasma levels of carnosine, subjective well-being, and muscle strength. Together, this shows the multifaceted and organ-specific roles of carnosine peptides and establishes *Gadl1* knockout mice as a versatile model to explore carnosine biology and its therapeutic potential.

INTRODUCTION

Carnosine (β -alanyl-L-histidine) is one of several dipeptides of β -alanine and histidine that are found in high concentrations in vertebrate tissues, particularly in the brain and skeletal muscle (SKM) tissues. In humans, carnosine and acetylcarnosine are most abundant. In contrast, many animals mainly synthesize the related β -alanine-containing peptides anserine or ophidine/balentine through methylation of the imidazole moiety of carnosine in the 1 or 3 position (1, 2). Here, we refer to this family of related peptides as “carnosine peptides.”

Carnosine peptides may have multiple biological functions, including calcium regulation, pH buffering, metal chelation, and antioxidant effects (1). β -Alanine, as well as its dipeptide derivatives, may also be neurotransmitters or neuromodulators in the central nervous system, especially in olfactory bulb (OB). In mammals, including mice, only two tissues have carnosine concentrations in the millimolar range, i.e., SKM and OB (1, 3). Various disorders and dysfunctions have been linked to alterations in β -alanine and carnosine metabolism. In β -alaninemia and carnosinemia, decreased degradation of these compounds is associated with neurological symptoms (4, 5). Conversely, it has been suggested that some age-related and neurological diseases, e.g., Alzheimer’s disease, Parkinson’s disease, multiple sclerosis (MS), and cancer, as well as diabetes complications, may benefit from carnosine supplementation (6).

β -Alanine supplementation increases carnosine content and improves contractility and muscle performance of human and rodent SKM, especially during short exercise intervals (7, 8). These findings have led to the widespread use of dietary β -alanine supplements, particularly among athletes and soldiers (9). β -Alanine and carnosine dietary supplementation have also shown some promising effects in the treatment of depression, anxiety, and autism symptoms in humans (10) and animal models (11, 12).

As most carnosine peptides are hydrolyzed after oral ingestion, either in enterocytes or in the blood circulation, the body mainly depends on de novo synthesis of these peptides. Dietary supplementation has side effects but requires a daily intake of several grams to increase muscle β -alanine and carnosine content and physical performance (13). The lack of suitable model systems and the need to supply pharmacological quantities of carnosine peptides have caused some uncertainty regarding the mechanisms of action and safety of these compounds. A more stable, synthetic analog of carnosine, carnosinol, was recently shown to protect against metabolic dysregulation and oxidative damage (14).

Synthesis of β -alanine appears to be a rate-limiting factor for carnosine peptide levels in mammals (15). In a large genome-wide association (GWA) study on plasma metabolites, it was estimated that 86% of the variation in carnosine levels could be attributed to genetic factors, making this peptide the most heritable metabolite among all compounds examined (16). Still, uncertainty remains regarding the identity of the genes and proteins involved in its synthesis. Carnosine synthase 1 (encoded by *CARN1*) produces carnosine from β -alanine and histidine and homocarnosine from γ -aminobutyric acid (GABA) and histidine. In animal tissues, β -alanine may be produced by reductive degradation of uracil (17). In contrast, some bacteria produce β -alanine by α -decarboxylation of aspartic acid (Asp), catalyzed by aspartate decarboxylase with the aid of a covalently bound pyruvoyl cofactor (18). In insects, an analogous vitamin B6 [pyridoxal

¹Department of Biomedicine, University of Bergen, Bergen, Norway. ²Division of Psychiatry, Haukeland University Hospital, Bergen, Norway. ³Department of Chemistry, University of Bergen, Bergen, Norway. ⁴Norwegian Geotechnical Institute, Oslo, Norway. ⁵Department of Cognitive Neuroscience, Donders Institute for Brain Cognition and Behavior, Radboud University Medical Center, Nijmegen, Netherlands. ⁶Conway Institute of Biomolecular and Biomedical Research, School of Medicine, University College Dublin, Belfield, Dublin 4, Ireland. ⁷Department of Pathology, Haukeland University Hospital, Bergen, Norway. ⁸Faculty of Biochemistry and Molecular Medicine, University of Oulu, Oulu, Finland. *Corresponding author. Email: jan.haavik@uib.no

phosphate (PLP)]-dependent enzyme L-aspartate- α -decarboxylase has evolved by convergent evolution (19). The formation of carnosine in the mouse SKM is dependent on vitamin B6, implicating a PLP-dependent enzyme in its synthesis in animals as well (20).

On the basis of its sequence similarity to glutamic acid decarboxylase (GAD), the PLP-dependent enzyme GAD-like protein 1 (GADL1; acidic amino acid decarboxylase) has been assigned a possible role in GABA synthesis and to be associated with lithium response in bipolar patients (21). Although this genetic association was not replicated in other clinical samples (22), these findings have triggered interest in the *in vivo* investigation of GADL1 function and biochemical properties. As cysteine sulfenic acid (CSA) is a substrate of GADL1, it was suggested that GADL1 is involved in the biosynthesis of hypotaurine and taurine (23). However, it has also been reported that purified human (23) and mouse (24) GADL1 can synthesize β -alanine from Asp, although at very low rates *in vitro*. This is consistent with recent crystallographic studies, showing that GADL1 shares structural features with both CSA decarboxylase (CSAD) and Asp decarboxylase (25). Moreover, a human genetic association study demonstrated that single-nucleotide polymorphisms (SNPs) in the *GADL1* intron are strongly associated with blood levels of acetyl-carnosine (26) that, in turn, are strongly correlated with carnosine levels (2). On the basis of these observations, we hypothesized that GADL1 could be involved in β -alanine and carnosine production in mammalian tissues.

Here, we describe the first *Gad1l* knockout (KO) mouse model and demonstrate an organ-specific role of GADL1 in the biosynthesis of carnosine peptides and protection against oxidative stress, particularly in the OB and SKM. To understand the substrate specificity of GADL1, we compared the three-dimensional (3D) structures of mouse GADL1 and related enzymes. Last, we investigate the association between common genetic variants in enzymes and transporters involved in carnosine homeostasis with multiple human traits and diseases and present an initial behavioral characterization of the *Gad1l* KO mouse.

RESULTS

Mice lacking GADL1 show age-related changes

Gad1l^{-/-} (null) mice were generated using *Cre/loxP* technology. Because of the proximity of the *Gad1l* gene to the *Tgfb2* gene that encodes a receptor with possible effects on growth and survival, we applied a conservative knocking out strategy, where only *Gad1l* exon 7, coding for part of the PLP-binding active site of GADL1, was deleted (Fig. 1A). *Gad1l*^{+/+}, *Gad1l*^{+/-}, and *Gad1l*^{-/-} mice were successfully generated in the expected Mendelian ratios by breeding from *Gad1l*^{+/-} mice. We observed no obvious physical abnormalities. Overall activity and feeding behavior, as well as initial growth curves, were similar across all genotypes. However, after 30 weeks of age, compared to *Gad1l*^{+/+} mice, female and male *Gad1l*^{-/-} mice exhibited relative growth retardation, compatible with age-related and possible degenerative changes (Fig. 1, B and C).

Genomic DNA sequencing and Southern blot analyses confirmed the elimination of exon 7 (Fig. 1, D and E). However, quantification of *Gad1l* mRNA from SKM and OB revealed that some *Gad1l* mRNA species could be detected across all genotypes. RNA sequencing showed that *Gad1l*^{-/-} mice lacked *Gad1l* exons 7 and 8. This was confirmed using quantitative reverse transcription polymerase chain reaction (qRT-PCR) of individual exons (see below). Bioinformatic

analyses showed that the deletion of exons 7 and 8 was coupled to the generation of a new RNA splicing site in the mutated mice (fig. S1).

Western blotting confirmed that GADL1 protein was present in *Gad1l*^{+/+} and *Gad1l*^{+/-} but not in *Gad1l*^{-/-} mice. In OB extracted from *Gad1l*^{+/+} mice, GADL1 appeared as a wide band, with an estimated molecular mass of 55 to 59 kDa (Fig. 1F). This corresponds to several predicted protein variants with 502 to 550 amino acids (24). Since exons 7 and 8 encode amino acids involved in cofactor binding, GADL1 lacking these amino acids was predicted to be enzymatically inactive. This was confirmed by expressing the protein lacking exons 7 and 8 in *Escherichia coli* and comparing it to the full-length protein (Fig. 1G and fig. S2). The mutant protein yield was only 17% compared to that of the full-length protein. Furthermore, the mutant protein was completely devoid of enzyme activity (Fig. 1H). This demonstrated that the elimination of gene function was successful and that the *Gad1l*^{-/-} mice did not have any residual GADL1 enzyme activity.

Elimination of *Gad1l* alters the OB transcriptome

To determine the effects of GADL1 depletion on gene expression, we sequenced and compared OB mRNA levels from *Gad1l*^{+/+}, *Gad1l*^{+/-}, and *Gad1l*^{-/-} mice (Fig. 1, I to K). The top 25 up- and down-regulated genes (\log_2 fold change either less than -1 or greater than +1 and $P \leq 0.05$) are shown in table S1 and fig. S3. Pathway enrichment analysis showed that the strongest affected group of genes is involved in drug metabolism [Kyoto Encyclopedia of Genes and Genomes (KEGG) pathway mmu00983; $P = 0.00016$, $q = 0.014$] (Table 1) (27). This pathway includes the *Upb1* gene (β -ureidopropionase 1), a transcript with a twofold increase in *Gad1l*^{-/-} mice ($P = 0.0154$). UPB1 catalyzes the last step in the formation of β -alanine from pyrimidines. This is consistent with a compensatory mechanism for maintaining β -alanine synthesis in the absence of GADL1. Moreover, in OB of *Gad1l*^{-/-} mice, we observed increased transcript levels of multiple isoforms of carboxylesterase 1, cytochrome P450, and myeloperoxidase.

A gene ontology (GO) pathway analysis (27, 28) of up- or down-regulated genes (\log_2 fold change either less than -1 or greater than +1 and $P \leq 0.05$) showed statistical significant alterations in 24 different biological processes, where the most significant alteration involves drug catabolism (GO:0042737; $P = 2.43 \times 10^{-7}$, $q = 0.0007$). Furthermore, biological processes involving circadian rhythms and sleep cycles seemed to be altered. Dopamine receptors (*Drd1* to *Drd3*) and adenosine A2a receptor (*Adora2a*) were the most consistently recurring genes throughout the GO analysis (table S2). It has been reported that the release of glutamate from terminals of carnosine containing olfactory neurons in OB glomeruli is modified by dopamine receptors (29). It is possible that the elimination of GADL1 and carnosine depletion also affected the expression of these modulatory transmitter receptors in the OB. Wu *et al.* (30) recently reported that GADL1 overexpression inhibited Potassium channel tetramerization domain containing 12 (KCTD12) expression. However, a comparison of *Gad1l*^{-/-} and *Gad1l*^{+/+} mice showed that RNA levels of KCTD12 were unaffected by the deletion of *Gad1l* ($P = 0.62$).

Deletion of *Gad1l* perturbs carnosine metabolism

To explore the biological function(s) of GADL1, we performed untargeted liquid chromatography-mass spectrometry (LC-MS) metabolomic analyses of eight different tissues from 20 *Gad1l*^{+/+} mice and 21 *Gad1l*^{-/-} mice that were matched across genotype and sex (Fig. 2). The number of identifiable metabolites varied between 541 and 720 in the cerebral cortex, OB, SKM, liver, cerebellum, heart,

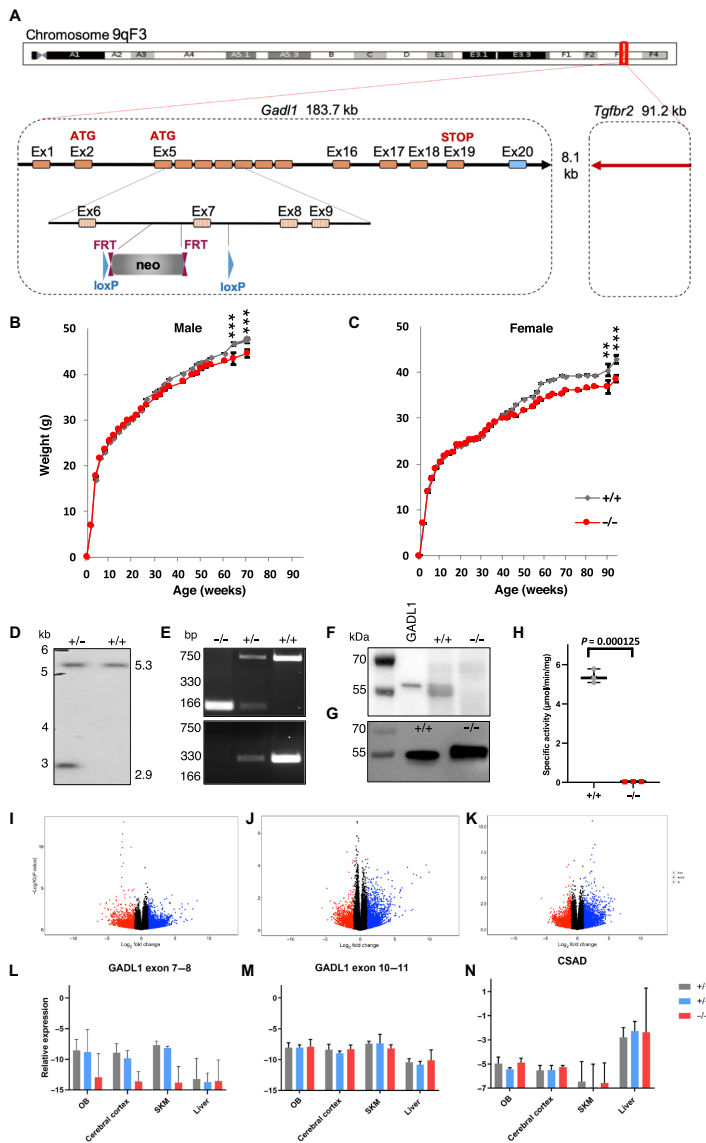


Fig. 1. Generation and characterization of GADL1 KO mice. (A) Targeting strategy for knocking out exon (Ex) 7 of the mouse *Gad1* locus on chromosome 9. *Gad1* coding sequences (hatched rectangles), noncoding exon portions (blue rectangle), and chromosome sequences (orange rectangles) are represented. The neomycin (neo)-positive selection cassette is indicated between loxP sites (blue triangles) and Flippase recognition target (FRT) sites (plum triangles). (B and C) Growth curves of *Gad1*^{+/+} (*n* = 4 to 34) and *Gad1*^{-/-} mice (*n* = 4 to 40), presented as means ± SD. Differences between genotypes were significant; *P* = 0.0008 (64 weeks) and *P* = 0.0005 (70 weeks) for males and *P* = 0.0084 (90 weeks) and *P* = 0.0001 (94 weeks) for females, respectively. (D) Southern blot analysis of genomic DNA from *Gad1*^{+/+} and *Gad1*^{-/-}. (E) Genotyping of the offspring from intercrosses of *Gad1*^{+/-} mice by polymerase chain reaction (PCR). The DNA band at 166 base pair (bp) is the KO allele (primer 3), while bands at 330 bp (primer 2 and 3) and 750 bp (primer 1) are the wild-type alleles. (F) Representative Western blots of OB samples from *Gad1*^{+/+} and *Gad1*^{-/-} mice (34 weeks old, female) using anti-GADL1 antibody. Positive control was recombinant His-tagged GADL1 (2 ng; lane 1). (G) Western blot of recombinant His-tagged truncated *Gad1*^{+/+} and *Gad1*^{-/-}. (H) Enzyme activity toward CSA of recombinant His-tagged truncated *Gad1*^{+/+} and *Gad1*^{-/-}; *P* < 0.001. (I to K). RNA expression levels (volcano plots) in OB tissue. (I) *Gad1*^{+/+}-to-*Gad1*^{+/+} ratio, (J) *Gad1*^{+/+}-to-*Gad1*^{-/-} ratio, and (K) *Gad1*^{-/-}-to-*Gad1*^{+/+} ratio. (L to N) Quantitative reverse transcription PCR (qRT-PCR) analysis of normalized mRNA expression in OB, brain, SKM, and liver tissues from 35-week-old female *Gad1*^{+/+} (gray), *Gad1*^{+/-} (blue), and *Gad1*^{-/-} (red) mice for (L) *Gad1* exons 7 and 8, (M) *Gad1* exons 10 and 11, and (N) CSAD. *n* = 3 for each genotype. Presented on an Ln y scale as mean of 2^{ΔCt} and upper limit (95%).

Table 1. Pathway enrichment analysis comparing *Gad1*^{-/-} to *Gad1*^{+/+}. Green, up-regulated; yellow, down-regulated.

Gene ID	Abbr.	Name	Log ₂ fold	P value	KEGG ID			
					mmu00983	mmu00830	mmu00980	mmu00380
					0.00016	0.00022	0.00025	0.00045
14869	Gstp2	Glutathione S-transferase, pi 2	-4.2819	0.0374				
13897	Ces1e	Carboxylesterase 1E	4.9087	0.0040				
104158	Ces1d	Carboxylesterase 1D	3.8723	0.0131				
234564	Ces1f	Carboxylesterase 1F	2.6056	0.0193				
17523	Mpo	Myeloperoxidase	2.4247	0.0001				
394432	Ugt1a7c	uridine 5'-diphospho glucuronosyltransferase 1A7C	1.0524	0.0019				
103149	Upb1	β-Ureidopropionase	1.0121	0.0154				
27400	Hsd17b6	Hydroxysteroid (17-β) dehydrogenase 6	4.0829	0.0103				
13087	Cyp2a5	Cytochrome P450 2A5	3.9985	0.0129				
213043	Aox2	Aldehyde oxidase 2	3.4965	0.0260				
13086	Cyp2a4	Cytochrome P450 2A4	3.1973	0.0157				
13076	Cyp1a1	Cytochrome P450 1A1	3.0800	0.0010				
11522	Adh1	Alcohol dehydrogenase 1, class 1	1.7208	0.0144				
13107	Cyp2f2	Cytochrome P450 2F2	2.9664	0.0024				
12409	Cbr2	Carbonyl reductase 2	1.2641	0.0012				
11298	Aanat	Arylalkylamine N-acetyltransferase	-1.3632	0.0008				
15930	Ido1	Indoleamine 2,3-dioxygenase 1	2.4039	0.0192				
21743	Inmt	Indolethylamine N-methyltransferase	1.2043	0.0401				

Table 2. Male and female mice used in the metabolomic study.

Genotype	Sex	Number (n)	Age (weeks ± SD)
<i>Gad1</i> ^{+/+}	Female	11	14.64 ± 7.85
<i>Gad1</i> ^{-/-}	Female	11	14.27 ± 7.85
<i>Gad1</i> ^{+/+}	Male	9	8.88 ± 3.98
<i>Gad1</i> ^{-/-}	Male	10	8.40 ± 3.81

serum, and kidney. Partial least squares–discriminant analyses (PLS-DA) were used to evaluate metabolic differences between *Gad1*^{+/+} and *Gad1*^{-/-} mice. This allowed identification of suitable markers responsible for the metabolic differences by variable important projection (VIP) scores.

The metabolic features with VIP scores higher than 2, responsible for the separation in each tissue, are depicted in Fig. 2 (A to D). Carnosine peptides showed the strongest difference between the genotypes in the OB and the cerebral cortex (Fig. 2E). Carnosine was also among the most strongly affected metabolites in SKM but not in the

liver (Fig. 2E). Although GADL1 has been postulated to synthesize GABA from glutamate, the levels of GABA and glutamate in *Gad1*^{+/+} and *Gad1*^{-/-} mice were similar in all tissues examined (fold difference of 0.88 to 1.15 for glutamate and 0.96 to 1.53 for GABA; *P* > 0.05). *Gad1*^{-/-} mice had significantly reduced levels of β-alanine in OB but nonsignificant reduction in the cerebral cortex and SKM and unaltered levels in the liver. In contrast, carnosine, acetylcarnosine, and anserine were significantly depleted in brain and SKM tissues. A nonsignificant reduction (~10%) of β-alanine and carnosine peptides was observed in the serum and whole blood (fig. S4A), as well as in the kidney, cerebellum, and heart. Together, this is consistent with the observed tissue distribution of GADL1 and demonstrates its key role in the metabolic pathway of β-alanine and carnosine peptides.

High-resolution magic angle spinning nuclear magnetic resonance spectroscopy confirms the depletion of carnosine in *Gad1*^{-/-} mice

To determine the role of GADL1 on carnosine content in intact tissue, we used fresh OB tissue where we found the highest expression GADL1. We performed high-resolution magic angle spinning (MAS) ¹H–nuclear magnetic resonance (NMR) spectroscopy on OB from

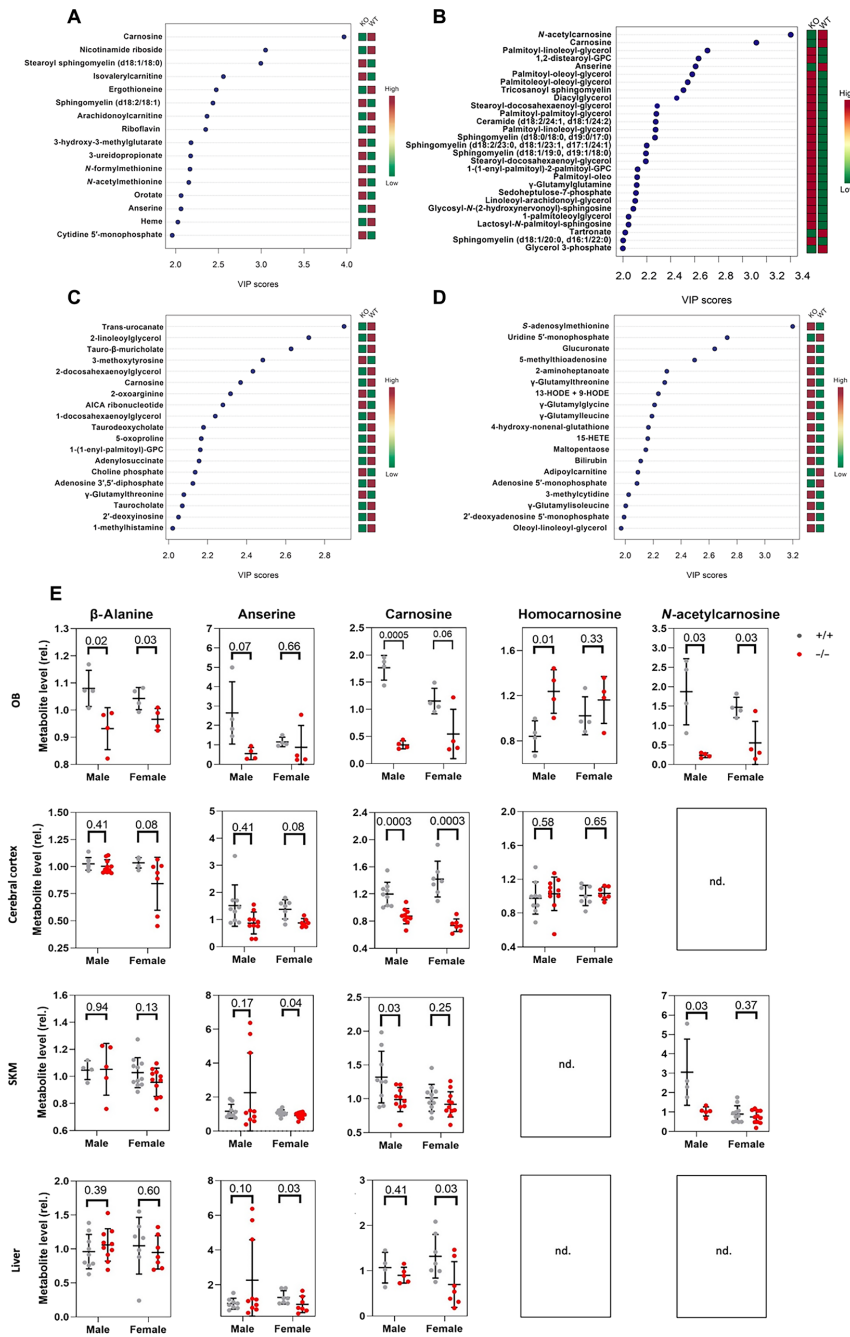


Fig. 2. Tissue-specific effects on metabolite levels in *Gald1*^{-/-} mice. (A to D) Top significant features of metabolites based on VIP scores of >2 of component 1 of PLS-DA. Untargeted metabolic profiling of (A) cerebral cortex, (B) OB, (C) SKM, and (D) liver tissue samples from *Gald1*^{+/+} (n = 20) and *Gald1*^{-/-} (n = 21) mice. WT, wild-type. (E) The relative levels of β-alanine and carnosine derivatives in *Gald1*^{+/+} (gray) and *Gald1*^{-/-} (red) mouse tissue. nd., not determined.

Gad11^{+/+} (*n* = 4), *Gad11*^{+/-} (*n* = 3), and *Gad11*^{-/-} (*n* = 3) mice. Characteristic features of carnosine (Fig. 3A) could be identified in the aromatic regions of the spectrum, in accordance with the quantification in tissue extracts (Fig. 3B). Compared to *Gad11*^{+/+}, *Gad11*^{+/-}, and *Gad11*^{-/-} mice had 34 and 70% (*P* = 0.0056) reduced carnosine content in the OB (Fig. 3C). To our knowledge, this is the first demonstration of carnosine measurement in intact brain tissue, also establishing MAS NMR spectroscopy as a fast and convenient way to determine carnosine in this tissue. Furthermore, we performed brain magnetic resonance imaging (MRI) on 94-week-old female *Gad11*^{+/+}, *Gad11*^{+/-}, and *Gad11*^{-/-} mice. There were no significant differences in the brain morphology of *Gad11* genotypes (Fig. 3, E to F).

Substrate specificity of GADL1

Many PLP-dependent enzymes have multiple substrates (31). To explore whether the divergent metabolic changes observed in *Gad11*^{-/-} mice could be secondary to changes in β -alanine levels or were due to the parallel chemical conversion of multiple substrates by GADL1, we solved the crystal structure of mouse GADL1 (25). The structure of the closely related CSAD has been solved earlier but not published [Protein Data Bank (PDB) entry 2JIS]. With available crystal structures of GADL1, CSAD, and GAD (32), it is possible to identify determinants of substrate specificity in these acidic amino acid decarboxylases. GADL1 and CSAD have different, although slightly overlapping, physiological functions (24). GADL1, through the conversion of Asp to β -alanine, is important in carnosine peptide biosynthesis, while CSAD catalyzes the major pathway in taurine synthesis, using CSA as substrate. Despite similar chemical structures of the two substrates (Fig. 3G), these two highly similar enzymes can distinguish between them. Both Asp and CSA are smaller than Glu (Fig. 3H), explaining the inability of GADL1 and CSAD to function as glutamate decarboxylases (Fig. 3I). The carboxyl group in Asp is planar, while the sulfonic acid moiety of CSA is tetrahedral and has slightly longer bonds; effectively, CSA is slightly larger and can, perhaps, more specifically accommodate to a binding site due to its shape and charge.

As the chemical reaction catalyzed by the enzymes is identical, we can assume that the reactive groups bind in an identical manner, and the differences lie in recognizing the side chain of the substrate. GAD uses Glu as a substrate, while GADL1 acts on Asp, indicating that side-chain length is one determinant of productive binding. For binding a negatively charged side chain in the specificity pocket, one expects to find positive charge potential in the form of amino groups. For GAD, these interactions can be conceived; two backbone NH groups and a water molecule coordinated by a conserved His residue coordinate the side-chain carboxyl group in the model of the substrate complex, together with a Ser side chain. How is GADL1 different? The major difference is the substitution of this Ser with a Tyr residue (Fig. 3I), effectively making the binding cavity smaller. Interactions with the peptide backbone and the His-water unit are likely conserved for Asp binding to GADL1. The specificity pocket contains a Tyr (GADL1) or Phe (CSAD) residue, and the slightly different conformations of these residues are enough to cause this difference in substrate specificity.

Tissue-specific effects of GADL1 on the synthesis of taurine and its derivatives

On the basis of the ability of purified GADL1 to produce hypotaurine from CSA, it has been suggested that the primary biological func-

tion of GADL1 may be in taurine synthesis (23). However, the concentrations of the substrates and products in taurine synthesis were unaltered in the *Gad11*^{-/-} mice in the brain, OB, and liver. In contrast, levels of taurine derivatives were moderately reduced in SKM in *Gad11*^{-/-} (fig. S4). This is consistent with the observations that taurine mainly is synthesized by other routes, such as by CSAD (33), and our previous finding that CSAD is expressed in low amounts in SKM (24). In all tissues examined, CSAD protein has been reported to be more abundant than GADL1, and purified CSAD has a 5- to 35-fold higher specificity constant for decarboxylation of CSA than GADL1 (24). Moreover, as shown here, the qRT-PCR analysis showed that the levels of *Csad* mRNA were at least 10-fold higher than levels of *Gad11* and were unaffected by the deletion of *Gad11* exons (Fig. 2N). Thus, we conclude that in organs with a high content of CSAD, GADL1 has a minor role in taurine synthesis. In the absence of CSAD, levels of taurine in the mouse plasma, liver, and brain decreased by 70 to 90%, with the largest decrease in the liver and the smallest in the brain (33). This remaining taurine biosynthetic capacity has been attributed to an alternative biosynthetic route of taurine catalyzed by cysteamine dioxygenase from cysteamine, generated from coenzyme A (34). However, our results indicate that GADL1 has a small taurine biosynthetic capacity in vivo that may contribute to the overall production of taurine.

Oxidative stress markers

Several lines of evidence support a role of carnosine peptides in protection against oxidative stress (1, 35). To investigate the role of GADL1 in antioxidant defense, we compared levels of oxidative stress markers in *Gad11*^{+/+} and *Gad11*^{-/-} mice. *Gad11*^{-/-} mice had increased levels of oxidative stress markers, including methionine sulfide and γ -glutamyl peptides. These alterations are compatible with elevated glutathione synthesis and consistent with elevated oxidative stress. Some oxidative stress markers were strongly increased even in tissues with a moderate decrease in carnosine peptides, such as the liver. We also compared tissue levels of the antioxidant enzymes superoxide dismutase 1 (SOD1) (CuZnSOD), SOD2 (MnSOD), and glutathione reductase (GSR) in *Gad11*^{+/+} and *Gad11*^{-/-} mice (OB, cerebral cortex, and SKM) using Western blotting (Fig. 4). Unexpectedly, the most obvious difference was detected in the OB where the *Gad11*^{-/-} mice had a threefold increase in GSR levels (*P* = 0.0145) (Fig. 4A).

In contrast to carnosine and anserine, that were reduced in multiple tissues, levels of homocarnosine were significantly increased in the OB of *Gad11*^{-/-} mice (Fig. 2E). Several other metabolites related to β -alanine synthesis were also altered (fig. S4, G, I, and J).

Gad11^{-/-} mice had also increased levels of many lipid species, including sphingolipids, with the strongest effects in OB (Fig. 2, A to D, and fig. S4K). Notably, complex sphingolipids accumulate under inflammation and oxidative stress, conditions that *Gad11*^{-/-} mice seem more susceptible to. Moreover, sphingolipids may alter muscle contractility (36).

Animal behavior and tissue morphology

To examine the effects of *Gad11* deletion on brain function, we tested a range of mouse behaviors in *Gad11*^{+/+} (*n* = 13) and *Gad11*^{-/-} (*n* = 13) 22-week-old male mice. In the open field, the latency to first enter the center was significantly different between genotypes, with *Gad11*^{-/-} mice taking less time to enter the center (Fig. 5, A to E). However, the cumulative time spent in the center of the open field was not significant between groups nor was the elevated plus maze and resident

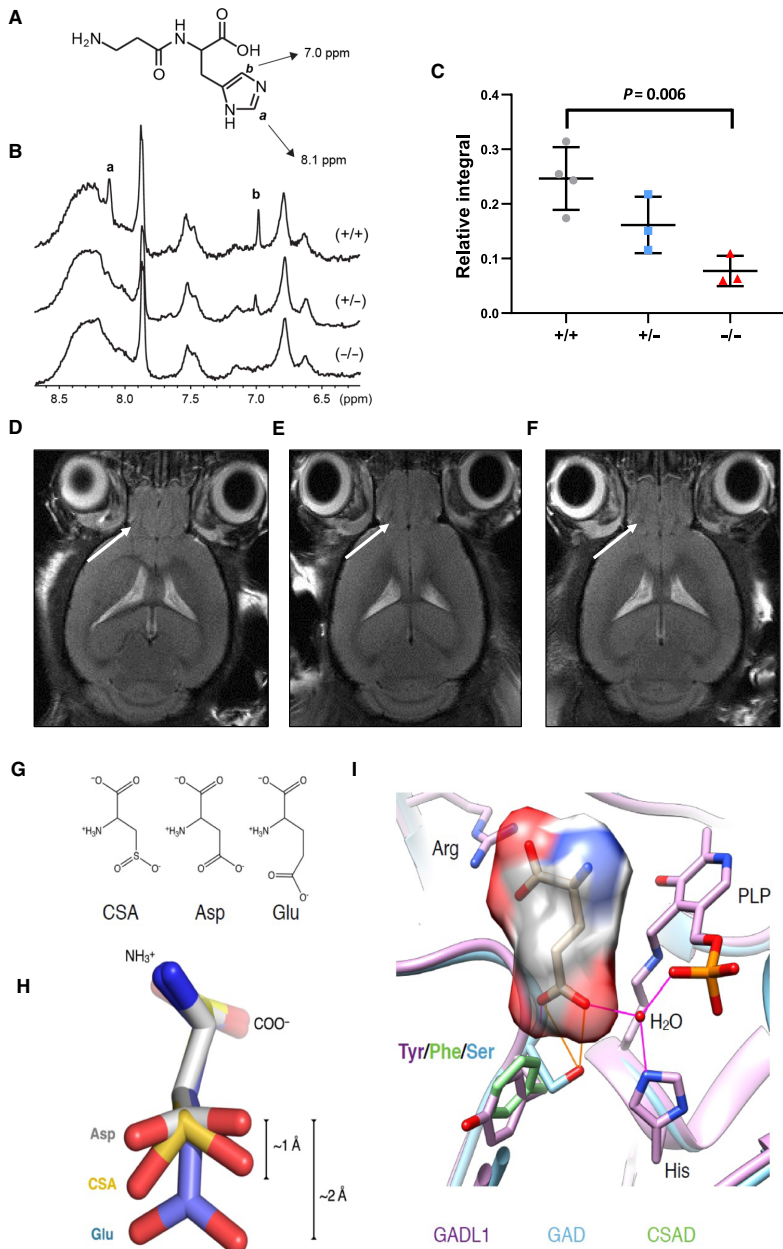


Fig. 3. $^1\text{H-NMR}$ and MRI of mouse tissues and substrate specificity of GADL1. (A to C) Measurement of carnosine in intact OB tissue. (A) Chemical structure of carnosine. ppm, parts per million. (B) MAS $^1\text{H-NMR}$ spectra of OB tissue samples from $Gad1^{+/+}$, $Gad1^{+/-}$, and $Gad1^{-/-}$ male mice (12 weeks). The two hydrogens of the imidazole ring in carnosine are marked a and b. (C) Relative integral based on NMR results, presented as means \pm SD. (D to F) MRI of the brain in (D) $Gad1^{+/+}$, (E) $Gad1^{+/-}$, and (F) $Gad1^{-/-}$ mice. The arrow indicates the OB. (G) Chemical structure comparison of GADL1 substrates CSA, Asp, and Glu. (H) 3D substrate structures to show the size and shape differences of Glu compared to CSA and Asp. (I) Active sites of GADL1, GAD, and CSAD and the predicted mode of binding of Glu to GAD. The prediction is based on the complex between GAD and the inhibitor chelidonic acid (63).

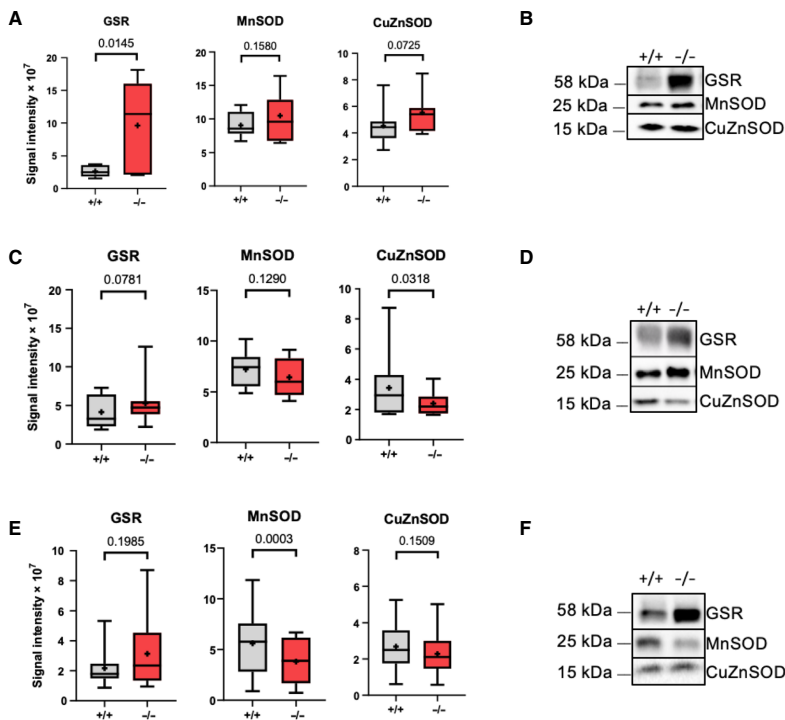


Fig. 4. Relative levels of antioxidant enzymes in *Gad1*^{-/-} mouse tissues. (A to E) Representative Western blots (B, D, and F) and normalized protein expression levels. (A), (C), and (E) for GSR, SOD1 (CuZnSOD), and SOD2 (Mn) in (A and B) OB, (C and D) cerebral cortex, and (E and F) SKM tissue from female *Gad1*^{+/+} and *Gad1*^{-/-} mice.

intruder test metrics. Only the difference in attack latency between initial testing and retesting 1 day later was significantly different between genotypes. Both genotypes showed a significant preference for the social versus nonsocial cylinder in the three-chamber task ($P < 0.0001$), but there was no significant difference between the genotypes. On this basis, it seems that a reduction of carnosine content in the mouse OB (~70%) and cerebral cortex (~40%) may result in the *Gad1*^{-/-} mice showing increased initiation to enter an exposed area (which is indicative of decreased anxiety). However, this should be tempered by the observation that the total time spent in the center of the open nor differences in the ratio of the time spent on closed versus open arms of the elevated plus maze were not different. Further investigation of any possible anxiolytic effect of *Gad1*^{-/-} mice is prudent.

To examine the effects of *Gad1* deletion on organ aging and morphology, we compared tissue sections from 33 mice aged 28 to 96 weeks, equally matched across different sex and genotypes. At the microscopic level, SKM, brain, and OB morphologies were not affected by the elimination of *Gad1* (fig. S5A).

Common genetic variants in the *GAD1* locus are associated with multiple human phenotypes

GWA studies (GWAS) have shown associations of the *GAD1* locus with multiple human traits and diseases, including eating disorders (37), kidney functions (38), and several blood metabolites. This includes a strong association with levels of acetylcarnosine ($P = 8.17 \times$

10^{-21}) in the *GAD1* locus at an intergenic SNP rs6804368 (13.9 kb from *GAD1* and 17.9 kb from *TGFBR2*) (26). The strongest association ($P = 5.50 \times 10^{-37}$) has been reported for the response to lithium (Li^+) in bipolar disorder at an SNP (rs17026688) located in intron 6 of *GAD1* (21). However, these findings were not replicated in other clinical samples (24).

To get an overview of genetic associations between human phenotypes and enzymes in carnosine metabolism, we conducted gene-based tests using the MAGMA software (39), mainly focusing on traits related to oxidative protection and brain functions. We included associations of common variants in *GAD1* and seven related genes (Fig. 5) (40). We limited the search to 21 phenotypes with openly available GWAS summary statistics obtained from large samples (total number of tests 167; Bonferroni-corrected P value threshold = 2.99×10^{-4}). Table S3 shows an overview of the data used.

GAD1 was associated with serum acetylcarnosine levels ($P = 1.25 \times 10^{-11}$), kidney function ($P = 1.03 \times 10^{-7}$), and subjective well-being ($P = 1.22 \times 10^{-4}$). *CARNMT1* was associated with body mass index ($P = 1.12 \times 10^{-4}$). *CARN1* was associated with right-hand grip strength (muscular strength) ($P = 4.98 \times 10^{-5}$). *SLC15A2* was associated with kidney function ($P = 8.60 \times 10^{-12}$). In addition, several tentative gene-phenotype associations did not pass the Bonferroni-corrected threshold for significance. In conclusion, of eight tested genes known to be involved in carnosine metabolism, *GAD1* and *SLC15A2* showed the strongest association with human phenotypes.

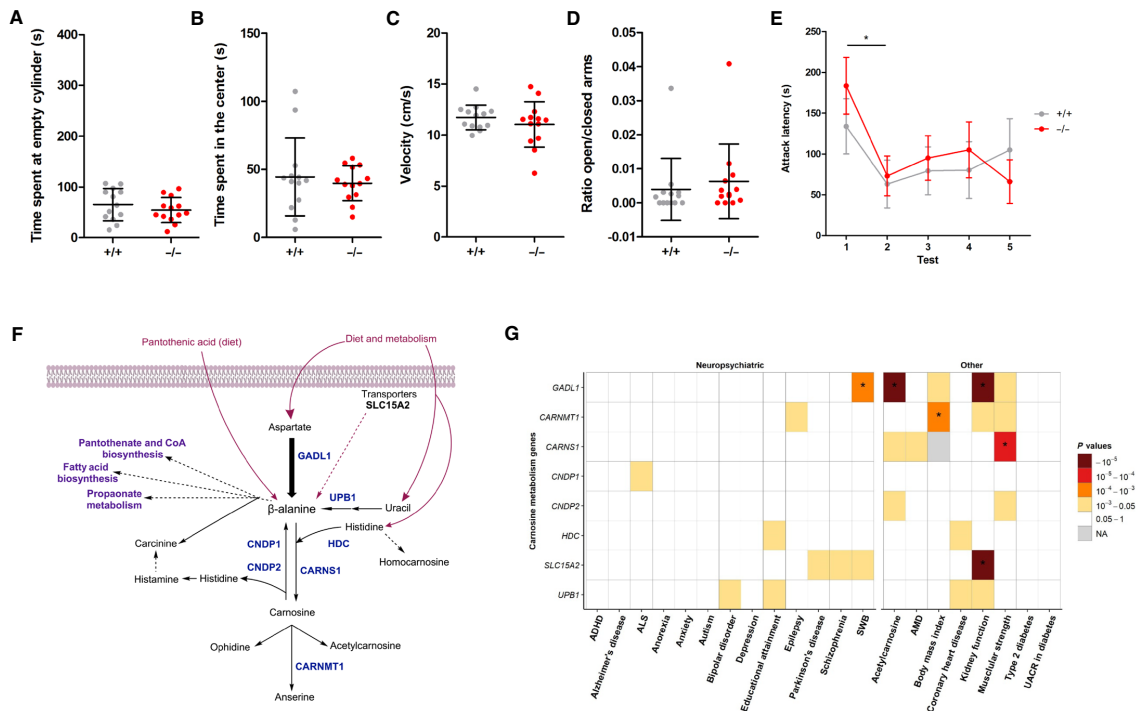


Fig. 5. Behavioral phenotypes associated with *Gad1*^{-/-} mice, carnine homeostasis and human phenotypes. (A) Three-chamber task: Time spent at each cylinder was not different between the genotypes. Both *Gad1*^{+/+} and *Gad1*^{-/-} mice prefer the social cylinder, indicating that sociability remains similar. (B) Open field task: The cumulative time spent in the center was not different between the genotypes. On this measure, no anti-anxiety effect was observed. However, on the latency to enter the center (another anxiety measure), *Gad1*^{-/-} was quicker to enter the center, which may suggest some anxiolytic effects of the *Gad1*^{-/-} phenotype that would require confirmation in additional studies. (C) Open field task: The exploration velocity was not different between the genotypes, indicating that there is no effect on motor function. Similar observations were made with the total distance moved data. Together, this suggests no effect of genotype on activity metrics. (D) Elevated plus maze: The ratio of the time spent (s) on the open and closed arms was found not to be different between the genotypes. Both genotypes prefer the closed (sheltered arm), suggesting no difference in anxiety on this measure. (E) Resident intruder paradigm: The attack latency against an intruder from the first to the fifth day (tests 1 to 5) was not different between the genotypes. Both genotypes attack faster on the second day compared to the first day after which the attack latency remains constant. This suggests no effect of genotype on aggression. (F) A summary overview of different pathways involving β-alanine. Genes analyzed in this study are marked in blue. (G) Association analyses of genes involved in the carnine metabolism. Asterisk indicates statistical significance after correction for multiple testing. ADHD, Attention deficiency hyperactivity disorder; ALS, Amyotrophic lateral sclerosis; SWB, subjective well being; AMD, age-related macular degeneration; UACR, Urine Albumin-to-Creatinine Ratio; NA, not applicable.

The most obvious associations were observed for acetylcarnosine levels, muscle strength, kidney function, and general well-being but not in a range of neuropsychiatric diseases that have been reported to respond to carnine treatment (Fig. 5, G and F) (14).

DISCUSSION

Carnosine peptides were found in 1900, yet their biological functions and biosynthetic routes are still being debated (1). Here, we report the first animal model lacking GADL1. We show that these animals have low levels of β-alanine and carnine peptides, consistent with a key role of GADL1 in their synthesis. This enzyme is analogous to Asp decarboxylases previously only found in prokaryotes and insects (23).

Carnosine peptides, except for homocarnosine, were significantly depleted in the brain and SKM. In contrast, the reduction was modest and nonsignificant in multiple other tissues including the kidney,

heart, whole blood, and serum. Furthermore, β-alanine was only reduced significantly in OB. As GADL1 activity was eliminated in *Gad1*^{-/-} mice, the remaining β-alanine and its peptide derivatives may be derived either from the diet, by gut bacteria, maternally transferred from heterozygous mothers used for breeding, or by de novo synthesis. Biochemical analyses of the standard plant-based rodent diet did confirm low levels of β-alanine and carnine, but we cannot exclude a possible small dietary contribution from β-alanine, pantothenic acid (vitamin B5), or carnine peptides (table S4). It is, however, more likely that there are several alternative biosynthetic routes for β-alanine and that these have different roles in different tissues. Thus, in tissues with the highest demands for carnine synthesis, i.e., SKM, brain, and particularly the OB, we demonstrate a critical role of de novo β-alanine biosynthesis to maintain its levels, as well as compensatory up-regulation of enzymes involved in alternative biosynthetic routes. As blood levels of β-alanine and carnine

peptides were moderately affected by elimination of GADL1, it seems that the muscle and brain are less dependent on uptake of these compounds from the circulation.

Alternative biosynthetic routes may include β -alanine synthesis by CSAD, which has a relatively low β -alanine synthetic specific activity but much higher tissue abundance than GADL1 (24), production of β -alanine from uracil by ureidopropionase 1 [β -alanine synthase, UPB1; N-carbamoyl- β -alanine amidohydrolase; (BUP1/UPB1)] (41), or by other enzymes, such as β -alanine-2-oxoglutarate transaminase (ABAT) or β -alanine pyruvate transaminase (AGXT2) (20). Our findings contrast earlier observations that found no decarboxylation of Asp in rat muscle (23). Dietary PLP supplementation significantly increases the concentrations of β -alanine and carnosine peptides in the SKM of rats (20). As GADL1 is dependent on PLP, this increase may be due to the activation of GADL1 by PLP. In contrast, PLP is not required for the production of β -alanine by UPB1. Our observation of increased *Upb1* transcript levels in the OB of *Gadl1*^{-/-} mice but unaltered levels of *Abat* and *Agxt2* indicates a role UPB1 in maintaining levels of β -alanine. However, this finding contradicts earlier observations of UPB1 protein in the rat liver and kidney but not in the brain, lung, SKM, or spleen (41).

In contrast to the reduced levels of β -alanine, carnosine, anserine, and acetylcarnosine, the levels of homocarnosine were increased. This is probably the result of a shortage of β -alanine precursor and carnosine peptides, indicating that the tissue levels of these dipeptides may be tightly regulated. Moreover, no significant difference in GABA between *Gadl1*^{+/+} and *Gadl1*^{-/-} mice was detected. Together with the observations of increased homocarnosine (a GABA-derived peptide), this indicates that GADL1, despite its name, does not catalyze the decarboxylation of glutamate to GABA. Figure 5F summarizes the different biosynthetic routes of carnosine peptides, and the main enzymes and transporters believed to be involved in this metabolism in mammalian tissues.

As the *Gadl1* locus on chromosome 3p24.1-3p23 is close to the *Tgfb2* locus (3p24.1) and genetic variants in the vicinity of *Gadl1* influence plasma levels of transforming growth factor- β (TGF- β) receptor type 2 (TGFB2), the gene-targeting strategy was designed to avoid regulatory sequences in this region. This strategy resulted in the expression of low amounts of a catalytically inactive and unstable partially truncated version of the GADL1 protein, but *Tgfb2* transcripts were unaltered.

To determine the substrate specificity of GADL1, we previously expressed the mouse enzyme in bacteria and screened purified GADL1 against all proteinogenic amino acids, as well as many other putative substrates and inhibitors, demonstrating decarboxylase activity against Asp, CSA, and cysteine (24). This substrate profile was similar to what Liu *et al.* (23) observed for the human enzyme. However, compared to other PLP-dependent decarboxylases, the affinity and selectivity were very low for all substrates tested. Liu *et al.* (23) reported that it was impossible to detect GADL1 enzyme activities in tissue lysates. Here, we show that, despite its extremely low activity in vitro, GADL1 is important for β -alanine and carnosine peptide synthesis, particularly in the OB, cerebral cortex, and SKM.

Gadl1^{-/-} mice also had decreased levels of taurine and multiple taurine derivatives in SKM, indicating that CSA also is a physiologically relevant substrate. *Gadl1*^{-/-} mice also showed other biochemical alterations that could be secondary to the depletion of β -alanine derivatives and antioxidant function or other effects of GADL1 inactivation. *Gadl1* deletion might alter energy metabolism through sev-

eral pathways. In addition to its role in carnosine synthesis, β -alanine is a component in pantothenic acid (vitamin B5) and coenzyme A, an essential cofactor for multiple biochemical pathways, including energy metabolism.

The role of GADL1 as a relatively nonspecific decarboxylase of low molecular weight acid substrates is consistent with its relatively high Michaelis-Menten constant (K_m) values and low catalytic efficacy (24). Mammalian genomes encode hundreds of PLP-dependent enzymes, many of which may catalyze new or unclassified reactions (31). In addition, because of their common mechanistic features and similar structures, many PLP-dependent enzymes can catalyze multiple biochemical reactions. This promiscuity makes it difficult to define their primary biological functions (31). Some enzymes have evolved to have multiple physiological substrates. Such a reactivity with multiple substrates may be advantageous for fitness (42). GADL1 may be an example of an enzyme with multiple biological activities. Although the strongest effect of GADL1 deletion seemed to be a decrease in β -alanine and carnosine peptides, with the taurine pathway being intact, the *Gadl1*^{-/-} mice also had slightly reduced levels of taurine derivatives in SKM, consistent with multiple catalytic functions of this enzyme. Similarly, while the accumulation of oxidative stress biomarkers in *Gadl1*^{-/-} mice is probably secondary to loss of β -alanine or carnosine peptides, we cannot exclude that the metabolic changes could be caused by other functions of GADL1.

Inspection of the catalytic site of mouse GADL1 shows that it might be accessible by different small, acidic, polar substrates. From the comparison (Fig. 3I), it can be observed that very minor changes in specificity-determining amino acids in the active site vicinity may dictate the function of an enzyme at the tissue and organism level. These structural features correspond well with the previously reported substrate specificity of purified mouse and human GADL1 (23–25). For a more detailed understanding of the catalytic properties of GADL1, as well as its closest homologs, high-resolution structural studies with active-site ligands, preferably with the flexible catalytic loop visible, will be required.

Both in vitro and in vivo experiments have shown that reactive oxygen species can decrease the levels of antioxidant enzymes, such as SOD and glutathione peroxidase, and that carnosine supplementation can restore depleted levels of these enzymes (1). Carnosine peptides are considered to be important in protection, e.g., against ischemia-related free radical damage (1). However, the protective function of carnosine has only been studied in vitro or in animals receiving large pharmacological doses of carnosine. Thus, β -alanine and carnosine dietary supplementation have widespread human use and are marketed to protect against oxidative stress (1). However, contradictory findings have been reported, and elevated levels of β -alanine were noted to reduce cellular taurine levels and to be associated with increased oxidative stress (43) and altered energy metabolism (44). Here, we show that the *Gadl1* deletion mice have increased levels of oxidative stress biomarkers and altered levels of several antioxidant enzymes. These findings establish this mouse model as a new tool to study not only β -alanine synthesis but also carnosine peptide biology and their relationship to oxidative stress and diseases.

Deletion of the mouse carnosine transporting dipeptide transporter *Pept2* (*SLC15A*) has previously been reported to alter carnosine levels in several organs but not as markedly as in the *Gadl1*^{-/-} mice (45). These organ-specific effects indicate that although β -alanine and carnosine peptides are mainly synthesized locally in the OB, other organs

mainly take up carnosine peptides and their precursors from the circulation. Carnosine homeostasis in SKM is regulated by multiple nutritional and hormonal stimuli in a complex interplay between transporters and enzymes, including *CARNS*, *CNDP2*, *PHT1*, *PHT2*, *TauT*, *PAT1*, *ABAT*, and *HDC* (Fig. 5F) (40). It was recently reported that in the SKM, *CARNS1* and *GADL1* are rapidly up-regulated upon high-intensity exercise, demonstrating the importance of carnosine in muscle function and physiological regulation of these enzymes (46). The importance of *GADL1* in carnosine synthesis is supported by human genetic studies showing a strong association of *GADL1* variants with blood levels of carnosine peptides (26). However, the tissue levels of carnosine peptides are reflecting levels of not only β -alanine and histidine and their biosynthetic enzymes but also other metabolites and enzymes. Thus, the enzymes and transporters involved in carnosine homeostasis are nonspecific and subjected to competitive inhibition by alternative substrates, which may differ between tissues (Fig. 5) (47).

Since *Gad11*^{-/-} mice displayed behavioral changes and β -alanine and carnosine peptides have been implicated in many different physiological functions and disease states, we performed a gene-based analysis of *GADL1* and enzymes and transporters directly involved in carnosine metabolism. We selected 21 human diseases and traits related to oxidative stress and where treatment with carnosine peptides has shown some promising effects (Fig. 5G) (12, 48). In addition to the strong associations with plasma carnosine peptide levels, common variants in the *GADL1* locus were associated with subjective well-being and muscle strength. The association with subjective well-being is particularly intriguing. This phenotype is genetically related to somatic complaints not only as bodily aches and pains but also as low energy, anxiety, and depression, traits that have all been shown in animal studies to be related to levels of carnosine peptides in the brain and SKM (49). However, for most of the diseases studied, we observed no significant associations with genes associated with carnosine homeostasis. Still, we cannot exclude possible effects of rare genetic variants or a role in other patient groups or populations. The behavioral data in the *Gad11*^{-/-} mice suggest that the link between *GADL1* with anxiety is worth exploring further, including the investigation of differences in sensory processing and alterations in fear-related behavior.

Brain metabolomics has revealed large regional differences, with particularly large concentration gradients for carnosine (50). However, it is still a mystery why *GADL1* and its carnosine peptide products are so abundant in OB. In zebrafish, high immunoreactivity for carnosine and anserine is found in sensory neurons and nonsensory cells of the olfactory epithelium, olfactory nerve, and the OB, indicating a specific role of these peptides in sensory organs (51). On the basis of the early occurrence of carnosine peptides during embryonic development, it has been suggested that these peptides play a role in the developing nervous system, specifically in the olfactory and visual function (51). Our findings of intact histological architecture and the modest behavioral effects of *Gad11* deletion may argue against this hypothesis. However, it is also possible that the remaining 10 to 30% carnosine peptides are adequate for maintaining these biological effects, as reported for other neurotrophic factors such as serotonin (52). Alternatively, a neuroprotective, antioxidant role of *GADL1* and carnosine peptides is conceivable. The olfactory epithelium provides a direct entry route from the environment to the OB and brain for substances that could cause oxidative stress. These substances can cause age-related cellular degeneration and olfactory damage, and

prevention of this damage depends on an intact antioxidant defense system. Although baseline *GADL1* levels are low, the levels of this enzyme may be up-regulated in response to oxidative damage and other physiological stressors, as shown in oligodendrocytes obtained from a mouse model of amyotrophic lateral sclerosis (53) and in SKM upon exercise (46).

CONCLUSIONS

GADL1 is essential for the production of β -alanine and carnosine peptides, particularly in the brain and SKM. Mice lacking *GADL1* have behavioral changes, increased oxidative stress markers, and age-related changes, underscoring the biological importance of these peptides. Common variants in the human *GADL1* locus are associated with plasma levels of acetylcarnosine, muscle strength, kidney function, and subjective well-being. Future studies should explore how this enzyme is regulated and its involvement in physiological functions, including antioxidant defense mechanisms, and pathological states.

MATERIALS

Chemicals in this study were purchased from Sigma-Aldrich if not otherwise stated. Probes for the qRT-PCR were from Thermo Fisher Scientific, the kits used were from Thermo Fisher Scientific or QIAGEN, agarose was from Apollo Scientific, and SDS-polyacrylamide gel electrophoresis (PAGE) gels were from Bio-Rad. O-Phthaldialdehyde reagent and 2-mercaptoethanol were from Merck Schuchardt. L-Carnosine nitrate salt was used as standard for NMR spectroscopy.

METHODS

Ethical statement

This study was carried out per Norwegian laws and regulations and the European Convention for the Protection of Vertebrate Animals used for Experimental and Other Scientific Purposes. The protocol was approved by the Animal Studies Committee, Norwegian Food Safety Authority (Mattilsynet, permit number 9468).

Generation of *Gad11*-null mice

Gad11-null (-) mice were generated by homologous recombination in C57BL/6N mice at genOway, Lyon, France. On the basis of the *Gad11* complementary DNA (cDNA) sequence NM_028638, the exon/intron organization of the gene was established. The mouse *Gad11* gene is located on chromosome 9 and extends over more than 183.6 kilobase pairs (kbp) (sequence map Chr9:115909455-116074347 bp, +strand). The mouse *Gad11* locus consists of 20 exons (Fig. 1). ATG initiation codons are located in exons 3, and stop codons are located in exons 19 and 20. Bioinformatic analysis identified three isoforms for *GADL1* protein and three predicted other splice variants of the *Gad11* gene. In the National Center for Biotechnology Information database release 106, four isoforms with predicted 518, 479, 362, and 502 amino acid residues (NM_028638) were identified. On the basis of sequence comparison and x-ray structural data (25), Lys⁴⁰⁵, Lys³³³, and His²¹⁹ are predicted to be essential amino acids of the PLP-binding region, and Arg⁴⁹⁴ and Gln¹²⁰ are essential amino acids of the substrate-binding region. Exon 7 is highly conserved and contains the substrate-binding residue Gln¹²⁰. This exon is present in all splice variants. In the mouse genome, the closest coding gene is *Tgfb2*, encoding the

TGFBR2 (sequence map Chr9:116087695-116175363 bp, –strand). This is involved in multiple biological pathways and cells. In addition, several noncoding genes and pseudogenes are located in this region. To minimize the risk of interfering with possible regulatory sequences, it was decided to delete only exon 7 in the *Gad1l* gene, resulting in the deletion of sequences encoding part of the active site domain of *Gad1l*, including Q120 (24). The mouse model was generated by homologous recombination in embryonic stem (ES) cells. For this purpose, a targeting vector containing regions homologous to the genomic *Gad1l* sequences was constructed. After its transfection into C57BL/6N ES cells, the recombined cell clones were injected into blastocysts. Mouse breeding was established with C57BL/6N Flp-deleter mice to remove the neomycin cassette. The heterozygous KO colony was produced by breeding with C57BL/6N Cre-deleter mice.

Breeding

Heterozygous siblings were mated to produce *Gad1l*^{-/-} homozygous pups. Further breeding and genotyping were performed at the animal facility at the University of Bergen (Bergen, Norway). Animals were group-housed in temperature- and light-controlled vivarium (21° ± 1°C; 12:12-hour light/dark artificial circadian rhythm). All experiments were conducted with 3- to 96-week-old mice of both sexes that were ad libitum fed using standard rodent diets [rat and mouse no. 1 (RM1)] during maintenance and RM3 during breeding (Scanbur/Special Diets Services, Witham, UK). These diets are plant-based. The content of natural amino acids is specified, but the content of carnosine peptides is not specified (<http://sdsdiets.com/pdfs/RM1-A-P.pdf>). Further analysis is shown in table S4.

Gad1l mouse genotype determination

DNA was extracted from mice ear samples at 2 weeks of age. Genotyping was performed using a multiplex PCR kit (#206143, QIAGEN). After initial heat activation at 94°C for 15 min, DNA was denatured at 94°C for 30 s, annealed at 60°C for 1.30 min, and extended at 72°C for 1.30 min. This cycle was repeated 25 times. DNA was extended for an additional 30 min after the last cycle. PCR products were analyzed using 2% agarose gel electrophoresis. The PCR product size was measured to 166 bp in the *Gad1l*^{-/-} mice and 330 and 750 bp in the *Gad1l*^{+/-} mice. All three base pair sizes were measured in the *Gad1l*^{+/-} mice (166, 330, and 750 bp). The sizes of PCR products and the primer sequences are summarized in table S5 and Fig. 1E.

Validation of the animal model

The deletion strategy was validated using DNA sequencing, RNA sequencing, proteomic analyses, and Western blotting. DNA sequencing confirmed that exon 7 was absent from the genomic DNA of the *Gad1l*^{-/-} mice. We determined branching scores that reflected each exon's splicing capability using the RNA splicing prediction tool SROOGLE (54). This gave a lower splicing score for exon 8 compared to exon 9, suggesting that splicing of exon 6 to exon 9 was favored over splicing to exon 8. The qRT-PCR data also suggested that the *Gad1l* mRNA from *Gad1l*^{-/-} mice was stable. However, sequence analysis showed that both exons 7 and 8 were absent from *Gad1l* mRNA in *Gad1l*^{-/-} mice. An mRNA devoid of exons 7 and 8 is expected to be stable and produce a truncated protein. Expression and purification of mouse GADL1 protein in *E. coli* were performed as described (fig. S2) (24). Site-directed mutagenesis of mouse GADL1 to generate a protein lacking exons 7 and 8 (coding protein sequence, NHPRFFNQLYAGLDYYSLAARIITEALNPSIYTYEVSPVFL-

VEEAVLKKMIECVGWKEGDGFNP) was performed using the following primers: GADL1, 5'-TTCAGAACCGCCTCTCCAC-3' (reverse), 5'-TCCAAGATTTTCAACCAGC-3' (forward), 5'-AGA-AAGCACCGCCGCTCCT-3' (forward), 5'-GGATGAGATAGACAGCCTGG-3' (forward), 5'-TTTCTGTTTCATGGGGTAAT-3' (forward), 5'-TGC GGATTTCGGAATCTTGC-3' (reverse), 5'-ACGCATCGTGGCCGGCATCA-3' (reverse), 5'-CGATTTCCGCC-TATTGGTTA-3' (forward), 5'-TGACAATCTTCTCGCGCAA-3' (reverse), 5'-ATGGGGGATCATGTAACCTCG-3' (forward), 5'-CTT-GCTGCAACTCTCTCAGG-3' (reverse), 5'-CGGATCAAGAGCT-ACCAACT-3' (forward), 5'-TAACGAAGCGCTGGCATTGA-3' (reverse), and 5'-GCCTTTGAGTGGCTGATAC-3' (forward).

Metabolomic studies using LC-MS

Animals were anesthetized using urethane (250 mg/ml) administered by intraperitoneal injection and adjusted to their individual weight (1.4 to 1.8 mg/kg). Tissues were perfused with 50 ml of 0.02% heparin-saline solution pumped through the heart's left ventricle before organ extraction. After dissection, the tissues were flash-frozen in liquid nitrogen and stored at -80°C until use. A total of 172 different tissue samples from 41 animals were shipped at -80°C to Metabolon Inc. (Durham, NC, USA) for further processing. Male and female mice were matched according to genotype and age. Table 2 shows the list of mice used in the metabolomic study.

All 41 animals were analyzed for brain, SKM, and liver metabolites. A subset of 21 animals (10 *Gad1l*^{+/-} and 11 *Gad1l*^{-/-}, 4.63 and 4.89 weeks, respectively) were analyzed for OB metabolites. Exploratory analyses were performed in the kidney, cerebellum, heart, whole blood, and serum from 12-week-old males (seven *Gad1l*^{+/-} and seven *Gad1l*^{-/-}). Because of limited capacity of the animal breeding facility, samples were dissected and shipped in three separate batches, with tissues from 10 (5 *Gad1l*^{+/-} and 5 *Gad1l*^{-/-}), 17 (8 *Gad1l*^{+/-} and 9 *Gad1l*^{-/-}), and 14 (7 *Gad1l*^{+/-} and 7 *Gad1l*^{-/-}) animals, respectively. All samples were processed using an identical pipeline.

At the Metabolon Company, samples were prepared using the automated Microlab STAR[®] system from the Hamilton Company. To remove protein, dissociate small molecules bound to protein or trapped in the precipitated protein matrix, and to recover chemically diverse metabolites, proteins were precipitated with methanol under vigorous shaking for 2 min (Glen Mills Geno/Grinder 2000), followed by centrifugation. The resulting extract was divided into four fractions for analysis using different chromatographic methods. Each sample extract was stored overnight under nitrogen before preparation for analysis. After that, the samples were reconstituted in appropriate solvents (according to the chromatographic method) contained a series of standards at fixed concentrations to ensure injection and chromatographic consistency.

Metabolomic analyses were performed through three chromatographic methods used that were based on reversed-phase/ultraperformance liquid chromatography (UPLC)-MS/MS chromatography with positive and negative ion mode electrospray ionization (ESI) and one chromatographic method using hydrophilic interaction liquid chromatography/UPLC-MS/MS with negative ion mode ESI. The columns used were Waters UPLC BEH C18 (2.1 mm by 100 mm, 1.7 μm) and Waters UPLC BEH Amide (2.1 mm by 150 mm, 1.7 μm).

Metabolomic analyses were performed at UPLC (Waters ACQUITY) coupled to Thermo Fisher Scientific Q Exactive high-resolution/accurate mass spectrometer interfaced with a heated ESI (HESI-II) source and Orbitrap mass analyzer operated at 35,000 mass resolution.

The MS analysis alternated between MS and MSⁿ scans using dynamic exclusion. The scan range varied slightly between methods but covered 70 to 1000 mass/charge ratio (*m/z*).

Compounds were identified by comparison to library entries of purified standards or recurrent unknown entities. Metabolon maintains a library based on authenticated standards that contain the retention time/index (RI), *m/z*, and chromatographic data (including MS/MS spectral data) on all molecules present in the library. Furthermore, biochemical identifications are based on three criteria: retention index within a narrow RI window of the proposed identification, accurate mass match to the library \pm 10 parts per million, and the MS/MS forward and reverse scores between the experimental data and authentic standards. The MS/MS scores are based on a comparison of the ions present in the experimental spectrum to the ions present in the library spectrum.

Normalized areas of each compound were rescaled to set the median equal to 1. The values obtained for each tissue were used for metabolomic analyses with MetaboAnalyst 4.0. Analyses of PLS-DA data were normalized using Pareto scaling.

¹H-NMR spectroscopy

MAS ¹H-NMR spectroscopy was performed using samples (13 to 20 mg of wet weight) of the OB from 12-week-old male mice of different genotypes *Gad1*^{-/-}, *Gad1*^{+/-}, and *Gad1*^{+/+}. After dissection, the samples were stored at -80°C before they were placed in 4-mm ZrO₂ MAS rotors with 50 μl of inserts and analyzed in a 500-MHz Bruker instrument at 4°C. Water signal decoupling was achieved by presaturation pulses. Each spectrum was recorded at an MAS rate of 5 kHz using 256 transients and a 5-s delay between each transient. To aid comparison, the maximal signal intensities were normalized to the same level for all samples.

¹H-MRI of living animals

Animals were anesthetized using 5 to 6% (v/v) sevoflurane (SevoFlo, Zoetis Inc., Kalamazoo, MI, USA) mixed with oxygen (200 cm³/min) for induction and ~3% for maintenance. During the MRI experiments, the respiration rate was monitored using a pressure sensor (SA Instruments, NY, USA). MRI investigations were performed with User PharmaScan 70/16 (7 T) scanner from Bruker (Bruker BioSpin GmbH, Ettlingen, Germany) using a 72-mm-inner diameter transmit coil together with a mouse brain four-element surface coil array for receiving the MR signal. We recorded 13 coronal T2-weighted images [slice thickness, 0.5 mm; slice distance, 0.05 mm; field of view (FOV), 20 mm by 20 mm; matrix size, 256 by 256] with fat suppression. The images were recorded with a turbo-RARE sequence [time to echo (TE), 38 ms; repetition time (TR), 3200 ms; four averages]. The FOV covered the whole brain including the OB. The software used with the scanner was ParaVision 6.0.1. Analysis of MR images was performed with Fiji ImageJ (version 1.46a, National Institute of Health, Bethesda, MD, USA). The OB was manually delineated in each image slice, and the number of pixels within each region of interest was translated to volume measurement.

RNA purification and qRT-PCR

Total RNA was purified from different tissues from both *Gad1*^{+/+} and *Gad1*^{-/-} mice using the RNeasy purification kit from QIAGEN (#741104; and for muscle tissue, #74704). cDNA was synthesized in triplicates from this RNA using a High-Capacity RNA-to-cDNA kit (#4387406, Applied Biosystems). qRT-PCR was performed using the TaqMan gene expression assay (TaqMan Gene Expression Master Mix, #4369016, Applied Biosystems). The TaqMan probes were as follows: Mm00520087_m1 (CSAD), Mm01348767_m1 (GADL1, exons 13 to

14), Mm01341531_m1 (GADL1, exons 3 to 4), Mm01341534_m1 (GADL1, exons 6 to 7), Mm99999915_g1 [glyceraldehyde-3-phosphate dehydrogenase (GAPDH)], and Mm00607939_s1 (β -actin). mRNA expression for all genotypes was normalized against the housekeeping genes GAPDH and β -actin using a variant (2 ^{ΔCt}) of the Livak method (2 ^{$-\Delta\text{Ct}$}), as described in the real-time PCR applications guide from Bio-Rad (55). Values are presented as means and upper 95% limit on an ln *y* scale.

RNA sequencing

RNA sequencing was performed using the TruSeq stranded mRNA prep kit from Illumina and an Illumina HiSeq 4000 instrument (paired end, 75 bp, \times 2 run). Raw data were quality controlled using the FastQC tool (available at www.bioinformatics.babraham.ac.uk/projects/fastqc). Raw reads were aligned to mouse genome M13 using HISAT2 (56). Read aligned to coding regions of the genome were counted using “FeatureCounts” (57). Normalization and differential gene expression were performed using DESeq2 (58). Transcripts from 27,878 genes at an average were detected. GO enrichment analysis was performed using tools “TopGo” and their dependencies in R environment (version 2.36.0). Biological pathways affected by the *Gad1* deletion were defined according to GO (27, 28) and the KEGG (27, 59). Among the 27,878 mouse genes reliably identified, we further analyzed up- or down-regulated genes with a log₂ fold change either less than -1 or greater than $+1$ and $P \leq 0.05$. Heat maps were made using ClustVis (59).

Western blotting

We used custom-made affinity-purified sheep antibodies generated against purified human GADL1 MBP (maltose-binding protein) fusion proteins (J. Hastie, University of Dundee). All the other antibodies were purchased from Abcam. The primary antibodies were anti-SOD1 (1:2000; CuZn; ab13498), anti-SOD2 (1:1000; Mn; ab68155), and anti-GLR1/GSR (1:5000; ab16801) prepared in 3% (w/v) bovine serum albumin (BSA) in 1 \times tris-buffered saline (20 mM Trizma base and 150 mM NaCl) with 0.1% (v/v) Tween 20 (TBST). Frozen tissue samples (OB, SKM, and cerebral cortex) were homogenized in radioimmunoprecipitation assay buffer containing a protease inhibitor cocktail. Equal amounts of protein (30 mg) were separated by SDS-PAGE and transferred to a nitrocellulose membrane (Bio-Rad) using a Trans-Blot Turbo transfer system (Bio-Rad) according to the manufacturer's protocols. Membranes were blocked with 3% BSA in TBST for 2 hours at room temperature before incubation with primary antibodies overnight at 4°C. The following day, membranes were incubated with the secondary antibody, anti-rabbit and goat anti-sheep horseradish peroxidase immunoglobulin G H + L (1:10,000; ab6721) (Bio-Rad, Hercules, CA), and developed with the enhanced chemiluminescence technique using a WesternBright Sirius kit (#K-12043-D20, Advansta) on a Gel DocTM XR+ system (Bio-Rad) with Image Lab software (version 6.0.1). All blots were normalized against the total protein load in a *Gad1*^{+/+} mouse.

Behavioral tests

There were 26 male mice, 13 mice from each genotype (*Gad1*^{+/+} and *Gad1*^{-/-}) tested for the behavioral experiments. The average age of *Gad1*^{+/+} and *Gad1*^{-/-} mice was 22.2 and 21.7 weeks, respectively. The order of testing of the mice was randomized for each test with the tasks following the order, three-chamber social interaction task, open field, elevated plus maze, and resident intruder task. Exclusively male mice were used to eliminate possible variation caused by the estrous cycle of female mice. Upon entry, all mice were provided with a unique tail number. All mice were housed at the institutional animal facility in an

individually ventilated cage (type 2L, Tecniplast S.p.A., Buguggiate, Italy) with an igloo as environmental enrichment and had ad libitum access to water and food. Mice were socially isolated before the open field task. The mice were housed under a reversed light/dark cycle (12:12 hours) in a ventilated cabinet, Scantainer (Scanbur, Karlslunde, Denmark), with sunset at 7:30 a.m. at a constant temperature of $24^{\circ} \pm 1^{\circ}\text{C}$. All experimental procedures were approved by the Committee of Animal Experiments of the Radboud University Medical Center (project number DEC2016-0094), Nijmegen, The Netherlands.

All the behavioral experiments were performed in the dark phase under red light conditions in the same experimental room. No experiments were performed within the first hour after the light/dark transition. All animals were given 1 month to acclimatize to the animal housing facility before behavioral testing. EthoVision XT9 software (Noldus, Wageningen, The Netherlands) was used for tracking the mice and analysis of the videos in the open field and elevated plus maze experiments with the Observer version 11 software (Noldus, Wageningen, The Netherlands) used for the assessment of the social interaction and resident intruder task experiments. All the behavioral tests were recorded using a high-speed (25 frames/s) infrared camera (GigE, Basler AG, Ahrensburg, Germany). MediaRecorder (Noldus, Wageningen, The Netherlands) was used to record these movies.

Open field

Locomotion activity was quantified in a 55 cm by 55 cm by 36 cm activity chamber that was positioned on a flat table with a camera directly above the center of the apparatus. The animals were placed in the center of the field where locomotion activity was then recorded for 5 min. The arena was divided into four quadrants in which the connected center points of all quadrants formed the center of the field and measured 27.5 cm by 27.5 cm. The total time in the center zone, outside the center, and time spent near the walls was measured, as well as the frequency of center visits. In addition, the latency to leave the center was used as an indication of immobility behavior. Reduced frequency of center visits, velocity, and distance traveled was used as indications of locomotor activity and anxiety behavior. Total distance traveled was measured by tracking movement from the center of the mice's body. The arena was cleaned with 70% alcohol between tests. Videotapes of the locomotion activity were examined using EthoVision XT9 (Noldus, Wageningen, The Netherlands).

Elevated plus maze

The apparatus provided by Noldus consisted of two open arms and two closed arms (36 cm by 6 cm, 15-cm-high walls) with a common central platform (6 cm²). The apparatus was placed 60 cm above the ground. At the start, animals were placed at the junction of the open and closed arms with the head facing the closed arms. The elevated plus maze was performed in the dark phase under dim light conditions. The time spent in the open and closed arms were examined as a time ratio (RT). The RT is the time spent in the open arms (TO) divided by total time spent in both closed (TC) and open arms (TO): $RT = TO / (TO + TC)$. Furthermore, the frequency of transition between the arms, the total distance traveled, and velocity was measured. Between each animal, the maze was cleaned with 70% ethanol and dried before testing the next animal.

Resident intruder paradigm

The resident intruder paradigm was performed to assess territorial aggression. On each testing day, an unfamiliar C57BL/6J intruder mouse was encountered, which was randomly assigned to a resident for each interaction. All animals, both resident and intruder, were tested once a day. The housing cage of the resident was used as the

interaction area. A transparent Plexiglas screen was placed in the middle of the cage to prevent direct interaction between animals but to enable visual, auditory, and olfactory perception. The intruder mouse was placed at the other side of the plastic screen for a period of 5 min. Hereafter, the screen was removed, and the interaction was videotaped for 5 min. After the test, the intruder was removed from the cage, and both animals were weighed and checked for wounds. The frequency of attacks and bites and the latency to the first attack were analyzed manually for all interaction days. An attack latency of 300 s was taken in case no attack occurred within the 5-min interaction window.

Three-chamber social interaction test

A standard three-chamber task arena (Noldus, Wageningen, The Netherlands) was used in a dark room with red overhead lighting. During the first 10 min of the test, the test mouse was placed alone in the arena to habituate to the new environment. In both the left and right chambers, an empty acrylic cylinder with bars was placed. After 10 min, an interaction mouse (C57BL/6J mouse, same age as test mouse) was placed in a cylinder, randomly in either the left or right cylinder. Testing was spread across 2 days with each C57BL/6J mouse used maximally four times as an interaction mouse. The order of testing was counterbalanced. For 10 min, test mice were allowed to investigate the arena with the interaction mouse in it.

Carnosine-related genes in human phenotypes

To conduct the gene-based analyses, we obtained openly available summary statistics from GWAS performed in individuals of European descent (table S3). We then restricted the data, where possible, to SNPs with a minor allele frequency of 1%, with good imputation quality (imputation information score, >0.8), and that were represented in more than 70% of the total meta-analyzed sample size. We then calculated the eight genes of interest's association with the chosen phenotypes using MAGMA (39). The gene-phenotype associations were calculated using the individual SNPs' *P* values for association with the respective phenotypes. SNPs were assigned to a gene if their chromosomal location were within the start and end of the gene transcripts (i.e., the standard settings of MAGMA). We used the 1000 genomes CEU (Northern Europeans from Utah) population as the reference panel to correct for linkage disequilibrium.

Variant effect prediction

In total, Ensembl reported 23,292 SNPs in human GADL1, with 78% of them being intronic. Among the coding variants, 67% were presented as missense, 23% as synonymous, 5% as frameshift, 3% as stop gained, and 1% as in-frame deletion.

Structural analyses

For comparative protein structure analysis, the structures of mouse GADL1 (25) (PDB entry 6enz), human CSAD (PDB entry 2jis), and human GAD65 (60) (PDB entries 2okk) were used. To predict the binding mode of Glu into GAD65, its structure was re-refined and observed to contain the inhibitor chelidonic acid, based on which the Glu binding mode can easily be obtained because of the presence of two appropriately spaced carboxyl groups. Structures were superposed in COOT (61) and visualized in Chimera (62).

Hematoxylin and eosin staining

For the histochemistry studies, the organs were fixed with formalin. The samples were paraffin-embedded and sectioned into 40- μm -thick slices. For hematoxylin and eosin staining, sections were deparaffinized in Tissue-Clear II (2 \times 10 min) and rehydrated using 100% ethanol (2 \times 1 min each), followed by 96% ethanol (1 min) and then 70% ethanol for 1 min and double-distilled H₂O (ddH₂O) for 3 min.

Sections were then dipped in 0.2% hematoxylin (Histolab) for 5 min, eosin for 1 min, followed by a 5-s wash with ddH₂O. The sections were then rehydrated in 70% ethanol for 30 s, followed by dipping in 96% (2 min) and 100% ethanol (2 × 2 min). Last, the sections were dipped in xylene for 2 min, mounted on slides, and coverslipped. Hamamatsu slide scanner was used for scanning slides, and Aperio software was used to take pictures.

Statistics

All data, unless specified otherwise, are presented as means ± SD. The growth curves (Fig. 1, B and C), enzyme activity assay (Fig. 1H), NMR (Fig. 3C), MRI, and animal behavior (Fig. 5, A to E) were analyzed with unpaired Student's *t* test (two-tailed). Statistical significance was defined as $P \leq 0.05$. Metabolomics data (Fig. 2 and fig. S4) were analyzed with unpaired Student's *t* test (two-tailed) with Welch's correction. Antioxidant levels (Fig. 4) were analyzed with a ratio, paired *t* test (two-tailed) per experimental setup.

Study approval

The protocol used in this manuscript was approved by the Animal Studies Committee, Norwegian Food Safety Authority (Mattilsynet, permit number 9468).

SUPPLEMENTARY MATERIAL

Supplementary material for this article is available at <http://advances.sciencemag.org/cgi/content/full/6/29/eabb3713/DC1>

[View/request a protocol for this paper from Bio-protocol.](#)

REFERENCES AND NOTES

- A. A. Boldyrev, G. Aldini, W. Derave, Physiology and pathophysiology of carnosine. *Physiol. Rev.* **93**, 1803–1845 (2013).
- R. Chaleckis, I. Murakami, J. Takada, H. Kondoh, M. Yanagida, Individual variability in human blood metabolites identifies age-related differences. *Proc. Natl. Acad. Sci. U.S.A.* **113**, 4252–4259 (2016).
- A. R. Hipkiss, Is carnosine a naturally occurring suppressor of oxidative damage in olfactory neurons? *Rejuvenation Res.* **7**, 253–255 (2004).
- T. L. Perry, S. Hansen, B. Tischler, R. Bunting, K. Berry, Carnosine — A new metabolic disorder associated with neurologic disease and mental defect. *N. Engl. J. Med.* **277**, 1219–1227 (1967).
- K. Wisniewski, L. Fleisher, D. Rassin, H. Lassmann, Neurological disease in a child with carnosinase deficiency. *Neuropediatrics* **12**, 143–151 (1981).
- J. H. Cararo, E. L. Streck, P. F. Schuck, G. da C. Ferreira, Carnosine and related peptides: Therapeutic potential in age-related disorders. *Aging Dis.* **6**, 369–379 (2015).
- R. M. Hobson, B. Saunders, G. Ball, R. C. Harris, C. Sale, Effects of β -alanine supplementation on exercise performance: A meta-analysis. *Amino Acids* **43**, 25–37 (2012).
- A. E. Smith, A. A. Walter, J. L. Graef, K. L. Kendall, J. R. Moon, C. M. Lockwood, D. H. Fukuda, T. W. Beck, J. T. Cramer, J. R. Stout, Effects of β -alanine supplementation and high-intensity interval training on endurance performance and body composition in men; a double-blind trial. *J. Int. Soc. Sports Nutr.* **6**, 5 (2009).
- B. Saunders, K. Elliott-Sale, G. G. Artioli, P. A. Swinton, E. Dolan, H. Roschel, C. Sale, B. Gualano, β -alanine supplementation to improve exercise capacity and performance: A systematic review and meta-analysis. *Br. J. Sports Med.* **51**, 658–669 (2016).
- M. G. Chez, C. P. Buchanan, M. C. Aimonovitch, M. Becker, K. Schaefer, C. Black, J. Komen, Double-blind, placebo-controlled study of L-carnosine supplementation in children with autistic spectrum disorders. *J. Child Neurol.* **17**, 833–837 (2002).
- T. Murakami, M. Furuse, The impact of taurine- and beta-alanine-supplemented diets on behavioral and neurochemical parameters in mice: Antidepressant versus anxiolytic-like effects. *Amino Acids* **39**, 427–434 (2010).
- M. Schön, A. Mousa, M. Berk, W. L. Chia, J. Ukropec, A. Majid, B. Ukropcová, B. de Courten, The potential of carnosine in brain-related disorders: A comprehensive review of current evidence. *Nutrients* **11**, 1196 (2019).
- G. G. Artioli, B. Gualano, A. Smith, J. Stout, A. H. Lanch Jr., Role of β -alanine supplementation on muscle carnosine and exercise performance. *Med. Sci. Sports Exerc.* **42**, 1162–1173 (2010).
- E. J. Anderson, G. Vistoli, L. A. Katunga, K. Funai, L. Regazzoni, T. Blake Monroe, E. Gilardoni, L. Cannizzaro, M. Colzani, D. De Maddis, G. Rossini, R. Canevotti, S.agliardi, M. Carini, G. Aldini, A carnosine analog mitigates metabolic disorders of obesity by reducing carbonyl stress. *J. Clin. Invest.* **128**, 5280–5293 (2018).
- M. Dunnett, R. C. Harris, Influence of oral β -alanine and L-histidine supplementation on the carnosine content of the *gluteus medius*. *Equine Vet. J. Suppl.* **30**, 499–504 (1999).
- E. P. Rhee, J. E. Ho, M.-H. Chen, D. Shen, S. Cheng, M. G. Larson, A. Ghorbani, X. Shi, I. T. Helenius, C. J. O'Donnell, A. L. Souza, A. Deik, K. A. Pierce, K. Bullock, G. A. Walford, R. S. Vasan, J. C. Florez, C. Clish, J.-R. J. Yeh, T. J. Wang, R. E. Gerszten, A genome-wide association study of the human metabolome in a community-based cohort. *Cell Metab.* **18**, 130–143 (2013).
- R. Zrenner, H. Riegler, C. R. Marquard, P. R. Lange, C. Gericke, C. E. Bartosz, C. T. Chen, R. D. Slocum, A functional analysis of the pyrimidine catabolic pathway in Arabidopsis. *New Phytol.* **183**, 117–132 (2009).
- F. Schmitzberger, M. L. Kilkenny, C. M. C. Lobley, M. E. Webb, M. Vinkovic, D. Matak-Vinkovic, M. Witty, D. Y. Chirgadzhe, A. G. Smith, C. Abell, T. L. Bundell, Structural constraints on protein self-processing in L-aspartate- α -decarboxylase. *EMBO J.* **22**, 6193–6204 (2003).
- S. Chopra, H. Pai, A. Ranganathan, Expression, purification, and biochemical characterization of *Mycobacterium tuberculosis* aspartate decarboxylase, PanD. *Protein Expr. Purif.* **25**, 533–540 (2002).
- S. Suidasari, J. Stauteamas, S. Uragami, N. Yanaka, W. Derave, N. Kato, Carnosine content in skeletal muscle is dependent on vitamin B6 status in rats. *Front. Nutr.* **2**, 39 (2015).
- C.-H. Chen, C.-S. Lee, M.-T. M. Lee, W.-C. Ouyang, C.-C. Chen, M.-Y. Chong, J.-Y. Wu, H. K.-L. Tan, Y.-C. Lee, L.-J. Chuo, N.-Y. Chiu, H.-Y. Tsang, T.-J. Chang, F.-W. Lung, C.-H. Chiu, C.-H. Chang, Y.-S. Chen, Y.-M. Hou, C.-C. Chen, T.-J. Lai, C.-L. Tung, C.-Y. Chen, H.-Y. Lane, T.-P. Su, J. Feng, J.-Y. Lin, C.-J. Chang, P.-R. Teng, C.-Y. Liu, C.-K. Chen, I.-C. Liu, J.-J. Chen, T. Lu, C.-C. Fan, C.-K. Wu, C.-F. Li, K. H.-T. Wang, L. S.-H. Wu, H.-L. Peng, C.-P. Chang, L.-S. Lu, Y.-T. Chen, A. T.-A. Cheng, Taiwan Bipolar Consortium, Variant GADL1 and response to lithium therapy in bipolar I disorder. *N. Engl. J. Med.* **370**, 119–128 (2014).
- C. Cruceanu, M. Alda, P. A. Dion, G. Turecki, G. A. Rouleau, No evidence for GADL1 variation as a bipolar disorder susceptibility factor in a Caucasian lithium-responsive cohort. *Am. J. Psychiatry* **172**, 94–95 (2015).
- P. Liu, X. Ge, H. Ding, H. Jiang, B. M. Christensen, J. Li, Role of glutamate decarboxylase-like protein 1 (GADL1) in taurine biosynthesis. *J. Biol. Chem.* **287**, 40898–40906 (2012).
- I. Winge, K. Teigen, A. Fossbakk, E. Mahootchi, R. Kleppe, F. Skoldberg, O. Kämpe, J. Haavik, Mammalian CSAD and GADL1 have distinct biochemical properties and patterns of brain expression. *Neurochem. Int.* **90**, 173–184 (2015).
- A. Raasakka, E. Mahootchi, I. Winge, W. Luan, P. Kursula, J. Haavik, Structure of the mouse acidic amino acid decarboxylase GADL1. *Acta Crystallogr. F. Struct. Biol. Commun.* **74** (Pt 1), 65–73 (2018).
- S.-Y. Shin, E. B. Fauman, A.-K. Petersen, J. Krumsiek, R. Santos, J. Huang, M. Arnold, I. Erte, V. Forgetta, T.-P. Yang, K. Walter, C. Menni, L. Chen, L. Vasquez, A. M. Valdes, C. L. Hyde, V. Wang, D. Ziemek, P. Roberts, L. Xi, E. Grundberg: The Multiple Tissue Human Expression Resource (MUTHER) Consortium, M. Waldenberger, J. B. Richards, R. P. Mohney, M. V. Milburn, S. L. John, J. Trimmer, F. J. Theis, J. P. Overington, K. Suhre, M. J. Broxnan, C. Gieger, G. Kastenmüller, T. D. Spector, N. Soranzo, An atlas of genetic influences on human blood metabolites. *Nat. Genet.* **46**, 543–550 (2014).
- M. Kanehisa, S. Goto, KEGG: Kyoto encyclopedia of genes and genomes. *Nucleic Acids Res.* **28**, 27–30 (2000).
- The Gene Ontology Consortium, Gene Ontology Consortium: Going forward. *Nucleic Acids Res.* **43** (Database issue), D1049–D1056 (2015).
- R. M. Kream, F. L. Margolis, Olfactory marker protein: Turnover and transport in normal and regenerating neurons. *J. Neurosci.* **4**, 868–879 (1984).
- T.-N. Wu, C.-K. Chen, C.-S. Lee, B.-J. Wu, H.-J. Sun, C.-H. Chang, C.-Y. Chen, L. S.-H. Wu, A. T.-A. Cheng, Lithium and GADL1 regulate glycogen synthase kinase-3 activity to modulate *KCTD12* expression. *Sci. Rep.* **9**, 10255 (2019).
- R. Percudani, A. Peracchi, A genomic overview of pyridoxal-phosphate-dependent enzymes. *EMBO Rep.* **4**, 850–854 (2003).
- G. Fenalti, R. H. P. Law, A. M. Buckle, C. Langendorf, K. Tuck, C. J. Rosado, N. G. Faux, K. Mahmood, C. S. Hampe, J. P. Banga, M. Wilce, J. Schmidberger, J. Rosjohn, O. El-Kabbani, R. N. Pike, A. I. Smith, I. R. Mackay, M. R. Rowley, J. C. Whisstock, GABA production by glutamic acid decarboxylase is regulated by a dynamic catalytic loop. *Nat. Struct. Mol. Biol.* **14**, 208–286 (2007).
- E. Park, S. Y. Park, C. Dobkin, G. Schuller-Levis, Development of a novel cysteine sulfonic acid decarboxylase knockout mouse: Dietary taurine reduces neonatal mortality. *J. Amino Acids* **2014**, 346809 (2014).
- J. E. Dominy Jr., C. R. Simmons, L. H. Hirschberger, J. Hwang, R. M. Coloso, M. H. Stipanuk, Discovery and characterization of a second mammalian thiol dioxygenase, cysteamine dioxygenase. *J. Biol. Chem.* **282**, 25189–25198 (2007).

35. A. A. Boldyrev, Carnosine: New concept for the function of an old molecule. *Biochemistry (Moscow)* **77**, 313–326 (2012).
36. M. N. Nikolova-Karakashian, M. B. Reid, Sphingolipid metabolism, oxidant signaling, and contractile function of skeletal muscle. *Antioxid. Redox Signal.* **15**, 2501–2517 (2011).
37. T. D. Wade, S. Gordon, S. Medland, C. M. Bulik, A. C. Heath, G. W. Montgomery, N. G. Martin, Genetic variants associated with disordered eating. *Int. J. Eat. Disord.* **46**, 594–608 (2013).
38. M. Wuttke, Y. Li, M. Li, K. B. Sieber, M. F. Feitosa, M. Gorski, A. Tin, L. Wang, A. Y. Chu, A. Hoppmann, H. Kirsten, A. Giri, J.-F. Chai, G. Sveinbjornsson, B. O. Tayo, T. Nutile, C. Fuchsberger, J. Marten, M. Cocca, S. Ghasemi, Y. Xu, K. Horn, D. Noce, P. J. van der Most, S. Sedaghat, Z. Yu, M. Akiyama, S. Afaq, T. S. Ahluwalia, P. Almgren, N. Amin, J. Ärnlöv, S. J. L. Bakker, N. Bansal, D. Baptista, S. Bergmann, M. L. Biggs, G. Biino, M. Boehnke, E. Boerwinkle, M. Boissel, E. P. Bottinger, T. S. Boutin, H. Brenner, M. Brumat, R. Burkhardt, A. S. Butterworth, E. Campana, A. Campbell, H. Campbell, M. Canouil, R. J. Carroll, E. Catamo, J. C. Chambers, M.-L. Chee, M.-L. Chee, X. Chen, C.-Y. Cheng, Y. Cheng, K. Christensen, R. Cifkova, M. Giulio, M. P. Concas, J. P. Cook, J. Coresh, T. Corre, C. F. Sala, D. Cusi, J. Danesh, E. W. Daw, M. H. de Borst, A. De Grandi, R. de Mutser, A. P. J. de Vries, F. Degenhardt, G. Delgado, A. Demirkan, E. D. Angelantonio, K. Dittrich, J. Divers, R. Dorajoo, K.-U. Eckardt, G. Ehret, P. Elliott, K. Endlich, M. K. Evans, J. F. Felix, V. H. X. Foo, O. H. Franco, A. Franke, B. I. Freedman, S. Freitag-Wolf, Y. Friedlander, P. Froguel, R. T. Gansevoort, H. Gao, P. Gasparini, J. M. Gaziano, V. Giedraitis, C. Gieger, G. Girotto, F. Giulianini, M. Gögele, S. D. Gordon, D. F. Gudbjartsson, V. Gudnason, T. Haller, P. Hamet, T. B. Harris, C. A. Hartman, C. Hayward, J. N. Hellwege, C.-K. Heng, A. A. Hicks, E. Hofer, W. Huang, N. Hutri-Kähönen, S.-J. Hwang, M. A. Ikram, O. S. Indridason, E. Ingelsson, M. Ising, V. W. V. Jaddoe, J. Jakobsdottir, J. B. Jonas, P. K. Joshi, N. S. Josyula, B. Jung, M. Kähönen, Y. Kamatani, C. M. Kammerer, M. Kanai, M. Katarinen, S. M. Kerr, C.-C. Khor, W. Kiess, M. E. Kleber, W. Koenig, J. S. Koener, A. Körner, P. Kovacs, A. T. Kraja, A. Kravjovicova, H. Kramer, B. K. Krämer, F. Kronenberg, M. Kubo, B. Kühnel, M. Kuokkanen, J. Kuusisto, M. L. Bianca, M. Laakso, L. A. Lange, C. D. Langefeld, J. J.-M. Lee, B. Lehne, T. Lehtimäki, W. Lieb, L. C. Study, S.-C. Lim, L. Lind, C. M. Lindgren, J. Liu, J. Liu, M. Loeffler, R. J. F. Loos, S. Lucae, M. A. Lukas, L.-P. Lyttikäinen, R. Mägi, P. K. E. Magnusson, A. Mahajan, N. G. Martin, J. Martyn, W. März, D. Mascalcioni, K. Matsuda, C. Meisinger, T. Meitinger, O. Melander, A. Metspalu, E. K. Mikaelssdottir, Y. Milaneschi, K. Milku, P. P. Mishra; A. M. Million Veteran Program, K. L. Mohlke, N. Mononen, G. W. Montgomery, D. O. Mook-Kanamori, J. C. Mychaleckyj, G. N. Nadkarni, M. A. Nalls, M. Nauck, K. Nikus, B. Ning, I. M. Nolte, R. Noordam, J. O'Connell, M. L. O'Donoghue, I. Olafsson, A. J. Oldehinkel, M. Orho-Melander, W. H. Ouwehand, S. Padmanabhan, N. D. Palmer, R. Palsson, B. W. J. H. Penninx, T. Perls, M. Perola, M. Pirastu, N. Pirastu, G. Pistis, A. I. Podgorina, O. Polasek, B. Ponte, D. J. Porteous, T. Poulain, P. P. Pramstaller, M. H. Preuss, B. P. Prins, M. A. Province, T. J. Rabelink, L. M. Raffield, O. T. Raitakari, D. F. Reilly, R. Rettig, M. Rheinberger, K. M. Rice, P. M. Ridker, F. Rivadeneira, F. Rizzati, D. J. Roberts, A. Robino, P. Rossing, I. Rudan, R. Rueedi, D. Ruggiero, K. A. Ryan, Y. Saba, C. Sabanayagam, V. Salomaa, E. Salvi, K.-U. Saum, H. Schmidt, R. Schmidt, B. Schöttker, C.-A. Schulz, N. Schuh, C. M. Shaffer, Y. Shi, A. V. Smith, B. H. Smith, N. Soranzo, C. N. Spracklen, K. Strauch, M. H. Stringham, M. Stumvoll, P. O. Svensson, S. Szymczak, E.-S. Tai, S. M. Tajuddin, N. Y. Q. Tan, K. D. Taylor, A. Teren, Y.-C. Tham, J. Thiery, C. H. L. Thio, H. Thomsen, G. Thorleifsson, D. Toniolo, A. Tönjes, J. Tremblay, I. Tzoulaki, A. G. Uitterlinden, S. Vaccargiu, R. M. van Dam, P. van der Harst, C. M. van Duijn, D. R. Velez Edward, N. Verweij, S. Voegelzang, U. Volker, P. Vollenweider, G. Waeber, M. Waldenberger, L. Wallentin, Y. X. Wang, C. Wang, D. M. Waterworth, B. W. Wei, H. White, J. B. Whitfield, S. H. Wild, J. F. Wilson, M. K. Wojczynski, C. Wong, T.-Y. Wong, L. Xu, Q. Yang, M. Yasuda, L. M. Yerges-Armstrong, W. Zhang, A. B. Zonderman, J. I. Rotter, M. Bochud, B. M. Psaty, V. Vitart, J. G. Wilson, A. Dehghan, A. Parsa, D. I. Chasman, K. Ho, A. P. Morris, O. Devuyst, S. Akilesh, S. A. Pendergrass, X. Sim, C. A. Böger, Y. Okada, T. L. Edwards, H. Snieder, K. Stefansson, A. M. Hung, I. M. Heid, M. Scholz, A. Teumer, A. Köttgen, C. Pattaro, A catalog of genetic loci associated with kidney function from analyses of a million individuals. *Nat. Genet.* **51**, 957–972 (2019).
39. C. A. de Leeuw, J. M. Mooij, T. Heskes, D. Posthuma, MAGMA: Generalized gene-set analysis of GWAS data. *PLoS Comput. Biol.* **11**, e1004219 (2015).
40. I. Everaert, H. De Naeyer, Y. Taes, W. Deraeve, Gene expression of carnosine-related enzymes and transporters in skeletal muscle. *Eur. J. Appl. Physiol.* **113**, 1169–1179 (2013).
41. M. M. Matthews, T. W. Traut, Regulation of *N*-carbamoyl- β -alanine amidohydrolase, the terminal enzyme in pyrimidine catabolism, by ligand-induced change in polymerization. *J. Biol. Chem.* **262**, 7232–7237 (1987).
42. A. Peracchi, The limits of enzyme specificity and the evolution of metabolism. *Trends Biochem. Sci.* **43**, 984–996 (2018).
43. A. Shetewy, K. Shimada-Takaura, D. Warner, C. J. Jong, A.-B. Al Mehdi, M. Alexeyev, K. Takahashi, S. W. Schaffer, Mitochondrial defects associated with β -alanine toxicity: Relevance to hyper-beta-alaninemia. *Mol. Cell. Biochem.* **416**, 11–22 (2016).
44. T. Gemelli, R. B. de Andrade, D. B. Rojas, N. F. Bonorino, P. N. Mazzola, L. S. Tortorelli, C. Funchal, C. S. D. Filho, C. M. D. Wannmacher, Effects of β -alanine administration on selected parameters of oxidative stress and phosphoryltransfer network in cerebral cortex and cerebellum of rats. *Mol. Cell. Biochem.* **380**, 161–170 (2013).
45. M. A. Kamal, H. Jiang, Y. Hu, R. F. Keep, D. E. Smith, Influence of genetic knockout of *Pept2* on the in vivo disposition of endogenous and exogenous carnosine in wild-type and *Pept2* null mice. *Am. J. Physiol. Regul. Integr. Comp. Physiol.* **296**, R986–R991 (2009).
46. E. Miyamoto-Mikami, K. Tsuji, N. Horii, N. Hasegawa, S. Fujie, T. Homma, M. Uchida, T. Hamaoka, H. Kanehisa, I. Tabata, M. Iemitsu, Gene expression profile of muscle adaptation to high-intensity intermittent exercise training in young men. *Sci. Rep.* **8**, 16811 (2018).
47. J. Drozak, M. Veiga-da-Cunha, D. Vertommen, V. Stroobant, E. Van Schaftingen, Molecular identification of carnosine synthase as ATP-grasp domain-containing protein 1 (ATPGD1). *J. Biol. Chem.* **285**, 9346–9356 (2010).
48. B. Janssen, D. Hohenadel, P. Brinkkoetter, V. Peters, N. Rind, C. Fischer, I. Rychlik, M. Cerna, M. Romzova, E. de Heer, H. Baelde, S. J. L. Bakker, M. Zirie, E. Rondeau, P. Mathieson, M. A. Saleem, J. Meyer, H. Köppel, S. Sauerhofer, C. R. Bartram, P. Nawroth, H.-P. Hammes, B. A. Yard, J. Zschocke, F. J. van der Woude, Carnosine as a protective factor in diabetic nephropathy: Association with a leucine repeat of the carnosinase gene *CNDP1*. *Diabetes* **54**, 2320–2327 (2005).
49. M. A. Babizhayev, Biochemical, biomedical and metabolic aspects of imidazole-containing dipeptides with the inherent complexity to neurodegenerative diseases and various states of mental well-being: A challenging correction and neurotherapeutic pharmaceutical biotechnology for treating cognitive deficits, depression and intellectual disabilities. *Curr. Pharm. Biotechnol.* **15**, 738–778 (2014).
50. J. Ivanisevic, A. A. Epstein, M. E. Kurczak, P. H. Benton, W. Uritboonthai, H. S. Fox, M. D. Boska, H. E. Gendelman, G. Sluzdak, Brain region mapping using global metabolomics. *Chem. Biol.* **21**, 1575–1584 (2014).
51. M.-C. Senut, S. Azher, F. L. Margolis, K. Patel, A. Mousa, A. Majid, Distribution of carnosine-like peptides in the nervous system of developing and adult zebrafish (*Danio rerio*) and embryonic effects of chronic carnosine exposure. *Cell Tissue Res.* **337**, 45–61 (2009).
52. N. Alerina, D. Kikic, M. Todiras, V. Mosienko, F. Qadri, R. Plehm, P. Boyé, L. Villanovitch, R. Sohr, K. Tenner, H. Hörtnagl, M. Bader, Growth retardation and altered autonomic control in mice lacking brain serotonin. *Proc. Natl. Acad. Sci. U.S.A.* **106**, 10332–10337 (2009).
53. S. Sun, Y. Sun, S.-C. Ling, L. Ferraiuolo, M. McAlonis-Downes, Y. Zou, K. Drenner, Y. Wang, D. Ditsworth, S. Tokunaga, A. Kopelevich, B. K. Kaspar, C. Lagier-Tourenne, D. W. Cleveland, Translational profiling identifies a cascade of damage initiated in motor neurons and spreading to glia in mutant SOD1-mediated ALS. *Proc. Natl. Acad. Sci. U.S.A.* **112**, E6993–E7002 (2015).
54. S. Schwartz, E. Hall, G. Ast, SROOGLE: Webserver for integrative, user-friendly visualization of splicing signals. *Nucleic Acids Res.* **37**, W189–W192 (2009).
55. K. J. Livak, T. D. Schmittgen, Analysis of relative gene expression data using real-time quantitative PCR and the $2^{-\Delta\Delta Ct}$ method. *Methods* **25**, 402–408 (2001).
56. D. Kim, B. Langmead, S. L. Salzberg, HISAT: A fast spliced aligner with low memory requirements. *Nat. Methods* **12**, 357–360 (2015).
57. Y. Liao, G. K. Smyth, W. Shi, featureCounts: An efficient general purpose program for assigning sequence reads to genomic features. *Bioinformatics* **30**, 923–930 (2014).
58. M. I. Love, W. Huber, S. Anders, Moderated estimation of fold change and dispersion for RNA-seq data with DESeq2. *Genome Biol.* **15**, 550 (2014).
59. T. Metsalu, J. Vilo, ClustVis: A web tool for visualizing clustering of multivariate data using principal component analysis and heatmap. *Nucleic Acids Res.* **43** (W1), W566–W570 (2015).
60. G. Fenalti, C. S. Hampe, K. O'Connor, J. P. Banga, I. R. Mackay, M. J. Rowley, O. El-Kabbani, Molecular characterization of a disease associated conformational epitope on GAD65 recognised by a human monoclonal antibody b96.11. *Mol. Immunol.* **44**, 1178–1189 (2007).
61. P. Emsley, B. Lohkamp, W. G. Scott, K. Cowtan, Features and development of Coot. *Acta Crystallogr. D Biol. Crystallogr.* **66** (Pt 4), 486–501 (2010).
62. E. F. Pettersen, T. D. Goddard, C. C. Huang, G. S. Couch, D. M. Greenblatt, E. C. Meng, T. E. Ferrin, UCSF Chimera—A visualization system for exploratory research and analysis. *J. Comput. Chem.* **25**, 1605–1612 (2004).
63. C. G. Langendorf, K. L. Tuck, T. L. G. Key, G. Fenalti, R. N. Pike, C. J. Rosado, A. S. M. Wong, A. M. Buckle, R. H. P. Law, J. C. Whistock, Structural characterization of the mechanism through which human glutamic acid decarboxylase auto-activates. *Biosci. Rep.* **33**, 137–144 (2013).
64. D. Demontis, R. K. Walters, J. Martin, M. Mattheisen, T. D. Als, E. Agerbo, G. Baldursson, R. Belliveau, J. Bybjerg-Grauholm, M. Bækvad-Hansen, F. Cerrato, K. Chambert, C. Churchhouse, A. Dumont, N. Eriksson, M. Gandalf, J. I. Goldstein, K. L. Grasby, J. Grove, O. O. Gudmundsson, C. S. Hansen, M. E. Hauberg, M. V. Hollegaard, D. P. Howrigan, H. Huang, J. B. Maller, A. R. Martin, N. G. Martin, J. Moran, J. Pallesen, D. S. Palmer, C. B. Pedersen, M. G. Pedersen, T. Poterba, J. B. Poulsen, S. Ripke, E. B. Robinson,

- F. K. Satterstrom, H. Stefansson, C. Stevens, P. Turley, G. M. Walters, H. Won, M. J. Wright; ADHD Working Group of the Psychiatric Genomics Consortium (PGC); Early Lifecourse & Genetic Epidemiology (EAGLE) Consortium; 23andMe Research Team, O. A. Andreassen, P. Asherson, C. L. Burton, D. I. Boomsma, B. Cormand, S. Dalsgaard, B. Franke, J. Gelernter, D. Geschwind, H. Hakonarson, J. Haavik, H. R. Kranzler, J. Kuntsi, K. Langley, K.-P. Lesch, C. Middeldorp, A. Reif, L. A. Rohde, P. Roussos, R. Schachar, P. Sklar, E. J. S. Sonuga-Barke, P. F. Sullivan, A. Thapar, J. Y. Tung, I. D. Waldman, S. E. Medland, K. Stefansson, M. Nordentoft, D. M. Hougaard, T. Werge, O. Mors, P. B. Mortensen, M. J. Daly, S. V. Faraone, A. D. Børglum, B. M. Neale, Discovery of the first genome-wide significant risk loci for attention deficit/hyperactivity disorder. *Nat. Genet.* **51**, 63–75 (2019).
65. L. G. Fritsche, W. Igl, J. N. C. Bailey, F. Grassmann, S. Sengupta, J. L. Bragg-Gresham, K. P. Burdon, S. J. Hebbking, C. Wen, M. Gorski, I. K. Kim, D. Cho, D. Zack, E. Souied, H. P. N. Scholl, E. Bala, K. E. Lee, D. J. Hunter, R. J. Sardell, P. Mitchell, J. E. Merriam, V. Cipriani, J. D. Hoffman, T. Schick, Y. T. E. Lechanteur, R. H. Guymer, M. P. Johnson, Y. Jiang, C. M. Stanton, G. H. S. Buitendijk, X. Zhan, A. B. M. Kwong, A. Boleda, M. Brooks, L. Gieser, R. Ratnapriya, K. E. Branham, J. R. Foerster, J. R. Heckenlively, M. I. Othman, B. J. Vote, H. H. Liang, E. Souzeau, I. L. McAllister, T. Isaacs, J. Hall, S. Lake, D. A. Mackey, I. J. Constable, J. E. Craig, T. E. Kitchner, Z. Yang, Z. Su, H. Luo, D. Chen, H. Ouyang, K. Flagg, D. Lin, G. Mao, H. Ferreyra, K. Stark, C. N. von Strachwitz, A. Wolf, C. Brandl, G. Rudolph, M. Olden, M. A. Morrison, D. J. Morgan, M. Schu, J. Ahn, G. Silvestri, E. E. Tsironi, K. H. Park, L. A. Farrer, A. Orlin, A. Brucker, M. Li, C. A. Curcio, S. Mohand-Said, J.-A. Sahel, I. Audo, M. Benchaboune, A. J. Cree, C. A. Rennie, S. V. Goverdhan, M. Grunin, S. Hagbi-Levi, P. Campochiaro, N. Katsanis, F. G. Holz, F. Blond, H. Blanché, J.-F. Deleuze, R. P. Igo Jr, B. Truitt, N. S. Peachey, S. M. Meuer, C. E. Myers, E. L. Moore, R. Klein, M. A. Hauser, E. A. Postel, M. D. Courtenay, S. G. Schwartz, J. L. Kovach, W. K. Scott, G. Liew, A. G. Tan, B. Gopinath, J. C. Merriam, R. T. Smith, J. C. Khan, H. Shahid, A. T. Moore, J. A. McGrath, R. Lax, M. A. Brantley Jr, A. Agarwal, L. Ersoy, A. Caramoy, T. Langmann, N. T. M. Saksens, E. K. de Jong, C. B. Hoyng, M. S. Cain, A. J. Richardson, T. M. Martin, J. Blangero, D. E. Weeks, B. Dhillon, C. M. van Duijn, K. F. Doheny, J. Romm, C. C. W. Klaver, C. Hayward, M. B. Gorin, M. L. Klein, P. N. Baird, A. I. den Hollander, S. Fausner, J. R. W. Yates, R. Allikmets, J. J. Wang, D. A. Schaumberg, B. E. K. Klein, S. A. Hagstrom, I. Chowers, A. J. Lotery, T. Léveillard, K. Zhang, M. H. Brilliant, A. W. Hewitt, A. Swaroop, E. Y. Chew, M. A. Perica-Vance, M. De Angelis, D. Stambolian, J. L. Haines, S. K. Iyengar, B. H. F. Weber, G. R. Abecasis, I. M. Heid, A large genome-wide association study of age-related macular degeneration highlights contributions of rare and common variants. *Nat. Genet.* **48**, 134–143 (2016).
66. J. Grove, S. Ripke, T. D. Als, M. Mattheisen, R. K. Walters, H. Won, J. Pallesen, E. Agerbo, O. A. Andreassen, R. Anney, S. Awasthi, R. Belliveau, F. Bettella, J. D. Buxbaum, J. Bybjerg-Grauholm, M. Bækvad-Hansen, F. Cerrato, K. Chambert, J. H. Christensen, C. Churchhouse, K. Dellennvall, D. Demontis, S. De Rubeis, B. Devlin, S. Djurovic, A. L. Dumont, J. I. Goldstein, C. S. Hansen, M. E. Hauberg, M. V. Hollegaard, S. Hope, D. P. Howrigan, H. Huang, C. M. Hultman, L. Klei, J. Maller, J. Martin, A. R. Martin, J. L. Moran, M. Nyegaard, T. Nærdal, D. S. Palmer, A. Palotie, C. B. Pedersen, M. G. Pedersen, T. dPoterba, J. B. Poulsen, B. S. Pourcain, P. Qvist, K. Rehnström, A. Reichenberger, J. Reichert, E. B. Robinson, K. Roeder, P. Roussos, E. Saemundsen, S. Sandin, F. K. Satterstrom, G. D. Smith, H. Stefansson, S. Steinberg, C. R. Stevens, P. F. Sullivan, P. Turley, G. M. Walters, X. Xu; Autism Spectrum Disorder Working Group of the Psychiatric Genomics Consortium; BUPGEN; Major Depressive Disorder Working Group of the Psychiatric Genomics Consortium; 23andMe Research Team, K. Stefansson, D. H. Geschwind, M. Nordentoft, D. M. Hougaard, T. Werge, O. Mors, P. B. Mortensen, B. M. Neale, M. J. Daly, A. D. Børglum, Identification of common genetic risk variants for autism spectrum disorder. *Nat. Genet.* **51**, 431–444 (2019).
67. I. E. Jansen, J. E. Savage, K. Watanabe, J. Bryois, D. M. Williams, S. Steinberg, J. Sealock, I. K. Karlsson, S. Hägg, L. Athanasiu, N. Voyle, P. Proitsi, A. Witoelar, S. Stringer, D. Aarsland, I. S. Almdahl, F. Andersen, S. Bergh, F. Bettella, S. Björnsson, A. Brækhus, G. Bräthen, C. de Leeuw, S. S. Desikan, S. Djurovic, L. Dumitrescu, T. Fladby, T. J. Hohman, P. V. Jonsson, S. J. Kiddle, A. Rongve, I. Saltvedt, S. B. Sando, G. Selbæk, M. Shoaib, N. G. Skene, J. Snaedal, E. Stordal, I. D. Ulstein, Y. Wang, L. R. White, J. Hardy, J. Hjerling-Leffler, P. F. Sullivan, W. M. van der Flier, R. Dobson, L. K. Davis, H. Stefansson, K. Stefansson, N. L. Pedersen, S. Ripke, O. A. Andreassen, D. Posthuma, Genome-wide meta-analysis identifies new loci and functional pathways influencing Alzheimer's disease risk. *Nat. Genet.* **51**, 404–413 (2019).
68. J. J. Lee, R. Wedow, A. Okbay, E. Kong, O. Maghzian, M. Zacher, T. A. Nguyen-Viet, P. Bowers, J. Sidorenko, R. K. Linnér, M. A. Fontana, T. Kundu, C. Lee, H. Li, R. Li, R. Royer, P. N. Timshe, R. K. Walters, E. A. Willoughby, L. Yengo; 23andMe Research Team; COGENT (Cognitive Genomics Consortium); Social Science Genetic Association Consortium, M. Alver, Y. Bao, D. W. Clark, F. R. Day, N. A. Furlotte, P. K. Joshi, K. E. Kemper, A. Kleinman, C. Langenberg, R. Mägi, J. W. Trampush, S. S. Verma, Y. Wu, M. Lam, J. H. Zhao, Z. Zheng, J. D. Boardman, H. Campbell, J. Freese, K. M. Harris, C. Hayward, P. Herd, M. Kumari, T. Lencz, J. Luan, A. K. Malhotra, A. Metspalu, L. Milani, K. K. Ong, J. R. B. Perry, D. J. Porteous, M. D. Ritchie, M. C. Smart, B. H. Smith, J. Y. Tung, N. J. Wareham, J. F. Wilson, J. P. Beauchamp, D. C. Conley, T. Esko, S. F. Lehrner, P. K. E. Magnusson, S. Oskarsson, T. H. Pers, M. R. Robinson, K. Thom, C. Watson, C. F. Chabris, M. N. Meyer, D. I. Laibson, J. Yang, M. Johannesson, P. D. Koellinger, P. Turley, P. M. Visscher, D. J. Benjamin, D. Cesarini, Gene discovery and polygenic prediction from a genome-wide association study of educational attainment in 1.1 million individuals. *Nat. Genet.* **50**, 1112–1121 (2018).
69. M. A. Nalls, C. Blauwendraat, C. L. Vallerga, K. Heilbron, S. Bandres-Ciga, D. Chang, M. Tan, D. A. Kia, A. J. Noyce, A. Xue, J. Bras, E. Young, R. von Coelln, J. Simón-Sánchez, C. Schulte, M. Sharma, L. Krohn, L. Pihlström, A. Siitonen, H. Iwaki, H. Leonard, F. Faghri, J. R. Gibbs, D. G. Hernandez, S. W. Scholz, J. A. Botia, M. Martinez, J.-C. Corvol, J. S. Lesage, J. Jankovic, L. M. Shulman, M. Sutherland, P. Tienari, K. Majamaa, M. Toft, O. A. Andreassen, T. Bangale, A. Brice, J. Yang, Z. Gan, R. T. Gasser, P. Heutink, J. M. Shulman, N. W. Wood, D. A. Hinds, J. A. Hardy, H. R. Morris, J. Gratten, P. M. Visscher, R. R. Graham, A. B. Singleton; 23andMe Research Team; System Genomics of Parkinson's Disease Consortium; International Parkinson's Disease Genomics Consortium, Identification of novel risk loci, causal insights, and heritable risk for Parkinson's disease: A meta-analysis of genome-wide association studies. *Lancet Neurol.* **18**, 1091–1102 (2019).
70. A. Nicolas, K. P. Kenna, A. E. Renton, N. Ticozzi, F. Faghri, R. Chia, J. A. Dominov, B. J. Kenna, M. A. Nalls, P. Keagle, A. M. Rivera, W. van Rheenen, N. A. Murphy, J. J. F. A. van Vugt, J. T. Geiger, R. A. Van der Spek, H. A. Pliner, Shankaracharya, B. N. Smith, G. Marangi, S. D. Topp, Y. Abramson, A. S. Gkazi, J. D. Eicher, A. Kenna; ITALSGEN Consortium, G. Mora, A. Calvo, L. Mazzini, N. Riva, J. Mandrioli, C. Caponnetto, S. Battistini, P. Volanti, V. L. Bella, F. L. Conforti, G. Borghero, S. Messina, I. L. Simone, F. Trojsi, F. Salvi, F. O. Logullo, S. D'Alfonso, L. Corrado, M. Capasso, L. Ferrucci; Genomic Translation for ALS Care (GTAC) Consortium, C. de Araujo Martins Moreno, S. Kamalakaran, D. B. Goldstein; ALS Sequencing Consortium, A. D. Gitler, T. Harris, R. M. Myers; NYCG ALS Consortium, H. Phatnani, R. L. Musunuri, U. S. Evani, A. Abhyankar, M. C. Zody; Answer ALS Foundation, J. Kaye, S. Finkbeiner, S. K. Wyman, A. L. Naili, L. Lima, E. Fraenkel, C. N. Svendsen, L. M. Thompson, J. E. Van Eyk, J. D. Berry, T. M. Miller, S. J. Kolb, M. Cudkovic, E. Baxi; Clinical Research in ALS and Related Disorders for Therapeutic Development (CReATe) Consortium, M. Benatar, J. P. Taylor, E. Rempersaud, G. Wu, J. Wu; SLAGEN Consortium, G. Lauria, F. Verde, I. Fogh, C. Tiloca, G. P. Comi, G. Soraru, C. Cereda; French ALS Consortium, P. Corcia, H. Laaksvirta, L. Myllykangas, L. Jansson, M. Valori, J. Ealing, H. Hamdalla, S. Rollinson, S. Pickering-Brown, R. W. Orell, K. C. Sidle, A. Malaspina, J. Hardy, A. B. Singleton, J. O. Johnson, S. Arepalli, P. C. Sapp, D. McKenna-Yasek, M. Polak, S. Asress, S. Al-Sarraj, A. King, C. Troakes, C. Vance, J. de Bellerocque, F. Baas, A. L. M. A. Ten Asbroek, J. L. Muñoz-Blanco, D. G. Hernandez, J. Ding, J. R. Gibbs, S. W. Scholz, M. K. Floeter, R. H. Campbell, F. Landi, R. Bowser, S. M. Pulst, J. M. Ravits, D. J. L. Mac Gowan, J. Kirby, E. P. Piro, R. Pamphlett, J. Broach, G. Gerhard, T. L. Dunckley, K. B. Brady, N. W. Kowall, J. C. Troncoso, I. L. Ber, K. Mouzat, S. Lumbroso, T. D. Heiman-Patterson, F. Kamel, J. Van Den Bosch, R. H. Baloh, T. M. Strom, T. Meitinger, A. Shatunov, K. R. Van Eijk, M. de Carvalho, M. Kooyman, B. Middelkoop, M. Moisse, R. L. McLaughlin, M. A. Van Es, M. Weber, K. B. Boylan, M. Van Blitterswijk, R. Rademakers, K. E. Morrison, A. N. Basak, J. S. Mora, V. E. Drory, P. J. Shaw, M. R. Turner, K. Talbot, O. Hardiman, K. L. Williams, J. A. Fifita, G. A. Nicholson, I. P. Blair, G. A. Rouleau, J. Esteban-Pérez, A. García-Redondo, A. Al-Chalabi; Project MinE ALS Sequencing Consortium, E. Rogava, L. Zinman, L. W. Ostrow, N. J. Maragakis, J. D. Rothstein, Z. Simmons, J. Cooper-Knock, A. Brice, S. A. Goutman, E. L. Feldman, S. B. Gibson, F. Taroni, A. Ratti, C. Gellera, P. Van Damme, W. Robberecht, P. Fratta, M. Sabatelli, C. Lunetta, A. C. Ludolph, P. M. Andersen, J. H. Weishaupt, W. Camu, J. Q. Trojanowski, V. M. Van Deerlin, R. H. Brown Jr, L. H. van den Berg, J. H. Veldink, M. B. Harms, J. D. Glass, D. J. Stone, P. Tienari, V. Silani, A. Chiò, C. E. Shaw, B. J. Traynor, J. E. Landers, Genome-wide analyses identify KIF5A as a novel ALS gene. *Neuron* **97**, 1268–1283.e6 (2018).
71. T. Otowa, K. Heck, M. Lee, E. M. Byrne, S. S. Mirza, M. G. Nivard, T. Bigdeli, S. H. Aggen, D. Adkins, A. Wolen, A. Fanous, M. C. Keller, E. Castelazo, Z. Kutalik, S. Van der Auwera, G. Homuth, M. Nauck, A. Teumer, Y. Milaneschi, J.-J. Hottenga, N. Direk, A. Hofman, A. Utterlinden, C. L. Mulder, A. K. Henders, S. E. Medland, S. Gordon, A. C. Heath, P. A. F. Madden, M. L. Pergadia, P. J. van der Most, I. M. Nolte, F. V. A. van Oort, C. A. Hartman, A. J. Oldehinkel, M. Preisig, H. J. Grabe, C. M. Middeldorp, B. W. J. H. Penninx, D. Boomsma, N. G. Martin, G. Montgomery, B. S. Maher, E. J. van den Oord, N. R. Wray, H. Tiemeier, J. M. Hettema, Meta-analysis of genome-wide association studies of anxiety disorders. *Mol. Psychiatry* **21**, 1485 (2016).
72. E. A. Stahl, G. Breen, A. J. Forstner, A. M. Quillin, S. Ripke, V. Trubetskoy, M. Mattheisen, Y. Wang, J. R. I. Coleman, H. A. Gaspar, C. A. de Leeuw, S. Steinberg, J. M. Whitehead Pavlides, M. Trzaskowski, E. M. Byrne, T. H. Pers, P. A. Holmans, A. L. Richards, L. Abbott, E. Agerbo, H. Akil, D. Albani, N. Alliey-Rodriguez, T. D. Als, A. Anjorin, V. Antilla, S. Awasthi, J. A. Badner, M. Bækvad-Hansen, J. D. Barchas, N. Bass, M. Bauer, R. Belliveau, S. E. Bergen, C. B. Pedersen, E. Bøen, M. P. Boks, J. Boocock, M. Budde, W. Bunney, M. Chamberst, J. Bybjerg-Grauholm, W. Burcher, M. Casas, F. Cerrato, P. Cervantes, K. Burneister, A. W. Charney, D. Chen, C. Churchhouse, T.-K. Clarke, W. Coryell, D. W. Craig, C. Cruceanu, D. Curtis, P. M. Czerski, A. M. Dale,

- S. de Jong, F. Degenhardt, J. Del-Favero, J. R. De Pau, S. Djurovic, A. L. Dobbyn, A. Dumont, T. Elväsahagen, V. Escott-Price, C. C. Fan, S. B. Fischer, M. Flickinger, T. M. Foroud, F. Forty, J. Frank, C. Fraser, N. B. Freimer, L. Frisén, K. Gade, D. Gage, J. Garnham, C. Giambartolomei, M. G. Pedersen, J. Goldstein, S. D. Gordon, K. Gordon-Smith, E. K. Green, M. J. Green, T. A. Greenwood, J. Grove, W. Guan, J. Guzman-Parra, M. L. Hamshere, M. Hautzinger, U. Heilbronner, S. Herms, M. Hipolito, P. Hoffmann, D. Holland, L. Huckins, S. Jamain, J. S. Johnson, A. Juréus, R. Kandaswamy, R. Karlsson, J. L. Kennedy, S. Kittel-Schneider, A. J. Knowles, M. Kogevinas, A. C. Koller, R. Kupka, C. Lavebratt, J. Lawrence, W. B. Lawson, M. Leber, P. H. Lee, S. E. Levy, J. Z. Li, C. Liu, S. Lucae, A. Maaser, D. J. MacIntyre, P. B. Mahon, W. Maier, L. Martinsson, S. M. Carroll, P. M. Guffin, M. G. McInnis, J. D. McKay, H. Medeiros, S. E. Medland, F. Meng, L. Milani, G. W. Montgomery, D. W. Morris, T. W. Mühleisen, N. Mullins, H. Nguyen, C. M. Nievergelt, A. N. Adolphson, E. A. Nwulia, C. O'Donovan, L. M. Olde Loohuis, A. P. S. Ori, L. Oruc, U. Ösby, R. H. Perlis, A. Perry, A. Pfennig, J. B. Potash, S. M. Purcell, E. J. Regeer, A. Reif, C. S. Reinbold, J. P. Rice, F. Rivas, M. Rivera, P. Roussos, D. M. Ruderfer, E. Ryu, C. Sánchez-Mora, A. F. Schatzberg, W. A. Scheftner, N. J. Schork, C. S. Weickert, T. Shekhtman, P. D. Shilling, E. Sigurdsson, G. Slaney, O. B. Smeland, J. L. Sobell, C. S. Hansen, A. T. Spijkier, D. S. Clair, M. Steffens, J. S. Strauss, F. Streit, J. Strohmaier, S. Szlinger, R. C. Thompson, T. E. Thorgeirsson, J. Treutlein, H. Vedder, W. Wang, S. J. Watson, T. W. Weickert, S. H. Witt, S. Xi, W. Xu, A. H. Young, P. Zandi, P. Zhang, S. Zollner; eQTLGen Consortium; BIOS Consortium, R. Adolphson, I. Agartz, M. Alda, L. Backlund, B. T. Baune, F. Bellivier, W. H. Berrettini, J. M. Biernacka, D. H. R. Blackwood, M. Boehnke, A. D. Børglum, A. Corvin, N. Craddock, M. J. Daly, U. Dannlowski, T. Esko, B. Etain, M. Frye, J. M. Fullerton, E. S. Gershon, M. Gill, F. Goes, M. Grigoriou-Serbanescu, J. Hauser, D. M. Hougaard, C. M. Hultman, J. Jones, L. S. Kahn, G. Kirov, M. Landén, M. Leboyer, C. M. Lewis, Q. S. Li, J. Lissowska, N. G. Martin, F. Mayoral, S. L. McElroy, A. M. McIntosh, F. J. McMahon, I. Melle, A. Metspalu, P. B. Mitchell, G. Morken, O. Mors, P. B. Mortensen, B. Müller-Myhsok, R. M. Myers, B. M. Neale, V. Nimgaonkar, M. Nordentoft, M. M. Nöthen, M. C. O'Donovan, K. J. Oedegaard, M. J. Owen, S. A. Paciga, C. Pató, M. T. Pató, D. Posthuma, J. A. Ramos-Quiroga, M. Ribasés, M. Rietschel, G. A. Rouleau, M. Schalling, P. R. Schofield, T. G. Schulze, A. Serretti, J. W. Smoller, H. Stefansson, K. Stefansson, E. Stordal, P. F. Sullivan, G. Turecki, A. E. Vaaler, E. Vieta, J. B. Vincent, T. Werge, J. I. Nurnberger, N. R. Wray, A. D. Florio, H. J. Edenberg, S. Cichon, R. A. Ophoff, L. J. Scott, O. A. Andreassen, J. Kelseo, P. Sklar; the Bipolar Disorder Working Group of the Psychiatric Genomics Consortium, Genome-wide association study identifies 30 loci associated with bipolar disorder. *Nat. Genet.* **51**, 793–803 (2019).
73. A. Teumer, A. Tin, R. Sorice, M. Gorski, N. C. Yeo, A. Y. Chu, M. Li, Y. Li, Y. Mijatovic, Y.-A. Ko, D. Taliun, A. Luciani, M.-H. Chen, Q. Yang, M. C. Foster, M. Olden, L. T. Hiraki, B. O. Tayo, C. Fuchsberger, A. K. Dieffenbach, A. R. Shuldiner, A. V. Smith, A. M. Zappa, A. Lupo, B. Kollerits, B. Ponte, B. Stengel, B. K. Krämer, B. Paulweber, B. D. Mitchell, C. Hayward, C. Helmer, C. Meisinger, C. Gieger, C. M. Shaffer, C. Müller, C. Langenberg, D. Ackermann, D. Siscovick; DCCT/EDIC, E. Boerwinkle, F. Kronenberg, G. B. Ehret, G. Homuth, G. Waeber, G. Navis, G. Gambaro, G. Malerba, G. Eiriksdottir, G. Li, H. E. Wichmann, H. Grallert, H. Wallaschowski, H. Völzke, H. Brenner, H. Kramer, I. M. Leach, I. Rudan, H. L. Hillege, J. S. Beckmann, J. C. Lambert, J. Luan, J. H. Zhao, J. Chalmers, J. Coresh, J. C. Denny, K. Butterbach, L. J. Launer, L. Ferrucci, L. Kedenko, M. Haun, M. Metzger, M. Woodward, M. J. Hoffman, M. Nauck, M. Waldenberger, M. Pruijm, M. Bochud, M. Rheinberger, N. Verweij, N. J. Wareham, N. Endlich, N. Soranzo, O. Polasek, P. van der Harst, P. P. Pramstaller, P. Vollenweider, P. S. Wild, R. T. Gansevoort, R. Rettig, R. Biffar, R. J. Carroll, R. Katz, R. J. F. Loos, S.-J. Hwang, S. Coassin, S. Bergmann, S. E. Rosas, S. Stracke, T. B. Harris, T. Corre, T. Zeller, T. Illig, T. Aspelund, T. Tanaka, U. Lendeckel, U. Völker, V. Gudnason, V. Chouraki, W. Koenig, Z. Kutalik, J. R. O'Connell, A. Parsa, I. M. Heid, A. D. Paterson, I. H. de Boer, O. Devuyst, J. Lazar, K. Endlich, K. Suszta, J. Tremblay, P. Hameit, H. J. Jacob, C. A. Böger, C. S. Fox, C. Pattaro, A. Köttgen, Genome-wide association studies identify genetic loci associated with albuminuria in diabetes. *Diabetes* **65**, 803–817 (2016).
74. P. van der Harst, N. Verweij, Identification of 64 novel genetic loci provides an expanded view on the genetic architecture of coronary artery disease. *Circ. Res.* **122**, 433–443 (2018).
75. H. J. Watson, Z. Yilmaz, L. M. Thornton, C. Hübel, J. R. I. Coleman, H. A. Gaspar, J. Bryois, A. Hinney, V. M. Leppä, M. Mattheisen, S. E. Medland, S. Ripke, S. Yao, P. Giusti-Rodríguez; Anorexia Nervosa Genetics Initiative, K. B. Hanscombe, K. L. Purves; Eating Disorders Working Group of the Psychiatric Genomics Consortium, R. A. H. Adan, L. Alfredsson, T. Ando, O. A. Andreassen, J. H. Baker, W. H. Berrettini, I. Boehm, C. Boni, V. B. Perica, K. Buehren, R. Burghardt, M. Cassina, S. Cichon, M. Clementi, R. D. Cone, P. Courtet, S. Crow, J. J. Crowley, U. N. Danner, O. S. P. Davis, M. de Zwaan, G. Dedoussis, D. Degortes, J. E. De Socio, D. M. Dick, D. Dikeos, C. Dina, M. Dmitrak-Weglarz, E. Docampo, L. E. Duncan, K. Egberts, S. Ehrlich, G. Escaramis, T. Esko, X. Estivill, A. Farmer, A. Favarro, F. Fernández-Aranda, M. M. Fichter, K. Fischer, M. Föcker, L. Foretova, A. J. Forstner, M. Forzan, C. S. Franklyn, S. Gallinger, I. Giegling, J. Giuarana, F. Gonidakis, P. Greenwood, M. G. Mayora, S. Guillaume, Y. Guo, H. Hakonarson, K. Hatzikotoulas, J. Hauser, J. Hebebrand, S. G. Helder, S. Herms, B. Herpertz-Dahlmann, W. Herzog, L. M. Huckins, J. I. Hudson, H. Imgart, H. Inoko, V. Janout, S. Jiménez-Murcia, A. Julià, G. Kalsi, D. Kaminská, J. Kaprio, L. Karhunen, A. Karwaart, M. J. H. Kas, J. L. Kennedy, A. Keski-Rahkonen, K. Kiezebrink, Y.-R. Kim, L. Klarskog, K. L. Klump, G. P. S. Knudsen, M. C. La Via, S. L. Hellard, R. D. Levitan, D. Li, L. Lilienfeld, B. D. Lin, J. Lissowska, J. Luyck, P. J. Magistretti, M. Maj, K. Mannik, S. Marsal, C. R. Marshall, M. Mattingsdal, S. M. Devitt, P. M. Guffin, A. Metspalu, I. Meulenbelt, N. Micali, K. Mitchell, A. M. Monteleone, P. Monteleone, M. A. Munn-Chernoff, B. Nacmias, M. Navratilova, I. Ntalla, J. K. O'Toole, R. A. Ophoff, L. Padyukov, A. Palotie, J. Pantel, H. Papezova, D. Pinto, R. Rabionet, A. Raevuori, N. Ramoz, T. Reichborn-Kjennerud, V. Ricca, S. Ripatti, F. Ritschel, M. Roberts, A. Rotondo, D. Rujescu, F. Rybakowski, P. Santonastaso, A. Scherag, S. W. Scherer, U. Schmidt, N. J. Schork, A. Schosser, J. Seitz, L. Slachetova, P. E. Slagboom, M. C. T. Slof-Op't Landt, A. Slopian, S. Sorbi, B. Świątkowska, J. Z. Sztatkiewicz, I. Tachmazidou, E. Tenconi, A. Tortorella, F. Tozzi, J. Treasure, A. Tsitsika, M. Tyszkiewicz-Nwafor, K. Tziouvas, A. A. van Elburg, E. F. van Furth, G. Wagner, E. Walton, E. Widen, E. Zeggini, S. Zerwas, S. Zifpel, A. W. Bergen, J. M. Boden, H. Brandt, S. Crawford, K. A. Halmi, L. J. Horwood, C. Johnson, A. S. Kaplan, W. H. Kaye, J. E. Mitchell, C. M. Olsen, J. F. Pearson, N. L. Pedersen, M. Strober, T. Werge, D. C. Whiteman, D. B. Woodside, G. D. Stuber, S. Gordon, J. Grove, A. K. Henders, A. Juréus, K. M. Kirk, J. T. Larsen, R. Parker, L. Petersen, J. Jordan, M. Kennedy, G. W. Montgomery, T. D. Wade, A. Birgegard, P. Lichtenstein, C. Norring, M. Landén, N. G. Martin, P. B. Mortensen, P. F. Sullivan, G. Green, C. M. Bulik, Genome-wide association study identifies eight risk loci and implicates metabo-psychiatric origins for anorexia nervosa. *Nat. Genet.* **51**, 1207–1214 (2019).
76. N. R. Wray, S. Ripke, M. Mattheisen, M. Trzaskowski, E. M. Byrne, A. Abdellaoui, M. J. Adams, E. Agerbo, T. M. Air, T. M. F. Andlauer, S.-A. Bacanu, M. Bækvaag-Hansen, A. F. T. Beekman, T. B. Bigdeli, E. B. Binder, D. R. H. Blackwood, J. Bryois, H. N. Büttenschon, J. Bybjerg-Grauholm, N. Cai, E. Castelao, J. H. Christensen, T.-K. Clarke, J. I. R. Coleman, L. Colodro-Conde, B. Couvy-Duchesne, N. Craddock, G. E. Crawford, C. A. Crowley, H. S. Dashti, G. Davies, J. J. Deary, F. Degenhardt, E. M. Derks, N. Direk, C. V. Dolan, E. C. Dunn, T. C. Eley, N. Eriksson, V. Escott-Price, F. H. F. Kiadeh, H. K. Finucane, A. J. Forstner, J. Frank, H. A. Gaspar, M. Gill, P. Giusti-Rodríguez, F. S. Goes, S. D. Gordon, J. Grove, L. S. Hall, E. Hannon, C. S. Hansen, T. F. Hansen, S. Herms, I. B. Hickie, P. Hoffmann, G. Homuth, C. Horn, J.-J. Hottenga, D. M. Hougaard, M. Hu, C. L. Hyde, M. Ising, R. Jansen, F. Jin, E. Jorgenson, J. A. Knowles, I. S. Kohane, J. Kraft, W. W. Kretschmar, J. Krogh, Z. Kutalik, J. M. Lane, Y. Li, Y. Li, P. A. Lind, X. Liu, L. Lu, D. J. Macintyre, D. F. Mackinnon, R. M. Maier, W. Maier, J. Marchini, H. Mbarek, P. M. Grath, P. M. Guffin, S. E. Medland, D. Mehta, C. M. Middeldorp, E. Mihailov, Y. Milaneschi, L. Milani, J. Mill, F. M. Mondimore, G. W. Montgomery, S. Mostafavi, N. Mullins, M. Nauck, B. Ng, M. G. Nivard, D. R. Nyholt, P. F. O'Reilly, H. Oskarsson, M. J. Owen, J. N. Painter, C. B. Pedersen, M. G. Pedersen, R. E. Peterson, E. Pettersson, W. J. Peyrot, G. Pistis, D. Posthuma, S. M. Purcell, J. A. Quiroz, P. Qvist, J. P. Rice, B. P. Riley, M. Rivera, S. S. Mirza, R. Saxena, R. Schoevers, E. Schulte, L. Shen, J. Shi, S. I. Shyn, E. Sigurdsson, G. B. C. Sinnamon, J. H. Smith, D. J. Smith, H. Stefansson, S. Steinberg, C. A. Stockmeier, F. Streit, J. Strohmaier, K. E. Tansey, H. Teismann, A. Teumer, W. Thompson, P. A. Thomson, T. E. Thorgeirsson, C. Tian, M. Traylor, J. Treutlein, V. Trubetskoy, A. G. Uitterlinden, D. Umbrecht, S. Van der Auwera, A. M. van Hemert, A. Viktorin, P. M. Visscher, Y. Wang, B. T. Webb, S. M. Weinsheimer, J. Wellmann, G. Willemssen, S. H. Witt, Y. Wu, H. S. Xi, J. Yang, F. Zhang; eQTLGen; 23andMe, V. Arolt, B. T. Baune, K. Berger, D. I. Boomsma, S. Cichon, U. Dannlowski, E. C. J. de Geus, J. R. De Paulo, E. Domenici, K. Domschke, T. Esko, H. J. Grabe, S. P. Hamilton, C. Hayward, A. C. Heath, D. A. Hinds, K. S. Kendler, S. Kloiber, G. Lewis, Q. S. Li, S. Lucae, P. F. A. Madden, P. K. Magnusson, N. G. Martin, A. M. McIntosh, A. Metspalu, O. Mors, P. B. Mortensen, B. Müller-Myhsok, M. Nordentoft, M. M. Nöthen, M. C. O'Donovan, S. A. Paciga, N. L. Pedersen, B. W. J. H. Penninx, R. H. Perlis, D. J. Porteous, J. B. Potash, M. Preisig, M. Rietschel, C. Schaefer, T. G. Schulze, J. W. Smoller, K. Stefansson, H. Tiemeier, R. Uher, H. Völzke, M. Weissman, T. Werge, A. R. Winslow, C. M. Lewis, D. F. Levinson, G. Breen, A. D. Børglum, P. F. Sullivan; the Major Depressive Disorder Working Group of the Psychiatric Genomics Consortium, Genome-wide association analyses identify 44 risk variants and refine the genetic architecture of major depression. *Nat. Genet.* **50**, 668–681 (2018).
77. A. Xue, Y. Wu, Z. Zhu, F. Zhang, K. E. Kemper, Z. Zheng, L. Yengo, L. R. Lloyd-Jones, J. Sidorenko, Y. Wu; eQTLGen Consortium, A. F. McRae, P. M. Visscher, J. Zeng, J. Yang, Genome-wide association analyses identify 143 risk variants and putative regulatory mechanisms for type 2 diabetes. *Nat. Commun.* **9**, 2941 (2018).
78. L. Yengo, J. Sidorenko, K. E. Kemper, Z. Zheng, A. R. Wood, M. N. Weedon, T. M. Frayling, J. Hirschhorn, J. Yang, P. M. Visscher; GIANT Consortium, Meta-analysis of genome-wide association studies for height and body mass index in approximately 700000 individuals of European ancestry. *Hum. Mol. Genet.* **27**, 3641–3649 (2018).
79. International League Against Epilepsy Consortium on Complex Epilepsies, Genetic determinants of common epilepsies: A meta-analysis of genome-wide association studies. *Lancet Neurol.* **13**, 893–903 (2014).

80. A. Okbay, B. M. L. Baselmans, J.-E. De Neve, P. Turley, M. G. Nivard, M. A. Fontana, S. F. W. Meddens, R. K. Linnér, C. A. Rietveld, J. Derringer, J. Gratten, J. J. Lee, J. Z. Liu, R. de Vlaming, T. S. Ahluwalia, J. Buchwald, A. Cavadiño, A. C. Frazier-Wood, N. A. Furlotte, V. Garfield, M. H. Geisel, J. R. Gonzalez, S. Haitjema, R. Karlsson, S. W. van der Laan, K.-H. Ladwig, J. Lahti, S. J. van der Lee, P. A. Lind, T. Liu, L. Matteson, E. Mihailov, M. B. Miller, C. C. Minica, I. M. Nolte, D. Mook-Kanamori, P. J. van der Most, C. Oldmeadow, Y. Qian, O. Raitakari, R. Rawal, A. Realo, R. Rueedi, B. Schmidt, A. V. Smith, E. Stergiakouli, T. Tanaka, K. Taylor, G. Thorleifsson, J. Wedenoja, J. Wellmann, H.-J. Westra, S. M. Willems, W. Zhao; Life Lines Cohort Study, N. Amin, A. Bakshi, S. Bergmann, G. Björnsdóttir, P. A. Boyle, S. Cherney, S. R. Cox, G. Davies, O. S. P. Davis, J. Ding, N. Direk, P. Eibich, R. T. Emeny, G. Fatemifar, J. D. Faul, L. Ferrucci, A. J. Forstner, C. Gieger, R. Gupta, T. B. Harris, J. M. Harris, E. G. Holliday, J.-J. Hottenga, P. L. De Jager, M. A. Kaakinen, E. Kajantie, V. Karhunen, I. Kolcic, M. Kumari, L. J. Launer, L. Franke, R. Li-Gao, D. C. Liewald, M. Koini, A. Loukola, P. Marques-Vidal, G. W. Montgomery, M. A. Mosing, L. Paternoster, A. Pattie, K. E. Petrovic, L. Pulkki-Råback, L. Quaye, K. Raikönen, I. Rudan, R. J. Scott, J. A. Smith, A. R. Sutin, M. Trzaskowski, A. E. Vinkhuyzen, L. Yu, D. Zabaneh, J. R. Attia, D. A. Bennett, K. Berger, L. Bertram, D. I. Boomsma, H. Snieder, S.-C. Chang, F. Cucca, I. J. Deary, C. M. van Duijn, J. G. Eriksson, U. Bültmann, E. J. C. de Geus, P. J. F. Groenen, V. Gudnason, T. Hansen, C. A. Hartman, C. M. A. Haworth, C. Hayward, A. C. Heath, D. A. Hinds, E. Hyppönen, W. G. Iacono, M.-R. Järvelin, K.-H. Jöckel, J. Kaprio, S. L. R. Kardia, L. Keltikangas-Järvinen, P. Kraft, L. D. Kubzansky, T. Lehtimäki, P. K. E. Magnusson, N. G. Martin, M. M. Gue, A. Metspalu, M. Mills, R. de Mutsert, A. J. Oldehinkel, G. Pasterkamp, N. L. Pedersen, R. Plomin, O. Polasek, C. Power, S. S. Rich, F. R. Rosendaal, H. M. den Ruijter, D. Schlessinger, H. Schmidt, R. Svento, R. Schmidt, B. Z. Alizadeh, T. I. A. Sørensen, T. D. Spector, J. M. Starr, K. Stefansson, A. Steptoe, A. Terracciano, U. Thorsteinsdóttir, A. R. Thurik, N. J. Timpson, H. Tiemeier, A. G. Uitterlinden, P. Vollenweider, G. G. Wagner, D. R. Weir, J. Yang, D. C. Conley, G. D. Smith, A. Hofman, M. Johannesson, D. I. Laibson, S. E. Medland, M. N. Meyer, J. K. Pickrell, T. Esko, R. F. Krueger, J. P. Beauchamp, P. D. Koellinger, D. J. Benjamin, M. Bartels, D. Cesarini, Genetic variants associated with subjective well-being, depressive symptoms, and neuroticism identified through genome-wide analyses. *Nat. Genet.* **48**, 624–633 (2016).
81. Schizophrenia Working Group of the Psychiatric Genomics Consortium, Biological insights from 108 schizophrenia-associated genetic loci. *Nature* **511**, 421–427 (2014).

Acknowledgments: We thank T. Zayats and A. Srivastava for help with analyzing genetic data and L. E. Schiro, H. O. Rølfesnes, H. Dale, and B. Nordanger for expert technical assistance.

Funding: This work has received funding from Stiftelsen Kristian Gerhard Jebsen (SKJ-MED-02), the Regional Health Authority of Western Norway (no. 25048), and the Innovative Medicines Initiative 2 Joint Undertaking under grant agreement no. 115916 (PRISM). This Joint Undertaking receives support from the European Union's Horizon 2020 research and innovation programme and EFPIA. The Genomics Core Facility (GCF) at the University of Bergen, which is a part of the NorSeq consortium, provided services on RNA sequencing. GCF is supported in part by major grants from the Research Council of Norway (grant no. 245979/F50) and Trond Mohn Stiftelse (grant no. BFS2016-genom). **Author contribution:** E.M. characterized all aspects of the mutated mice, performed mice dissection, genotyping, enzyme and Western blotting assays, analyzed the MR and NMR data, and wrote the manuscript. S.C.H. performed Western blotting assays, analyzed mouse tissue lysates and RNA data, and helped with the preparation of the manuscript. R.K. helped in the analyses of metabolomic data. I.W. performed genotyping and qRT-PCR. T.-A.H. performed the gene-based human analyses and helped in the analyses of metabolomic data. R.M.-P. performed the statistical analyses of metabolomic data. C.T. performed the NMR spectroscopic experiments. F.M. performed the mouse behavioral studies. A.B. performed the qRT-PCR studies. J.C.G. supervised the mouse behavioral studies. H.M. performed histological examination of mouse tissues. P.K. analyzed and compared the protein structures. J.H. conceived and supervised the study and wrote the manuscript. **Competing interests:** The authors declare that they have no competing interests. **Data and materials availability:** All data needed to evaluate the conclusions in the paper are present in the paper and/or the Supplementary Materials. Additional data related to this paper may be requested from the authors.

Submitted 19 February 2020

Accepted 5 June 2020

Published 17 July 2020

10.1126/sciadv.abb3713

Citation: E. Mahootchi, S. Cannon Homaei, R. Kleppe, I. Winge, T.-A. Hegvik, R. Megias-Perez, C. Totland, F. Mogavero, A. Baumann, J. C. Glennon, H. Miletic, P. Kursula, J. Haavik, GADL1 is a multifunctional decarboxylase with tissue-specific roles in β -alanine and carnosine production. *Sci. Adv.* **6**, eabb3713 (2020).

GADL1 is a multifunctional decarboxylase with tissue-specific roles in α -alanine and carnosine production

Elaheh MahootchiSelina Cannon HomaeiRune KleppelIngeborg WingeTor-Arne HegvikRoberto Megias-PerezChristian TotlandFloriana MogaveroAnne BaumannJeffrey Colm GlennonHrvoje MileticPetri KursulaJan Haavik

Sci. Adv., 6 (29), eabb3713. • DOI: 10.1126/sciadv.abb3713

View the article online

<https://www.science.org/doi/10.1126/sciadv.abb3713>

Permissions

<https://www.science.org/help/reprints-and-permissions>

Use of this article is subject to the [Terms of service](#)

Supplementary Materials for

GADL1 is a multifunctional decarboxylase with tissue-specific roles in β -alanine and carnosine production

Elaheh Mahootchi, Selina Cannon Homaei, Rune Kleppe, Ingeborg Winge, Tor-Arne Hegvik, Roberto Megias-Perez, Christian Totland, Floriana Mogavero, Anne Baumann, Jeffrey Colm Glennon, Hrvoje Miletic, Petri Kursula, Jan Haavik*

*Corresponding author. Email: jan.haavik@uib.no

Published 17 July 2020, *Sci. Adv.* 6, eabb3713 (2020)
DOI: 10.1126/sciadv.abb3713

The PDF file includes:

Tables S1, S3 to S5
Figs. S1 to S5
References

Other Supplementary Material for this manuscript includes the following:

(available at advances.sciencemag.org/cgi/content/full/6/29/eabb3713/DC1)

Table S2

Table S1 A. Top 25 upregulated genes in OB tissue samples from *Gad11^{-/-}* compared to *Gad11^{+/+}* mice.

ENSEMBL ID	Abbreviation	Name	Log2Fold	P-value
ENSMUSG00000032226	<i>Gcn3</i>	Glucosaminyl (N-acetyl) transferase 3, mucin type	6.05	0.00084
ENSMUSG00000020159	<i>Gabrp</i>	γ -aminobutyric acid (GABA) A receptor, pi	5.77	0.01167
ENSMUSG00000085224	<i>Gm13425</i>	Predicted gene 13425	5.40	0.00262
ENSMUSG00000038805	<i>Six3</i>	Sine oculis-related homeobox 3	5.23	0.00077
ENSMUSG00000093894	<i>Ighv1-53</i>	Immunoglobulin heavy variable 1-53	5.22	0.02869
ENSMUSG00000096225	<i>Lhx8</i>	LIM homeobox protein 8	5.17	0.00055
ENSMUSG00000045620	<i>Odf3l1</i>	Outer dense fiber of sperm tails 3-like 1	4.97	0.00314
ENSMUSG00000061959	<i>Ces1e</i>	Carboxylesterase 1E	4.91	0.00405
ENSMUSG00000004341	<i>Gpx6</i>	Glutathione peroxidase 6	4.86	0.00372
ENSMUSG00000029866	<i>Kel</i>	Kell blood group	4.67	0.00028
ENSMUSG00000046975	<i>Olfir1020</i>	Olfactory receptor 1020	4.57	0.01397
ENSMUSG00000027902	<i>Chil6</i>	Chitinase like 6	4.55	0.00405
ENSMUSG00000024681	<i>Ms4a3</i>	Membrane-spanning 4-domains A3	4.49	0.02221
ENSMUSG00000112343	<i>Sfta3-ps</i>	Surfactant associated 3, pseudogene	4.38	0.02155
ENSMUSG00000082308	<i>Gm15770</i>	Predicted gene 15770	4.36	0.03261
ENSMUSG00000083986	<i>Gm12213</i>	Predicted gene 12213	4.36	0.02563
ENSMUSG00000090475	<i>Gm6245</i>	Predicted gene 6245	4.36	0.02527
ENSMUSG00000074665	<i>Bptfb4</i>	BPI fold containing family B4	4.35	0.01778
ENSMUSG00000073920	<i>Olfir661</i>	Olfactory receptor 661	4.30	0.02962
ENSMUSG00000058884	<i>Olfir1025-ps1</i>	Olfactory receptor 1025, pseudogene 1	4.30	0.03356
ENSMUSG00000087340	<i>Gm15228</i>	Predicted gene 15228	4.25	0.02579
ENSMUSG00000094872	<i>Igkv9-120</i>	Immunoglobulin kappa chain variable 9-120	4.22	0.01533
ENSMUSG00000066108	<i>Muc5b</i>	Mucin 5, subtype B, tracheobronchial	4.21	0.00077
ENSMUSG00000105906	<i>Igcl1</i>	Immunoglobulin lambda constant 1	4.18	0.01064
ENSMUSG00000095765	<i>Olfir741</i>	Olfactory receptor 741	4.16	0.00863

Table S1 B. Top 25 downregulated genes in OB tissue samples from *Gadd1^{-/-}* compared to *Gadd1^{+/+}* mice.

ENSEMBL ID	Abbreviation	Name	Log2Fold	P-value
ENSMUSG00000022485	<i>Hoxc5</i>	Homeobox Protein Hox C5	-8.25	0.00033
ENSMUSG00000038700	<i>Hoxb5</i>	Homeobox Protein Hox B5	-7.65	0.00325
ENSMUSG000000087658	<i>Hotairm1</i>	Hoxa transcript antisense RNA, myeloid-specific 1	-6.90	0.00079
ENSMUSG000000038253	<i>Hoxa5</i>	Homeobox Protein Hox A5	-6.46	0.00381
ENSMUSG000000056423	<i>Uts2b</i>	Urotensin-2B	-6.04	0.00188
ENSMUSG000000048763	<i>Hoxb3</i>	Homeobox Protein Hox B3	-5.99	0.00081
ENSMUSG000000001661	<i>Hoxc6</i>	Homeobox Protein Hox C6	-5.97	0.01110
ENSMUSG000000056468	<i>5730596B20Rik</i>	RIKEN cDNA 5730596B20 gene	-5.84	0.03447
ENSMUSG000000084844	<i>Hoxb3os</i>	Homeobox B3 and homeobox B2, opposite strand	-5.76	0.03083
ENSMUSG000000075394	<i>Hoxc4</i>	Homeobox Protein Hox C4	-5.67	0.00327
ENSMUSG000000085696	<i>Hoxaas3</i>	Hoxa cluster antisense RNA 3	-5.02	0.00906
ENSMUSG000000060738	<i>Prl7c1</i>	Prolactin 7c1	-4.85	0.00353
ENSMUSG000000005503	<i>Eyx1</i>	Even-skipped homeobox 1	-4.65	0.03972
ENSMUSG000000067684	<i>Obpl1a</i>	Odorant binding protein 1A	-4.55	0.02233
ENSMUSG000000001670	<i>Tat</i>	Tyrosine aminotransferase	-4.48	0.02410
ENSMUSG000000103430	<i>Gm36996</i>	Predicted gene 36996	-4.45	0.01718
ENSMUSG000000108282	<i>Gm44317</i>	Predicted gene 44317	-4.41	0.01906
ENSMUSG000000026976	<i>Pax8</i>	Paired box 8	-4.29	0.00069
ENSMUSG000000038155	<i>Gstp2</i>	Glutathione S-transferase, pi 2	-4.28	0.03740
ENSMUSG000000042279	<i>H1foo</i>	H1.8 linker histone	-4.27	0.02103
ENSMUSG000000109753	<i>Gm45633</i>	Predicted gene 45633	-4.26	0.02596
ENSMUSG000000041333	<i>Mup4</i>	Major urinary protein 4	-4.26	0.02462
ENSMUSG000000073242	<i>Dnmt3aos</i>	DNA methyltransferase 3A, opposite strand	-4.18	0.02929
ENSMUSG000000074385	<i>Gm10684</i>	Predicted gene 10684	-4.14	0.00057
ENSMUSG000000029844	<i>Hoxal</i>	Homeobox Protein Hox A1	-4.11	0.03148

Table S1 C. Transcript levels of 30 predicted genes close to the *Gad11* locus (yellow: downregulated in knockout, green: upregulated in knockout, blank: not detected).

Gene name	ENSEMBL ID	Log2FoldChange	P-value
<i>Loc102633324 (Gm16142)</i>	ENSMUSG00000087469	-1.145644169	0.331003828
<i>Loc102633106 (Gm31014)</i>			
<i>Loc102633399 (Gm31234)</i>			
<i>Loc102633476 (Gm31292)</i>			
<i>Tgfbr2</i>	ENSMUSG00000032440	0.153321074	0.11705412
<i>Gm9385</i>	ENSMUSG00000080848	-0.131387484	0.400319186
<i>Gm5921</i>	ENSMUSG00000074034	-0.062966245	0.955064616
<i>Gm9385</i>	ENSMUSG00000080848	-0.131387484	0.400319186
<i>Rbms3</i>	ENSMUSG00000039607	-0.041538879	0.816216697
<i>Cmc1</i>	ENSMUSG00000039163	0.043065942	0.678703046
<i>Azi2</i>	ENSMUSG00000039285	0.113416692	0.251718473
<i>Stt3b</i>	ENSMUSG00000032437	0.143339379	0.156764486
<i>Gm18328</i>			
<i>Gm40582</i>			
<i>d73003k21rik</i>			
<i>Gm39447</i>			
<i>Gm40587</i>			
<i>Mir467h</i>			
<i>Gm9487</i>			
<i>4930428G15rik</i>			
<i>Gm30762</i>			
<i>Stmn1-rs1</i>			
<i>Gm31599</i>			
<i>Gm39449</i>			
<i>Gm18489</i>			
<i>Gm39452</i>			
<i>Loc102635502</i>			
<i>Gm36451</i>			
<i>Gm39450</i>			
<i>Loc108167721</i>			
<i>Gm4668</i>			
<i>Gm48038</i>			
<i>Gm31410</i>			

Table S1 D. Transcript levels of ABAT or AGXT2 in the OB extracts of *Gad11*^{+/+} and *Gad11*^{-/-} mice. (yellow: downregulated in knockout, green: upregulated in knockout, blank: not detected).

Gene name	ENSEMBL ID	Log2FoldChange	P-value
<i>Abat</i>	ENSMUSG00000057880	0.063686739	0.554421048
<i>Agxt2</i>	ENSMUSG00000089678	-1.638874888	0.686109037

Table S3. Overview of the data used for genetic analysis using MAGMA software.

phenotype	Sample size*	Reference and data source
Neuropsychiatric		
ADHD**	53,293	Demontis et al. (64)
Alzheimer's disease	452,010	Jansen et al. (67)
ALS***	80,610	Nicolas et al.(70, 75)
Anorexia	72,517	Watson et al.(75)
Anxiety	18,186	Otowa et al. (71)
Autism	46,351	Grove et al. (66)
Bipolar disorder	51,710	Stahl et al. (72)
Depression	173,005	Wray et al. (76)
Educational attainment	766,345	Lee et al. (68)
Epilepsy	34,852	International League Against Epilepsy Consortium on Complex Epilepsies (79)
Parkinson's disease	482,730	Nalls et al. (69)
Schizophrenia	77,096	Ripke et al. (81)
SWB****	298,420	Okbay et al. (82)
Acetyl carnosine (in blood serum)	6279	Shm et al. (27)
AMD	33,976	Fritsche et al. (65)
Body mass index	795,640	Yengo et al. (78)
Coronary heart disease	547,261	van der Harst & Verweij (74)
Muscular strength*****	335,842	UKBIOBANK http://www.nealelab.is/uk-biobank http://ldsc.broadinstitute.org/
Type 2 diabetes	605,056	Xue et al. (77)
Kidney function*	567,460	Wuttke et al. (39)
UACR in diabetes**	5826	Teumer et al.(73)

*Maximum total sample size

** Attention-deficit/hyperactivity disorder

*** Amyotrophic lateral sclerosis

**** Subjective well-being

***** Age-related macular degeneration

***** Right hand grip strength

* glomerular filtration rate estimated from serum creatinine (eGFR)

** urinary albumin-to-creatinine ratio among individuals with diabetes

Table S4. Analysis of mouse diet

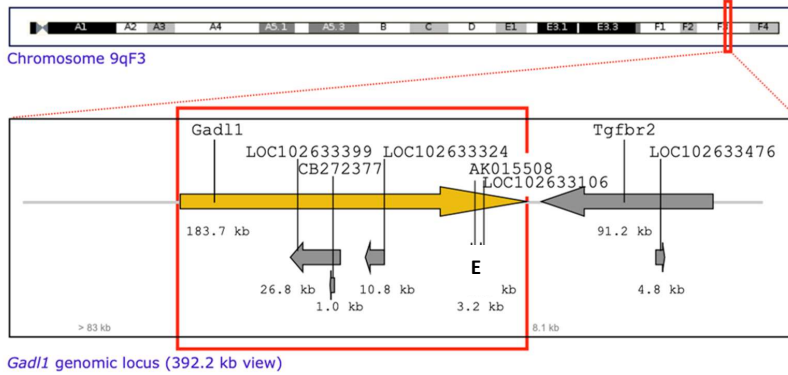
Parameter analyzed	Result (g/kg)
1-Methylhistidine (Free)	<0.5
3-Methylhistidine (Free)	<0.5
Alanine (Free)	<0.5
Alpha-Amino adipic acid (Free)	<0.5
Alpha-Amino-n-butyric acid (Free)	<0.5
Anserine (Free)	<0.5
Arginine (Free)	<0.5
Asparagine (Free)	0.535
Aspartic Acid (Free)	<0.5
β -Alanine (Free)	<0.5
β -Aminoisobutyric acid (Free)	<0.5
Carnosine	<0.5
Citrulline	<0.5
Cystathionine (Free)	<0.5
Cystin (Free)	<0.5
Delta-Hydroxylysine (Free)	<0.5
Ethanolamine	<0.5
γ -Amino-butyric acid (Free)	<0.5
Glutamic acid (Free)	<0.5
Glutamine (Free)	<0.5
Glycine (Free)	<0.5
Histidine (Free)	<0.5
Homocysteine (Free)	<0.5
Hydroxyproline (Free)	<0.5
Isoleucine (Free)	<0.5
Leucine (Free)	<0.5
Lysine (Free)	0.843
Methionine (Free)	<0.5
Ornithine (Free)	<0.5
Phenylalanine (Free)	<0.5
Phosphothanolamine (Free)	<0.5
Phosphoserine (Free)	<0.5
Proline (Free)	<0.5
Sarcosine (Free)	<0.5
Serine (Free)	<0.5
Taurine (Free)	<0.5
Threonine (Free)	<0.5
Tryptophan (Free)	<0.5
Tyrosine (Free)	<0.5
Urea	<0.5

Table S5. Sequences of PCR primers and sizes of PCR products.

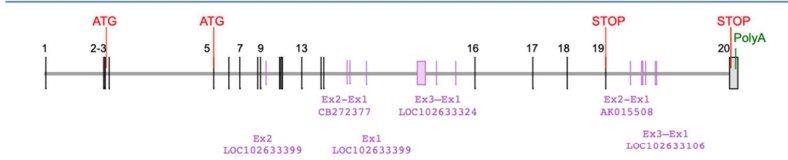
Primer	Primer Sequence 5'-3'	PCR Product Size	
		WT	KO
136258Cre-HAA2	TCAGTTGAGAAGCCCTTCCTTGGTGTA	330 and 750 bp	166 bp
136249Cre-HAA2	CCTTGAACGTGGTTCTCTAGTAGCCACC		
136248Cre-HAA2	AGACCTGGTTAAGCAACTCTCCACTAACTCC		

Supplementary Figures

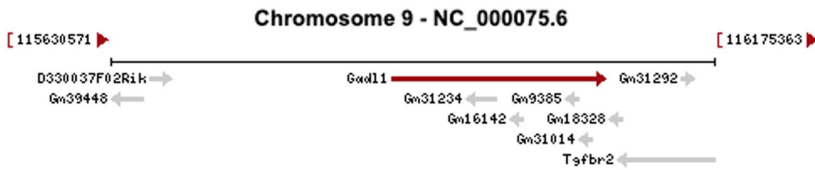
A



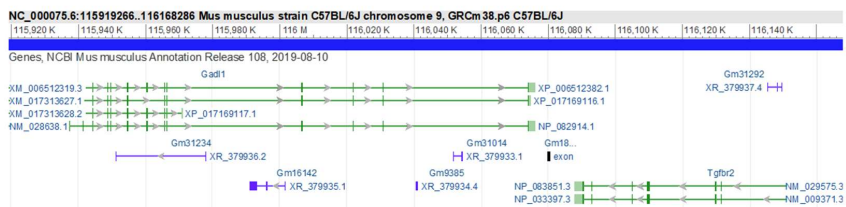
B



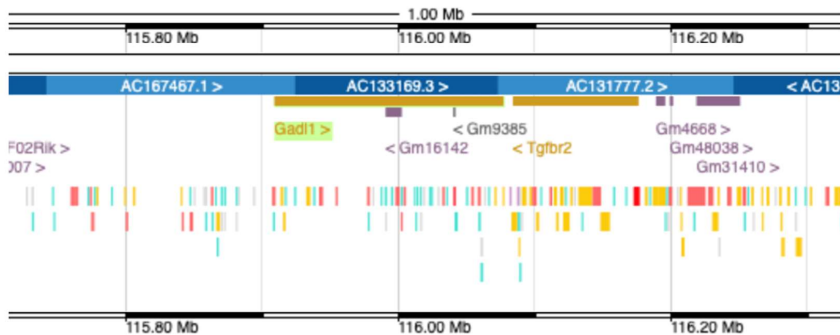
C



D



E



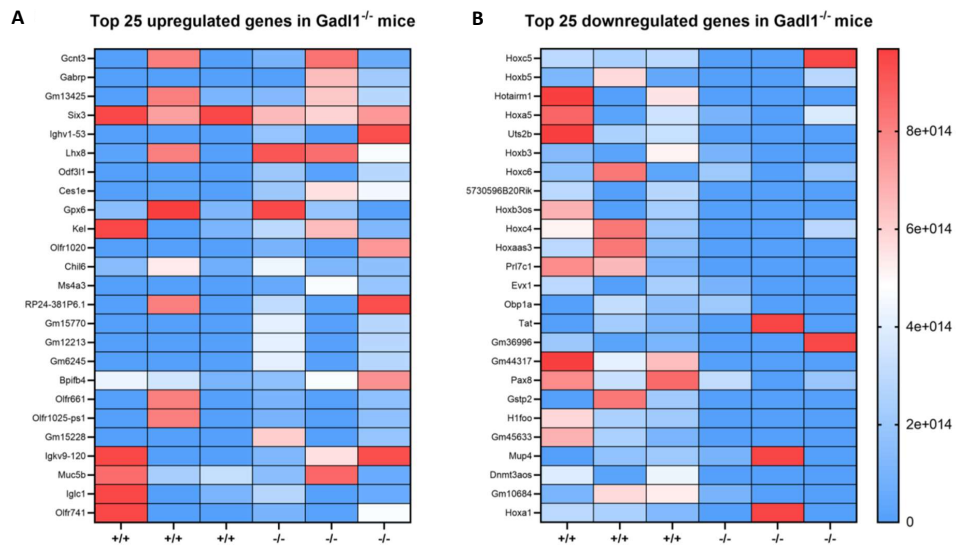
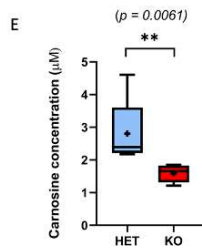
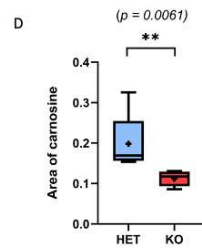
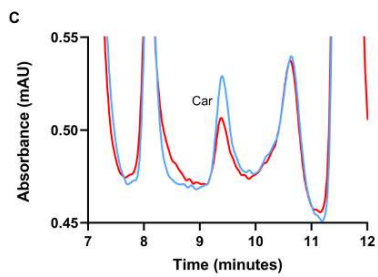
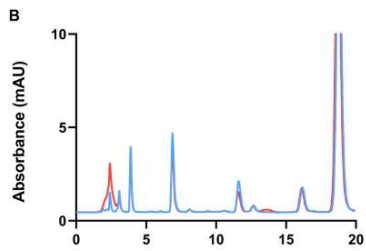
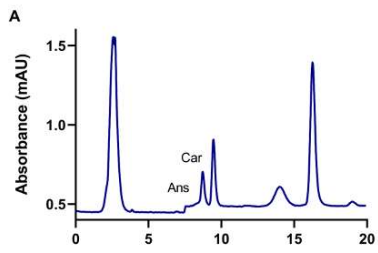
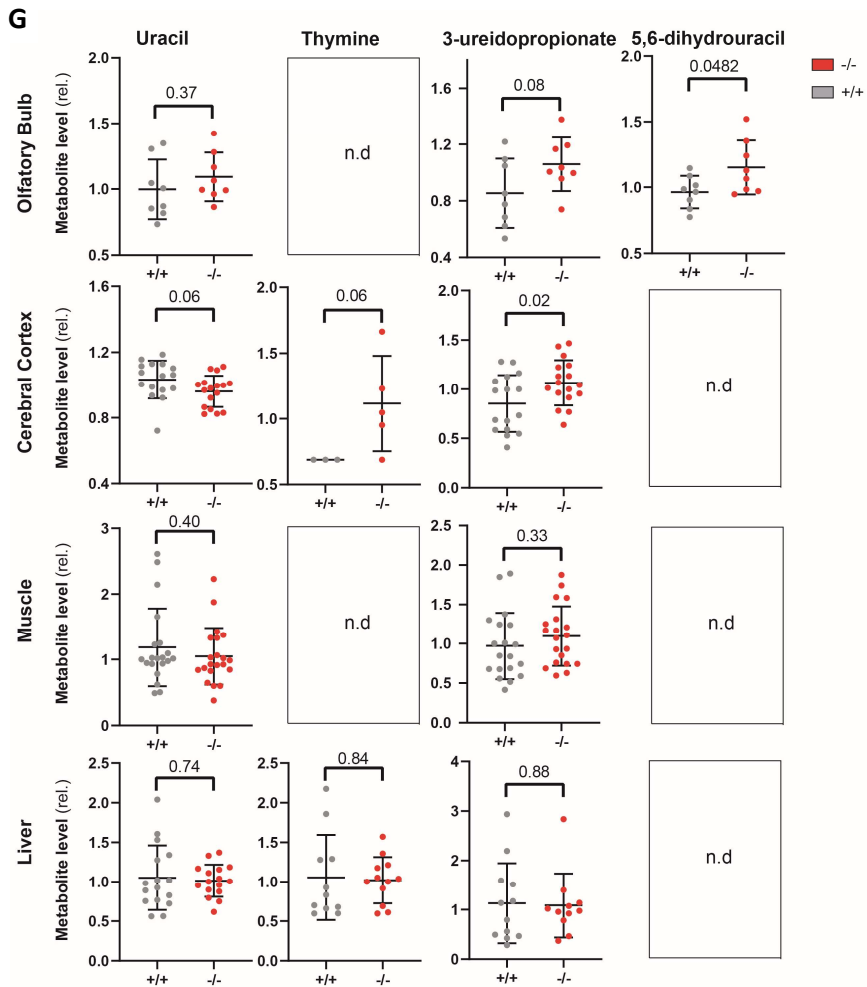
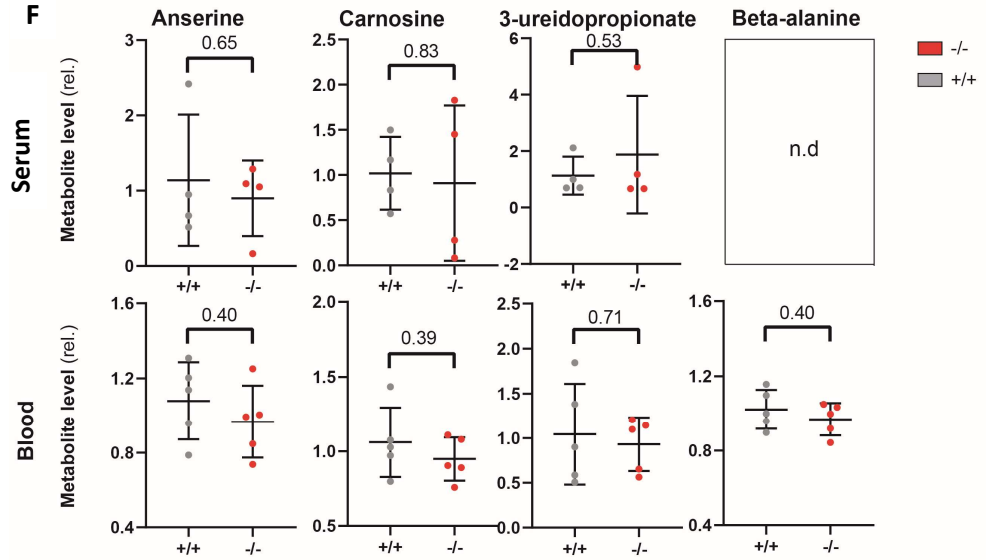
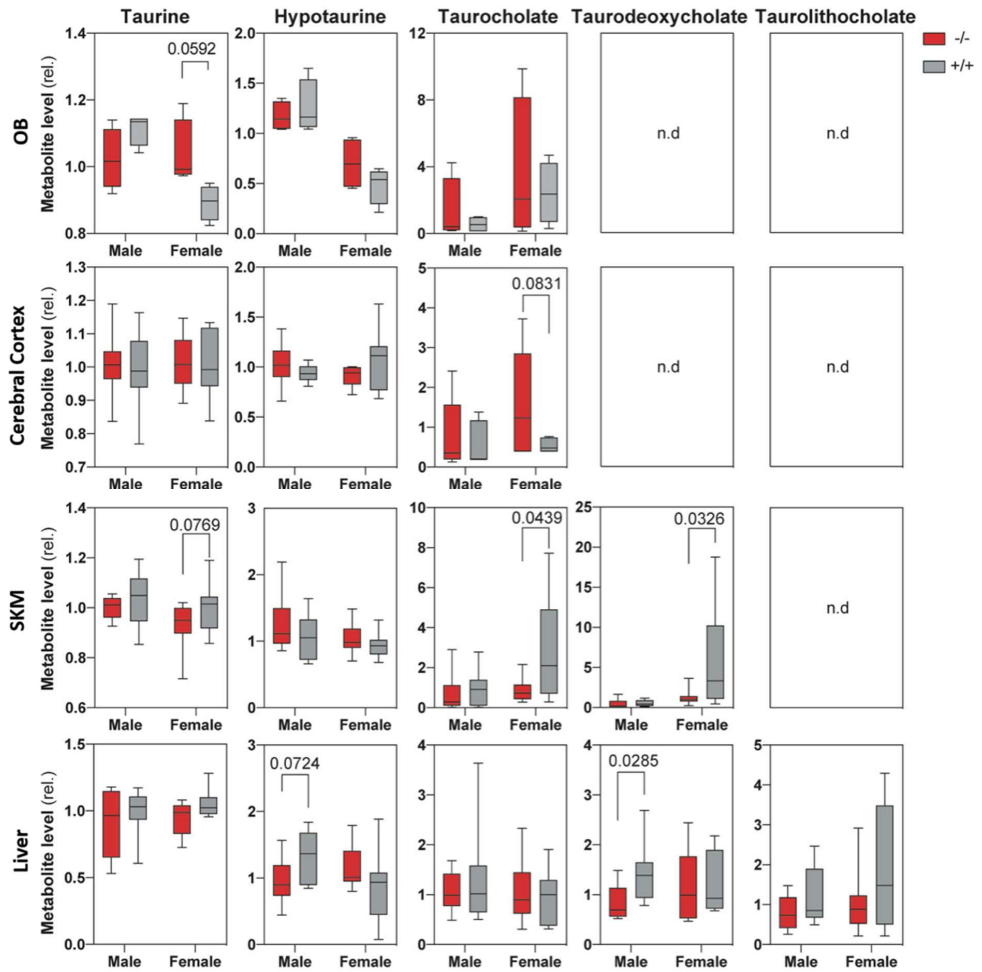
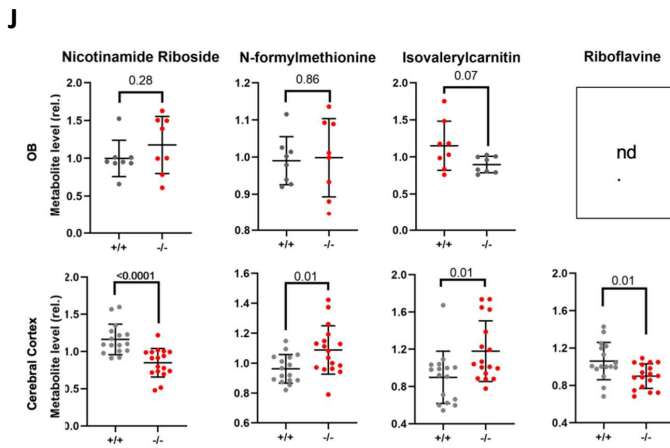
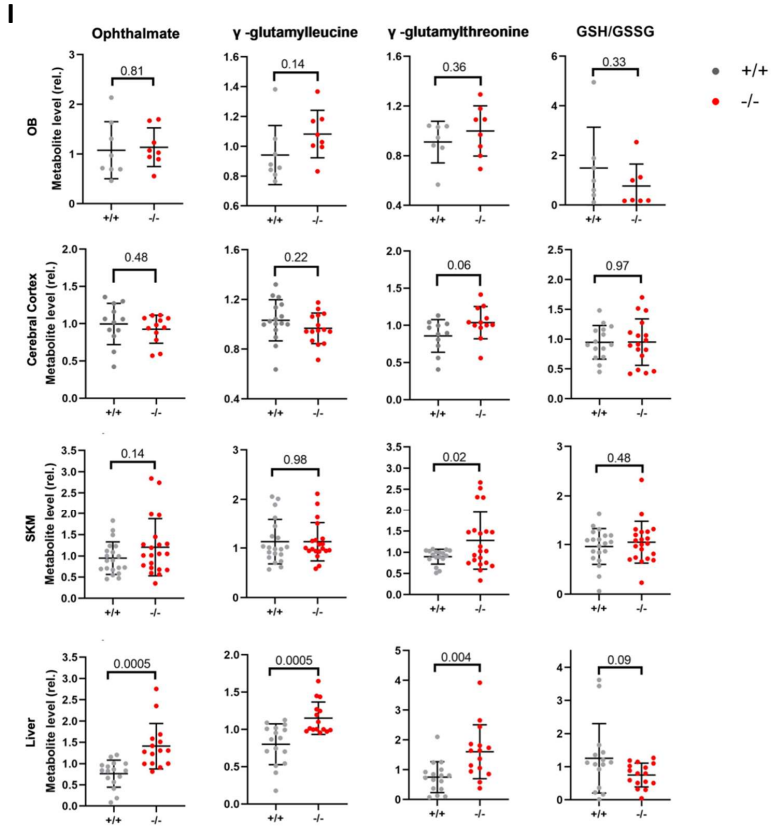


Fig. S3. Top 25 up (A) and down (B) regulated genes in olfactory bulb when comparing *Gad1*^{-/-} (n=3) to *Gad1*^{+/+} (n=3).





H



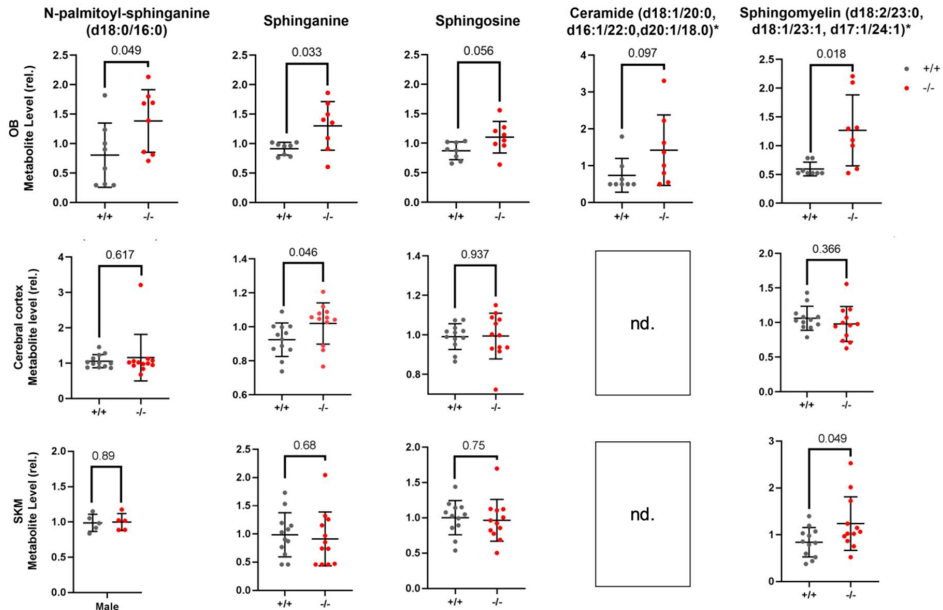
K

Fig. S4. Metabolite levels in mouse tissues. (A, B, C, D and E) Measurements of carnosine peptides in extracts of cerebral cortex from female *Gad11*^{+/-} (n=5) and *Gad11*^{-/-} (n=5) mice (18-22 weeks) using an isocratic RP-HPLC system. Injection of 20µl (A) L-anserine nitrate salt and L-carnosine, and (B and C) cerebral cortex lysates from female *Gad11*^{+/-} (n=5) and *Gad11*^{-/-} (n=5) mice (18-22 weeks). The box plots show (D) mean area and (E) relative level of carnosine concentration in cortex extracts. The decrease in carnosine levels was 40.46 ± 12.18 % from *Gad11*^{+/-} to *Gad11*^{-/-}. Median is presented as a line and mean as a plus (+) sign. Whiskers are drawn from min to max value. Statistical significance ($p < 0.05$) was determined with a ratio, paired t-test and significant differences are indicated with an asterisk (*). Relative levels of (F) 3-ureido-propionate, β-alanine, anserine, and carnosine in whole blood and serum (n=5). Relative levels of various metabolites in OB, cerebral cortex, SKM, and liver tissue extracts from *Gad11*^{+/+} (grey) and *Gad11*^{-/-} (red) mice (n=5-21); (G) uracil and thymine derivatives, (H) taurine and taurine derivatives, (I) Glutamate peptides and related oxidative stress markers, (J) Nicotinamide riboside, N-formylmethionine, isovalerylcarnitine, riboflavin, (K) sphingolipids and ceramide.

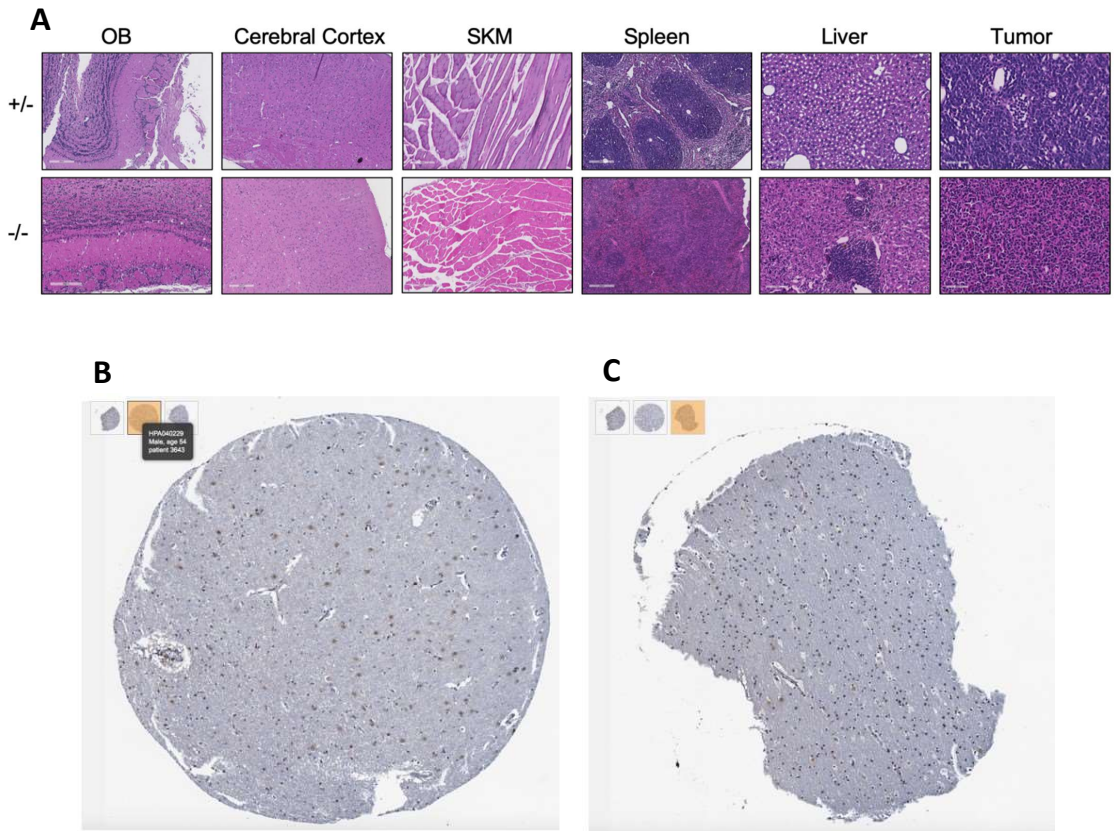


Fig. S5. Tissue distribution of GADL1 (A) Hematoxylin and Eosin (HE) staining of mouse *Gad1*^{+/+} and *Gad1*^{-/-} OB, cerebral cortex, SKM, spleen, liver and tumor. (B-C) Immunohistochemistry for GADL1 of (B) grey and (C) white matter using commercial antibody adapted from Human Protein Atlas.

Links to databases:

Human Protein Atlas

<https://www.proteinatlas.org/ENSG00000144644-GADL1/tissue>

alliance of genome resources

<http://www.informatics.jax.org/marker/MGI:1920998>

REFERENCES AND NOTES

1. A. A. Boldyrev, G. Aldini, W. Derave, Physiology and pathophysiology of carnosine. *Physiol. Rev.* **93**, 1803–1845 (2013).
2. R. Chaleckis, I. Murakami, J. Takada, H. Kondoh, M. Yanagida, Individual variability in human blood metabolites identifies age-related differences. *Proc. Natl. Acad. Sci. U.S.A.* **113**, 4252–4259 (2016).
3. A. R. Hipkiss, Is carnosine a naturally occurring suppressor of oxidative damage in olfactory neurones? *Rejuvenation Res.* **7**, 253–255 (2004).
4. T. L. Perry, S. Hansen, B. Tischler, R. Bunting, K. Berry, Carnosinemia — A new metabolic disorder associated with neurologic disease and mental defect. *N. Engl. J. Med.* **277**, 1219–1227 (1967).
5. K. Wisniewski, L. Fleisher, D. Rassin, H. Lassmann, Neurological disease in a child with carnosinase deficiency. *Neuropediatrics* **12**, 143–151 (1981).
6. J. H. Cararo, E. L. Streck, P. F. Schuck, G. da C Ferreira, Carnosine and related peptides: Therapeutic potential in age-related disorders. *Aging Dis.* **6**, 369–379 (2015).
7. R. M. Hobson, B. Saunders, G. Ball, R. C. Harris, C. Sale, Effects of β -alanine supplementation on exercise performance: A meta-analysis. *Amino Acids* **43**, 25–37 (2012).
8. A. E. Smith, A. A. Walter, J. L. Graef, K. L. Kendall, J. R. Moon, C. M. Lockwood, D. H. Fukuda, T. W. Beck, J. T. Cramer, J. R. Stout, Effects of β -alanine supplementation and high-intensity interval training on endurance performance and body composition in men; a double-blind trial. *J. Int. Soc. Sports Nutr.* **6**, 5 (2009).
9. B. Saunders, K. Elliott-Sale, G. G. Artioli, P. A. Swinton, E. Dolan, H. Roschel, C. Sale, B. Gualano, β -alanine supplementation to improve exercise capacity and performance: A systematic review and meta-analysis. *Br. J. Sports Med.* **51**, 658–669 (2016).
10. M. G. Chez, C. P. Buchanan, M. C. Aimonovitch, M. Becker, K. Schaefer, C. Black, J. Komen, Double-blind, placebo-controlled study of L-carnosine supplementation in children with autistic spectrum disorders. *J. Child Neurol.* **17**, 833–837 (2002).
11. T. Murakami, M. Furuse, The impact of taurine- and beta-alanine-supplemented diets on behavioral and neurochemical parameters in mice: Antidepressant versus anxiolytic-like effects. *Amino Acids* **39**, 427–434 (2010).

12. M. Schön, A. Mousa, M. Berk, W. L. Chia, J. Ukropec, A. Majid, B. Ukropcová, B. de Courten, The potential of carnosine in brain-related disorders: A comprehensive review of current evidence. *Nutrients* **11**, 1196 (2019).
13. G. G. Artioli, B. Gualano, A. Smith, J. Stout, A. H. Lanch Jr., Role of β -alanine supplementation on muscle carnosine and exercise performance. *Med. Sci. Sports Exerc.* **42**, 1162–1173 (2010).
14. E. J. Anderson, G. Vistoli, L. A. Katunga, K. Funai, L. Regazzoni, T. Blake Monroe, E. Gilardoni, L. Cannizzaro, M. Colzani, D. De Maddis, G. Rossoni, R. Canevotti, S. Gagliardi, M. Carini, G. Aldini, A carnosine analog mitigates metabolic disorders of obesity by reducing carbonyl stress. *J. Clin. Invest.* **128**, 5280–5293 (2018).
15. M. Dunnett, R. C. Harris, Influence of oral β -alanine and L-histidine supplementation on the carnosine content of the *gluteus medius*. *Equine Vet. J. Suppl.* **30**, 499–504 (1999).
16. E. P. Rhee, J. E. Ho, M.-H. Chen, D. Shen, S. Cheng, M. G. Larson, A. Ghorbani, X. Shi, I. T. Helenius, C. J. O'Donnell, A. L. Souza, A. Deik, K. A. Pierce, K. Bullock, G. A. Walford, R. S. Vasani, J. C. Florez, C. Clish, J.-R. J. Yeh, T. J. Wang, R. E. Gerszten, A genome-wide association study of the human metabolome in a community-based cohort. *Cell Metab.* **18**, 130–143 (2013).
17. R. Zrenner, H. Riegler, C. R. Marquard, P. R. Lange, C. Geserick, C. E. Bartosz, C. T. Chen, R. D. Slocum, A functional analysis of the pyrimidine catabolic pathway in *Arabidopsis*. *New Phytol.* **183**, 117–132 (2009).
18. F. Schmitzberger, M. L. Kilkenny, C. M. C. Lobley, M. E. Webb, M. Vinkovic, D. Matak-Vinkovic, M. Witty, D. Y. Chirgadze, A. G. Smith, C. Abell, T. L. Blundell, Structural constraints on protein self-processing in L-aspartate- α -decarboxylase. *EMBO J.* **22**, 6193–204 (2003).
19. S. Chopra, H. Pai, A. Ranganathan, Expression, purification, and biochemical characterization of *Mycobacterium tuberculosis* aspartate decarboxylase, PanD. *Protein Expr. Purif.* **25**, 533–540 (2002).
20. S. Suidasari, J. Stautemas, S. Urugami, N. Yanaka, W. Derave, N. Kato, Carnosine content in skeletal muscle is dependent on vitamin B6 status in rats. *Front. Nutr.* **2**, 39 (2015).
21. C.-H. Chen, C.-S. Lee, M.-T. M. Lee, W.-C. Ouyang, C.-C. Chen, M.-Y. Chong, J.-Y. Wu, H. K.-L. Tan, Y.-C. Lee, L.-J. Chuo, N.-Y. Chiu, H.-Y. Tsang, T.-J. Chang, F.-W. Lung, C.-

- H. Chiu, C.-H. Chang, Y.-S. Chen, Y.-M. Hou, C.-C. Chen, T.-J. Lai, C.-L. Tung, C.-Y. Chen, H.-Y. Lane, T.-P. Su, J. Feng, J.-J. Lin, C.-J. Chang, P.-R. Teng, C.-Y. Liu, C.-K. Chen, I.-C. Liu, J.-J. Chen, T. Lu, C.-C. Fan, C.-K. Wu, C.-F. Li, K. H.-T. Wang, L. S.-H. Wu, H.-L. Peng, C.-P. Chang, L.-S. Lu, Y.-T. Chen, A. T.-A. Cheng; Taiwan Bipolar Consortium, Variant GADL1 and response to lithium therapy in bipolar I disorder. *N. Engl. J. Med.* **370**, 119–128 (2014).
22. C. Cruceanu, M. Alda, P. A. Dion, G. Turecki, G. A. Rouleau, No evidence for *GADL1* variation as a bipolar disorder susceptibility factor in a Caucasian lithium-responsive cohort. *Am. J. Psychiatry* **172**, 94–95 (2015).
23. P. Liu, X. Ge, H. Ding, H. Jiang, B. M. Christensen, J. Li, Role of glutamate decarboxylase-like protein 1 (*GADL1*) in taurine biosynthesis. *J. Biol. Chem.* **287**, 40898–40906 (2012).
24. I. Winge, K. Teigen, A. Fossbakk, E. Mahootchi, R. Kleppe, F. Skoldberg, O. Kämpe, J. Haavik, Mammalian CSAD and *GADL1* have distinct biochemical properties and patterns of brain expression. *Neurochem. Int.* **90**, 173–184 (2015).
25. A. Raasakka, E. Mahootchi, I. Winge, W. Luan, P. Kursula, J. Haavik, Structure of the mouse acidic amino acid decarboxylase *GADL1*. *Acta Crystallogr. F. Struct. Biol. Commun.* **74** (Pt 1), 65–73 (2018).
26. S.-Y. Shin, E. B. Fauman, A.-K. Petersen, J. Krumsiek, R. Santos, J. Huang, M. Arnold, I. Erte, V. Forgetta, T.-P. Yang, K. Walter, C. Menni, L. Chen, L. Vasquez, A. M. Valdes, C. L. Hyde, V. Wang, D. Ziemek, P. Roberts, L. Xi, E. Grundberg; The Multiple Tissue Human Expression Resource (Mu THER) Consortium, M. Waldenberger, J. B. Richards, R. P. Mohney, M. V. Milburn, S. L. John, J. Trimmer, F. J. Theis, J. P. Overington, K. Suhre, M. J. Brosnan, C. Gieger, G. Kastenmüller, T. D. Spector, N. Soranzo, An atlas of genetic influences on human blood metabolites. *Nat. Genet.* **46**, 543–550 (2014).
27. M. Kanehisa, S. Goto, KEGG: Kyoto encyclopedia of genes and genomes. *Nucleic Acids Res.* **28**, 27–30 (2000).
28. The Gene Ontology Consortium, Gene Ontology Consortium: Going forward. *Nucleic Acids Res.* **43** (Database issue), D1049–D1056 (2015).
29. R. M. Kream, F. L. Margolis, Olfactory marker protein: Turnover and transport in normal and regenerating neurons. *J. Neurosci.* **4**, 868–879 (1984).

30. T.-N. Wu, C.-K. Chen, C.-S. Lee, B.-J. Wu, H.-J. Sun, C.-H. Chang, C.-Y. Chen, L. S.-H. Wu, A. T.-A. Cheng, Lithium and GADL1 regulate glycogen synthase kinase-3 activity to modulate *KCTD12* expression. *Sci. Rep.* **9**, 10255 (2019).
31. R. Percudani, A. Peracchi, A genomic overview of pyridoxal-phosphate-dependent enzymes. *EMBO Rep.* **4**, 850–854 (2003).
32. G. Fenalti, R. H. P. Law, A. M. Buckle, C. Langendorf, K. Tuck, C. J. Rosado, N. G. Faux, K. Mahmood, C. S. Hampe, J. P. Banga, M. Wilce, J. Schmidberger, J. Rossjohn, O. El-Kabbani, R. N. Pike, A. I. Smith, I. R. Mackay, M. J. Rowley, J. C. Whisstock, GABA production by glutamic acid decarboxylase is regulated by a dynamic catalytic loop. *Nat. Struct. Mol. Biol.* **14**, 280–286 (2007).
33. E. Park, S. Y. Park, C. Dobkin, G. Schuller-Levis, Development of a novel cysteine sulfinic acid decarboxylase knockout mouse: Dietary taurine reduces neonatal mortality. *J. Amino Acids* **2014**, 346809 (2014).
34. J. E. Dominy Jr., C. R. Simmons, L. L. Hirschberger, J. Hwang, R. M. Coloso, M. H. Stipanuk, Discovery and characterization of a second mammalian thiol dioxygenase, cysteamine dioxygenase. *J. Biol. Chem.* **282**, 25189–25198 (2007).
35. A. A. Boldyrev, Carnosine: New concept for the function of an old molecule. *Biochemistry (Mosc.)* **77**, 313–326 (2012).
36. M. N. Nikolova-Karakashian, M. B. Reid, Sphingolipid metabolism, oxidant signaling, and contractile function of skeletal muscle. *Antioxid. Redox Signal.* **15**, 2501–2517 (2011).
37. T. D. Wade, S. Gordon, S. Medland, C. M. Bulik, A. C. Heath, G. W. Montgomery, N. G. Martin, Genetic variants associated with disordered eating. *Int. J. Eat. Disord.* **46**, 594–608 (2013).
38. M. Wuttke, Y. Li, M. Li, K. B. Sieber, M. F. Feitosa, M. Gorski, A. Tin, L. Wang, A. Y. Chu, A. Hoppmann, H. Kirsten, A. Giri, J.-F. Chai, G. Sveinbjornsson, B. O. Tayo, T. Nutile, C. Fuchsberger, J. Marten, M. Cocca, S. Ghasemi, Y. Xu, K. Horn, D. Noce, P. J. van der Most, S. Sedaghat, Z. Yu, M. Akiyama, S. Afaq, T. S. Ahluwalia, P. Almgren, N. Amin, J. Ärnlöv, S. J. L. Bakker, N. Bansal, D. Baptista, S. Bergmann, M. L. Biggs, G. Biino, M. Boehnke, E. Boerwinkle, M. Boissel, E. P. Bottinger, T. S. Boutin, H. Brenner, M. Brumat, R. Burkhardt, A. S. Butterworth, E. Campana, A. Campbell, H. Campbell, M. Canouil, R. J. Carroll, E. Catamo, J. C. Chambers, M.-L. Chee, M.-L. Chee, X. Chen, C.-Y. Cheng, Y.

Cheng, K. Christensen, R. Cifkova, M. Ciullo, M. P. Concas, J. P. Cook, J. Coresh, T. Corre, C. F. Sala, D. Cusi, J. Danesh, E. W. Daw, M. H. de Borst, A. De Grandi, R. de Mutsert, A. P. J. de Vries, F. Degenhardt, G. Delgado, A. Demirkan, E. D. Angelantonio, K. Dittrich, J. Divers, R. Dorajoo, K.-U. Eckardt, G. Ehret, P. Elliott, K. Endlich, M. K. Evans, J. F. Felix, V. H. X. Foo, O. H. Franco, A. Franke, B. I. Freedman, S. Freitag-Wolf, Y. Friedlander, P. Froguel, R. T. Gansevoort, H. Gao, P. Gasparini, J. M. Gaziano, V. Giedraitis, C. Gieger, G. Giroto, F. Giulianini, M. Gögele, S. D. Gordon, D. F. Gudbjartsson, V. Gudnason, T. Haller, P. Hamet, T. B. Harris, C. A. Hartman, C. Hayward, J. N. Hellwege, C.-K. Heng, A. A. Hicks, E. Hofer, W. Huang, N. Hutri-Kähönen, S.-J. Hwang, M. A. Ikram, O. S. Indridason, E. Ingelsson, M. Ising, V. W. V. Jaddoe, J. Jakobsdottir, J. B. Jonas, P. K. Joshi, N. S. Josyula, B. Jung, M. Kähönen, Y. Kamatani, C. M. Kammerer, M. Kanai, M. Kastarinen, S. M. Kerr, C.-C. Khor, W. Kiess, M. E. Kleber, W. Koenig, J. S. Kooner, A. Körner, P. Kovacs, A. T. Kraja, A. Krajcoviechova, H. Kramer, B. K. Krämer, F. Kronenberg, M. Kubo, B. Kühnel, M. Kuokkanen, J. Kuusisto, M. L. Bianca, M. Laakso, L. A. Lange, C. D. Langefeld, J. J.-M. Lee, B. Lehne, T. Lehtimäki, W. Lieb, L. C. Study, S.-C. Lim, L. Lind, C. M. Lindgren, J. Liu, J. Liu, M. Loeffler, R. J. F. Loos, S. Lucae, M. A. Lukas, L.-P. Lyytikäinen, R. Mägi, P. K. E. Magnusson, A. Mahajan, N. G. Martin, J. Martins, W. März, D. Mascalzoni, K. Matsuda, C. Meisinger, T. Meitinger, O. Melander, A. Metspalu, E. K. Mikaelsdottir, Y. Milaneschi, K. Miliku, P. P. Mishra; V. A. Million Veteran Program, K. L. Mohlke, N. Mononen, G. W. Montgomery, D. O. Mook-Kanamori, J. C. Mychaleckyj, G. N. Nadkarni, M. A. Nalls, M. Nauck, K. Nikus, B. Ning, I. M. Nolte, R. Noordam, J. O'Connell, M. L. O'Donoghue, I. Olafsson, A. J. Oldehinkel, M. Orho-Melander, W. H. Ouwehand, S. Padmanabhan, N. D. Palmer, R. Palsson, B. W. J. H. Penninx, T. Perls, M. Perola, M. Pirastu, N. Pirastu, G. Pistis, A. I. Podgornaia, O. Polasek, B. Ponte, D. J. Porteous, T. Poulain, P. P. Pramstaller, M. H. Preuss, B. P. Prins, M. A. Province, T. J. Rabelink, L. M. Raffield, O. T. Raitakari, D. F. Reilly, R. Rettig, M. Rheinberger, K. M. Rice, P. M. Ridker, F. Rivadeneira, F. Rizzi, D. J. Roberts, A. Robino, P. Rossing, I. Rudan, R. Rueedi, D. Ruggiero, K. A. Ryan, Y. Saba, C. Sabanayagam, V. Salomaa, E. Salvi, K.-U. Saum, H. Schmidt, R. Schmidt, B. Schöttker, C.-A. Schulz, N. Schupf, C. M. Shaffer, Y. Shi, A. V. Smith, B. H. Smith, N. Soranzo, C. N. Spracklen, K. Strauch, H. M. Stringham, M. Stumvoll, P. O. Svensson, S. Szymczak, E.-S. Tai, S. M. Tajuddin, N. Y. Q. Tan, K. D. Taylor, A.

- Teren, Y.-C. Tham, J. Thiery, C. H. L. Thio, H. Thomsen, G. Thorleifsson, D. Toniolo, A. Tönjes, J. Tremblay, I. Tzoulaki, A. G. Uitterlinden, S. Vaccargiu, R. M. van Dam, P. van der Harst, C. M. van Duijn, D. R. Velez Edward, N. Verweij, S. Vogelesang, U. Völker, P. Vollenweider, G. Waeber, M. Waldenberger, L. Wallentin, Y. X. Wang, C. Wang, D. M. Waterworth, W. B. Wei, H. White, J. B. Whitfield, S. H. Wild, J. F. Wilson, M. K. Wojczynski, C. Wong, T.-Y. Wong, L. Xu, Q. Yang, M. Yasuda, L. M. Yerges-Armstrong, W. Zhang, A. B. Zonderman, J. I. Rotter, M. Bochud, B. M. Psaty, V. Vitart, J. G. Wilson, A. Dehghan, A. Parsa, D. I. Chasman, K. Ho, A. P. Morris, O. Devuyst, S. Akilesh, S. A. Pendergrass, X. Sim, C. A. Böger, Y. Okada, T. L. Edwards, H. Snieder, K. Stefansson, A. M. Hung, I. M. Heid, M. Scholz, A. Teumer, A. Köttgen, C. Pattaro, A catalog of genetic loci associated with kidney function from analyses of a million individuals. *Nat. Genet.* **51**, 957–972 (2019).
39. C. A. de Leeuw, J. M. Mooij, T. Heskes, D. Posthuma, MAGMA: Generalized gene-set analysis of GWAS data. *PLOS Comput. Biol.* **11**, e1004219 (2015).
40. I. Everaert, H. De Naeyer, Y. Taes, W. Derave, Gene expression of carnosine-related enzymes and transporters in skeletal muscle. *Eur. J. Appl. Physiol.* **113**, 1169–1179 (2013).
41. M. M. Matthews, T. W. Traut. Regulation of *N*-carbamoyl- β -alanine amidohydrolase, the terminal enzyme in pyrimidine catabolism, by ligand-induced change in polymerization. *J. Biol. Chem.* **262**, 7232–7237 (1987).
42. A. Peracchi The limits of enzyme specificity and the evolution of metabolism. *Trends Biochem. Sci.* **43**, 984–996 (2018).
43. A. Shetewy, K. Shimada-Takaura, D. Warner, C. J. Jong, A.-B. Al Mehdi, M. Alexeyev, K. Takahashi, S. W. Schaffer, Mitochondrial defects associated with β -alanine toxicity: Relevance to hyper-beta-alaninemia. *Mol. Cell. Biochem.* **416**, 11–22 (2016).
44. T. Gemelli, R. B. de Andrade, D. B. Rojas, N. F. Bonorino, P. N. Mazzola, L. S. Tortorelli, C. Funchal, C. S. D. Filho, C. M. D. Wannmacher, Effects of β -alanine administration on selected parameters of oxidative stress and phosphoryltransfer network in cerebral cortex and cerebellum of rats. *Mol. Cell. Biochem.* **380**, 161–170 (2013).
5. M. A. Kamal, H. Jiang, Y. Hu, R. F. Keep, D. E. Smith, Influence of genetic knockout of *Pept2* on the in vivo disposition of endogenous and exogenous carnosine in wild-type and *Pept2* null mice. *Am. J. Physiol. Regul. Integr. Comp. Physiol.* **296**, R986–R991 (2009).

6. E. Miyamoto-Mikami, K. Tsuji, N. Horii, N. Hasegawa, S. Fujie, T. Homma, M. Uchida, T. Hamaoka, H. Kanehisa, I. Tabata, M. Iemitsu, Gene expression profile of muscle adaptation to high-intensity intermittent exercise training in young men. *Sci. Rep.* **8**, 16811 (2018).
47. J. Drozak, M. Veiga-da-Cunha, D. Vertommen, V. Stroobant, E. Van Schaftingen, Molecular identification of carnosine synthase as ATP-grasp domain-containing protein 1 (ATPGD1). *J. Biol. Chem.* **285**, 9346–9356 (2010).
48. B. Janssen, D. Hohenadel, P. Brinkkoetter, V. Peters, N. Rind, C. Fischer, I. Rychlik, M. Cerna, M. Romzova, E. de Heer, H. Baelde, S. J. L. Bakker, M. Zirie, E. Rondeau, P. Mathieson, M. A. Saleem, J. Meyer, H. Köppel, S. Sauerhoefer, C. R. Bartram, P. Nawroth, H.-P. Hammes, B. A. Yard, J. Zschocke, F. J. van der Woude, Carnosine as a protective factor in diabetic nephropathy: Association with a leucine repeat of the carnosinase gene CNDP1. *Diabetes* **54**, 2320–2327 (2005).
49. M. A. Babizhayev, Biochemical, biomedical and metabolic aspects of imidazole-containing dipeptides with the inherent complexity to neurodegenerative diseases and various states of mental well-being: A challenging correction and neurotherapeutic pharmaceutical biotechnology for treating cognitive deficits, depression and intellectual disabilities. *Curr. Pharm. Biotechnol.* **15**, 738–778 (2014).
50. J. Ivanisevic, A. A. Epstein, M. E. Kurczy, P. H. Benton, W. Uritboonthai, H. S. Fox, M. D. Boska, H. E. Gendelman, G. Siuzdak, Brain region mapping using global metabolomics. *Chem. Biol.* **21**, 1575–1584 (2014).
51. M.-C. Senut, S. Azher, F. L. Margolis, K. Patel, A. Mousa, A. Majid, Distribution of carnosine-like peptides in the nervous system of developing and adult zebrafish (*Danio rerio*) and embryonic effects of chronic carnosine exposure. *Cell Tissue Res.* **337**, 45–61 (2009).
2. N. Alenina, D. Kikic, M. Todiras, V. Mosienko, F. Qadri, R. Plehm, P. Boyé, L. Vilianovitch, R. Sohr, K. Tenner, H. Hörtnagl, M. Bader, Growth retardation and altered autonomic control in mice lacking brain serotonin. *Proc. Natl. Acad. Sci. U.S.A.* **106**, 10332–10337 (2009).
53. S. Sun, Y. Sun, S.-C. Ling, L. Ferraiuolo, M. McAlonis-Downes, Y. Zou, K. Drenner, Y. Wang, D. Ditsworth, S. Tokunaga, A. Kopelevich, B. K. Kaspar, C. Lagier-Tourenne, D. W. Cleveland, Translational profiling identifies a cascade of damage initiated in motor neurons

- and spreading to glia in mutant SOD1-mediated ALS. *Proc. Natl. Acad. Sci. U.S.A.* **112**, E6993–E7002 (2015).
54. S. Schwartz, E. Hall, G. Ast, SROOGLE: Webserver for integrative, user-friendly visualization of splicing signals. *Nucleic Acids Res.* **37**, W189–W192 (2009).
 55. K. J. Livak, T. D. Schmittgen, Analysis of relative gene expression data using real-time quantitative PCR and the $2^{-\Delta\Delta C_T}$ method. *Methods* **25**, 402–408 (2001).
 56. D. Kim, B. Langmead, S. L. Salzberg, HISAT: A fast spliced aligner with low memory requirements. *Nat. Methods* **12**, 357–360 (2015).
 57. Y. Liao, G. K. Smyth, W. Shi, featureCounts: An efficient general purpose program for assigning sequence reads to genomic features. *Bioinformatics* **30**, 923–930 (2014).
 58. M. I. Love, W. Huber, S. Anders, Moderated estimation of fold change and dispersion for RNA-seq data with DESeq2. *Genome Biol.* **15**, 550 (2014).
 59. T. Metsalu, J. Vilo, ClustVis: A web tool for visualizing clustering of multivariate data using principal component analysis and heatmap. *Nucleic Acids Res.* **43** (W1), W566–W570 (2015).
 0. G. Fenalti, C. S. Hampe, K. O'Connor, J. P. Banga, I. R. Mackay, M. J. Rowley, O. El-Kabbani, Molecular characterization of a disease associated conformational epitope on GAD65 recognised by a human monoclonal antibody b96.11. *Mol. Immunol.* **44**, 1178–1189 (2007).
 61. P. Emsley, B. Lohkamp, W G Scott, K. Cowtan, Features and development of Coot. *Acta Crystallogr. D Biol. Crystallogr.* **66** (Pt 4), 486–501 (2010).
 62. E. F. Pettersen, T. D. Goddard, C. C. Huang, G. S. Couch, D. M. Greenblatt, E. C. Meng, T. E. Ferrin, UCSF Chimera—A visualization system for exploratory research and analysis. *J. Comput. Chem.* **25**, 1605–1612 (2004).
 63. C. G. Langendorf, K. L. Tuck, T. L. G. Key, G. Fenalti, R. N. Pike, C. J. Rosado, A. S. M. Wong, A. M. Buckle, R. H. P. Law, J. C. Whisstock, Structural characterization of the mechanism through which human glutamic acid decarboxylase auto-activates. *Biosci. Rep.* **33**, 137–144 (2013).
 64. D. Demontis, R. K. Walters, J. Martin, M. Mattheisen, T. D. Als, E. Agerbo, G. Baldursson, R. Belliveau, J. Bybjerg-Grauholm, M. Bækvad-Hansen, F. Cerrato, K. Chambert, C. Churchhouse, A. Dumont, N. Eriksson, M. Gandal, J. I. Goldstein, K. L. Grasby, J. Grove, O.

O. Gudmundsson, C. S. Hansen, M. E. Hauberg, M. V. Hollegaard, D. P. Howrigan, H. Huang, J. B. Maller, A. R. Martin, N. G. Martin, J. Moran, J. Pallesen, D. S. Palmer, C. B. Pedersen, M. G. Pedersen, T. Poterba, J. B. Poulsen, S. Ripke, E. B. Robinson, F. K. Satterstrom, H. Stefansson, C. Stevens, P. Turley, G. B. Walters, H. Won, M. J. Wright; ADHD Working Group of the Psychiatric Genomics Consortium (PGC); Early Lifecourse & Genetic Epidemiology (EAGLE) Consortium; 23andMe Research Team, O. A. Andreassen, P. Asherson, C. L. Burton, D. I. Boomsma, B. Cormand, S. Dalsgaard, B. Franke, J. Gelernter, D. Geschwind, H. Hakonarson, J. Haavik, H. R. Kranzler, J. Kuntsi, K. Langley, K.-P. Lesch, C. Middeldorp, A. Reif, L. A. Rohde, P. Roussos, R. Schachar, P. Sklar, E. J. S. Sonuga-Barke, P. F. Sullivan, A. Thapar, J. Y. Tung, I. D. Waldman, S. E. Medland, K. Stefansson, M. Nordentoft, D. M. Hougaard, T. Werge, O. Mors, P. B. Mortensen, M. J. Daly, S. V. Faraone, A. D. Børglum, B. M. Neale, Discovery of the first genome-wide significant risk loci for attention deficit/hyperactivity disorder. *Nat. Genet.* **51**, 63–75 (2019).

65. L. G. Fritsche, W. Igl, J. N. C. Bailey, F. Grassmann, S. Sengupta, J. L. Bragg-Gresham, K. P. Burdon, S. J. Hebring, C. Wen, M. Gorski, I. K. Kim, D. Cho, D. Zack, E. Souied, H. P. N. Scholl, E. Bala, K. E. Lee, D. J. Hunter, R. J. Sardell, P. Mitchell, J. E. Merriam, V. Cipriani, J. D. Hoffman, T. Schick, Y. T. E. Lechanteur, R. H. Guymer, M. P. Johnson, Y. Jiang, C. M. Stanton, G. H. S. Buitendijk, X. Zhan, A. M. Kwong, A. Boleda, M. Brooks, L. Gieser, R. Ratnapriya, K. E. Branham, J. R. Foerster, J. R. Heckenlively, M. I. Othman, B. J. Vote, H. H. Liang, E. Souzeau, I. L. McAllister, T. Isaacs, J. Hall, S. Lake, D. A. Mackey, I. J. Constable, J. E. Craig, T. E. Kitchner, Z. Yang, Z. Su, H. Luo, D. Chen, H. Ouyang, K. Flagg, D. Lin, G. Mao, H. Ferreyra, K. Stark, C. N von Strachwitz, A. Wolf, C. Brandl, G. Rudolph, M. Olden, M. A. Morrison, D. J. Morgan, M. Schu, J. Ahn, G. Silvestri, E. E. Tsironi, K. H. Park, L. A. Farrer, A. Orlin, A. Brucker, M. Li, C. A. Curcio, S. Mohand-Saïd, J.-A. Sahel, I. Audo, M. Benchaboune, A. J. Cree, C. A. Rennie, S. V. Goverdhan, M. Grunin, S. Hagbi-Levi, P. Campocharo, N. Katsanis, F. G. Holz, F. Blond, H. Blanché, J.-F. Deleuze, R. P. Igo Jr., B. Truitt, N. S. Peachey, S. M. Meuer, C. E. Myers, E. L. Moore, R. Klein, M. A. Hauser, E. A. Postel, M. D. Courtenay, S. G. Schwartz, J. L. Kovach, W. K. Scott, G. Liew, A. G. Tan, B. Gopinath, J. C. Merriam, R. T. Smith, J. C. Khan, H. Shahid, A. T. Moore, J. A. McGrath, R. Laux, M. A. Brantley Jr., A. Agarwal, L. Ersoy, A. Caramoy, T. Langmann, N. T. M. Saksens, E. K. de Jong, C. B. Hoyng, M. S. Cain, A. J. Richardson,

- T. M. Martin, J. Blangero, D. E. Weeks, B. Dhillon, C. M van Duijn, K. F. Doheny, J. Romm, C. C. W. Klaver, C. Hayward, M. B. Gorin, M. L. Klein, P. N. Baird, A. I den Hollander, S. Fauser, J. R. W. Yates, R. Allikmets, J. J. Wang, D. A. Schaumberg, B. E. K. Klein, S. A. Hagstrom, I. Chowers, A. J. Lotery, T. Léveillard, K. Zhang, M. H. Brilliant, A. W. Hewitt, A. Swaroop, E. Y. Chew, M. A. Pericak-Vance, M. De Angelis, D. Stambolian, J. L. Haines, S. K. Iyengar, B. H. F. Weber, G. R. Abecasis, I. M. Heid, A large genome-wide association study of age-related macular degeneration highlights contributions of rare and common variants. *Nat. Genet.* **48**, 134–143 (2016).
66. J. Grove, S. Ripke, T. D. Als, M. Mattheisen, R. K. Walters, H. Won, J. Pallesen, E. Agerbo, O. A. Andreassen, R. Anney, S. Awashti, R. Belliveau, F. Bettella, J. D. Buxbaum, J. Bybjerg-Grauholm, M. Bækvad-Hansen, F. Cerrato, K. Chambert, J. H. Christensen, C. Churchhouse, K. Dellenvall, D. Demontis, S. De Rubeis, B. Devlin, S. Djurovic, A. L. Dumont, J. I. Goldstein, C. S. Hansen, M. E. Hauberg, M. V. Hollegaard, S. Hope, D. P. Howrigan, H. Huang, C. M. Hultman, L. Klei, J. Maller, J. Martin, A. R. Martin, J. L. Moran, M. Nyegaard, T. Nærland, D. S. Palmer, A. Palotie, C. B. Pedersen, M. G. Pedersen, T. dPoterba, J. B. Poulsen, B. S. Pourcain, P. Qvist, K. Rehnström, A. Reichenberg, J. Reichert, E. B. Robinson, K. Roeder, P. Roussos, E. Saemundsen, S. Sandin, F. K. Satterstrom, G. D. Smith, H. Stefansson, S. Steinberg, C. R. Stevens, P. F. Sullivan, P. Turley, G. B. Walters, X. Xu; Autism Spectrum Disorder Working Group of the Psychiatric Genomics Consortium; BUPGEN; Major Depressive Disorder Working Group of the Psychiatric Genomics Consortium; 23andMe Research Team, K. Stefansson, D. H. Geschwind, M. Nordentoft, D. M. Hougaard, T. Werge, O. Mors, P. B. Mortensen, B. M. Neale, M. J. Daly, A. D. Børglum, Identification of common genetic risk variants for autism spectrum disorder. *Nat. Genet.* **51**, 431–444 (2019).
67. I. E. Jansen, J. E. Savage, K. Watanabe, J. Bryois, D. M. Williams, S. Steinberg, J. Sealock, I. K. Karlsson, S. Hägg, L. Athanasiu, N. Voyle, P. Proitsi, A. Witoelar, S. Stringer, D. Aarsland, I. S. Almdahl, F. Andersen, S. Bergh, F. Bettella, S. Bjornsson, A. Brækhus, G. Bråthen, C. de Leeuw, R. S. Desikan, S. Djurovic, L. Dumitrescu, T. Fladby, T. J. Hohman, P. V. Jonsson, S. J. Kiddle, A. Rongve, I. Saltvedt, S. B. Sando, G. Selbæk, M. Shoai, N. G. Skene, J. Snaedal, E. Stordal, I. D. Ulstein, Y. Wang, L. R. White, J. Hardy, J. Hjerling-Leffler, P. F. Sullivan, W. M. van der Flier, R. Dobson, L. K. Davis, H. Stefansson, K.

- Stefansson, N. L. Pedersen, S. Ripke, O. A. Andreassen, D. Posthuma, Genome-wide meta-analysis identifies new loci and functional pathways influencing Alzheimer's disease risk. *Nat. Genet.* **51**, 404–413 (2019).
68. J. J. Lee, R. Wedow, A. Okbay, E. Kong, O. Maghzian, M. Zacher, T. A. Nguyen-Viet, P. Bowers, J. Sidorenko, R. K. Linnér, M. A. Fontana, T. Kundu, C. Lee, H. Li, R. Li, R. Royer, P. N. Timshel, R. K. Walters, E. A. Willoughby, L. Yengo; 23andMe Research Team; COGENT (Cognitive Genomics Consortium); Social Science Genetic Association Consortium, M. Alver, Y. Bao, D. W. Clark, F. R. Day, N. A. Furlotte, P. K. Joshi, K. E. Kemper, A. Kleinman, C. Langenberg, R. Mägi, J. W. Trampush, S. S. Verma, Y. Wu, M. Lam, J. H. Zhao, Z. Zheng, J. D. Boardman, H. Campbell, J. Freese, K. M. Harris, C. Hayward, P. Herd, M. Kumari, T. Lencz, J. Luan, A. K. Malhotra, A. Metspalu, L. Milani, K. K. Ong, J. R. B. Perry, D. J. Porteous, M. D. Ritchie, M. C. Smart, B. H. Smith, J. Y. Tung, N. J. Wareham, J. F. Wilson, J. P. Beauchamp, D. C. Conley, T. Esko, S. F. Lehrer, P. K. E. Magnusson, S. Oskarsson, T. H. Pers, M. R. Robinson, K. Thom, C. Watson, C. F. Chabris, M. N. Meyer, D. I. Laibson, J. Yang, M. Johannesson, P. D. Koellinger, P. Turley, P. M. Visscher, D. J. Benjamin, D. Cesarini, Gene discovery and polygenic prediction from a genome-wide association study of educational attainment in 1.1 million individuals. *Nat. Genet.* **50**, 1112–1121 (2018).
69. M. A. Nalls, C. Blauwendraat, C. L. Vallerga, K. Heilbron, S. Bandres-Ciga, D. Chang, M. Tan, D. A. Kia, A. J. Noyce, A. Xue, J. Bras, E. Young, R. von Coelln, J. Simón-Sánchez, C. Schulte, M. Sharma, L. Krohn, L. Pihlström, A. Siitonen, H. Iwaki, H. Leonard, F. Faghri, J. R. Gibbs, D. G. Hernandez, S. W. Scholz, J. A. Botia, M. Martinez, J.-C. Corvol, S. Lesage, J. Jankovic, L. M. Shulman, M. Sutherland, P. Tienari, K. Majamaa, M. Toft, O. A. Andreassen, T. Bangale, A. Brice, J. Yang, Z. Gan-Or, T. Gasser, P. Heutink, J. M. Shulman, N. W. Wood, D. A. Hinds, J. A. Hardy, H. R. Morris, J. Gratten, P. M. Visscher, R. R. Graham, A. B. Singleton; 23andMe Research Team; System Genomics of Parkinson's Disease Consortium; International Parkinson's Disease Genomics Consortium, Identification of novel risk loci, causal insights, and heritable risk for Parkinson's disease: A meta-analysis of genome-wide association studies. *Lancet Neurol.* **18**, 1091–1102 (2019).
70. A. Nicolas, K. P. Kenna, A. E. Renton, N. Ticozzi, F. Faghri, R. Chia, J. A. Dominov, B. J. Kenna, M. A. Nalls, P. Keagle, A. M. Rivera, W. van Rheenen, N. A. Murphy, J. J. F. A. van

Vugt, J. T. Geiger, R. A. Van der Spek, H. A. Pliner, Shankaracharya, B. N. Smith, G. Marangi, S. D. Topp, Y. Abramzon, A. S. Gkazi, J. D. Eicher, A. Kenna; ITALSGEN Consortium, G. Mora, A. Calvo, L. Mazzini, N. Riva, J. Mandrioli, C. Caponnetto, S. Battistini, P. Volanti, V. L. Bella, F. L. Conforti, G. Borghero, S. Messina, I. L. Simone, F. Trojsi, F. Salvi, F. O. Logullo, S. D'Alfonso, L. Corrado, M. Capasso, L. Ferrucci; Genomic Translation for ALS Care (GTAC) Consortium, C. de Araujo Martins Moreno, S. Kamalakaran, D. B. Goldstein; ALS Sequencing Consortium, A. D. Gitler, T. Harris, R. M. Myers; NYGC ALS Consortium, H. Phatnani, R. L. Musunuri, U. S. Evani, A. Abhyankar, M. C. Zody; Answer ALS Foundation, J. Kaye, S. Finkbeiner, S. K. Wyman, A. L. Nail, L. Lima, E. Fraenkel, C. N. Svendsen, L. M. Thompson, J. E. Van Eyk, J. D. Berry, T. M. Miller, S. J. Kolb, M. Cudkowicz, E. Baxi; Clinical Research in ALS and Related Disorders for Therapeutic Development (CRATE) Consortium, M. Benatar, J Paul Taylor, E. Rempersaud, G. Wu, J. Wu; SLAGEN Consortium, G. Lauria, F. Verde, I. Fogh, C. Tiloca, G. P. Comi, G. Sorarù, C. Cereda; French ALS Consortium, P. Corcia, H. Laaksovirta, L. Myllykangas, L. Jansson, M. Valori, J. Ealing, H. Hamdalla, S. Rollinson, S. Pickering-Brown, R. W. Orrell, K. C. Sidle, A. Malaspina, J. Hardy, A. B. Singleton, J. O. Johnson, S. Arepalli, P. C. Sapp, D. McKenna-Yasek, M. Polak, S. Asress, S. Al-Sarraj, A. King, C. Troakes, C. Vance, J. de Belleruche, F. Baas, A. L. M. A. Ten Asbroek, J. L. Muñoz-Blanco, D. G. Hernandez, J. Ding, J. R. Gibbs, S. W. Scholz, M. K. Floeter, R. H. Campbell, F. Landi, R. Bowser, S. M. Pulst, J. M. Ravits, Daniel J L Mac Gowan, J. Kirby, E. P. Pioro, R. Pamphlett, J. Broach, G. Gerhard, T. L. Dunkley, C. B. Brady, N. W. Kowall, J. C. Troncoso, I. L. Ber, K. Mouzat, S. Lumbroso, T. D. Heiman-Patterson, F. Kamel, L. Van Den Bosch, R. H. Baloh, T. M. Strom, T. Meitinger, A. Shatunov, K. R. Van Eijk, M. de Carvalho, M. Kooyman, B. Middelkoop, M. Moisse, R. L. Mc Laughlin, M. A. Van Es, M. Weber, K. B. Boylan, M. Van Blitterswijk, R. Rademakers, K. E. Morrison, A. N. Basak, J. S. Mora, V. E. Drory, P. J. Shaw, M. R. Turner, K. Talbot, O. Hardiman, K. L. Williams, J. A. Fifita, G. A. Nicholson, I. P. Blair, G. A. Rouleau, J. Esteban-Pérez, A. García-Redondo, A. Al-Chalabi; Project MinE ALS Sequencing Consortium, E. Rogaeva, L. Zinman, L. W. Ostrow, N. J. Maragakis, J. D. Rothstein, Z. Simmons, J. Cooper-Knock, A. Brice, S. A. Goutman, E. L. Feldman, S. B. Gibson, F. Taroni, A. Ratti, C. Gellera, P. Van Damme, W. Robberecht, P. Fratta, M. Sabatelli, C. Lunetta, A. C. Ludolph, P. M. Andersen, J. H.

Weishaupt, W. Camu, J. Q. Trojanowski, V. M. Van Deerlin, R. H. Brown Jr., L. H. van den Berg, J. H. Veldink, M. B. Harms, J. D. Glass, D. J. Stone, P. Tienari, V. Silani, A. Chiò, C. E. Shaw, B. J. Traynor, J. E. Landers, Genome-wide analyses identify KIF5A as a novel ALS gene. *Neuron* **97**, 1268–1283.e6 (2018).

71. T. Otowa, K. Hek, M. Lee, E. M. Byrne, S. S. Mirza, M. G. Nivard, T. Bigdeli, S. H. Aggen, D. Adkins, A. Wolen, A. Fanous, M. C. Keller, E. Castelao, Z. Kutalik, S. Van der Auwera, G. Homuth, M. Nauck, A. Teumer, Y. Milaneschi, J.-J. Hottenga, N. Direk, A. Hofman, A. Uitterlinden, C. L. Mulder, A. K. Henders, S. E. Medland, S. Gordon, A. C. Heath, P. A. F. Madden, M. L. Pergadia, P. J. van der Most, I. M. Nolte, F. V. A. van Oort, C. A. Hartman, A. J. Oldehinkel, M. Preisig, H. J. Grabe, C. M. Middeldorp, B. W. J. H. Penninx, D. Boomsma, N. G. Martin, G. Montgomery, B. S. Maher, E. J. van den Oord, N. R. Wray, H. Tiemeier, J. M. Hettema, Meta-analysis of genome-wide association studies of anxiety disorders. *Mol. Psychiatry* **21**, 1485 (2016).
72. E. A. Stahl, G. Breen, A. J. Forstner, A. M. Quillin, S. Ripke, V. Trubetskoj, M. Mattheisen, Y. Wang, J. R. I. Coleman, H. A. Gaspar, C. A. de Leeuw, S. Steinberg, J. M. Whitehead Pavlides, M. Trzaskowski, E. M. Byrne, T. H. Pers, P. A. Holmans, A. L. Richards, L. Abbott, E. Agerbo, H. Akil, D. Albani, N. Alliey-Rodriguez, T. D. Als, A. Anjorin, V. Antilla, S. Awasthi, J. A. Badner, M. Bækvad-Hansen, J. D. Barchas, N. Bass, M. Bauer, R. Belliveau, S. E. Bergen, C. B. Pedersen, E. Bøen, M. P. Boks, J. Boocock, M. Budde, W. Bunnay, M. Burmeister, J. Bybjerg-Grauholm, W. Byerley, M. Casas, F. Cerrato, P. Cervantes, K. Chambert, A. W. Charney, D. Chen, C. Churchhouse, T.-K. Clarke, W. Coryell, D. W. Craig, C. Cruceanu, D. Curtis, P. M. Czerski, A. M. Dale, S. de Jong, F. Degenhardt, J. Del-Favero, J. R. De Paulo, S. Djurovic, A. L. Dobbyn, A. Dumont, T. Elvsåshagen, V. Escott-Price, C. C. Fan, S. B. Fischer, M. Flickinger, T. M. Foroud, L. Forty, J. Frank, C. Fraser, N. B. Freimer, L. Frisén, K. Gade, D. Gage, J. Garnham, C. Giambartolomei, M. G. Pedersen, J. Goldstein, S. D. Gordon, K. Gordon-Smith, E. K. Green, M. J. Green, T. A. Greenwood, J. Grove, W. Guan, J. Guzman-Parra, M. L. Hamshere, M. Hautzinger, U. Heilbronner, S. Herms, M. Hipolito, P. Hoffmann, D. Holland, L. Huckins, S. Jamain, J. S. Johnson, A. Juréus, R. Kandaswamy, R. Karlsson, J. L. Kennedy, S. Kittel-Schneider, J. A. Knowles, M. Kogevinas, A. C. Koller, R. Kupka, C. Lavebratt, J. Lawrence, W. B. Lawson, M. Leber, P. H. Lee, S. E. Levy, J. Z. Li, C. Liu, S. Lucae, A. Maaser, D. J.

Mac Intyre, P. B. Mahon, W. Maier, L. Martinsson, S. M. Carroll, P. M. Guffin, M. G. McInnis, J. D. Mc Kay, H. Medeiros, S. E. Medland, F. Meng, L. Milani, G. W. Montgomery, D. W. Morris, T. W. Mühleisen, N. Mullins, H. Nguyen, C. M. Nievergelt, A. N. Adolfsson, E. A. Nwulia, C. O'Donovan, L. M. Olde Loohuis, A. P. S. Ori, L. Oruc, U. Ösby, R. H. Perlis, A. Perry, A. Pfennig, J. B. Potash, S. M. Purcell, E. J. Regeer, A. Reif, C. S. Reinbold, J. P. Rice, F. Rivas, M. Rivera, P. Roussos, D. M. Ruderfer, E. Ryu, C. Sánchez-Mora, A. F. Schatzberg, W. A. Scheftner, N. J. Schork, C. S. Weickert, T. Shekhtman, P. D. Shilling, E. Sigurdsson, C. Slaney, O. B. Smeland, J. L. Sobell, C. S. Hansen, A. T. Spijker, D. S. Clair, M. Steffens, J. S. Strauss, F. Streit, J. Strohmaier, S. Szlinger, R. C. Thompson, T. E. Thorgeirsson, J. Treutlein, H. Vedder, W. Wang, S. J. Watson, T. W. Weickert, S. H. Witt, S. Xi, W. Xu, A. H. Young, P. Zandi, P. Zhang, S. Zöllner; eQTLGen Consortium; BIOS Consortium, R. Adolfsson, I. Agartz, M. Alda, L. Backlund, B. T. Baune, F. Bellivier, W. H. Berrettini, J. M. Biernacka, D. H. R. Blackwood, M. Boehnke, A. D. Børglum, A. Corvin, N. Craddock, M. J. Daly, U. Dannlowski, T. Esko, B. Etain, M. Frye, J. M. Fullerton, E. S. Gershon, M. Gill, F. Goes, M. Grigoriu-Serbanescu, J. Hauser, D. M. Hougaard, C. M. Hultman, I. Jones, L. A. Jones, R. S. Kahn, G. Kirov, M. Landén, M. Leboyer, C. M. Lewis, Q. S. Li, J. Lissowska, N. G. Martin, F. Mayoral, S. L. Mc Elroy, A. M. McIntosh, F. J. McMahon, I. Melle, A. Metspalu, P. B. Mitchell, G. Morken, O. Mors, P. B. Mortensen, B. Müller-Myhsok, R. M. Myers, B. M. Neale, V. Nimgaonkar, M. Nordentoft, M. M. Nöthen, M. C. O'Donovan, K. J. Oedegaard, M. J. Owen, S. A. Paciga, C. Pato, M. T. Pato, D. Posthuma, J. A. Ramos-Quiroga, M. Ribasés, M. Rietschel, G. A. Rouleau, M. Schalling, P. R. Schofield, T. G. Schulze, A. Serretti, J. W. Smoller, H. Stefansson, K. Stefansson, E. Stordal, P. F. Sullivan, G. Turecki, A. E. Vaaler, E. Vieta, J. B. Vincent, T. Werge, J. I. Nurnberger, N. R. Wray, A. D. Florio, H. J. Edenberg, S. Cichon, R. A. Ophoff, L. J. Scott, O. A. Andreassen, J. Kelsoe, P. Sklar; the Bipolar Disorder Working Group of the Psychiatric Genomics Consortium, Genome-wide association study identifies 30 loci associated with bipolar disorder. *Nat. Genet.* **51**, 793–803 (2019).

73. A. Teumer, A. Tin, R. Sorice, M. Gorski, N. C. Yeo, A. Y. Chu, M. Li, Y. Li, V. Mijatovic, Y.-A. Ko, D. Taliun, A. Luciani, M.-H. Chen, Q. Yang, M. C. Foster, M. Olden, L. T. Hiraki, B. O. Tayo, C. Fuchsberger, A. K. Dieffenbach, A. R. Shuldiner, A. V. Smith, A. M. Zappa,

A. Lupo, B. Kollerits, B. Ponte, B. Stengel, B. K. Krämer, B. Paulweber, B. D. Mitchell, C. Hayward, C. Helmer, C. Meisinger, C. Gieger, C. M. Shaffer, C. Müller, C. Langenberg, D. Ackermann, D. Siscovick; DCCT/EDIC, E. Boerwinkle, F. Kronenberg, G. B. Ehret, G. Homuth, G. Waeber, G. Navis, G. Gambaro, G. Malerba, G. Eiriksdottir, G. Li, H. E. Wichmann, H. Grallert, H. Wallaschofski, H. Völzke, H. Brenner, H. Kramer, I. M. Leach, I. Rudan, H. L. Hillege, J. S. Beckmann, J. C. Lambert, J. Luan, J. H. Zhao, J. Chalmers, J. Coresh, J. C. Denny, K. Butterbach, L. J. Launer, L. Ferrucci, L. Kedenko, M. Haun, M. Metzger, M. Woodward, M. J. Hoffman, M. Nauck, M. Waldenberger, M. Pruijm, M. Bochud, M. Rheinberger, N. Verweij, N. J. Wareham, N. Endlich, N. Soranzo, O. Polasek, P. van der Harst, P. P. Pramstaller, P. Vollenweider, P. S. Wild, R. T. Gansevoort, R. Rettig, R. Biffar, R. J. Carroll, R. Katz, R. J. F. Loos, S.-J. Hwang, S. Coassin, S. Bergmann, S. E. Rosas, S. Stracke, T. B. Harris, T. Corre, T. Zeller, T. Illig, T. Aspelund, T. Tanaka, U. Lendeckel, U. Völker, V. Gudnason, V. Chouraki, W. Koenig, Z. Kutalik, J. R. O'Connell, A. Parsa, I. M. Heid, A. D. Paterson, I. H. de Boer, O. Devuyst, J. Lazar, K. Endlich, K. Susztak, J. Tremblay, P. Hamet, H. J. Jacob, C. A. Böger, C. S. Fox, C. Pattaro, A. Köttgen, Genome-wide association studies identify genetic loci associated with albuminuria in diabetes. *Diabetes* **65**, 803–817 (2016).

74. P. van der Harst, N. Verweij, Identification of 64 novel genetic loci provides an expanded view on the genetic architecture of coronary artery disease. *Circ. Res.* **122**, 433–443 (2018).
75. H. J. Watson, Z. Yilmaz, L. M. Thornton, C. Hübel, J. R. I. Coleman, H. A. Gaspar, J. Bryois, A. Hinney, V. M. Leppä, M. Mattheisen, S. E. Medland, S. Ripke, S. Yao, P. Giusti-Rodríguez; Anorexia Nervosa Genetics Initiative, K. B. Hanscombe, K. L. Purves; Eating Disorders Working Group of the Psychiatric Genomics Consortium, R. A. H. Adan, L. Alfredsson, T. Ando, O. A. Andreassen, J. H. Baker, W. H. Berrettini, I. Boehm, C. Boni, V. B. Perica, K. Buehren, R. Burghardt, M. Cassina, S. Cichon, M. Clementi, R. D. Cone, P. Courtet, S. Crow, J. J. Crowley, U. N. Danner, O. S. P. Davis, M. de Zwaan, G. Dedoussis, D. Degortes, J. E. De Socio, D. M. Dick, D. Dikeos, C. Dina, M. Dmitrzak-Weglarz, E. Docampo, L. E. Duncan, K. Egberts, S. Ehrlich, G. Escaramis, T. Esko, X. Estivill, A. Farmer, A. Favaro, F. Fernández-Aranda, M. M. Fichter, K. Fischer, M. Föcker, L. Foretova, A. J. Forstner, M. Forzan, C. S. Franklin, S. Gallinger, I. Giegling, J. Giuranna, F. Gonidakis, P. Gorwood, M. G. Mayora, S. Guillaume, Y. Guo, H. Hakonarson, K. Hatzikotoulas, J.

Hauser, J. Hebebrand, S. G. Helder, S. Herms, B. Herpertz-Dahlmann, W. Herzog, L. M. Huckins, J. I. Hudson, H. Imgart, H. Inoko, V. Janout, S. Jiménez-Murcia, A. Julià, G. Kalsi, D. Kaminská, J. Kaprio, L. Karhunen, A. Karwautz, M. J. H. Kas, J. L. Kennedy, A. Keski-Rahkonen, K. Kiezebrink, Y.-R. Kim, L. Klareskog, K. L. Klump, G. P. S. Knudsen, M. C. La Via, S. L. Hellard, R. D. Levitan, D. Li, L. Lilenfeld, B. D. Lin, J. Lissowska, J. Luykx, P. J. Magistretti, M. Maj, K. Mannik, S. Marsal, C. R. Marshall, M. Mattingsdal, S. M. Devitt, P. M. Guffin, A. Metspalu, I. Meulenbelt, N. Micali, K. Mitchell, A. M. Monteleone, P. Monteleone, M. A. Munn-Chernoff, B. Nacmias, M. Navratilova, I. Ntalla, J. K. O'Toole, R. A. Ophoff, L. Padyukov, A. Palotie, J. Pantel, H. Papezova, D. Pinto, R. Rabionet, A. Raevuori, N. Ramoz, T. Reichborn-Kjennerud, V. Ricca, S. Ripatti, F. Ritschel, M. Roberts, A. Rotondo, D. Rujescu, F. Rybakowski, P. Santonastaso, A. Scherag, S. W. Scherer, U. Schmidt, N. J. Schork, A. Schosser, J. Seitz, L. Slachtova, P. E. Slagboom, M. C. T. Slof-Op 't Landt, A. Slopien, S. Sorbi, B. Świątkowska, J. P. Szatkiewicz, I. Tachmazidou, E. Tenconi, A. Tortorella, F. Tozzi, J. Treasure, A. Tsitsika, M. Tyszkiewicz-Nwafor, K. Tziouvas, A. A. van Elburg, E. F. van Furth, G. Wagner, E. Walton, E. Widen, E. Zeggini, S. Zerwas, S. Zipfel, A. W. Bergen, J. M. Boden, H. Brandt, S. Crawford, K. A. Halmi, L. John Horwood, C. Johnson, A. S. Kaplan, W. H. Kaye, J. E. Mitchell, C. M. Olsen, J. F. Pearson, N. L. Pedersen, M. Strober, T. Werge, D. C. Whiteman, D. B. Woodside, G. D. Stuber, S. Gordon, J. Grove, A. K. Henders, A. Juréus, K. M. Kirk, J. T. Larsen, R. Parker, L. Petersen, J. Jordan, M. Kennedy, G. W. Montgomery, T. D. Wade, A. Birgegård, P. Lichtenstein, C. Norring, M. Landén, N. G. Martin, P. B. Mortensen, P. F. Sullivan, G. Breen, C. M. Bulik, Genome-wide association study identifies eight risk loci and implicates metabo-psychiatric origins for anorexia nervosa. *Nat. Genet.* **51**, 1207–1214 (2019).

76. N. R. Wray, S. Ripke, M. Mattheisen, M. Trzaskowski, E. M. Byrne, A. Abdellaoui, M. J. Adams, E. Agerbo, T. M. Air, T. M. F. Andlauer, S.-A. Bacanu, M. Bækvad-Hansen, A. F. T. Beekman, T. B. Bigdeli, E. B. Binder, D. R. H. Blackwood, J. Bryois, H. N. Buttenschön, J. Bybjerg-Grauholm, N. Cai, E. Castela, J. H. Christensen, T.-K. Clarke, J. I. R. Coleman, L. Colodro-Conde, B. Couvy-Duchesne, N. Craddock, G. E. Crawford, C. A. Crowley, H. S. Dashti, G. Davies, I. J. Deary, F. Degenhardt, E. M. Derks, N. Direk, C. V. Dolan, E. C. Dunn, T. C. Eley, N. Eriksson, V. Escott-Price, F. H. F. Kiadeh, H. K. Finucane, A. J. Forstner, J. Frank, H. A. Gaspar, M. Gill, P. Giusti-Rodríguez, F. S. Goes, S. D. Gordon, J.

Grove, L. S. Hall, E. Hannon, C. S. Hansen, T. F. Hansen, S. Herms, I. B. Hickie, P. Hoffmann, G. Homuth, C. Horn, J.-J. Hottenga, D. M. Hougaard, M. Hu, C. L. Hyde, M. Ising, R. Jansen, F. Jin, E. Jorgenson, J. A. Knowles, I. S. Kohane, J. Kraft, W. W. Kretzschmar, J. Krogh, Z. Kutalik, J. M. Lane, Y. Li, Y. Li, P. A. Lind, X. Liu, L. Lu, D. J. MacIntyre, D. F. MacKinnon, R. M. Maier, W. Maier, J. Marchini, H. Mbarek, P. M. Grath, P. M. Guffin, S. E. Medland, D. Mehta, C. M. Middeldorp, E. Mihailov, Y. Milaneschi, L. Milani, J. Mill, F. M. Mondimore, G. W. Montgomery, S. Mostafavi, N. Mullins, M. Nauck, B. Ng, M. G. Nivard, D. R. Nyholt, P. F. O'Reilly, H. Oskarsson, M. J. Owen, J. N. Painter, C. B. Pedersen, M. G. Pedersen, R. E. Peterson, E. Pettersson, W. J. Peyrot, G. Pistis, D. Posthuma, S. M. Purcell, J. A. Quiroz, P. Qvist, J. P. Rice, B. P. Riley, M. Rivera, S. S. Mirza, R. Saxena, R. Schoevers, E. C. Schulte, L. Shen, J. Shi, S. I. Shyn, E. Sigurdsson, G. B. C. Sinnamon, J. H. Smit, D. J. Smith, H. Stefansson, S. Steinberg, C. A. Stockmeier, F. Streit, J. Strohmaier, K. E. Tansey, H. Teismann, A. Teumer, W. Thompson, P. A. Thomson, T. E. Thorgeirsson, C. Tian, M. Traylor, J. Treutlein, V. Trubetsky, A. G. Uitterlinden, D. Umbricht, S. Van der Auwera, A. M. van Hemert, A. Viktorin, P. M. Visscher, Y. Wang, B. T. Webb, S. M. Weinsheimer, J. Wellmann, G. Willemsen, S. H. Witt, Y. Wu, H. S. Xi, J. Yang, F. Zhang; eQTLGen; 23andMe, V. Arolt, B. T. Baune, K. Berger, D. I. Boomsma, S. Cichon, U. Dannlowski, E. C. J. de Geus, J. R. De Paulo, E. Domenici, K. Domschke, T. Esko, H. J. Grabe, S. P. Hamilton, C. Hayward, A. C. Heath, D. A. Hinds, K. S. Kendler, S. Kloiber, G. Lewis, Q. S. Li, S. Lucae, P. F. A. Madden, P. K. Magnusson, N. G. Martin, A. M. Mc Intosh, A. Metspalu, O. Mors, P. B. Mortensen, B. Müller-Myhsok, M. Nordentoft, M. M. Nöthen, M. C. O'Donovan, S. A. Paciga, N. L. Pedersen, B. W. J. H. Penninx, R. H. Perlis, D. J. Porteous, J. B. Potash, M. Preisig, M. Rietschel, C. Schaefer, T. G. Schulze, J. W. Smoller, K. Stefansson, H. Tiemeier, R. Uher, H. Völzke, M. M. Weissman, T. Werge, A. R. Winslow, C. M. Lewis, D. F. Levinson, G. Breen, A. D. Børglum, P. F. Sullivan; the Major Depressive Disorder Working Group of the Psychiatric Genomics Consortium, Genome-wide association analyses identify 44 risk variants and refine the genetic architecture of major depression. *Nat. Genet.* **50**, 668–681 (2018).

77. A. Xue, Y. Wu, Z. Zhu, F. Zhang, K. E. Kemper, Z. Zheng, L. Yengo, L. R. Lloyd-Jones, J. Sidorenko, Y. Wu; eQTLGen Consortium, A. F. McRae, P. M. Visscher, J. Zeng, J. Yang,

Genome-wide association analyses identify 143 risk variants and putative regulatory mechanisms for type 2 diabetes. *Nat. Commun.* **9**, 2941 (2018).

78. L. Yengo, J. Sidorenko, K. E. Kemper, Z. Zheng, A. R. Wood, M. N. Weedon, T. M. Frayling, J. Hirschhorn, J. Yang, P. M. Visscher; GIANT Consortium, Meta-analysis of genome-wide association studies for height and body mass index in approximately 700000 individuals of European ancestry. *Hum. Mol. Genet.* **27**, 3641–3649 (2018).
79. International League Against Epilepsy Consortium on Complex Epilepsies, Genetic determinants of common epilepsies: A meta-analysis of genome-wide association studies. *Lancet Neurol.* **13**, 893–903 (2014).
80. A. Okbay, B. M. L. Baselmans, J.-E. De Neve, P. Turley, M. G. Nivard, M. A. Fontana, S. F. W. Meddens, R. K. Linnér, C. A. Rietveld, J. Derringer, J. Gratten, J. J. Lee, J. Z. Liu, R. de Vlaming, T. S. Ahluwalia, J. Buchwald, A. Cavadino, A. C. Frazier-Wood, N. A. Furlotte, V. Garfield, M. H. Geisel, J. R. Gonzalez, S. Haitjema, R. Karlsson, Sander W van der Laan, K.-H. Ladwig, J. Lahti, S. J. van der Lee, P. A. Lind, T. Liu, L. Matteson, E. Mihailov, M. B. Miller, C. C. Minica, I. M. Nolte, D. Mook-Kanamori, P. J. van der Most, C. Oldmeadow, Y. Qian, O. Raitakari, R. Rawal, A. Realo, R. Rueedi, B. Schmidt, A. V. Smith, E. Stergiakouli, T. Tanaka, K. Taylor, G. Thorleifsson, J. Wedenoja, J. Wellmann, H.-J. Westra, S. M. Willems, W. Zhao; Life Lines Cohort Study, N. Amin, A. Bakshi, S. Bergmann, G. Bjornsdottir, P. A. Boyle, S. Cherny, S. R. Cox, G. Davies, O. S. P. Davis, J. Ding, N. Direk, P. Eibich, R. T. Emeny, G. Fatemifar, J. D. Faul, L. Ferrucci, A. J. Forstner, C. Gieger, R. Gupta, T. B. Harris, J. M. Harris, E. G. Holliday, J.-J. Hottenga, P. L. De Jager, M. A. Kaakinen, E. Kajantie, V. Karhunen, I. Kolcic, M. Kumari, L. J. Launer, L. Franke, R. Li-Gao, D. C. Liewald, M. Koini, A. Loukola, P. Marques-Vidal, G. W. Montgomery, M. A. Mosing, L. Paternoster, A. Pattie, K. E. Petrovic, L. Pulkki-Råback, L. Quaye, K. Räikkönen, I. Rudan, R. J. Scott, J. A. Smith, A. R. Sutin, M. Trzaskowski, A. E. Vinkhuyzen, L. Yu, D. Zabaneh, J. R. Attia, D. A. Bennett, K. Berger, L. Bertram, D. I. Boomsma, H. Snieder, S.-C. Chang, F. Cucca, I. J. Deary, C. M. van Duijn, J. G. Eriksson, U. Bültmann, E. J. C. de Geus, P. J. F. Groenen, V. Gudnason, T. Hansen, C. A. Hartman, C. M. A. Haworth, C. Hayward, A. C. Heath, D. A. Hinds, E. Hyppönen, W. G. Iacono, M.-R. Jarvelin, K.-H. Jöckel, J. Kaprio, S. L. R. Kardia, L. Keltikangas-Järvinen, P. Kraft, L. D. Kubzansky, T. Lehtimäki, P. K. E. Magnusson, N. G. Martin, M. M. Gue, A. Metspalu, M. Mills, R. de Mutsert, A. J.

Oldehinkel, G. Pasterkamp, N. L. Pedersen, R. Plomin, O. Polasek, C. Power, S. S. Rich, F. R. Rosendaal, H. M. den Ruijter, D. Schlessinger, H. Schmidt, R. Svento, R. Schmidt, B. Z. Alizadeh, T. I. A. Sørensen, T. D. Spector, J. M. Starr, K. Stefansson, A. Steptoe, A. Terracciano, U. Thorsteinsdottir, A. R. Thurik, N. J. Timpson, H. Tiemeier, A. G. Uitterlinden, P. Vollenweider, G. G. Wagner, D. R. Weir, J. Yang, D. C. Conley, G. D. Smith, A. Hofman, M. Johannesson, D. I. Laibson, S. E. Medland, M. N. Meyer, J. K. Pickrell, T. Esko, R. F. Krueger, J. P. Beauchamp, P. D. Koellinger, D. J. Benjamin, M. Bartels, D. Cesarini, Genetic variants associated with subjective well-being, depressive symptoms, and neuroticism identified through genome-wide analyses. *Nat. Genet.* **48**, 624–633 (2016).

81. Schizophrenia Working Group of the Psychiatric Genomics Consortium, Biological insights from 108 schizophrenia-associated genetic loci. *Nature* **511**, 421–427 (2014).

III



Structure of the mouse acidic amino acid decarboxylase GADL1

Arne Raasakka,^{a,†} Elaheh Mahootchi,^{a,b,†} Ingeborg Winge,^{a,b} Weisha Luan,^c
Petri Kursula^{a,c,*} and Jan Haavik^{a,b,d,*}

Received 9 October 2017
Accepted 13 December 2017

Edited by I. Tanaka, Hokkaido University, Japan

† These authors made equal contributions.

Keywords: decarboxylases; pyridoxal phosphate; catalysis; conformational change.

PDB reference: mouse GADL1, 6enz

Supporting information: this article has supporting information at journals.iucr.org/f

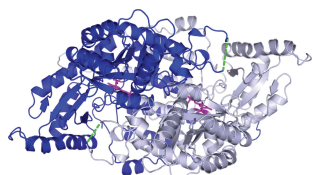
^aDepartment of Biomedicine, University of Bergen, Jonas Lies Vei 91, 5009 Bergen, Norway, ^bK. G. Jebsen Centre for Research on Neuropsychiatric Disorders, University of Bergen, Jonas Lies Vei 91, 5009 Bergen, Norway, ^cFaculty of Biochemistry and Molecular Medicine, University of Oulu, PO Box 5400, 90014 Oulu, Finland, and ^dDivision of Psychiatry, Haukeland University Hospital, Bergen, Norway. *Correspondence e-mail: petri.kursula@uib.no, jan.haavik@uib.no

Pyridoxal 5'-phosphate (PLP) is a ubiquitous cofactor in various enzyme classes, including PLP-dependent decarboxylases. A recently discovered member of this class is glutamic acid decarboxylase-like protein 1 (GADL1), which lacks the activity to decarboxylate glutamate to γ -aminobutyrate, despite its homology to glutamic acid decarboxylase. Among the acidic amino acid decarboxylases, GADL1 is most similar to cysteine sulfinic acid decarboxylase (CSAD), but the physiological function of GADL1 is unclear, although its expression pattern and activity suggest a role in neurotransmitter and neuroprotectant metabolism. The crystal structure of mouse GADL1 is described, together with a solution model based on small-angle X-ray scattering data. While the overall fold and the conformation of the bound PLP are similar to those in other PLP-dependent decarboxylases, GADL1 adopts a more loose conformation in solution, which might have functional relevance in ligand binding and catalysis. The structural data raise new questions about the compactness, flexibility and conformational dynamics of PLP-dependent decarboxylases, including GADL1.

1. Introduction

Pyridoxal 5'-phosphate (PLP), or vitamin B₆, is a versatile cofactor that is involved in many enzymatic reactions spanning multiple enzyme classes and chemical reactions (Percudani & Peracchi, 2003). PLP-dependent decarboxylases constitute a large family of enzymes that catalyze a range of metabolic reactions. Many of these enzymes catalyze biologically well defined processes; inactivating mutations affecting them are associated with severe phenotypes, and some of them are treatment targets in human disease (Baekkeskov *et al.*, 1990; Eliot & Kirsch, 2004; El-Sayed & Shindia, 2011; Paiardini *et al.*, 2014; Sköldbberg *et al.*, 2004).

Despite extensive research, the biological functions of many PLP-dependent enzymes are still unclear. One such enzyme is glutamic acid decarboxylase-like protein 1 (GADL1), which was originally named based on its sequence homology to glutamic acid decarboxylase (GAD), which synthesizes the inhibitory neurotransmitter γ -aminobutyric acid (GABA; Fenalti *et al.*, 2007). However, GADL1 has no reactivity towards glutamic acid and therefore is unlikely to be involved in GABA signalling (Liu *et al.*, 2012; Winge *et al.*, 2015). It has been suggested that GADL1 is involved in taurine production (Liu *et al.*, 2012). On the other hand, in our recent comparative study of GADL1 and cysteine sulfinic acid decarboxylase (CSAD), an enzyme homologous to GADL1 that is involved in taurine biosynthesis, we showed that these enzymes act



OPEN ACCESS

Table 1
Crystallization.

Crystal form	1	2
Method	Sitting-drop vapour diffusion	Sitting-drop vapour diffusion
Plate type	Swissci 3-drop 96-well plate	Swissci 3-drop 96-well plate
Temperature (K)	293	281
Protein concentration (mg ml ⁻¹)	7.5	7
Buffer composition of protein solution	20 mM HEPES pH 7.4, 200 mM NaCl	20 mM HEPES pH 7.4, 200 mM NaCl
Composition of reservoir solution	80 mM sodium cacodylate pH 6.0, 14% PEG 8000, 160 mM calcium acetate, 15% glycerol	80 mM sodium cacodylate pH 7.0, 13% PEG 8000, 160 mM calcium acetate, 15% glycerol
Volume and ratio (protein:well solution) of drop	0.3 µl (1:1)	1.5 µl (1:2)
Volume of reservoir (µl)	40	40
Cryoprotection solution	75%(v/v) reservoir + 25%(v/v) PEG 200	80%(v/v) reservoir + 20%(v/v) glycerol

differently. Compared with CSAD, the activity of GADL1 towards cysteine sulfinic acid (CSA) as a substrate is much lower, and GADL1 has a stronger preference for aspartate, suggesting that GADL1 may be involved in the biosynthesis of β-alanine and its peptide derivatives, such as the neuro-protectant carnosine (Min *et al.*, 2008; Park *et al.*, 2014; Winge *et al.*, 2015).

We showed in our earlier study that mouse and human brain have distinct patterns of expression of CSAD and GADL1 (Winge *et al.*, 2015). Whereas both CSAD and GADL1 were expressed in neurons, only the CSAD mRNA was detected in astrocytes. Using a homology model of GADL1 based on the crystal structure of human CSAD (*HsCSAD*), we performed *in silico* screening of potential substrate analogues and discovered the first generation of inhibitors with partial selectivity against either GADL1 or CSAD. However, detailed mechanistic studies have been hampered by the lack of structural information.

In this study, we describe the crystal structure of mouse GADL1 (*MmGADL1*). Additionally, we used small-angle X-ray scattering (SAXS) to elucidate the solution shape of *MmGADL1*. The overall fold of *MmGADL1* is similar to those of CSAD and other close homologues, with a flexible loop, not defined in electron density, from the apposing monomer covering the active site, which is possibly relevant in catalysis. SAXS data demonstrate that *MmGADL1* adopts a loosened state in solution, which might correspond to an open conformation significant for cofactor or substrate binding.

2. Materials and methods

2.1. Macromolecule production

2.1.1. Construct preparation, protein expression and purification. The expression vector for *MmGADL1* was prepared in the Gateway system using pTH27 (Hammarström *et al.*, 2006) as the destination vector. Cloning involved a two-step PCR protocol and homologous recombination into Gateway vectors using standard procedures. The resulting construct codes for an N-terminal His₆ tag, a *Tobacco etch virus* (TEV) protease cleavage site and *MmGADL1* residues 1–502 (UniProt entry E9QP13). A longer isoform of *MmGADL1* also exists (UniProtKB entry Q80WP8), and the construct corresponds to residues 49–550 of this isoform.

2.1.2. Expression and purification of *MmGADL1*. His₆-tagged *MmGADL1* was expressed in *Escherichia coli* BL21-CodonPlus(DE3)-RIPL cells (Stratagene) at 288 K using 150 mM IPTG induction. Cell pellets were lysed by sonication in a buffer consisting of 50 mM sodium phosphate buffer pH 7.4, 500 mM NaCl, 20 mM imidazole, 0.2 mg ml⁻¹ lysozyme, 1 mM MgCl₂, 2 mM pyridoxine hydrochloride and cOmplete EDTA-free protease inhibitors (Roche). Phenylmethylsulfonyl fluoride was added to 1 mM immediately following sonication. The unclarified lysate was applied directly onto an IMAC HiTrap TALON crude column (GE Healthcare). The column was washed with 50 mM sodium phosphate pH 7.4, 500 mM NaCl, 50 mM sodium phosphate pH 7.4, 500 mM NaCl, 20 mM imidazole. Elution was carried out with 100 mM imidazole in 50 mM sodium phosphate pH 7.4, 500 mM NaCl. Size-exclusion chromatography was performed using a Superdex HR 200 column (GE Healthcare) equilibrated with 20 mM HEPES, 200 mM NaCl pH 7.5.

2.2. Crystallization

Initial crystallization conditions for *MmGADL1* were obtained from the JCSG-*plus* screen (Molecular Dimensions) using sitting-drop vapour diffusion. The crystallization conditions, which yielded crystals with a needle morphology arranged as single crystals or point-originated clusters, were comprised of 80 mM sodium cacodylate pH 6.0–7.4, 13–14%(w/v) PEG 8000, 120–160 mM calcium acetate, 15.0–17.5%(w/v) glycerol. 0.3–1.5 µl drops with different volume ratios of protein solution (6.5–7.5 mg ml⁻¹ in 20 mM HEPES pH 7.4, 200 mM NaCl) and reservoir solution were used at 281 and 293 K, equilibrating against 40 µl reservoir solution. Crystals were briefly soaked in cryoprotectant solutions and flash-cooled in liquid N₂. The detailed conditions used to obtain the crystals used for data collection are given in Table 1.

2.3. Data collection, structure solution and refinement

The *MmGADL1* structure was solved from the two crystal forms by molecular replacement in *Phaser* (McCoy *et al.*, 2007) using the structure of *HsCSAD* (PDB entry 2jis; Structural Genomics Consortium, unpublished work) as the search model. Crystal form 1 diffracted to 3 Å resolution, while crystal form 2, which was used for initial structure solution, diffracted to 2.4 Å resolution; the latter suffered from near-

Table 2
Data collection, processing and structure refinement.

Values in parentheses are for the highest resolution shell.

Crystal form	1	2
Data-collection statistics		
Wavelength (Å)	1.0332	0.9763
Space group	C2	P2 ₁
<i>a</i> , <i>b</i> , <i>c</i> (Å)	137.4, 80.6, 128.5	80.9, 121.7, 101.1
α , β , γ (°)	90, 117.9, 90	90, 90.08, 90
Resolution range (Å)	50–3.00 (3.08–3.00)	50–2.40 (2.46–2.40)
Completeness (%)	99.4 (99.5)	98.7 (95.9)
Multiplicity	6.4 (6.0)	3.6 (3.1)
$\langle I/\sigma(I) \rangle^\dagger$	7.1 (0.7)	5.9 (0.9)
R_{meas}	0.328 (3.535)	0.188 (1.466)
$R_{\text{p.i.m.}}$	0.130 (1.443)	0.099 (0.832)
CC _{1/2} (%)	98.9 (28.4)	99.3 (61.4)
Overall <i>B</i> factor from Wilson plot (Å ²)	67	44
Refinement statistics		
Resolution range (Å)	50–3.0	—
Final R_{cryst}	0.236	—
Final R_{free}	0.288	—
R.m.s.d.s		
Bond lengths (Å)	0.003	—
Bond angles (°)	0.7	—
Average <i>B</i> factor (Å ²)	91.0	—
Ramachandran plot		
Favoured (%)	92.0	—
Outliers (%)	0.6	—
<i>MolProbity</i> score [percentile]	1.98 [99th]	—
Twin operator/twin fraction (%)	—	<i>h</i> , $-k$, $-l/45$
Pseudotranslation operator/fraction (%)	—	0.060, -0.500 , $0.417/38$

[†] The mean $\langle I/\sigma(I) \rangle$ in the outermost shell falls below 2.0 at 3.3 Å for crystal form 1 and 2.7 Å for crystal form 2.

perfect pseudomeroherdral twinning and high translational pseudosymmetry. Owing to these observations, both crystal forms were solved and initially refined, and the lower resolution structure, which completely lacked twinning and pseudotranslation, was considered to be better for final refinement. In essence, despite the higher nominal resolution, the twinned crystal suffering from pseudotranslation gave lower-quality electron-density maps. The twinning and pseudotranslation operations are given in Table 2. NCS restraints were employed throughout refinement. Refinement was performed with *phenix.refine* (Afonine *et al.*, 2012) and model building with *Coot* (Emsley & Cowtan, 2004). The structure was validated with *MolProbity* (Chen *et al.*, 2010). Data collection and refinement statistics can be found in Table 2. The resolution limits used were based on recent studies (Karplus & Diederichs, 2015) showing that useful information is available for refinement even for data with a CC_{1/2} much lower than 50%.

2.4. Small-angle X-ray scattering

Synchrotron SAXS data were collected on the EMBL/DESY BioSAXS beamline P12 (Blanchet *et al.*, 2015). The protein was at 1.6–6.5 mg ml⁻¹ in 20 mM HEPES pH 7.4, 200 mM NaCl. The scattering data were processed and analyzed with programs from the *ATSAS* package (Konarev *et al.*, 2006). The molecular weight was determined by comparison of the forward scattering intensity, $I(0)$, with a fresh

monomeric bovine serum albumin standard. Models of *MmGADL1* were built with *GASBOR* (Svergun *et al.*, 2001) and *SREFLEX* (Panjkovich & Svergun, 2016), using data extrapolated to zero concentration. Theoretical scattering curves from crystal structure coordinates were calculated with *CRY SOL* (Svergun *et al.*, 1995). Model superposition was performed using *SUPCOMB* (Kozin & Svergun, 2001). Details of SAXS data collection, processing and analysis are given in Table 3, and the raw SAXS scattering data are provided as Supporting Information.

2.5. Sequence and structure analysis

APBS (Unni *et al.*, 2011), *UCSF Chimera* (Pettersen *et al.*, 2004), *PyMOL* (<http://www.pymol.org>), *ProtParam* (Gasteiger *et al.*, 2005), *PDBeFold* (Krisinel & Henrick, 2004), *MUSCLE* (Edgar, 2004) and *ESPrpt3.0* (Robert & Gouet, 2014) were used for bioinformatics and structure analyses.

3. Results and discussion

3.1. The crystal structure of *MmGADL1*

Initial screening for crystallization conditions of *MmGADL1* resulted in a single condition that produced diffracting crystals. Crystals formed with a needle morphology, often growing in bunches or clusters and generally being very thin, with maximum lengths reaching 500 µm. The diffraction quality was initially poor, with diffraction limits of around 6–7 Å and highly smeared reflections. By optimizing the size, the amount of nucleation, and the general appearance of the crystals, the conditions given in Table 1 produced thin but nonfragile crystals that allowed structure refinement in two crystal forms to resolutions of 2.4 and 3.0 Å; the higher resolution data set was plagued by significant twinning and pseudotranslation (Table 2). Thus, the structure of the nontwinned crystal form is discussed here; essentially all features can also be seen in the twinned crystal.

The crystal structure revealed a single *MmGADL1* homodimer in the asymmetric unit, which was the expected oligomeric state based on other PLP-dependent decarboxylases (Fig. 1*a*). For both chains, residues 11–502 could be built, with the flexible loop common to PLP-dependent decarboxylases (Fenalti *et al.*, 2007) being absent from the electron density (approximately residues 340–350). The overall conformation of the two chains was nearly identical (Fig. 1*b*).

In the crystal lattice, the protein dimers form layers in the *xy* plane, separated by a rather uniform spacing (Fig. 1*c*). As the first ~30 amino acids of the tagged protein were not visible, they are most likely to occupy the space between protein dimers in the crystal. This is the likely source of the high mosaicity and incomplete lattice arrangement in the current *MmGADL1* crystals.

Both active sites in the dimer are occupied by the PLP cofactor, which is covalently bound to the N^ε atom of Lys314 in each chain through a Schiff base linkage, being located at the dimer interface (Fig. 1*d*). Closer observation of the active-site cavity reveals that only the active imine of the linked PLP

Table 3
Small-angle X-ray scattering.

Data-collection parameters	
Protein	<i>MmGADL1</i> , His-tagged
Instrument	P12, PETRA III, EMBL/DESY with Dectris PILATUS 2M detector (Blanchet <i>et al.</i> , 2015)
Wavelength (nm)	0.124
Beam size (μm)	200×120
Detector distance (m)	3.1
Angular range (nm^{-1})	0.018–4.607
Exposure time per frame (s)	0.045
No. of frames per sample	20
Monitoring for radiation damage	Data frame-by-frame comparison
Scaling method	Buffer-subtracted data normalized to 1 mg ml^{-1}
Normalization	To transmitted intensity by beamstop counter (Blanchet <i>et al.</i> , 2015)
Concentration range (mg ml^{-1})	1.6, 3.3, 6.5
Temperature (K)	293
Structural parameters	
R_g from crystal structure (nm)	2.95
D_{max} from crystal structure (nm)	10.67
Guinier analysis	
$I(0)$ from Guinier (relative)	2519
R_g from Guinier (nm)	3.62
s_{min} (nm^{-1})	0.143
sR_g range	0.52–1.30
Fidelity	0.92
$p(r)$ analysis	
$I(0)$ from $p(r)$ (relative)	2557
R_g from $p(r)$ (nm)	3.80
D_{max} (nm)	13.67
s range (nm^{-1})	0.143–1.98
Quality of fit (total estimate from <i>GNOM</i>)	0.83
Porod volume (nm^3) (ratio to calculated molecular mass in kDa)	196 (1.6)
Molecular-mass determination	
Molecular mass from $I(0)$ using $p(r)$ (kDa) (ratio to theoretical monomer)	121.0 (2.0)
Molecular mass from $I(0)$ using Guinier (kDa) (ratio to theoretical monomer)	120.6 (2.0)
Theoretical monomeric molecular mass from sequence (kDa)	60.4
Shape and atomistic modelling	
<i>CRY SOL</i> (comparison to crystal structure)	
χ^2 value versus crystal structure	41.9
s range (nm^{-1})	0.018–4.607
<i>GASBOR</i> (<i>ab initio</i> chain-like modelling)	
χ^2 value	1.7
s range (nm^{-1})	0.143–4.607
Symmetry	<i>P2</i>
<i>SREFLEX</i> (modelling of flexibility based on crystal structure)	
χ^2 value	5.7
s range (nm^{-1})	0.018–4.607
Software	
Data processing and basic analyses	
	<i>SASFLOW</i> (Franke <i>et al.</i> , 2012; Blanchet <i>et al.</i> , 2015) and <i>PRIMUSqt</i> (Petoukhov <i>et al.</i> , 2012)
Distance distribution analysis	<i>GNOM</i> (Svergun, 1992) through <i>PRIMUSqt</i> (Petoukhov <i>et al.</i> , 2012)
<i>Ab initio</i> analysis	<i>GASBOR</i> (Svergun <i>et al.</i> , 2001) via <i>ATSAS</i> online (https://www.embl-hamburg.de/biosaxs/atsas-online/)
Conformational analysis	<i>SREFLEX</i> (Panjkovich & Svergun, 2016) via <i>ATSAS</i> online (https://www.embl-hamburg.de/biosaxs/atsas-online/)
Comparison to crystal structure	<i>CRY SOL</i> (Svergun <i>et al.</i> , 1995)
Graphics representation	<i>PyMOL</i> (http://www.pymol.org)
Extinction coefficient estimate	<i>ProtParam</i> (Gasteiger <i>et al.</i> , 2005)

is solvent-exposed, and it resides at the end of a narrow cavity, which represents the substrate-binding pocket (Fig. 2*a*). Electrostatic surface analysis reveals the GADL1 active site to have a high positive charge potential (Fig. 2*b*). This is logical, as the substrates of GADL1 are acidic amino acids; the basic nature of the binding cavity is involved in electrostatic interactions that attract and bind the substrate, orienting it correctly for catalysis.

In our earlier work, we showed that GADL1 can use aspartate and CSA as substrates, but not glutamate (Winge *et*

al., 2015). While the catalytic cavities of GAD and GADL1 are very similar, it is currently difficult to pinpoint which features of the active site might be responsible for selectivity between such similar substrates. High-resolution structures of GADL1 and its closest homologues with bound active-site ligands will clearly be required. Importantly, a large part of the active-site cavity wall will be formed by the flexible loop in the substrate-bound state; the flexible loop is invisible in most PLP-dependent decarboxylase crystal structures, but harbours a Tyr residue that is likely to be important for catalysis.

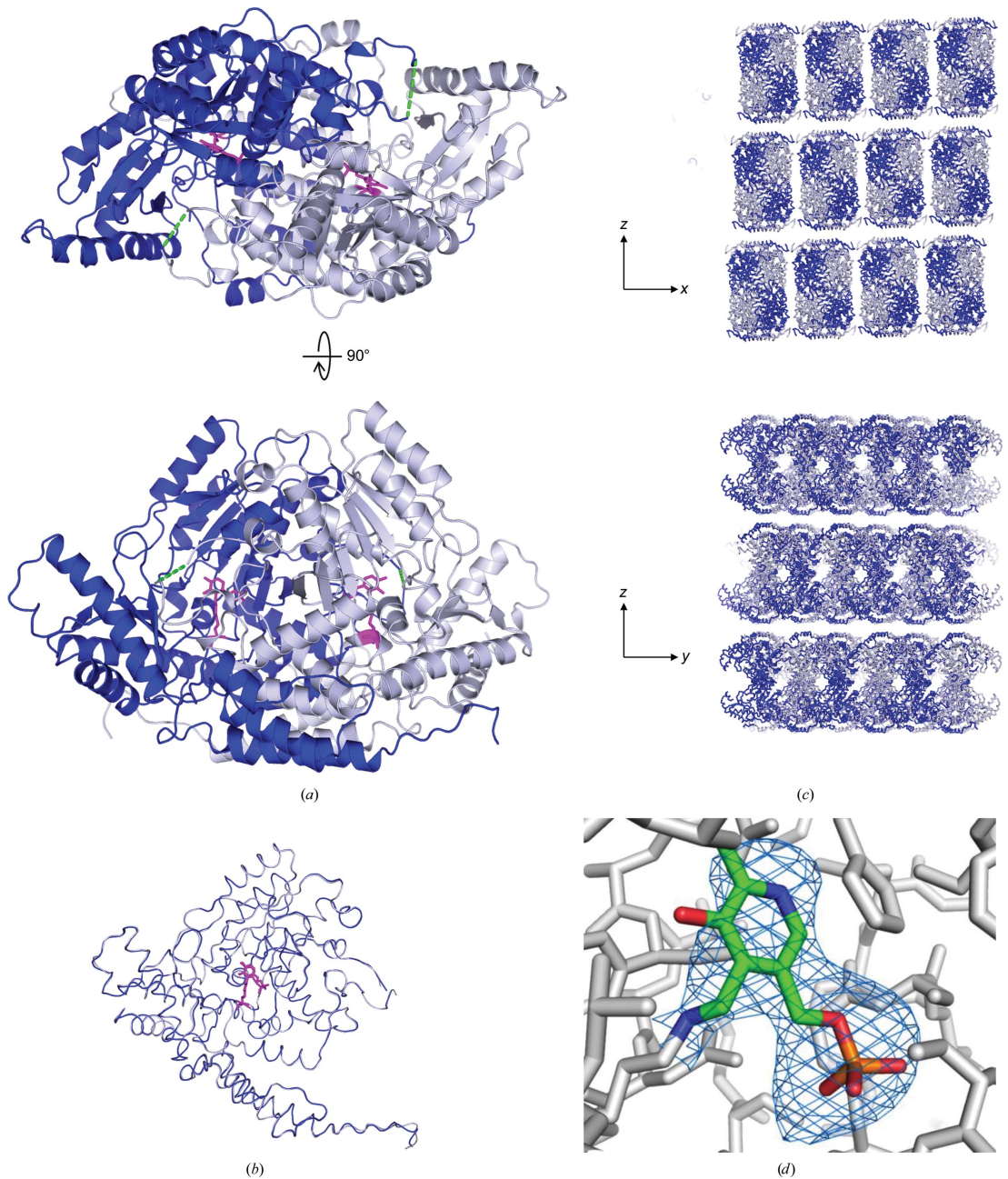


Figure 1
 Overall structure of *MmGADL1*. (a) The *MmGADL1* dimer. The PLP molecule covalently bound to Lys314 is shown in magenta. The green dashed line indicates the position of the flexible loop covering the active site. (b) Superposition of the two *MmGADL1* monomers in the homodimer. The covalently bound PLP is shown in magenta. The two monomers are essentially identical. (c) Crystal lattice arrangement of *MmGADL1* in two different planes. Note the uniform 11 Å cavities in the xy plane between protein layers. (d) Omit $F_o - F_c$ difference map (blue mesh) contoured at 2σ for the covalently bound PLP cofactor on Lys314.

3.2. *MmGADL1* adopts an open conformation in solution

We used SAXS to validate the crystal structure and to determine the conformation of *MmGADL1* in solution (Fig. 3, Table 3). As is apparent from the scattering data and the dimensionless Kratky plot, GADL1 presents a folded shape. While the molecular mass calculated from the forward scattering intensity accurately matches that of a dimer, the theoretical scattering curve calculated from the crystal structure differs significantly. The shape in solution is more elongated than in the crystal. The radii of gyration between the theoretical scattering curve from the crystal structure and the experimental value from Guinier analysis differ by nearly 1 nm, indicating a large difference in conformation. The maximum diameter is 3 nm larger in solution than in the crystal state.

The *GASBOR* chain-like dummy residue model of *MmGADL1* is elongated compared with the crystal structure (Fig. 3e). Attempts to model the missing N-terminal portion, while keeping the dimeric crystal structure fixed, did not fit the experimental SAXS data well (data not shown). We thus employed the recently described *SREFLEX* method (Panjkovich & Svergun, 2016) to take advantage of normal-

mode analysis of the crystal structure in SAXS modelling. The *SREFLEX* model fits the scattering data well and suggests a clearly loosened solution conformation (Fig. 3f), in contrast to the compact globular structures observed for PLP-dependent decarboxylases in the crystalline state. The open conformation is not similar to the open conformation observed for DOPA decarboxylase in the crystalline state (Giardina *et al.*, 2011; Fig. 3g), in which case the opening occurs in the centre of the dimer. The observed open–close movement is likely to be of functional relevance in the GADL1 catalytic cycle. Whether the different conformations are linked to the binding of ligands remains to be studied. While our GADL1 preparation is enzymatically active (Winge *et al.*, 2015), and the crystal is apparently fully occupied with covalently bound PLP, we cannot currently rule out the presence of PLP-deficient GADL1 in the purified SAXS sample, since crystallization might have enriched a cofactor-bound conformation of the protein.

3.3. Comparison to other PLP-dependent decarboxylases

While *MmGADL1* and its homologues show low sequence conservation, apart from a few fully conserved core elements

Table 4
Structural homologues of *MmGADL1*.

The homologues were detected by an *SSM* analysis using *PDBeFold*.

Protein	Organism	PDB entry	Reference	Chain	<i>Q</i> -score	R.m.s.d. (Å)	Sequence identity (%)	UniProtKB entry	Aligned residues
<i>MmGADL1</i>	<i>Mus musculus</i>	6enz	This study	A	—	—	—	E9QP13	1–502
<i>HsCSAD</i>	<i>Homo sapiens</i>	2jis	Unpublished work	B	0.586	0.85	62.0	Q9Y600	1–493
<i>HsGAD65</i>	<i>Homo sapiens</i>	2okk	Fenalti <i>et al.</i> (2007)	A	0.565	1.06	49.4	Q05329	88–584
<i>HsGAD67</i>	<i>Homo sapiens</i>	2okj	Fenalti <i>et al.</i> (2007)	B	0.532	1.15	50.9	Q9925	93–594
<i>SiPDD</i>	<i>Sphaerobacter thermophilus</i>	4rit	Unpublished work	B	0.461	1.96	28.9	D1C7D8	1–483
<i>RUMGNA_01526</i>	<i>Ruminococcus gnavus</i>	4obu	Williams <i>et al.</i> (2014)	H	0.492	1.79	25.6	A7B1V0	1–490
<i>VpGAD</i>	<i>Vibrio parahaemolyticus</i>	2qma	Unpublished work	B	0.442	2.16	25.8	Q87NC6	464–957
<i>HsHDC</i>	<i>Homo sapiens</i>	4e1o	Komori <i>et al.</i> (2012)	C	0.425	2.13	26.1	P19113	2–477
<i>HsDDC</i>	<i>Homo sapiens</i>	3rbl	Giardina <i>et al.</i> (2011)	A	0.397	2.61	23.3	P20711	1–480

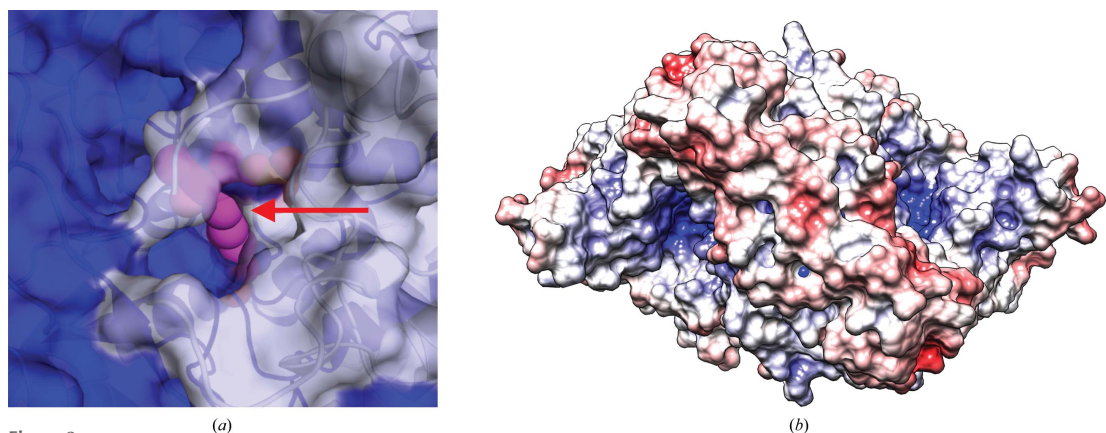


Figure 2
The *MmGADL1* active site. (a) Close-up view of the active-site cavity with the reactive moiety of PLP (magenta) visible (red arrow). Note how the cofactor lies at the interface between two protein monomers (blue and grey). (b) Surface electrostatics of *MmGADL1*. The positively charged cavity corresponds to the active site (blue).

around the active site (Fig. 4*a*), comparison of the structures of *Mm*GADL1 and its homologues reveals a conserved structural fold with little variance in the arrangement of the PLP-linked Lys residue (Figs. 4*b* and 4*c*, Table 4). The sequence conservation between *Mm*GADL1, *Hs*CSAD and *Hs*GADs (Fenalti *et al.*, 2007) is higher than those with human histidine decarboxylase (HDC; Komori *et al.*, 2012) and DOPA decarboxylase (DDC; Giardina *et al.*, 2011; Winge *et al.*, 2015). The latter present similar levels of sequence homology to GADL1 as the bacterial enzymes *Sphaerobacter thermophilus* PLP-dependent decarboxylase (StPDD), *Vibrio parahaemolyticus* GAD (VpGAD) and the tryptamine-synthesizing enzyme from the gut bacterium *Ruminococcus gnavus* (RUMGNA_01526; Williams *et al.*, 2014). Despite low sequence homology, the *R. gnavus* enzyme displays high structural similarity to GADL1, suggesting conservation of the fold of PLP-

dependent decarboxylases involved in neurotransmitter synthesis. It is interesting to note that the absence of PLP in the active site neither alters the overall tightness of the superposed proteins nor changes the position of the conserved Lys in most structures. In the future, experimental solution-state methods, such as SAXS, may help to distinguish functionally relevant conformational states from possible crystallographic artifacts. These observations conflict with earlier results described for *Hs*DDC in the beginning of its PLP accumulation-dependent conformational landscape, where a more open conformation was evident in the crystalline state with the active-site Lys residue oriented away from the PLP-binding pocket (Giardina *et al.*, 2011).

The substrate specificity and physiological function of GADL1 remain enigmatic. However, the conserved structural details and distinct expression patterns of GADL1 suggest

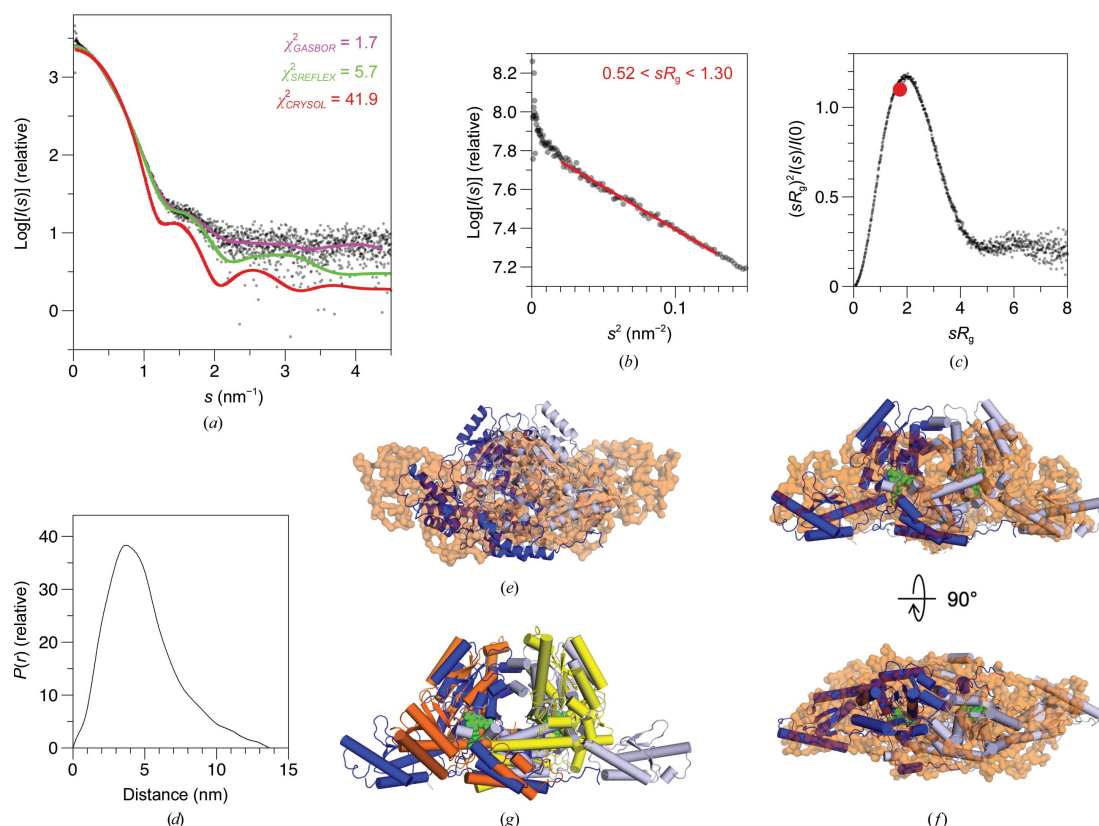


Figure 3

Structure of *Mm*GADL1 in solution determined by SAXS. (a) Raw SAXS data (dots) overlaid with *GASBOR* (pink) and *SREFLEX* (green) model fits, as well as the theoretical scattering curve calculated from the crystal structure using *CRY SOL* (red). (b) Guinier plot. (c) The dimensionless Kratky plot indicates that *Mm*GADL1 is folded, with limited flexibility. The red dot indicates the theoretical position of the peak in a folded globular protein. (d) Distance distribution of *Mm*GADL1. (e) The *GASBOR* model (orange) superimposed with the crystal structure of *Mm*GADL1 indicates a much more elongated conformation in solution. (f) Superposition of the *SREFLEX* (blue/grey) and *GASBOR* (orange) models suggests conformational changes relative to the crystal structure. (g) Comparison of the 'open' conformation of DDC (orange/yellow; Giardina *et al.*, 2011) and the open conformation of *Mm*GADL1 (blue/grey) seen here in solution.

research communications

that it plays a specific physiological role. Variants of GADL1 have been linked to lithium response in bipolar disorder patients (Chen *et al.*, 2014), suggesting a role for GADL1 in lithium pharmacodynamics or kinetics. However, these findings have not been replicated by others, and they have been subject to much controversy (Birnbaum *et al.*, 2014; Cruceanu *et al.*, 2015; Kotambail *et al.*, 2015; Winge *et al.*, 2015; Chen *et al.*, 2016).

Owing to their common mechanistic features, many PLP-dependent enzymes are able to catalyze multiple biochemical reactions, making it difficult to define their primary biological function (Percudani & Peracchi, 2003). Of the known GADL1

substrates, Asp appears as the most characteristic substrate for GADL1 (Winge *et al.*, 2015), although the K_m is relatively high and the catalytic efficiency is low. Nevertheless, the K_m of GADL1 for Asp is in the physiological range, and one could speculate that GADL1 is involved in sensing selected metabolite levels. Relatively low binding affinity is a hallmark of many proteins with signalling roles, which have evolved as sensors of ligand availability; such proteins include, for example, the calcium sensors calmodulin and annexin (Kursula, 2014; Monastyrskaya *et al.*, 2007). Conformational flexibility, as observed here for GADL1 in solution, might have relevance in such a function.

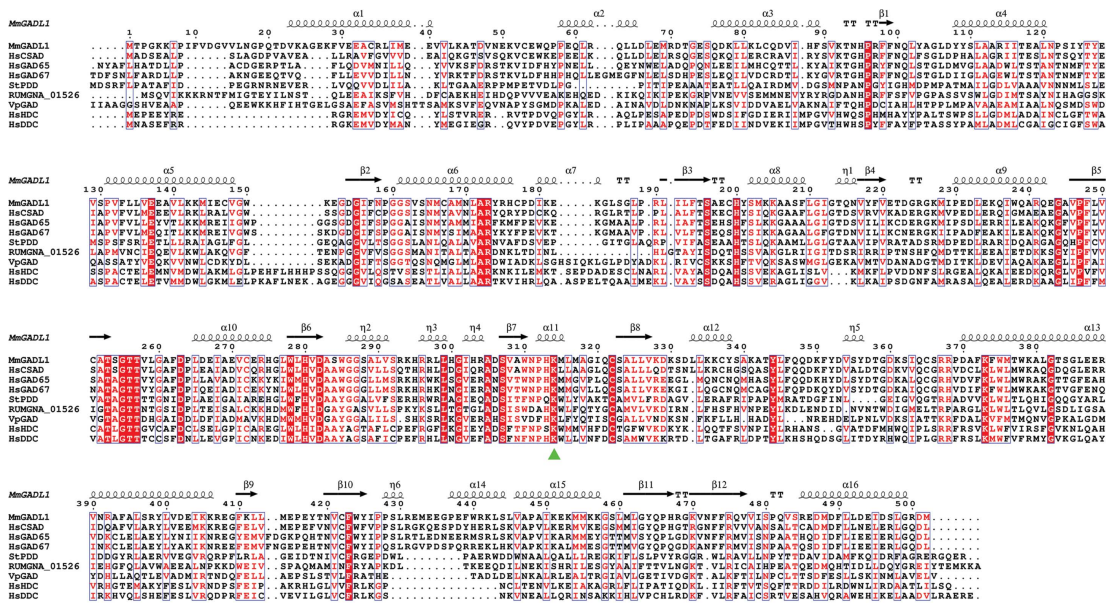


Figure 4
 Comparison of *MmGADL1* with other PLP-dependent decarboxylases. (a) Sequence alignment of *MmGADL1* with homologous structures. The conserved PLP-modified lysine is indicated (green triangle). Secondary structure elements and sequence numbering correspond to *MmGADL1*. (b) Stereo image of a structural superposition of PLP-dependent decarboxylase homologues, viewed towards the active-site cavity. The covalently linked *MmGADL1* PLP moiety is depicted as red spheres. The black arrow shows the position of the active-site-covering loop, which is disordered in the *MmGADL1* crystal structure. (c) Conservation of PLP conformation in the superposed PLP-dependent decarboxylase structures.

4. Concluding remarks

The physiological functions and enzymatic properties of GADL1 are subject to further studies. The structure of *Mm*GADL1 and its flexibility in solution, coupled to structural conservation with other PLP-dependent enzymes, point towards functional relevance of these features within the enzyme family. Important future work will concentrate on high-resolution structural details of substrate and inhibitor binding by GADL1, and on comparing these with those of CSAD, GAD and other PLP-dependent decarboxylases. Crucial topics to address will include the fine details of substrate specificity determinants in PLP-dependent decarboxylases, as well as the relevance of the conformational changes observed here to the catalytic cycle of this family of enzymes.

Acknowledgements

We gratefully acknowledge access to the synchrotron-radiation facilities and the outstanding beamline support at EMBL/DESY, Hamburg, Germany.

Funding information

Funding for this research was provided by: Helse Vest (grant to Jan Haavik); Norges Forskningsråd (grant to Petri Kursula); Sigrid Juséliuksen Säätiö (grant to Petri Kursula); Stiftelsen Kristian Gerhard Jebsen (grant to Jan Haavik); Seventh Framework Programme (grant No. 602805 to Jan Haavik).

References

Afonine, P. V., Grosse-Kunstleve, R. W., Echols, N., Headd, J. J., Moriarty, N. W., Mustyakimov, M., Terwilliger, T. C., Urzhumtsev, A., Zwart, P. H. & Adams, P. D. (2012). *Acta Cryst.* **D68**, 352–367.

Baekkeskov, S., Aanstoot, H.-J., Christgau, S., Reetz, A., Solimena, M., Cascalho, M., Folli, F., Richter-Olesen, H. & Camilli, P.-D. (1990). *Nature (London)*, **347**, 151–156.

Birnbaum, R., Shin, J. H. & Weinberger, D. (2014). *N. Engl. J. Med.* **370**, 1855–1856.

Blanchet, C. E., Spilotros, A., Schwemmer, F., Graewert, M. A., Kikhney, A., Jeffries, C. M., Franke, D., Mark, D., Zengerle, R., Cipriani, F., Fiedler, S., Roessle, M. & Svergun, D. I. (2015). *J. Appl. Cryst.* **48**, 431–443.

Chen, C.-H. *et al.* (2014). *N. Engl. J. Med.* **370**, 119–128.

Chen, C.-K., Lee, C.-S., Chen, H.-Y., Wu, L. S.-H., Chang, J.-C., Liu, C.-Y. & Cheng, A. T.-A. (2016). *BJPsych Open*, **2**, 301–306.

Chen, V. B., Arendall, W. B., Headd, J. J., Keedy, D. A., Immormino, R. M., Kapral, G. J., Murray, L. W., Richardson, J. S. & Richardson, D. C. (2010). *Acta Cryst.* **D66**, 12–21.

Cruceanu, C., Alda, M., Dion, P. A., Turecki, G. & Rouleau, G. A. (2015). *Am. J. Psychiatry*, **172**, 94–95.

Edgar, R. C. (2004). *Nucleic Acids Res.* **32**, 1792–1797.

Eliot, A. & Kirsch, J. (2004). *Annu. Rev. Biochem.* **73**, 383–415.

El-Sayed, A. S. & Shindia, A. A. (2011). *Targets in Gene Therapy*, edited by Y. You, ch. 7. Rijeka: Intech. <https://doi.org/10.5772/17449>.

Emsley, P. & Cowtan, K. (2004). *Acta Cryst.* **D60**, 2126–2132.

Fenalti, G. *et al.* (2007). *Nature Struct. Mol. Biol.* **14**, 280–286.

Franke, D., Kikhney, A. G. & Svergun, D. I. (2012). *Nucl. Instrum. Methods Phys. Res. A*, **689**, 52–59.

Gasteiger, E., Hoogland, C., Gattiker, A., Duvaud, S., Wilkins, M. R., Appel, R. D. & Bairoch, A. (2005). *The Proteomics Protocols Handbook*, edited by J. M. Walker, pp. 571–607. Totowa: Humana Press.

Giardina, G., Montioli, R., Gianni, S., Cellini, B., Paiardini, A., Voltattorni, C. B. & Cutruzzola, F. (2011). *Proc. Natl Acad. Sci. USA*, **108**, 20514–20519.

Hammarström, M., Woestenenk, E., Hellgren, N., Härd, T. & Berglund, H. (2006). *J. Struct. Funct. Genomics*, **7**, 1–14.

Karplus, P. A. & Diederichs, K. (2015). *Curr. Opin. Struct. Biol.* **34**, 60–68.

Komori, H., Nitta, Y., Ueno, H. & Higuchi, Y. (2012). *J. Biol. Chem.* **287**, 29175–29183.

Konarev, P. V., Petoukhov, M. V., Volkov, V. V. & Svergun, D. I. (2006). *J. Appl. Cryst.* **39**, 277–286.

Kotambail, A., Mathur, A., Bhat, S. M., Rai, P. S., Sharma, P. S. & Satyamoorthy, K. (2015). *Psychiatr. Genet.* **25**, 39–40.

Kozin, M. B. & Svergun, D. I. (2001). *J. Appl. Cryst.* **34**, 33–41.

Krissinel, E. & Henrick, K. (2004). *Acta Cryst.* **D60**, 2256–2268.

Kursula, P. (2014). *Amino Acids*, **46**, 2295–2304.

Liu, P., Ge, X., Ding, H., Jiang, H., Christensen, B. M. & Li, J. (2012). *J. Biol. Chem.* **287**, 40898–40906.

McCoy, A. J., Grosse-Kunstleve, R. W., Adams, P. D., Winn, M. D., Storoni, L. C. & Read, R. J. (2007). *J. Appl. Cryst.* **40**, 658–674.

Min, J., Senut, M., Rajanikant, K., Greenberg, E., Bandagi, R., Zemke, D., Mousa, A., Kassab, M., Farooq, M. U., Gupta, R. & Majid, A. (2008). *J. Neurosci. Res.* **86**, 2984–2991.

Monastyrskaya, K., Babiychuk, E. B., Hostettler, A., Rescher, U. & Draeger, A. (2007). *Cell Calcium*, **41**, 207–219.

Paiardini, A., Contestabile, R., Buckle, A. M. & Cellini, B. (2014). *Biomed. Res. Int.* **2014**, 856076.

Panjikovich, A. & Svergun, D. I. (2016). *Phys. Chem. Chem. Phys.* **18**, 5707–5719.

Park, H., Han, K., Shin, J., Park, J., Song, K. & Kim, D. (2014). *J. Korean. Neurosurg. Soc.* **55**, 125–130.

Percudani, R. & Peracchi, A. (2003). *EMBO Rep.* **4**, 850–854.

Petoukhov, M. V., Franke, D., Shkumatov, A. V., Tria, G., Kikhney, A. G., Gajda, M., Gorba, C., Mertens, H. D. T., Konarev, P. V. & Svergun, D. I. (2012). *J. Appl. Cryst.* **45**, 342–350.

Pettersen, E. F., Goddard, T. D., Huang, C. C., Couch, G. S., Greenblatt, D. M., Meng, E. C. & Ferrin, T. E. (2004). *J. Comput. Chem.* **25**, 1605–1612.

Robert, X. & Guet, P. (2014). *Nucleic Acids Res.* **42**, W320–W324.

Sköldbberg, F., Rorsman, F., Perheentupa, J., Landin-Olsson, M., Husebye, E., Gustafsson, J. & Kämpe, O. (2004). *J. Clin. Endocrinol. Metab.* **89**, 1636–1640.

Svergun, D. I. (1992). *J. Appl. Cryst.* **25**, 495–503.

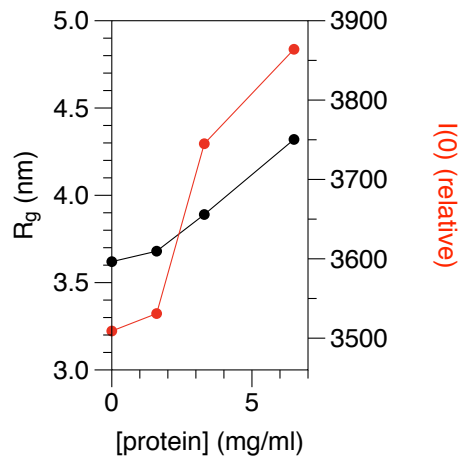
Svergun, D., Barberato, C. & Koch, M. H. J. (1995). *J. Appl. Cryst.* **28**, 768–773.

Svergun, D. I., Petoukhov, M. V. & Koch, M. H. J. (2001). *Biophys. J.* **80**, 2946–2953.

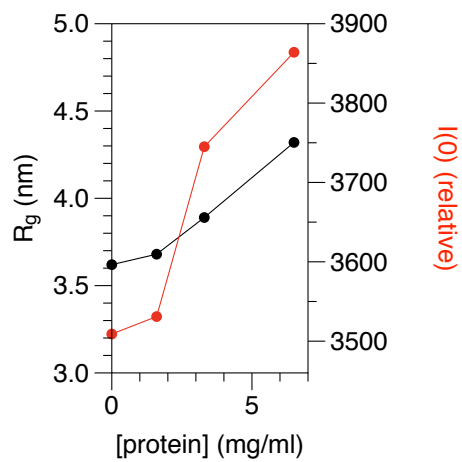
Unni, S., Huang, Y., Hanson, R., Tobias, M., Krishnan, S., Li, W. W., Nielsen, J. E. & Baker, N. A. (2011). *J. Comput. Chem.* **32**, 1488–1491.

Williams, B. B., Van Benschoten, A. H., Cimermancic, P., Donia, M. S., Zimmermann, M., Tacketani, M., Ishihara, A., Kashyap, P. C., Fraser, J. S. & Fischbach, M. A. (2014). *Cell Host Microbe*, **16**, 495–503.

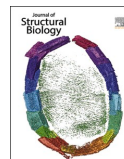
Winge, I., Teigen, K., Fossbakk, A., Mahootchi, E., Kleppe, R., Sköldbberg, F., Kämpe, O. & Haavik, J. (2015). *Neurochem. Int.* **90**, 173–184.



Supplementary Figure 1. R_g and $I(0)$ as a function of protein concentration in the SAXS experiment. The dataset extrapolated to zero concentration and used in all the analyses is included.



Supplementary Figure 1. R_g and $I(0)$ as a function of protein concentration in the SAXS experiment. The dataset extrapolated to zero concentration and used in all the analyses is included.



Structure and substrate specificity determinants of the taurine biosynthetic enzyme cysteine sulphinic acid decarboxylase

Elaheh Mahootchi^{a,1}, Arne Raasakka^{a,1}, Weisha Luan^b, Gopinath Muruganandam^{c,d}, Remy Loris^{c,d}, Jan Haavik^{a,e,*}, Petri Kursula^{a,b,f,*}

^a Department of Biomedicine, University of Bergen, Bergen, Norway

^b Faculty of Biochemistry and Molecular Medicine, University of Oulu, Oulu, Finland

^c VIB-VUB Center for Structural Biology, Vlaams Instituut voor Biotechnologie, Brussels, Belgium

^d Structural Biology Brussels, Department of Bioengineering Sciences, Vrije Universiteit Brussel, Brussels, Belgium

^e Bergen Center of Brain Plasticity, Division of Psychiatry, Haukeland University Hospital, Bergen, Norway

^f Biocenter Oulu, University of Oulu, Oulu, Finland

ARTICLE INFO

Keywords:

Cysteine sulphinic acid
Enzyme structure
Reaction mechanism
Substrate specificity
Pyridoxal phosphate

ABSTRACT

Pyridoxal 5'-phosphate (PLP) is an important cofactor for amino acid decarboxylases with many biological functions, including the synthesis of signalling molecules, such as serotonin, dopamine, histamine, γ -aminobutyric acid, and taurine. Taurine is an abundant amino acid with multiple physiological functions, including osmoregulation, pH regulation, antioxidative protection, and neuromodulation. In mammalian tissues, taurine is mainly produced by decarboxylation of cysteine sulphinic acid to hypotaurine, catalysed by the PLP-dependent cysteine sulphinic acid decarboxylase (CSAD), followed by oxidation of the product to taurine. We determined the crystal structure of mouse CSAD and compared it to other PLP-dependent decarboxylases in order to identify determinants of substrate specificity and catalytic activity. Recognition of the substrate involves distinct side chains forming the substrate-binding cavity. In addition, the backbone conformation of a buried active-site loop appears to be a critical determinant for substrate side chain binding in PLP-dependent decarboxylases. Phe94 was predicted to affect substrate specificity, and its mutation to serine altered both the catalytic properties of CSAD and its stability. Using small-angle X-ray scattering, we further showed that CSAD presents open/close motions in solution. The structure of apo-CSAD indicates that the active site gets more ordered upon internal aldimine formation. Taken together, the results highlight details of substrate recognition in PLP-dependent decarboxylases and provide starting points for structure-based inhibitor design with the aim of affecting the biosynthesis of taurine and other abundant amino acid metabolites.

1. Introduction

Pyridoxal 5-phosphate (PLP), the active form of vitamin B6, is a ubiquitous cofactor essential for a number of enzymes. PLP-dependent enzymes, which mainly use PLP as a covalently bound coenzyme, account for 4% of total cellular enzymatic activity (Percudani and Peracchi, 2003; Thornton et al., 2000). Mammalian genomes encode several PLP-dependent enzymes, which catalyse a variety of biochemical

reactions using different substrates (Percudani and Peracchi, 2003; Liang et al., 2019). Many PLP-dependent enzymes use amino acids as substrates and play central roles in cellular metabolism.

PLP-dependent enzymes are established drug targets in cancer and neurological diseases. Inhibitors of γ -aminobutyric acid (GABA) aminotransferase are of therapeutic interest in central nervous system disorders, being used in the treatment of epilepsy (Sarup et al., 2003), and inhibitors of L-DOPA decarboxylase (DDC) are used in treating

Abbreviations: CA, cysteic acid; CD, circular dichroism; CSA, cysteine sulphinic acid; CSAD, cysteine sulphinic acid decarboxylase; DDC, L-DOPA decarboxylase; DSF, differential scanning fluorimetry; GABA, γ -aminobutyric acid; GAD, Glu decarboxylase; GADL1, GAD-like protein 1; HDC, histidine decarboxylase; MALS, multi-angle static light scattering; PLP, pyridoxal 5'-phosphate; PLP-DC, PLP-dependent decarboxylase; SAXS, small-angle X-ray scattering; SEC, size-exclusion chromatography; WT, wild-type.

* Corresponding authors at: Department of Biomedicine, University of Bergen, Bergen, Norway.

E-mail addresses: jan.haavik@uib.no (J. Haavik), petri.kursula@uib.no (P. Kursula).

¹ Equal contribution.

<https://doi.org/10.1016/j.jsb.2020.107674>

Received 3 October 2020; Received in revised form 13 November 2020; Accepted 21 November 2020

Available online 27 November 2020

1047-8477/© 2020 The Authors. Published by Elsevier Inc. This is an open access article under the CC BY license (<http://creativecommons.org/licenses/by/4.0/>).

Parkinson's disease (Bartholini and Pletscher, 1975; Sletzing et al., 1963). Furthermore, recessive mutations in PLP-dependent enzymes are associated with severe neurological syndromes (Brun et al., 2010; Ercan-Sencicek et al., 2010; Haavik et al., 2008). PLP-dependent enzymes can be autoantigens and targets of the immune system in autoimmune disorders, e.g. Glu decarboxylase 65 (GAD65; GAD2) in type 1 diabetes (Baekkeskov et al., 1990), GAD67 (GAD1) and GAD65 in several neurological disorders (Graus et al., 2020), and cysteine sulphonic acid decarboxylase (CSAD) in autoimmune polyendocrine syndrome 1 (Sköldbberg et al., 2004).

The sulphur-containing amino acid taurine is the most abundant free amino acid in mammals (Lourenco and Camilo, 2002; Samuelsson et al., 2012, 2013). Taurine is implicated in numerous physiological functions and attracts increasing attention as a biomarker for different disease states (Lourenco and Camilo, 2002; Samuelsson et al., 2012, 2013). It has a regulatory role in the maintenance of osmotic pressure and structural integrity of biological membranes (Hoffmann and Pedersen, 2006; Schaffer et al., 2010). In the nervous system, taurine may serve as a growth factor (Hernandez-Benitez et al., 2010; Pasantes-Morales and Hernández-Benítez, 2010) or a neurotransmitter/neuromodulator (Jia et al., 2008; Lähdesmäki et al., 1977). In many species, taurine deficiency can be lethal or associated with severe disease (Hoffmann and Pedersen, 2006), and in humans, altered levels of taurine have been reported in e.g. attention deficit hyperactivity disorder and autism (Hobert et al., 2014). In addition, taurine levels significantly decrease after electroconvulsive treatment in depressed patients, and this decrease strongly correlated with clinical improvements (Samuelsson et al., 2012, 2013). Plasma taurine levels were reduced by 83% in CSAD-deficient mice, and most offspring from 2nd-generation *Csad*^{-/-} mice died shortly after birth, unless given taurine supplementation (Park et al., 2014), indicating a crucial physiological role for CSAD in taurine biosynthesis.

In mammalian tissues, taurine is mainly synthesised from cysteine in a three-step pathway, involving oxidation by cysteine dioxygenase (E.C. 1.13.11.20), decarboxylation of cysteine sulphonic acid (CSA) by CSAD (E.C. 4.1.1.29), and oxidation of hypotaurine to taurine. CSA can additionally be decarboxylated by the related enzyme glutamic acid decarboxylase-like protein 1 (GADL1) (Winge et al., 2015), and taurine can be formed from cysteamine by cysteamine dioxygenase (E.C. 1.13.11.19) (Stipanuk et al., 2009).

Both CSAD and GADL1 are PLP-dependent decarboxylases (PLP-DC). GADL1, being the closest homologue, displays similar activity as CSAD (Winge et al., 2015). GADL1 plays a role in the decarboxylation of Asp to β -alanine and, thus, functions in the biosynthesis of the abundant dipeptides anserine and carnosine (Mahootchi et al., 2020). CSAD and GADL1 have distinct expression patterns in mouse and human brain (Winge et al., 2015). In the brain, CSAD has been detected in neurons and astrocytes in the cerebellum and hippocampus (Reymond et al., 1996; Chan-Palay et al., 1982). GADL1 is expressed in muscle, kidney, olfactory bulb, and isolated neurons (Winge et al., 2015; Liu et al., 2012). CSA is the preferred substrate for both CSAD and GADL1, although both are able to decarboxylate cysteic acid (CA) and Asp (Winge et al., 2015).

In an attempt to understand the molecular mechanisms underlying the catalysis and regulation of GADL1 and CSAD, and to enable future development of optimised inhibitors, we previously solved the crystal structure of mouse GADL1 (Raasakka et al., 2018). Here, we determined the crystal structure of mouse CSAD (*MmCSAD*) in the presence and absence of PLP. Comparisons of the active sites of PLP-DCs highlight substrate recognition determinants within the structurally conserved enzyme family. The structure of CSAD helps to understand the details in the biosynthesis of taurine, one of the most abundant amino acids and dietary supplements.

2. Results and discussion

Taurine, the most abundant free intracellular amino acid in humans, has been implicated in a range of different physiological functions, and it is valuable as an industrial product and dietary supplement. PLP-dependent decarboxylation of CSA was observed in liver extracts from several mammalian species in the 1950s (Sörbo and Heyman, 1957; Chatagner et al., 1958), and since then, the properties of CSAD and related PLP-dependent enzymes have been extensively studied. Our aim was to better understand biosynthesis of taurine and the substrate specificity of PLP-DCs, by way of structural characterisation of CSAD, which catalyses the conversion of CSA into hypotaurine (Fig. 1A).

2.1. The crystal structure of *MmCSAD*

A structure of human CSAD has been available at the PDB (entry 2JIS). However, no detailed information, comparative studies with related enzymes, or mechanistic investigations of CSAD are available. We solved the crystal structure of *MmCSAD*, in order to provide a tool for further studies on CSAD catalysis and facilitate the design of small molecules that could be used to modify taurine-related metabolic pathways.

The crystal structure of *MmCSAD* was solved at 2.1-Å resolution using synchrotron radiation (Table 1, Fig. 1B,C). The active site is fully occupied with PLP covalently attached to Lys305 as an internal aldimine, indicating that the structure corresponds to the catalytically competent form of *MmCSAD*.

The electrostatic potential surface of CSAD (Fig. 1D) shows a high positive charge in the active-site cavity, and it is conceivable that this property is important in attracting negatively charged substrates. CSAD and GADL1 prefer amino acids with short acidic side chains as substrates, i.e. Asp, CA, and CSA, of which CSA is most favoured for both enzymes (Winge et al., 2015). On the other hand, Glu, homocysteic acid, and homocysteine sulphonic acid have been reported not to be substrates of CSAD (Winge et al., 2015; Do and Tappaz, 1996).

MmCSAD presents the conserved fold of PLP-DCs, with the closest structural homologues in the PDB being human CSAD and mouse GADL1 (Table 2). A sequence alignment of selected homologues with known structure is shown in Fig. 2. High structural similarity was expected, since the chemical reaction catalysed by PLP-DCs is essentially identical, and the substrates differ from each other only by their respective side chain moieties. It is possible, however, that substrate side chain recognition in different PLP-DCs may cause small changes in the positioning of the reactive groups, thereby leading to different kinetic properties.

In addition to the catalytically crucial residue Lys305, which in all PLP-DCs forms the internal aldimine with PLP, other residues in the active site are relevant for substrate binding and catalysis (Fig. 3A). The residues interacting with PLP are highly conserved and include His191, which is stacked above the PLP aromatic ring. His191 is fully conserved in the PLP-DC family, and in addition to fixing PLP in a reactive conformation, its roles have been suggested to be central in coordinating the carboxyl group that will be released as CO₂ (Komori et al., 2012), as well as in protonating the quinonoid intermediate resulting from decarboxylation (Liang et al., 2019, 2017).

An additional crystal structure was solved and turned out to be the apo form of CSAD, with no electron density for PLP in the active site (Supplementary Fig. 1). Hence, this structure represents an inactive form of CSAD. The main difference between the apo and holo forms is the rotation of the His191 side chain to a conformation not compatible with the presence of PLP (Fig. 3B). Overall, the active site of CSAD is less ordered in the absence of PLP; thus, PLP binding will stabilise a catalytically competent conformation of the cavity. No larger-scale conformational changes were observed between the apo and holo enzymes, which is different from DDC, in which the structure of the apo form presented an open conformation, suggested to be linked to the mechanism of cofactor loading (Giardina et al., 2011). Interestingly, not

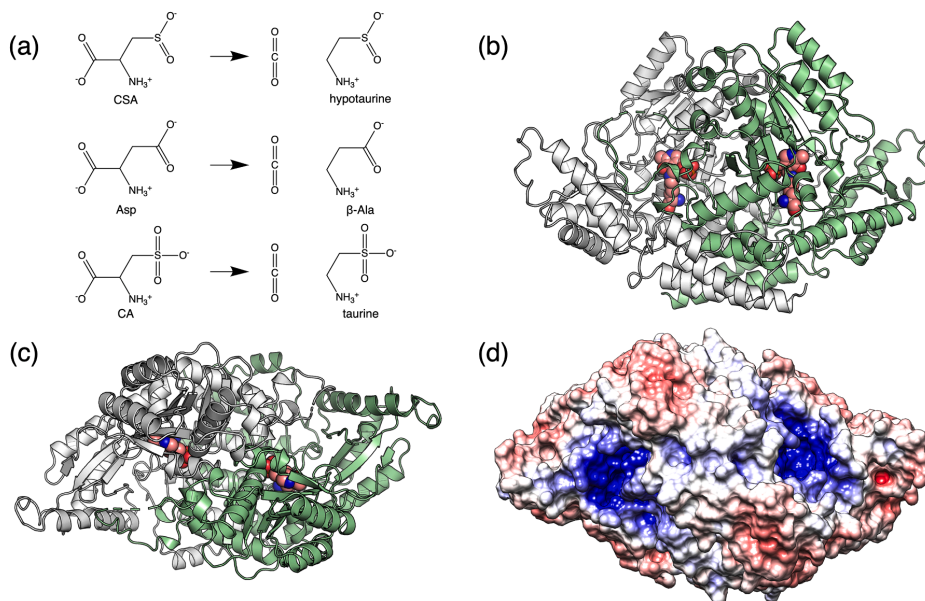


Fig. 1. Overall structure of *MmCSAD*. (a) Reactions catalysed by CSAD. CSA is the preferred substrate. (b) Side view of the dimer. The active site is indicated by the internal aldimine between PLP and Lys305 (spheres). (c) Top view of the CSAD dimer. (d) Electrostatic surface shows positive potential (blue) in the active-site cavity (top view). (For interpretation of the references to colour in this figure legend, the reader is referred to the web version of this article.)

Table 1

Crystallographic data collection and refinement. Values in parentheses correspond to the highest-resolution shell.

Structure	CSAD holo	CSAD apo
Space group	P2 ₁	P2 ₁
Unit cell dimensions	a = 72.9, b = 113.3, c = 113.4 Å = γ = 90°, β = 95.8°	a = 73.1, b = 114.9, c = 113.8 Å = γ = 90°, β = 95.8°
Data processing		
Resolution range (Å)	50–2.10 (2.15–2.10)	50–2.80 (2.87–2.80)
Completeness (%)	90.7 (88.5)	98.6 (98.6)
R _{sym} (%)	12.5 (116.5)	42.6 (323.1)
R _{meas} (%)	15.1 (141.1)	50.4 (380.9)
(I/σ(I))	7.7 (0.9)	3.4 (0.4)
CC _{1/2} (%)	99.3 (38.9)	94.9 (18.4)
Redundancy	2.7 (2.7)	3.4 (3.5)
Wilson B factor (Å ²)	39.2	55.1
Structure refinement		
R _{cryst} /R _{free} (%)	17.9/23.5	24.3/29.2
RMSD bond length (Å)	0.007	0.003
RMSD bond angle (°)	0.9	0.6
Ramachandran favoured/outliers (%)	96.3/0.16	95.6/0.16
MolProbity score/percentile	1.61/96 th	1.49/100 th
PDB entry	6ZEK	7A0A

CSAD structures were obtained from the same protein batch, indicating that PLP has been lost during crystallisation of the apo form. One possibility is hydrolysis of the internal aldimine at the slightly acidic pH (6.5) of the conditions giving the apo CSAD crystals, eventually leading to loss of PLP from the active site.

2.2. Structure of CSAD in solution

In addition to the crystal structure, we studied CSAD conformation in

Table 2

Comparison of the mouse CSAD structure to selected PLP-DCs with known structure. Note how decrease in sequence identity has only minor effects on the similarity of the 3-dimensional fold.

Protein	PDB entry	C α RMSD (Å)	Sequence identity (%)	Reference
human CSAD	2JIS	0.5	90	–
mouse GADL1	6ENZ	1.0	62	(Raasakka et al., 2018)
human GAD65	2OKK	0.8	54	(Fenalti et al., 2007)
human GAD67	2OKJ	1.0	53	(Fenalti et al., 2007)
human HDC	4E1O	2.1	21	(Komori et al., 2012)
pig DDC	1JS6	2.2	22	(Burkhard et al., 2001)
<i>Arabidopsis thaliana</i> phenylacetaldehyde synthase	6EEI	2.1	13	(Torrens-Spence et al., 2020)

solution using synchrotron small-angle X-ray scattering (SAXS) (Fig. 4), in order to detect possible flexibility, as previously observed for GADL1 (Raasakka et al., 2018). Indeed, dimeric CSAD behaves much like GADL1 in solution, providing evidence for motions between open and closed states of the dimer. Such motions might be related to the catalytic cycle. They could be linked to the conformation of the flexible catalytic loop (residues 330–340), which is not fully visible in the CSAD crystal structure. Like in GADL1 (Raasakka et al., 2018), normal mode analysis identified an open conformation of the CSAD homodimer, which fits the SAXS data well (Fig. 4), but is different from that observed crystallographically for apo-DDC (Giardina et al., 2011). Whether open/close motions are unique to each class of PLP-DCs, or if all family members are equally dynamic, remains a subject for future research.

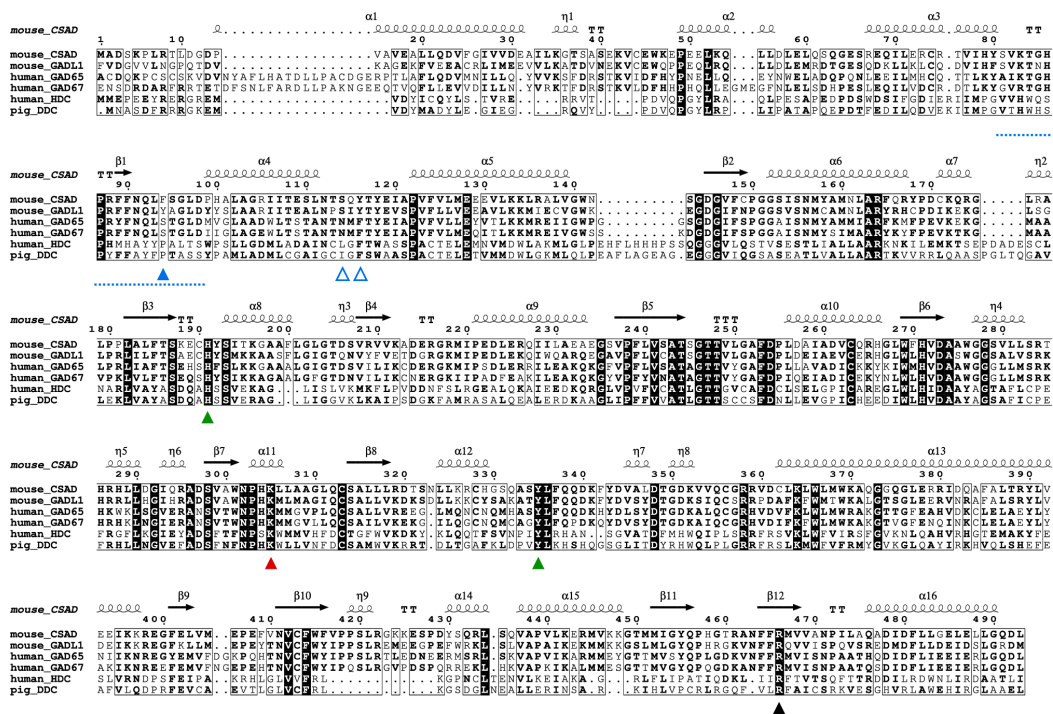


Fig. 2. Sequence alignment of PLP-DCs with known structure. Key elements discussed in the text are highlighted: Phe94 (blue), Ser114/Tyr116 (blue open), α 3- α 4 loop (blue dash), His191 (green), Lys305 (red), Tyr335 (green), Arg466 (black). Residue numbering corresponds to *MmCSAD*. (For interpretation of the references to colour in this figure legend, the reader is referred to the web version of this article.)

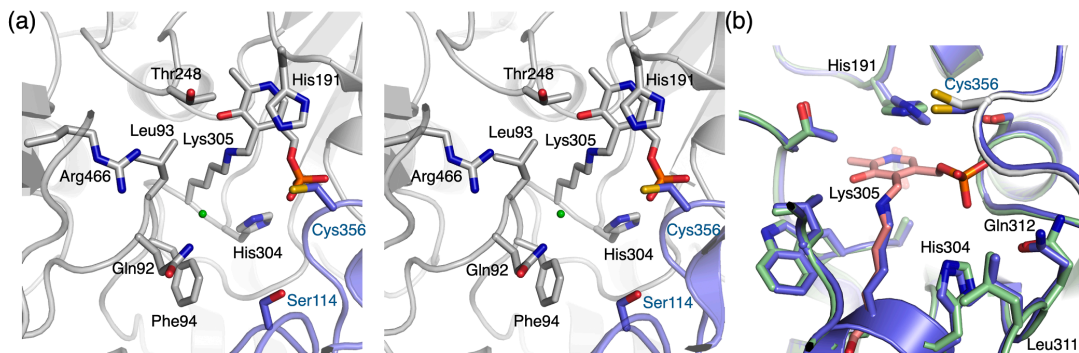


Fig. 3. The active site of *MmCSAD*. (a) Stereo view of the CSAD active site. The bound chloride ion is shown as a green sphere. Elements coming into the active site from the opposing monomer are in blue. (b) Comparison of the holo (green/pink) and apo (blue) CSAD active sites. (For interpretation of the references to colour in this figure legend, the reader is referred to the web version of this article.)

2.3. Importance of Phe94 for substrate specificity

When comparing the structures of CSAD and GAD, it can be concluded that Phe94 in CSAD may be important for substrate specificity. Apparently, Phe94 blocks the binding site for larger substrates; hence, Glu should not productively bind (Fig. 5A). The active site of GAD has a Ser residue at the corresponding position. In addition, GADL1 has a Tyr residue at this position, linked to a slightly different substrate preference (Winge et al., 2015). We previously identified this position as

a key difference in the substrate recognition pocket in the otherwise highly homologous acidic amino acid decarboxylases (Mahootchi et al., 2020). Thus, we mutated Phe94 to Ser in CSAD to evaluate the effects on enzymatic properties.

Activity assays of wild-type (WT) and F94S *MmCSAD* towards CSA and Asp were carried out using HPLC (Table 3, Fig. 5B). While the F94S mutation affected both K_m and k_{cat} of CSAD towards CSA and Asp, the mutant enzyme remained active. Specifically, the effects on K_m and k_{cat} revealed that F94S has a turnover number 5–10 times lower than WT

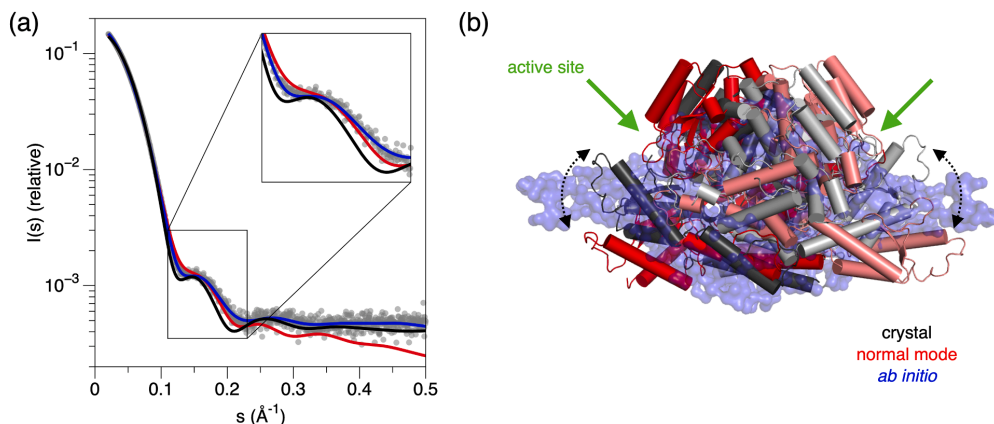


Fig. 4. Structure of *MmCSAD* in solution. (a) SAXS data (grey dots) overlaid with fits from the crystal structure (black), the *ab initio* model (red), and the normal mode-based conformation (blue). (b) Comparison of the crystal structure and models. The open/close motions and the active site location are indicated. (For interpretation of the references to colour in this figure legend, the reader is referred to the web version of this article.)

CSAD for both CSA and Asp, indicating an overall effect on catalysis. In the mutant, K_m increases by an order of magnitude for CSA, but not for Asp. Hence, Phe94 is specifically important for the binding of CSA, the preferred substrate of CSAD. k_{cat}/K_m values further support these observations, showing that the most effective combination by far is WT CSAD with CSA as substrate.

A test for GAD activity was carried out using Glu as substrate, as the mutation F94S mimics the GAD substrate binding site (Fig. 5C). While a trace level of activity is observed for WT CSAD, this activity is even weaker for F94S. The K_m values for both variants are an order of magnitude higher than for CSA and Asp. Hence, altering the substrate specificity towards Glu requires more than altering the obvious Phe94 to the corresponding Ser residue of GAD. Additional factors may include protein dynamics, effects of the catalytic loop – not visible in any structure of CSAD or GADL1 – as well as minor conformational changes in the active site caused by the mutation.

2.4. Folding and stability of WT *MmCSAD* and F94S

The folding and thermal stability of WT *MmCSAD* and F94S were examined using differential scanning fluorimetry (DSF) and circular dichroism (CD) spectroscopy. WT *MmCSAD* and F94S show CD spectra with two characteristic minima at 208 and 220 nm. Both spectra are essentially identical, indicating correct folding of the mutant (Fig. 5D). Both CD spectroscopy and DSF indicate decreased thermal stability for the F94S mutant (Table 4). From the CD melting curves, it follows that although WT *MmCSAD* and F94S have similar patterns of melting, F94S has a melting temperature $\sim 5^\circ\text{C}$ lower than the WT protein (Fig. 5E). While the DSF melting curves indicate a similar decrease in stability for F94S (Fig. 5F), the mutant appears to open up already at low temperatures. The differences in T_m between the methods, which are commonly seen, could be because of differences in the measurement method between CD and DSF. While CD measures the unfolding of secondary structures based on peptide backbone conformation, DSF follows access of a small-molecule dye to the protein hydrophobic core.

The effect of the F94S mutation on the oligomeric state and long-term stability of *MmCSAD* was further studied using size-exclusion chromatography (SEC) - multi-angle static light scattering (MALS), after freezing and thawing of a pure dimer fraction (Fig. 5G,H). Both WT *MmCSAD* and F94S displayed very similar elution profiles, which mainly correspond to a dimer (110 kDa). Both variants also have some tetramer and higher-order oligomers after freezing and thawing (Fig. 5H).

Notably, no monomeric form was detected, indicating high-affinity dimerisation; as the active site is formed at the dimer interface, this is expected.

Taken together, the F94S mutation does not affect the secondary structure content of CSAD, but it has a clear effect on protein stability. As the mutant displays lower activity than the WT enzyme, at least part of the effect could be from altered protein dynamics. These data indicate an important role for Phe94 in CSAD substrate binding and activity.

2.5. Comparison of the mouse CSAD active site with other decarboxylases

As far as enzymatic activity is concerned, CSAD is known to prefer CSA as substrate, while having weak activity towards CA and Asp (Winge et al., 2015; Do and Tappaz, 1996). The closest homologue, GADL1, is more active towards Asp than CSAD, although it is most active with CSA as substrate. Based on earlier studies, neither of the enzymes accept Glu as substrate, and Glu fails to act as an inhibitor (Winge et al., 2015), indicating lack of binding to the active site. It is possible that close members of the PLP-DC enzyme family have at least partially overlapping activities. Based on the observation that mice lacking GADL1 have organ-specific reductions of β -alanine and taurine levels, we recently suggested that this enzyme might have multiple physiological substrates also *in vivo* (Mahootchi et al., 2020). On the other hand, although our results indicate Glu is a very weak substrate for CSAD and GADL1, this activity is unlikely to be of any physiological relevance.

Using the high-resolution crystal structures of both CSAD and GADL1, as well as other PLP-DCs (Table 2), one can carry out an inspection of the corresponding active-site geometries underlying substrate specificity. As all PLP-DCs catalyse the same chemical reaction, amino acid decarboxylation, differences in the active site are expected to affect substrate specificity and/or affinity, rather than reaction mechanism *per se*. Hence, catalytically crucial features are expected to be conserved in sequence and 3D structure. For example, His191 is mechanistically important in PLP-DCs, possibly being involved in the protonation of the quinonoid reaction intermediate (Liang et al., 2019). Comparison of the apo and holo CSAD structures indicates that the conformation of His191 is linked to the presence of the PLP cofactor; it can be envisaged that His191 is important for the catalytically competent orientation of PLP and *vice versa*.

A comparison of CSAD and GADL1 should give indications on the structural properties causing their differential preference towards Asp,

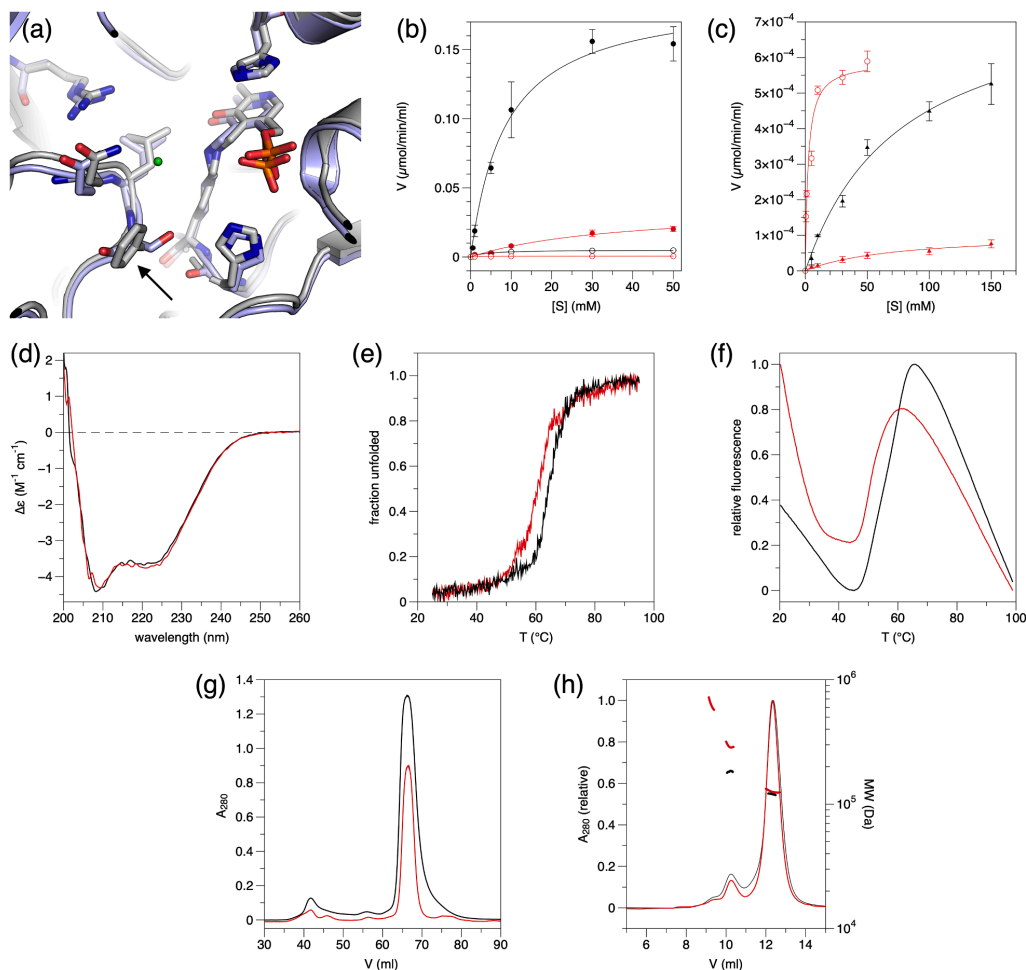


Fig. 5. Role of Phe94 in CSAD activity and stability. (a) Superposition of CSAD (grey) and GAD67 (light blue) active sites. The arrow indicates the position of CSAD Phe94. The chloride ion in CSAD is shown in green. (b) Activity assay with CSA (filled symbols) and Asp (open symbols). WT, black; mutant, red. (c) Activity assay with Glu (filled triangles). WT, black; mutant, red. The activity level of the mutant with Asp is shown for reference (red open circles). (d) CD spectra for WT (black) and mutant (red) CSAD. (e) CD melting curves. (f) DSF melting curves. (g) SEC during protein purification; the pure dimer peak at ~67 ml was picked for further experiments. (h) SEC-MALS after freezing and thawing of dimeric CSAD indicates presence of some higher-order oligomers in both WT and F94S. (For interpretation of the references to colour in this figure legend, the reader is referred to the web version of this article.)

Table 3

Enzymatic properties of CSAD towards acidic amino acids.

Substrate	WT CSAD		F94S			
	k_{cat} (s^{-1})	K_m (mM)	k_{cat}/K_m ($M^{-1} s^{-1}$)	k_{cat} (s^{-1})	K_m (mM)	k_{cat}/K_m ($M^{-1} s^{-1}$)
CSA	0.53 ± 0.02	8.6 ± 1.2	61.6	0.10 ± 0.01	36.8 ± 8.5	2.7
	0.014 ± 0.004	3.8 ± 0.5	3.7	0.0016 ± 0.00006	2.3 ± 0.4	0.7
Asp	0.0022 ± 0.0002	77.3 ± 12.2	0.03	0.00029 ± 0.00004	72.6 ± 20.9	0.004

Table 4Thermal stability of WT and F94S *Mm*CSAD.

Protein	DSF T_m ($^{\circ}C$)	CD T_m ($^{\circ}C$)
<i>Mm</i> CSAD	56.0 ± 0.2	64.6 ± 0.1
F94S	51.1 ± 0.2	60.5 ± 0.2

although CSA is the preferred substrate for both. Asp and CSA have slightly different geometries, in that the carboxyl group is planar while the sulphonic acid group is not. In addition, for the third known substrate, CA, the molecular size is larger, with 3 oxygen atoms interacting with the recognition pocket. In the predicted binding pocket for the acidic side-chain group, Phe94 in CSAD is replaced by Tyr in GADL1; while the hydroxyl group points away, minor changes in conformation and/or dynamics could explain the differences between CSAD and

GADL1. The Phe94 side chain and backbone of Gln92, Leu93, and Phe94 are likely to define the binding of the side chain in CSAD substrates (Fig. 5A).

When comparing CSAD and GAD65/67, it becomes obvious that Phe94 in CSAD is important for substrate specificity. It blocks the binding site for larger substrates, and the Ser residue at this position in GAD is likely to form hydrogen bonds to the Glu side chain carboxyl group (Fig. 6A). The binding mode of Glu into GAD can be deduced from the structure of GAD65 in complex with the inhibitor chelidonic acid

(Fig. 6A) (Fenalti et al., 2007). Original studies on this line of inhibitors indicated that the distance between the two carboxyl groups, corresponding to an extended Glu molecule, is important (Porter and Martin, 1985). The carboxyl groups of the inhibitor mimic those of Glu, and hydrogen bonds are seen to Ser183/192 and a water molecule coordinated by His395/404 at the bottom of the cavity (numbering for GAD65/67), and well as to the backbone amide groups of the α 3- α 4 recognition loop containing Ser183/192 (see below). The His residue and the water molecule are also present in CSAD, and CSA is likely to

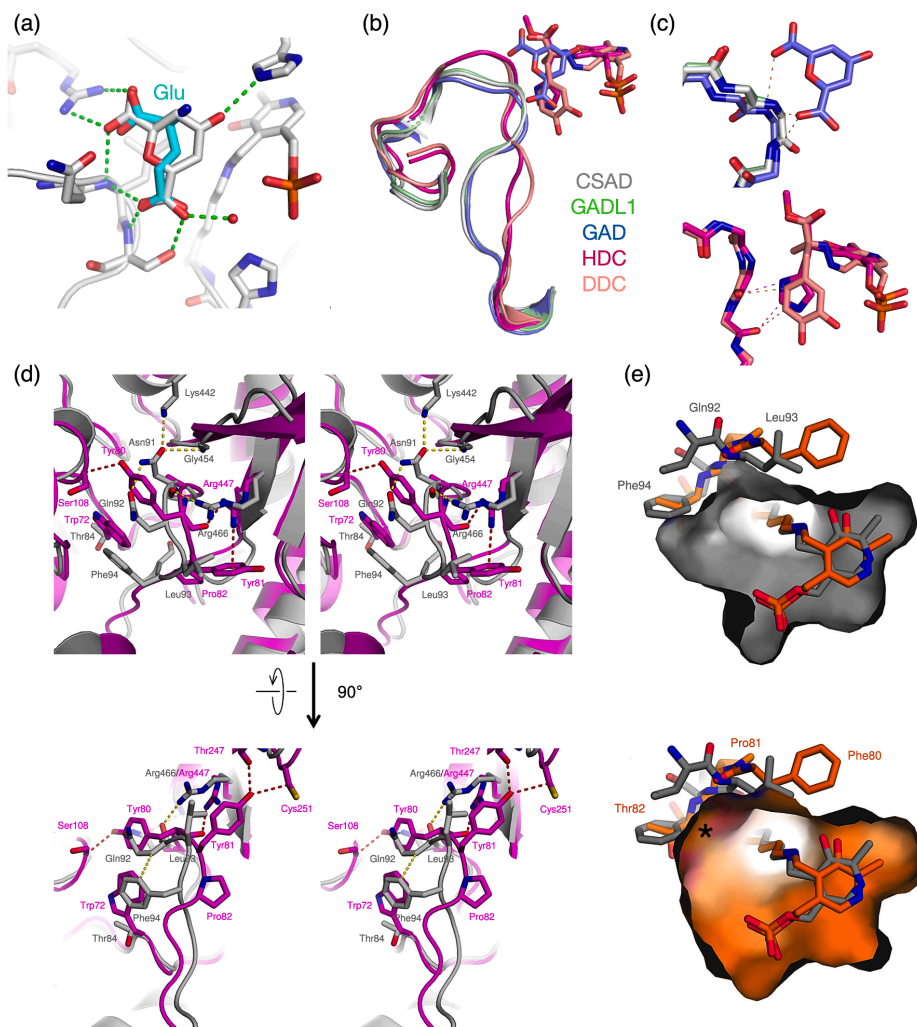


Fig. 6. Comparison to other decarboxylases. (a) GAD65 in complex with chelidonic acid, with hydrogen bonds shown in green. Based on the structure, a proposed mode of Glu substrate binding in GAD is shown (cyan). (b) Superposition of the α 3- α 4 loop in CSAD (grey), GADL1 (green), GAD65 (blue), HDC (magenta), and DDC (pink) highlights two subfamilies linked to substrate side chain size and properties. (c) Top: Backbone conformation in acidic amino acid decarboxylases (with chelidonic acid). Amino groups from the α 3- α 4 loop form direct hydrogen bonds (dashes) with the acidic substrate. Bottom: Backbone conformation in HDC and DDC; carbonyl groups interact with the substrate via hydrogen bonds and/or van der Waals interactions (dashes). (d) Stereo view of superposed CSAD (grey) and HDC (magenta) from two orientations. Key interactions of the α 3- α 4 loop of CSAD (yellow dashes) and HDC (red dashes) are shown. Additionally, large substituting changes between HDC and CSAD, such as Trp72/Thr84, are shown. (e) The α 3- α 4 loop and the internal aldimine in CSAD (grey) and DDC (orange). The surface at the top corresponds to CSAD and the one at the bottom to DDC. The black asterisk marks a volume present in DDC but not in CSAD, arising from the conformation of the α 3- α 4 loop. Relevant residues in the α 3- α 4 loop are labelled. (For interpretation of the references to colour in this figure legend, the reader is referred to the web version of this article.)

similarly hydrogen bond to this water molecule.

HDC has been crystallised with the non-cleavable His methyl ester trapped as a PLP adduct, thereby giving insights into the reaction mechanisms in the family (Komori et al., 2012). A similar conformation was observed for the inhibitor carbidopa in DDC (Burkhard et al., 2001). Phe94 in CSAD prevents the binding of such large substrates into the active site, but it is, in fact, not the only determinant. Comparing the acidic amino acid decarboxylases GAD65, GAD67, CSAD, and GADL1 with those acting on larger, non-acidic substrates, one should note the $\alpha 3$ - $\alpha 4$ loop, forming the active site cavity wall and intimately interacting with the substrate (Fig. 6B). The backbone conformation of the $\alpha 3$ - $\alpha 4$ loop is different between the two groups of enzymes, and the peptide bonds have opposite orientations, such that the NH groups point towards the substrate-binding cavity in GAD, CSAD, and GADL1 (Fig. 6C). In HDC and DDC, the carbonyl groups point into the same pocket, giving a different electrostatic environment and allowing the binding of positively charged and neutral substrates, such as His or L-DOPA, into the active site (Fig. 6C).

In addition to the active-site conformation, based on the sequence conservation of the $\alpha 3$ - $\alpha 4$ recognition loop in PLP-DCs (Fig. 2), CSAD, GADL1, and the GADs can be grouped together, while DDC and HDC form another group (Fig. 6B). A closer comparison of mouse CSAD and human HDC reveals that the loop is formed out of two overlapping motifs forming central interactions close to the active site (Fig. 6D). In CSAD, the first motif stretches from Phe90 to Phe94, with the consensus sequence FNQ[FYS] in the first group. In HDC, the stretch that superimposes with this sequence involves Ala79-Pro82, with the consensus sequence AY[YF]P in the second group. The backbone trace of this segment in both groups is similar, although the underlying interactions and side chain conformations differ drastically between CSAD and HDC. In group 1, the central Asn residue acts as a hub of weak interactions and hydrogen bonds, locking different structural elements in place. For CSAD, a noteworthy Asn91-interacting residue is Lys442, which is fully conserved in the first group and likely to draw the $\alpha 3$ - $\alpha 4$ loop towards helix $\alpha 15$. Worth noting is that Arg466 in CSAD (Arg447 in HDC) is fully conserved in PLP-DCs discussed above (Fig. 2), but may adopt different conformations. Its conservation is linked to its direct mechanistic interaction with the substrate α -carboxyl group.

Strikingly, the second stretch that follows after the conserved motif adopts a completely different conformation between the two groups of PLP-DCs (Fig. 6D). The conformation is influenced by the Pro residue replacing CSAD Phe94 in HDC and DDC, which leads to substantially more space in the active site of PLP-DCs with larger, non-acidic substrates (Fig. 6C,E). This is a key substrate binding determinant between the two groups of PLP-DCs. In addition to the conformational change resulting from the interaction network of the short sequence motifs, the rigidity of the $\alpha 3$ - $\alpha 4$ loop is most likely different between the two groups. HDC and DDC have a conserved Trp residue (Trp72 in HDC), which is replaced by Thr84 in CSAD (Fig. 6D); hence, the $\alpha 3$ - $\alpha 4$ loop in HDC and DDC may be more rigid. This is supported by lower *B* factors for the corresponding region ($10 - 11 \text{ \AA}^2$ in HDC bound to His methyl ester (resolution 1.8 \AA), $21 - 25 \text{ \AA}^2$ in apo-DDC (2.6 \AA), $27 - 31 \text{ \AA}^2$ in apo-CSAD (2.1 \AA)).

2.6. Substrate specificity and catalytic mechanism of CSAD and GADL1

The substrate specificity of CSAD has been subject to some controversy. Before the availability of recombinant, purified enzyme, a concern was that the ability of CSAD to accept multiple substrates could be due to contamination with other enzymes, mainly GAD (Do and Tappaz, 1996; Guion-Rain and Chatagner, 1972; Oertel et al., 1981). However, we now know that CSA is the preferred substrate for CSAD both *in vitro* and *in vivo* (Park et al., 2014; Winge et al., 2015; Agnello et al., 2013). In addition, CSAD isolated from marine bacteria, insects, and several mammalian species accept CA, the oxidised form of CSA, as substrate, with 3–13% rate constants relative to CSA (Agnello et al.,

2013; Liu et al., 2012). However, as the concentration of CA in the rat brain is 50–80% of CSA, decarboxylation of CA should have minor contribution to the overall synthesis of taurine (Ida and Kuriyama, 1983), at least in brain tissue. In addition, low Asp and Glu decarboxylase activity has been reported for CSAD (Winge et al., 2015; Weinstein and Griffith, 1987). Due to the presence of related enzymes with higher efficacy towards Asp and Glu (GADL1, GAD65, and GAD67), the physiological importance of such weak activity is unclear. However, the ability of the PLP-DCs to process a range of overlapping substrates may be metabolically advantageous, as observed for GADL1 knockout mice. These mice showed tissue-specific loss of both β -alanine and taurine derivatives, depending on the relative tissue abundance of the different enzymes (Mahootchi et al., 2020).

Insect aspartate decarboxylase (ADC), which has high homology and similar catalytic properties to CSAD, prefers CSA as substrate, but is also active towards Asp and CA (Liu et al., 2012). When ADC was incubated with CSA in the presence of each of the 20 proteinogenic amino acids, the preferred substrate was still CSA (Liu et al., 2013). Since insect ADC and human CSAD share $\sim 50\%$ sequence identity (Liu et al., 2019), one can expect similar properties for ADC and CSAD.

A number of ions were detected in the *Mm*CSAD structure; including an ion modelled as chloride in each active site (Fig. 3A,5A), interacting with the backbone amide groups of loop $\alpha 3$ - $\alpha 4$ discussed above. This site could be relevant for recognizing the substrate acidic side chain. In the structure of HDC with methylhistidine (Komori et al., 2012) covalently linked to the PLP cofactor, the binding determinants for the carboxyl and amino groups are well defined, while the inhibitor chelidonic acid bound to GAD (Fenalti et al., 2007a, 2007b) provides additional information. Using these structures as templates, one can dock in CSA, taking into account the anion-binding site in the active cavity (Fig. 7). We consider the latter to be a likely location for the CSA sulphonic acid group binding - or in the case of Asp, the side-chain carboxyl group. While both CSA and Asp require two hydrogen bonding partners for the side chain, CA needs three - it is likely that two of the hydrogen bonds are provided by the backbone amide groups in the $\alpha 3$ - $\alpha 4$ loop and the third one by the conserved water molecule.

The leaving carboxyl group, in a perpendicular position to the plane formed by the PLP ring and the Schiff base moiety, is stabilised by Arg466 (Fig. 7A). It may also be hydrogen-bonded to His191, a central residue in the PLP-DC mechanism, as seen in the structure of HDC (Komori et al., 2012). In apo CSAD, His191 is rotated, and it will reach its correct conformation upon PLP complex formation. Thus, the core active site of CSAD appears pre-organised for catalysis, but only in the presence of the cofactor internal aldimine.

A main obstacle in fully understanding the mechanistic details of CSAD and GADL1 catalysis is the flexible $\alpha 12$ - $\alpha 13$ loop covering the active site; this loop is not visible in any of the available CSAD or GADL1 crystal structures, but a conserved Tyr residue in it has been suggested to be a key player in catalysis by PLP-DCs, including GAD (Fenalti et al., 2007). This Tyr, Tyr335 in CSAD, is conserved in CSAD and GADL1 (Fig. 2). Importantly, in both DDC and HDC, the loop is susceptible to proteolysis, but gets protected, when an active-site ligand is bound (Burkhard et al., 2001; Fleming et al., 2004; Ishii et al., 1998). Hence, the dynamics of the loop are linked to the decarboxylase reaction cycle and occupancy of the active site. After decarboxylation, protonation of the reaction intermediate is carried out by Tyr335, which enables the reaction to proceed towards product release and reconstitution of the internal aldimine in the CSAD active site. The protonation could either occur directly (Fenalti et al., 2007) or be mediated through a water molecule coordinated by Tyr335 (Fernandes et al., 2017). Intriguingly, PLP-DCs can catalyse a different reaction involving molecular oxygen, if this Tyr residue is mutated to a Phe (Bertoldi et al., 2002; Bisello et al., 2020). His191 also appears to be relevant for the protonation step (Liang et al., 2019, 2017; Fernandes et al., 2017), but in light of current data, its likely role is the coordination of Tyr335.

A tripartite substrate selectivity motif was identified in GAD and

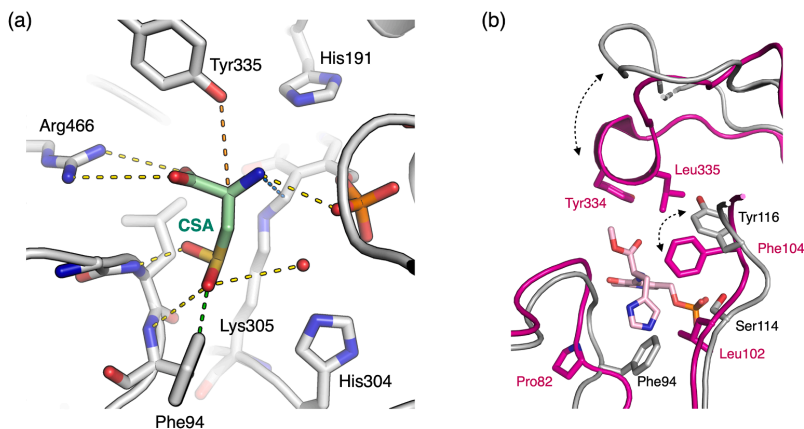


Fig. 7. Implications for the CSAD reaction mechanism. (a) Proposed model for CSA substrate binding to CSAD and depiction of catalytically important residues. Hydrogen bonds to active-site side chains, main-chain groups, the cofactor, and a conserved water molecule are shown in yellow dashes. A van der Waals interaction possibly relevant for CSAD substrate specificity to Phe94 is in green. The blue dash indicates the bond that will be formed upon external aldimine formation between Lys305 and CSA. Protonation of the quinonoid intermediate at the second stage of the reaction is likely catalysed by Tyr335 from the flexible $\alpha 2$ - $\alpha 3$ catalytic loop (here pictured in the position observed in the GAD65 crystal structure), from the other subunit. (b) The previously identified CSAD/GAD substrate selectivity motif consisting of Phe94, Ser114, and Tyr116 (Agnello et al., 2013), compared to that in HDC (magenta). Note how the incoming loop containing the catalytic Tyr residue pushes the aromatic residue (Tyr116 in CSAD) in close contact with the catalytic cavity. (For interpretation of the references to colour in this figure legend, the reader is referred to the web version of this article.)

CSAD, in a study focusing on taurine synthesis by marine bacteria (Agnello et al., 2013). The residues of this motif are Phe94, Ser114, and Tyr116 in CSAD. Essentially, while Phe94 was important for catalysis on CSA and CA, replacing Tyr116 with Phe (as in GAD, DDC, or HDC), allowed CSAD to use Glu as substrate (Agnello et al., 2013). This brings an added level of complexity to the mechanism. Comparing the structure of CSAD with the enzymes carrying Phe at this position reveals a completely different conformation in the crystal state (Fig. 7B). In HDC and GAD, it is clear that the catalytic loop pushes the Phe residue to the active site wall, when the Tyr in this loop reaches in for protonation of the reaction intermediate. In the structures of CSAD and GADL1, the catalytic loop is disordered, and Tyr116 is in a relaxed conformation. During the reaction cycle, it must be pushed further in, reducing the available space in the active site, but also providing a putative additional hydrogen bonding contact for substrate recognition (Fig. 7B). The latter could be important in making CSA the preferred substrate for CSAD.

2.7. Insights into inhibitor design

Rare mutations in enzymes responsible for the degradation of β -alanine, as well as its histidine derivatives carnosine and anserine, have been linked to the abnormal accumulation of these compounds in mammalian tissues and severe neurological diseases (Scriver et al., 1966; Willi et al., 1997). As the neurological symptoms have been unresponsive to dietary interventions, an alternative treatment strategy could be to inhibit their biosynthesis. The discovery (Mahootchi et al., 2020) that GADL1 functions in the biosynthesis of β -alanine and carnosine raises the possibility that it could be a target for inhibition therapy. The first generation of inhibitors targeting CSAD and GADL1 had modest affinity but promising selectivity (Winge et al., 2015). Since then, high-resolution structures for both enzymes have become available, providing a stepping stone for further knowledge-based optimisation of such compounds. The differences in activity towards closely related substrates, as well as the subtle differences in the respective active-site structures, can be utilised in the development of a next generation of potential inhibitors of acidic amino acid decarboxylases. These aspects are crucial in the development of *in silico* screening approaches.

A prime example of inhibitor design towards PLP-DCs is carbidopa

(Sletzinger et al., 1963), which is a DDC substrate analogue able to form a stable covalent adduct with the PLP cofactor. Carbidopa is in wide use in the treatment of Parkinson's disease, whereby it inhibits the conversion of L-DOPA to dopamine in peripheral tissues (Bartholini and Pletscher, 1975), leading to increased L-DOPA half-life and reduced side effects of dopamine. The crystal structure of DDC in complex with carbidopa (Burkhard et al., 2001) is, therefore, of high value in designing inhibitors towards other PLP-DCs. For example, for acidic amino acid decarboxylases, a similar approach targeting the external aldimine instead of a simple substrate analogue – as done previously (Winge et al., 2015; Porter and Martin, 1985; Liu et al., 2013) – would be a promising approach. In addition, mechanism-based inhibitors of CSAD activity, based on chemical substitutions on the β carbon, have been studied (Weinstein and Griffith, 1987; Griffith, 1983). Non-cleavable analogues of different stages of the acidic amino acid decarboxylase reaction mechanism could, hence, be targeted in a systematic manner instead of non-targeted screening or attempts at designing substrate analogues, which inherently will have rather low affinity in these enzymes.

3. Concluding remarks

Our work highlights central details of molecular mechanisms of taurine biosynthesis; in addition, substrate recognition determinants across the PLP-DC family have been elucidated. Substrate specificity in the family is clearly affected by both the amino acid side chains lining the catalytic cavity as well as direct backbone-substrate interactions. The latter divide PLP-DCs into two subclasses. These findings are central in understanding mechanistic details of catalysis, but also in research aimed at designing effectors of amino acid decarboxylation linked to the production of important metabolites and signalling molecules, such as taurine, β -alanine, carnosine, GABA, histamine, serotonin, and dopamine.

4. Materials and methods

4.1. Expression vector

Multiple mRNA transcripts of CSAD have been described, with alternative initiation codons and splicing events (Lourenco and Camilo,

2002). *MmCSAD* cDNA corresponding to the 493-amino-acid (55 kDa; UniProt entry Q9DBE0) isoform was subcloned into the expression vector pTH27 (Hammarström et al., 2006), which codes for an N-terminal His₆ tag. In order to examine structural determinants of substrate specificity of *MmCSAD*, the variant F94S was generated using the QuikChange kit (Agilent). The sequences of expression clones were verified by DNA sequencing.

4.2. Expression and purification of *MmCSAD*

WT and F94S His₆-CSAD were expressed in *Escherichia coli* BL21 CodonPlus (DE3)-RIPL cells (Stratagene) at +15 °C using 0.5 mM IPTG induction. Pyridoxine hydrochloride, a precursor of PLP biosynthesis, was added to the culture at 2 mM to improve protein solubility. Cell pellets were lysed by sonication in a buffer consisting of 50 mM sodium phosphate buffer pH 7.4, 500 mM NaCl, 20 mM imidazole, 0.2 mg/ml lysozyme, 1 mM MgCl₂, and cOmplete EDTA-free protease inhibitors (Roche). Phenylmethylsulphonyl fluoride was added to 1 mM immediately following sonication, and the unclarified lysate was applied onto an IMAC HiTrap TALON crude column (GE Healthcare). The column was washed first with 50 mM sodium phosphate pH 7.4, 500 mM NaCl, and then with the same buffer containing 20 mM imidazole. Elution was done with 100 mM imidazole in the same buffer. SEC was performed using a Superdex HR 200 column (GE Healthcare) equilibrated with 20 mM HEPES, 200 mM NaCl (pH 7.4). After elution, CSAD dimer fractions were combined and concentrated.

4.3. Crystallisation, data collection, structure solution, and refinement

MmCSAD crystals were obtained at +20 °C using sitting-drop vapour diffusion. Holo-CSAD crystals were grown in drops containing 200 nl of protein stock (10.3 mg/ml) and 100 nl of reservoir solution (0.15 M KBr, 30% PEG2000 monomethyl ether), and apo-CSAD crystals grew in drops of 100 nl protein and 200 nl reservoir (200 mM Na₂SO₄, 100 mM Bis-tris propane, pH 6.5, 20% PEG3350). Crystals were briefly soaked in a cryoprotectant solution containing 80% reservoir solution and 20% glycerol, and flash-cooled in liquid N₂ prior to data collection.

X-ray diffraction data were collected at 100 K on the automated MASSIF-1 synchrotron beamline at ESRF (Grenoble, France) (Bowler et al., 2015; Bowler et al., 2016; Svensson et al., 2015). The data were processed and scaled using XDS (Kabsch, 2010). The structure was solved by molecular replacement in PHASER (McCoy et al., 2007), using the human CSAD crystal structure (PDB entry 2JIS) as template. Refinement was done in phenix.refine (Afonine et al., 2012) and model rebuilding with Coot (Casañal et al., 2020). The structures were validated using MolProbity (Chen et al., 2010).

4.4. Small-angle X-ray scattering

SAXS data for *MmCSAD* were collected on the SWING beamline at the SOLEIL synchrotron (Gif-sur-Yvette, France). Scattering was measured in batch mode at three different protein concentrations (1–2.5 mg/ml), from a freshly purified monodisperse dimeric sample. The recorded frames were checked for radiation damage, and data from all concentrations were analysed to exclude interparticle effects. Data were processed using the beamline software Foxtrot 3.5.2 and analysed with ATSAS (Franke et al., 2017). *Ab initio* chain-like models were built with GASBOR (Svergun et al., 2001), normal mode-based conformations were analysed using SREFLEX (Panjkovich and Svergun, 2016), and the crystal structure was compared to the SAXS data with CRYSOLOG (Svergun et al., 1995).

4.5. Sequence and structure analysis

Structure superpositions were done with SSM (Krisinel and Henrick, 2004). Sequences were aligned with ClustalW (Thompson et al., 1994)

and visualised with ESPript (Gouet et al., 1999). Electrostatic surfaces were calculated using APBS and pdb2pqr (Unni et al., 2011) and visualised in UCSF Chimera (Pettersen et al., 2004). PyMOL (Schrödinger) was used for structure visualisation and analysis.

4.6. Circular dichroism spectroscopy

CD spectra between 200 and 260 nm were recorded in triplicate on a Jasco J-810 instrument. Measurements were done at a protein concentration of 0.6 mg/ml in a 1-mm quartz cuvette. The samples were diluted with 10 mM sodium phosphate (pH 7.4), and buffer spectra were subtracted. Thermal denaturation was measured using the CD signal at 222 nm from +25 to +95 °C, at a heating rate of 2 °C/min.

4.7. Differential scanning fluorimetry

A fluorescence-based thermal stability assay (differential scanning fluorimetry, DSF) (Ericsson et al., 2006) was performed using a Light-Cycler 480 II instrument (Roche). 20- μ l samples were analysed in 20 mM HEPES, 200 mM NaCl (pH 7.4). CSAD concentration was 0.1 mg/ml, and SYPRO® Orange was used at a 1:1000 (v/v) dilution. The instrument was set to detect emission between 300 and 570 nm. The heating rate was 2 °C/min from +20 to +99 °C. Five replicates of each sample were measured, using a 384-well plate with an optical film (Roche).

4.8. Quaternary structure analysis

Analytical SEC-MALS was employed to determine the oligomeric states of WT *MmCSAD* and F94S. SEC was done using the ÄKTA™Purifier FPLC system (GE Healthcare), which was coupled with a RefractoMax 520 module (ERC GmbH, Riemerling, Germany) for measuring refractive index for concentration determination, and a mini-DAWN TREOS light scattering detector (Wyatt Technology). Samples were diluted to 2 mg/ml and centrifuged at 16 000 g for 10 min at +4 °C. 200 μ g of the protein were applied onto a Superdex 200 Increase 10/300 GL column, pre-equilibrated with 20 mM HEPES, 200 mM NaCl (pH 7.4), at a flow rate of 0.4 ml/min. Astra software (Wyatt) was used for SEC-MALS data analysis.

4.9. Enzymatic activity assays

Catalytic activity of WT *MmCSAD* and F94S towards the known substrates CSA and Asp was measured at +37 °C, using a reaction mixture of 100 μ l containing 6 μ M CSAD, 60 mM potassium phosphate (pH 7.4), 5 mM DTT, and 0.5 μ M PLP. Adding the amino acid substrate started the reaction. To measure steady-state kinetic properties of the enzymes, 0–50 mM of the substrates were tested. After 60 min, the reaction was stopped by addition of an equal volume of ice-cold ethanol containing 5% acetic acid. For studying GAD activity with Glu as substrate, the reaction mixture of 100 μ l contained 60 mM potassium phosphate (pH 7.4), 5 mM DTT, and 2 mM PLP, and the reaction was stopped after 120 min.

The samples were centrifuged at 15,700 g for 10 min, and the supernatant was transferred onto a microtiter plate and analysed by HPLC. Samples were diluted with an equal volume of solvent (24% ethanol in 50 mM sodium phosphate, pH 6.0), and 4.2% *o*-phthalaldehyde (OPA) reagent was added. Mobile phase was a mix of 50% of 100 mM sodium phosphate, 20% ethanol, and 30% H₂O. Flow rate was set to 0.5 ml/min. Samples were injected into a Zorbax Eclipse XDB-C18 column, and the product was determined based on fluorescence detection of the OPA-conjugated amino acid, using excitation at 366 nm and emission at 455 nm. Retention time for hypotaurine was 24.1 min, β -alanine 19.8 min, and GABA 31.1 min. The software used for detecting the area was ChemStation 1100 from Agilent. Kinetic parameters were determined by nonlinear regression using the Michaelis–Menten equation in GraphPad Prism 8 (GraphPad Software, La Jolla, California, USA).

5. Accession numbers

PDB: 6ZEK, 7A0A
SASBDB: SASDJR7

CRediT authorship contribution statement

Elaheh Mahootechi: Conceptualization, Formal analysis, Investigation, Methodology, Validation, Writing - original draft. **Arne Raasakka:** Conceptualization, Formal analysis, Investigation, Methodology, Validation, Writing - original draft. **Weisha Luan:** Investigation, Resources, Writing - review & editing. **Gopinath Muruganandam:** Investigation, Resources. **Remy Loris:** Resources, Supervision, Writing - review & editing. **Jan Haavik:** Conceptualization, Funding acquisition, Project administration, Supervision, Validation, Writing - review & editing. **Petri Kursula:** Conceptualization, Data curation, Formal analysis, Methodology, Project administration, Supervision, Validation, Visualization, Writing - original draft.

Declaration of Competing Interest

The authors declare that they have no known competing financial interests or personal relationships that could have appeared to influence the work reported in this paper.

Acknowledgements

This work has received funding from the European Union Horizon 2020 research and innovation program under Grant Agreement No. 810384 (CoCA), Stiftelsen Kristian Gerhard Jebsen (SKJ-MED-02), and the Regional Health Authority of Western Norway (No. 25048). This publication reflects only the authors' view, and the European Commission is not responsible for any use that may be made of the information it contains. We wish to acknowledge access to and excellent support on synchrotron beamlines at SOLEIL and ESRF.

Appendix A. Supplementary data

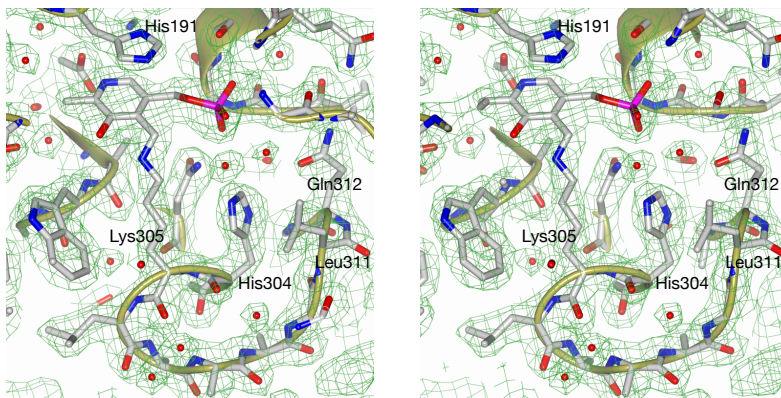
Supplementary data to this article can be found online at <https://doi.org/10.1016/j.jsb.2020.107674>.

References

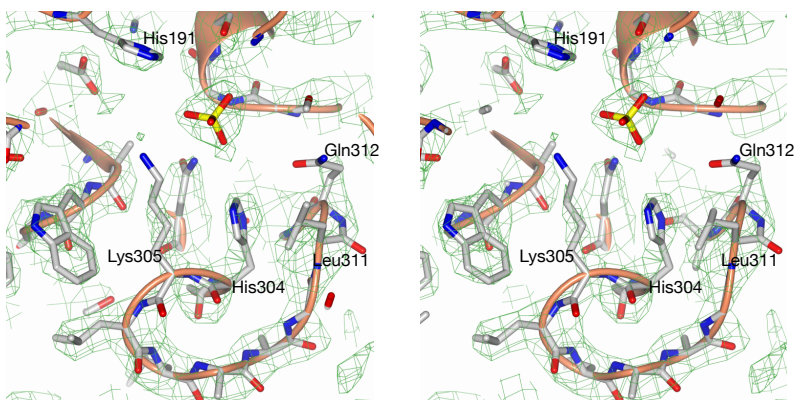
- Percudani, R., Peracchi, A., 2003. A genomic overview of pyridoxal-phosphate-dependent enzymes. *EMBO Rep* 4 (9), 850–854. <https://doi.org/10.1038/sj.embor.embor914>.
- Thornton, J.M., Todd, A.E., Milburn, D., Borkakoti, N., Orengo, C.A., 2000. From structure to function: Approaches and limitations. *Nat Struct Biol* 7 (Suppl), 991–994. <https://doi.org/10.1038/80784>.
- Liang, J., Han, Q., Tan, Y., Ding, H., Li, J., 2019. Current advances on structure-function relationships of pyridoxal 5'-phosphate-dependent enzymes. *Front Mol Biosci* 6, 4. <https://doi.org/10.3389/fmolb.2019.00004>.
- Sarup, A., Larsson, O.M., Schousboe, A., 2003. GABA transporters and GABA-transaminase as drug targets. *Curr Drug Targets CNS Neurol Disord* 2, 269–277. <https://doi.org/10.2174/1568007033482788>.
- Daidone F, Montoli R, Palearini A, Cellini B, Macchiarulo A, Giardina G, et al. (2012). Identification by virtual screening and in vitro testing of human DOPA decarboxylase inhibitors. *PLoS One* 7, e31610.
- Bartholini, G., Pletscher, A., 1975. Decarboxylase inhibitors. *Pharmacology & Therapeutics. Part B: General and Systematic Pharmacology* 1 (3), 407–421. [https://doi.org/10.1016/0306-039X\(75\)90047-1](https://doi.org/10.1016/0306-039X(75)90047-1).
- Slettinger, M., Chemerda, J.M., Bollinger, F.W., 1963. Potent decarboxylase inhibitors. *Annals of methyl dopa. J Med Chem* 6, 101–103. <https://doi.org/10.1021/jm0038a003>.
- Brun, L., Ngu, L.H., Keng, W.T., Ch'ng, G.S., Choy, S., Hwu, W.L., Lee, W.T., Willemsen, M.A.A.P., Verbeek, M.M., Wassenberg, T., Regal, L., Orcesi, S., Tonduti, D., Accorsi, P., Testard, H., Abdenur, J.E., Tay, S., Allen, G.F., Heales, S., Kern, I., Kato, M., Burlina, A., Manegold, C., Hoffmann, G.F., Blau, N., 2010. Clinical and biochemical features of aromatic L-amino acid decarboxylase deficiency. *Neurology* 75 (1), 64–71. <https://doi.org/10.1212/WNL.0b013e3181e620ae>.
- Ercan-Sencicek, A.G., Stillman, A.A., Ghosh, A.K., Bilguvar, K., O'Roak, B.J., Mason, C.E., Abbott, T., Gupta, A., King, R.A., Pauls, D.L., Tischfield, J.A., Heiman, G.A., Singer, H.S., Gilbert, D.L., Hoekstra, P.J., Morgan, T.M., Loring, E., Yasuno, K., Fernandez, T., Sanders, S., Louvi, A., Cho, J.H., Mane, S., Colangelo, C.M., Biederer, T., Lifton, R.P., Gunel, M., State, M.W., 2010. L-Histidine Decarboxylase and Tourette's Syndrome. *N Engl J Med* 362 (20), 1901–1908. <https://doi.org/10.1056/NEJMoa0907006>.
- Haavik, J., Blau, N., Thöny, B., 2008. Mutations in human monoamine-related neurotransmitter pathway genes. *Hum. Mutat.* 29 (7), 891–902. <https://doi.org/10.1002/humu.20700>.
- Baekkeskov, S., Aanstoot, H.-J., Christgai, S., Reetz, A., Solimena, M., Cascalho, M., Folli, F., Richter-Olesen, H., Camilli, P.-D., 1990. Identification of the 64K autoantigen in insulin-dependent diabetes as the GABA-synthesizing enzyme glutamic acid decarboxylase. *Nature* 347 (6289), 151–156. <https://doi.org/10.1038/347151a0>.
- Graus, F., Saiz, A., Dalmau, J., 2020. GAD antibodies in neurological disorders — insights and challenges. *Nat Rev Neurol* 16 (7), 353–365. <https://doi.org/10.1038/s41582-020-0359-x>.
- Skoldberg F., Rorsman F., Perheentupa J., Landin-Olsson M., Husebye E. S., Gustafsson J., et al. (2004). Analysis of antibody reactivity against cysteine sulfinic acid decarboxylase, a pyridoxal phosphate-dependent enzyme, in endocrine autoimmune disease. *J Clin Endocrinol Metab* 89, 1636–1640.
- Lourenco, R., Camilo, M.E., 2002. Taurine: A conditionally essential amino acid in humans? An overview in health and disease. *Nutr Hosp* 17, 262–270.
- Samuelsson, M., Gerdin, G., Öllinger, K., Vrethem, M., 2012. Taurine and glutathione levels in plasma before and after ECT treatment. *Psychiatry Research* 198 (1), 53–57. <https://doi.org/10.1016/j.psychres.2012.02.016>.
- Samuelsson, M., Skogh, E., Lundberg, K., Vrethem, M., Öllinger, K., 2013. Taurine and glutathione in plasma and cerebrospinal fluid in olanzapine treated patients with schizophrenia. *Psychiatry Research* 210 (3), 819–824. <https://doi.org/10.1016/j.psychres.2013.09.014>.
- Hoffmann, E.K., Pedersen, S.F., 2006. Sensors and signal transduction pathways in vertebrate cell volume regulation. *Contrib Nephrol* 152, 54–104. <https://doi.org/10.1159/000096318>.
- Schaffer, S.W., Ju Jong, C., KC, R., Azuma, J., 2010. Physiological roles of taurine in heart and muscle. *J Biomed Sci* 17 (Suppl 1), S2. <https://doi.org/10.1186/1423-0127-17-S1-S2>.
- Hernandez-Benitez, R., Pasantes-Morales, H., Saldana, I.T., Ramos-Mandujano, G., 2010. Taurine stimulates proliferation of mice embryonic cultured neural progenitor cells. *J Neurosci Res* 88, 1673–1681. <https://doi.org/10.1002/jnr.22328>.
- Pasantes-Morales, H., Hernández-Benitez, R., 2010. Taurine and Brain Development: Trophic or Cytoprotective Actions? *Neurochem Res* 35 (12), 1939–1943. <https://doi.org/10.1007/s11064-010-0262-8>.
- Jia, F., Yue, M., Chandra, D., Keramidis, A., Goldstein, P.A., Homanics, G.E., Harrison, N. L., 2008. Taurine Is a Potent Activator of Extrasynaptic GABAA Receptors in the Thalamus. *Journal of Neuroscience* 28 (1), 106–115. <https://doi.org/10.1523/JNEUROSCI.3996-07.2008>.
- Lähdesmäki, P., Kumpulainen, E., Raasakka, O., Kyrki, P., 1977. Interaction of taurine, GABA and glutamic acid with synaptic membranes. *J Neurochem* 29 (5), 819–826. <https://doi.org/10.1111/j.1471-4159.1977.tb10724.x>.
- Hobert, J.A., Embacher, R., Mester, J.L., Frazier Jr, T.W., Eng, C., 2014. Biochemical screening and PTEN mutation analysis in individuals with autism spectrum disorders and macrocephaly. *Eur J Hum Genet* 22 (2), 273–276. <https://doi.org/10.1038/ejhg.2013.114>.
- Park, E., Park, S.Y., Dobkin, C., Schuller-Levis, G., 2014. Development of a Novel Cysteine Sulfinic Acid Decarboxylase Knockout Mouse: Dietary Taurine Reduces Neonatal Mortality. *Journal of Amino Acids* 2014, 1–12. <https://doi.org/10.1155/2014/346809>.
- Winge, I., Teigen, K., Fossbakk, A., Mahootechi, E., Kleppe, R., Skoldberg, F., Kämpe, O., Haavik, J., 2015. Mammalian CSAD and GADL1 have distinct biochemical properties and patterns of brain expression. *Neurochemistry International* 90, 173–184. <https://doi.org/10.1016/j.neuint.2015.08.013>.
- Stipanuk, M.H., Ueki, I., Dornier Jr, J.E., Simmons, C.R., Hirschberger, L.L., 2009. Cysteine dioxygenase: a robust system for regulation of cellular cysteine levels. *Amino Acids* 37 (1). <https://doi.org/10.1007/s00726-008-0202-y>.
- Mahootechi, E., Cannon, H.S., Kleppe, R., Winge, I., Hegvik, T.A., Megias-Perez, R., et al., 2020. GADL1 is a multifunctional decarboxylase with tissue-specific roles in betanine and carnosine production. *Sci Adv* 6, eabb3713. <https://doi.org/10.1126/sciadv.abb3713>.
- Reymond, I., Almarghini, K., Tappaz, M., 1996. Immunocytochemical localization of cysteine sulfinic acid decarboxylase in astrocytes in the cerebellum and hippocampus: a quantitative double immunofluorescence study with glial fibrillary acidic protein and S-100 protein. *Neuroscience* 75 (2), 619–633. [https://doi.org/10.1016/0306-4522\(96\)00256-4](https://doi.org/10.1016/0306-4522(96)00256-4).
- Chan-Palay, V., Palay, S.L., Wu, J.-Y., 1982. Sagittal cerebellar microbands of taurine neurons: Immunocytochemical demonstration by using antibodies against the taurine-synthesizing enzyme cysteine sulfinic acid decarboxylase. *Proceedings of the National Academy of Sciences* 79 (13), 4221–4225. <https://doi.org/10.1073/pnas.79.13.4221>.
- Liu, P., Ge, X., Ding, H., Jiang, H., Christensen, B.M., Li, J., 2012. Role of Glutamate Decarboxylase-like Protein 1 (GADL1) in Taurine Biosynthesis. *J. Biol. Chem.* 287 (49), 40898–40906. <https://doi.org/10.1074/jbc.M112.393728>.
- Raasakka A., Mahootechi E., Winge I., Luan W., Kursula V. & Haavik J. (2018). Structure of the mouse acidic amino acid decarboxylase GADL1. *Acta Crystallogr F Struct Biol Commun* 74, 65–73.
- Sörbo, B., Heyman, T., 1957. On the purification of cysteinesulfinic acid decarboxylase and its substrate specificity. *Biochimica et Biophysica Acta* 23, 624–627. [https://doi.org/10.1016/0006-3002\(57\)90385-2](https://doi.org/10.1016/0006-3002(57)90385-2).

- Chatagner, F., Bergeret, B., Labouesse, J., 1958. Influence of thyroxin injection on the decarboxylation of L-glutamic acid by rat brain and of L-cysteine-sulfinate acid by rat liver. *Biochim Biophys Acta* 30, 422–423. [https://doi.org/10.1016/0006-3002\(58\)90067-2](https://doi.org/10.1016/0006-3002(58)90067-2).
- Do, K.Q., Tappaz, M.L., 1996. Specificity of cysteine sulfinate decarboxylase (CSD) for sulfur-containing amino-acids. *Neurochem Int* 28, 363–371. [https://doi.org/10.1016/0197-0186\(95\)00109-3](https://doi.org/10.1016/0197-0186(95)00109-3).
- Komori, H., Nitta, Y., Ueno, H., Higuchi, Y., 2012. Structural Study Reveals That Ser-354 Determines Substrate Specificity on Human Histidine Decarboxylase. *J. Biol. Chem.* 287 (34), 29175–29183. <https://doi.org/10.1074/jbc.M112.381897>.
- Liang, J., Han, Q., Ding, H., Li, J., 2017. Biochemical identification of residues that discriminate between 3,4-dihydroxyphenylalanine decarboxylase and 3,4-dihydroxyphenylacetaldehyde synthase-mediated reactions. *Insect Biochemistry and Molecular Biology* 91, 34–43. <https://doi.org/10.1016/j.ibmb.2017.10.001>.
- Giardina, G., Montoli, R., Gianni, S., Cellini, B., Paiardini, A., Voltattorni, C.B., Cutruzzola, F., 2011. Open conformation of human DOPA decarboxylase reveals the mechanism of PLP addition to Group II decarboxylases. *Proceedings of the National Academy of Sciences* 108 (15), 20514–20519. <https://doi.org/10.1073/pnas.1111456108>.
- Fenalti, G., Hampe, C.S., O'Connor, K., Banga, J.P., Mackay, I.R., Rowley, M.J., El-Kabbani, O., 2007a. Molecular characterization of a disease associated conformational epitope on GAD65 recognised by a human monoclonal antibody b96.11. *Molecular Immunology* 44 (6), 1178–1189. <https://doi.org/10.1016/j.molimm.2006.06.025>.
- Porter, T.G., Martin, D.L., 1985. Chelidonic acid and other conformationally restricted substrate analogues as inhibitors of rat brain glutamate decarboxylase. *Biochemical Pharmacology* 34 (23), 4145–4150. [https://doi.org/10.1016/0006-2952\(85\)90207-2](https://doi.org/10.1016/0006-2952(85)90207-2).
- Burkhard, P., Dominici, P., Borri-Voltattorni, C., Jansonius, J.N., Malashkevich, V.N., 2001. Structural insight into parkinson's disease treatment from drug-inhibited DOPA decarboxylase. *Nat Struct Biol* 8, 963–967. <https://doi.org/10.1038/nsb1101-963>.
- Guion-Rain, M.-C., Chatagner, F., 1972. Rat liver cysteine sulfinate decarboxylase: Some observations about substrate specificity. *Biochimica et Biophysica Acta (BBA) - Enzymology* 276 (1), 272–276. [https://doi.org/10.1016/0005-2744\(72\)90029-0](https://doi.org/10.1016/0005-2744(72)90029-0).
- Oertel, W.H., Schmechel, D.E., Weise, V.K., Ransom, D.H., Tappaz, M.L., Krutzsch, H.C., et al., 1981. Comparison of cysteine sulfinate acid decarboxylase isoenzymes and glutamic acid decarboxylase in rat liver and brain. *Neuroscience* 6, 2701–2714. [https://doi.org/10.1016/0306-4522\(81\)90114-7](https://doi.org/10.1016/0306-4522(81)90114-7).
- Agnello, G., Chang, L.L., Lamb, C.M., Georgiou, G., Stone, E.M., 2013. Discovery of a Substrate Selectivity Motif in Amino Acid Decarboxylases Unveils a Taurine Biosynthesis Pathway in Prokaryotes. *ACS Chem. Biol.* 8 (10), 2264–2271. <https://doi.org/10.1021/cb400335k>.
- Liu, P., Ding, H., Christensen, B.M., Li, J., 2012. Cysteine sulfinate acid decarboxylase activity of *Aedes aegypti* aspartate 1-decarboxylase: The structural basis of its substrate selectivity. *Insect Biochemistry and Molecular Biology* 42 (6), 396–403. <https://doi.org/10.1016/j.ibmb.2012.02.001>.
- Ida, S., Kuriyama, K., 1983. Simultaneous determination of cysteine sulfinate acid and cysteic acid in rat brain by high-performance liquid chromatography. *Analytical Biochemistry* 130 (1), 95–101. [https://doi.org/10.1016/0003-2697\(83\)90654-1](https://doi.org/10.1016/0003-2697(83)90654-1).
- Weinstein, C.L., Griffith, O.W., 1987. Multiple forms of rat liver cysteinesulfinate decarboxylase. *J Biol Chem* 262, 7254–7263.
- Liu, P., Torrens-Spence, M.P., Ding, H., Christensen, B.M., Li, J., 2013. Mechanism of cysteine-dependent inactivation of aspartate/glutamate/cysteine sulfinate acid alpha-decarboxylases. *Amino Acids* 44, 391–404. <https://doi.org/10.1007/s00726-012-1342-7>.
- Liu, Z., Zheng, W., Ye, W., Wang, C., Gao, Y., Cui, W., et al., 2019. Characterization of cysteine sulfinate acid decarboxylase from *Tribolium castaneum* and its application in the production of beta-alanine. *Appl Microbiol Biotechnol* 103, 9443–9453. <https://doi.org/10.1007/s00253-019-10139-z>.
- Fenalti, G., Law, R.H.P., Buckle, A.M., Langendorf, C., Tuck, K., Rosado, C.J., Faux, N.G., Mahmood, K., Hampe, C.S., Banga, J.P., Wilce, M., Schmidberger, J., Rossjohn, J., El-Kabbani, O., Pike, R.N., Smith, A.I., Mackay, I.R., Rowley, M.J., Whistock, J.C., 2007b. GABA production by glutamic acid decarboxylase is regulated by a dynamic catalytic loop. *Nat Struct Mol Biol* 14 (4), 280–286. <https://doi.org/10.1038/nsmb1228>.
- Fleming, J. V., Sanchez-Jimenez, F., Moya-Garcia, A. A., Langlois, M. R. & Wang T. C. (2004). Mapping of catalytically important residues in the rat l-histidine decarboxylase enzyme using bioinformatic and site-directed mutagenesis approaches. *Biochem J* 379, 253–261.
- Ishii, S., Hayashi, H., Okamoto, A., Kagamiyama, H., 1998. Aromatic L-amino acid decarboxylase: Conformational change in the flexible region around arg334 is required during the transamination process. *Protein Sci.* 7 (8), 1802–1810. <https://doi.org/10.1002/pro.5560070816>.
- Fernandes, H.S., Ramos, M.J., Cerqueira, N.M.F.S.A., 2017. The Catalytic Mechanism of the Pyridoxal-5'-phosphate-Dependent Enzyme, Histidine Decarboxylase: A Computational Study. *Chem. Eur. J.* 23 (38), 9162–9173. <https://doi.org/10.1002/chem.201701375>.
- Bertoldi, M., Gonsalvi, M., Contestabile, R., Voltattorni, C.B., 2002. Mutation of Tyrosine 332 to Phenylalanine Converts Dopa Decarboxylase into a Decarboxylation-dependent Oxidative Deaminase. *J. Biol. Chem.* 277 (39), 36357–36362. <https://doi.org/10.1074/jbc.M204867200>.
- Bisello, G., Longo, C., Rossignoli, G., Phillips, R.S., Bertoldi, M., 2020. Oxygen reactivity with pyridoxal 5'-phosphate enzymes: biochemical implications and functional relevance. *Amino Acids* 52 (8), 1089–1105. <https://doi.org/10.1007/s00726-020-02885-6>.
- Scriven, C.R., Pueschel, S., Davies, E., 1966. Hyper-beta-alaninemia associated with beta-aminoaciduria and gamma-aminobutyric aciduria, somnolence and seizures. *N Engl J Med* 274, 635–643. <https://doi.org/10.1056/NEJM196603242741201>.
- Willi, S.M., Zhang, Y., Hill, J.B., Phelan, M.C., Michaelis, R.C., Holden, K.R., 1997. A deletion in the long arm of chromosome 18 in a child with serum carnitine deficiency. *Pediatr Res* 41, 210–213. <https://doi.org/10.1203/00006450-199702000-00009>.
- Griffith, O.W., 1983. Cysteinesulfinate metabolism. Altered partitioning between transamination and decarboxylation following administration of beta-methyleneaspartate. *J Biol Chem* 258, 1591–1598.
- Hammarström, M., Woestenenk, E.A., Hellgren, N., Härd, T., Berglund, H., 2006. Effect of N-terminal solubility enhancing fusion proteins on yield of purified target protein. *J Struct Funct Genomics* 7 (1), 1–14. <https://doi.org/10.1007/s10969-005-9003-7>.
- Bowler M. W., Nurizzo D., Barrett T., Beteva A., Bodin M., Caserotto H., et al. (2015). MASSIF-1: A beamline dedicated to the fully automatic characterization and data collection from crystals of biological macromolecules. *Journal of synchrotron radiation* 22, 1540–1547.
- Bowler, M.W., Svensson, O., Nurizzo, D., 2016. Fully automatic macromolecular crystallography: the impact of MASSIF-1 on the optimum acquisition and quality of data. *Crystallography Reviews* 22 (4), 233–249. <https://doi.org/10.1080/0889311X.2016.1155050>.
- Svensson O., Malbet-Monaco S., Popov A., Nurizzo D. & Bowler M. W. (2015). Fully automatic characterization and data collection from crystals of biological macromolecules. *Acta Crystallographica Section D* 71, 1757–1767.
- Kabsch, W., 2010. XDS. *Acta Crystallogr D Biol Crystallogr* 66 (2), 125–132. <https://doi.org/10.1107/S0907444909047337>.
- McCoy, A.J., Grosse-Kunstleve, R.W., Adams, P.D., Winn, M.D., Storoni, L.C., Read, R.J., 2007. Phaser crystallographic software. *J Appl Crystallogr* 40 (4), 658–674. <https://doi.org/10.1107/S0021889807021206>.
- Afonine, P.V., Grosse-Kunstleve, R.W., Echols, N., Headd, J.J., Moriarty, N.W., Mustyakimov, M., Terwilliger, T.C., Urzhumtsev, A., Zwart, P.H., Adams, P.D., 2012. Towards automated crystallographic structure refinement with phenix.refine. *Acta Crystallogr D Biol Crystallogr* 68 (4), 352–367. <https://doi.org/10.1107/S0907444912001308>.
- Casana, A., Lohkamp, B., Emsley, P., 2020. Current developments in Coot for macromolecular model building of Electron Cryo-microscopy and Crystallographic Data. *Protein Science* 29 (4), 1055–1064. <https://doi.org/10.1002/pro.3791>.
- Chen, V.B., Arendall III, W.B., Headd, J.J., Keedy, D.A., Immormino, R.M., Kapral, G.J., Murray, L.W., Richardson, J.S., Richardson, D.C., 2010. MolProbity: all-atom structure validation for macromolecular crystallography. *Acta Crystallogr D Biol Crystallogr* 66 (1), 12–21. <https://doi.org/10.1107/S0907444909042073>.
- Franke D., Petoukhov M. V., Konarev P. V., Panjkovich A., Tuukkanen A., Mertens H. D. T., et al. (2017). *Atas 2.8: A comprehensive data analysis suite for small-angle scattering from macromolecular solutions.* *J Appl Crystallogr* 50, 1212–1225.
- Svergun, D.I., Petoukhov, M.V., Koch, M.H.J., 2001. Determination of Domain Structure of Proteins from X-Ray Solution Scattering. *Biophysical Journal* 80 (6), 2946–2953. [https://doi.org/10.1016/S0006-3495\(01\)76260-1](https://doi.org/10.1016/S0006-3495(01)76260-1).
- Panjukovich, A., Svergun, D.I., 2016. Deciphering conformational transitions of proteins by small angle X-ray scattering and normal mode analysis. *Phys. Chem. Chem. Phys.* 18 (8), 5707–5719. <https://doi.org/10.1039/C5CP04540A>.
- Svergun, D., Barberato, C., Koch, M.H.J., 1995. CRYSOLO – a Program to Evaluate X-ray Solution Scattering of Biological Macromolecules from Atomic Coordinates. *J Appl Crystallogr* 28 (6), 768–773. <https://doi.org/10.1107/S0021889895007047>.
- Krisinel, E., Henrick, K., 2004. Secondary-structure matching (SSM), a new tool for fast protein structure alignment in three dimensions. *Acta Crystallogr D Biol Crystallogr* 60 (12), 2256–2268. <https://doi.org/10.1107/S0907444904026460>.
- Thompson, J.D., Higgins, D.G., Gibson, T.J., 1994. CLUSTAL W: improving the sensitivity of progressive multiple sequence alignment through sequence weighting, position-specific gap penalties and weight matrix choice. *Nucl Acids Res* 22 (22), 4673–4680. <https://doi.org/10.1093/nar/22.22.4673>.
- Goet, P., Courcelle, E., Stuart, D., Metz, F., 1999. ESPript: analysis of multiple sequence alignments in PostScript. *Bioinformatics* 15 (4), 305–308. <https://doi.org/10.1093/bioinformatics/15.4.305>.
- Unni, S., Huang, Y., Hanson, R.M., Tobias, M., Krishnan, S., Li, W.W., Nielsen, J.E., Baker, N.A., 2011. Web servers and services for electrostatics calculations with APBS and PDB2PQR. *J. Comput. Chem.* 32 (7), 1488–1491. <https://doi.org/10.1002/jcc.21720>.
- Pettersen, E.F., Goddard, T.D., Huang, C.C., Couch, G.S., Greenblatt, D.M., Meng, E.C., Ferrin, T.E., 2004. UCSF Chimera?A visualization system for exploratory research and analysis. *J. Comput. Chem.* 25 (13), 1605–1612. <https://doi.org/10.1002/jcc.20084>.
- Ericsson, U.B., Hallberg, B.M., DeTitta, G.T., Dekker, N., Nordlund, P., 2006. Thermofluor-based high-throughput stability optimization of proteins for structural studies. *Analytical Biochemistry* 357 (2), 289–298. <https://doi.org/10.1016/j.ab.2006.07.027>.
- Torrens-Spence, M.P., Chiang, Y.-C., Smith, T., Vicent, M.A., Wang, Y.I., Weng, J.-K., 2020. Structural basis for divergent and convergent evolution of catalytic machineries in plant aromatic amino acid decarboxylase proteins. *Proc Natl Acad Sci USA* 117 (20), 10806–10817. <https://doi.org/10.1073/pnas.1920097117>.

holo-CSAD



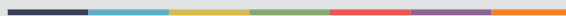
apo-CSAD



Supplementary Figure 1. Electron density maps for the holo (top) and apo (bottom) forms of CSAD. Shown are the final refined $2F_o - F_c$ maps contoured at 1σ . Both maps are shown in stereo view, and key residues either changing conformation or becoming more flexible in apo CSAD are labelled.



Graphic design: Communication Division, UIB / Print: Skjipes Kommunikasjon AS



uib.no

ISBN: 9788230856079 (print)
9788230848838 (PDF)